GREEN APPROACH TO FUNCTIONALIZE HIGHLY STABLE GRAPHENE NANOPLATELET COLLOID FOR HEAT-BASED APPLICATIONS

SITI SHAFIAH BINTI SHAZALI

FACULTY OF ENGINEERING
UNIVERSITY OF MALAYA
KUALA LUMPUR

2019

GREEN APPROACH TO FUNCTIONALIZE HIGHLY STABLE GRAPHENE NANOPLATELET COLLOID FOR HEAT-BASED APPLICATIONS

SITI SHAFIAH BINTI SHAZALI

THESIS SUBMITTED IN FULFILMENT OF THE REQUIREMENTS FOR THE DEGREE OF DOCTOR OF PHILOSOPHY

FACULTY OF ENGINEERING
UNIVERSITY OF MALAYA
KUALA LUMPUR

2019

UNIVERSITY OF MALAYA

ORIGINAL LITERARY WORK DECLARATION

Name of Candidate: Siti Shafiah binti Shazali

Matric No: KHA140129

Name of Degree: Doctor of Philosophy

Title of Project Paper/Research Report/Dissertation/Thesis ("this Work"):

Green approach to functionalize highly stable graphene nanoplatelet colloid for heat-based applications

Field of Study: Materials Engineering

I do solemnly and sincerely declare that:

(1) I am the sole author/writer of this Work;
(2) This Work is original;
(3) Any use of any work in which copyright exists was done by way of fair dealing and for permitted purposes and any excerpt or extract from, or reference to or reproduction of any copyright work has been disclosed expressly and sufficiently and the title of the Work and its authorship have been acknowledged in this Work;
(4) I do not have any actual knowledge nor do I ought reasonably to know that the making of this work constitutes an infringement of any copyright work;
(5) I hereby assign all and every rights in the copyright to this Work to the University of Malaya ("UM"), who henceforth shall be owner of the copyright in this Work and that any reproduction or use in any form or by any means whatsoever is prohibited without the written consent of UM having been first had and obtained;
(6) I am fully aware that if in the course of making this Work I have infringed any copyright whether intentionally or otherwise, I may be subject to legal action or any other action as may be determined by UM.

Candidate's Signature Date:

Subscribed and solemnly declared before,

Witness's Signature Date:

Name:

Designation:

ABSTRACT

In recent years, research efforts on the functionalization of graphene nanoplatelets (GNPs) have intensified due to the promisingly improved physical features and properties inherent within the modified structure that broaden its functionalities to suit diverse applications. In this research work, both covalent and non-covalent functionalization methods were applied on GNPs nanomaterials to enhance their stability and thermophysical attributes. Further investigation on the material performance based on different parameters in engineering applications (i.e., heat transfer and thermoelectrochemistry) was also carried out in this research. Researchers over the years have gone through the modification of GNPs structure in order to increase their colloidal stability to be used in specific applications. However, most of the studies involved hazardous chemicals and complex approaches. In this light, the focus of this research is directed toward the functionalization of GNPs material in a more environmentally friendly and facile method. Under covalent functionalization scheme, GNPs were derivatized with polymer and sugar alcohol using esterification process as well as subjected to doping process with nitrogen. On the other hand, a solvent-friendly surfactant with enhanced physical properties was chosen as the coating material for GNPs under non-covalent functionalization approach. A series of characterizations using spectroscopy, imaging, and electrophoresis instruments were conducted in order to examine the morphological structure, resolve the bond of functional groups, and also measure the colloidal stability of the functionalized GNPs. Thermal conductivity and viscosity properties in aqueous media improved significantly by using the functionalized GNPs. Finally, the functionalized GNPs materials were used as a solid additive in an aqueous solution that serves as heat transport media to improve the convective heat transfer performance under constant heat flux. Meanwhile, in thermoelectrochemistry application, the treated-GNPs materials were used as an additive in a redox solution to

increase the electrical performance with the increase of temperatures. All of the functionalized samples showed improved performance for the mentioned applications.

ABSTRAK

Dalam tahun-tahun kebelakangan ini, usaha penyelidikan mengenai fungsi graphene nanoplatelets (GNPs) telah dipergiatkan kerana ciri dan sifat fizikal yang lebih baik yang wujud dalam struktur yang diubah suai yang meluaskan fungsinya untuk disesuaikan dengan pelbagai aplikasi. Dalam kajian ini, kedua-dua kaedah fungsi kovalen dan bukan kovalen digunakan pada bahan nano GNPs untuk meningkatkan sifat kestabilan dan termofizikalnya. Penyiasatan lanjut mengenai prestasi bahan dalam aplikasi kejuruteraan (iaitu pemindahan haba dan termoelektrokimia) juga dilakukan dalam kajian ini. Penyelidik selama bertahun-tahun telah menjalani pengubahsuaian struktur GNPs untuk meningkatkan kestabilan koloid mereka bagi digunakan dalam aplikasi tertentu. Walau bagaimanapun, kebanyakan kajian yang terlibat menggunakan bahan kimia berbahaya dan pendekatan yang kompleks. Dalam kajian ini, tumpuan penyelidikan akan diarahkan kepada pengubahsuaian bahan GNPs dalam kaedah yang lebih mesra alam dan mudah. Di bawah skim fungsian kovalen, GNPs telah diubah dengan polimer dan gula alkohol menggunakan proses pengesteran serta menjalani proses penambahan dengan nitrogen. Sebaliknya, surfaktan mesra pelarut dengan sifat fizikal yang dipertingkatkan dipilih sebagai bahan salutan untuk GNP di bawah pendekatan pemfungsian bukan kovalen. Siri pencirian menggunakan instrumen spektroskopi, pengimejan, dan elektroforesis telah dijalankan untuk mengkaji struktur morfologi, menyelesaikan ikatan kumpulan berfungsi, dan juga untuk mengukur kestabilan koloid GNPs yang difungsikan. Keberkonduktan haba dan sifat-sifat kelikatan dalam media akueus telah meningkat dengan ketara hasil daripada penggunaan GNPs yang diubah suai. Akhir sekali, bahan GNPs yang diubah suai digunakan sebagai bahan tambah pepejal dalam larutan berair yang berfungsi sebagai media pengangkutan haba untuk meningkatkan prestasi perpindahan haba konvensional di bawah fluks haba yang berterusan. Sementara itu, dalam aplikasi termoelektrokimia, bahan GNPs yang dirawat berfungsi sebagai bahan tambah di dalam cecair redoks bagi

meningkatkan prestasi elektrikal dengan peningkatan suhu. Semua sampel yang difungsikan menunjukkan peningkatan prestasi untuk aplikasi yang disebutkan.

ACKNOWLEDGEMENTS

Firstly, I would like to express my sincere gratitude to my advisors Dr. Mohd. Nashrul Mohd. Zubir, Assoc. Prof. Ir. Dr. Mohd. Faizul Mohd. Sabri and Dr. Shaifulazuar Rozali, for the endless support of my PhD study and related research, for their patience, motivation, and immense knowledge. Their guidance helped me in all the time of research and writing of this thesis.

My sincere thanks also go to Assoc. Prof. Ir. Dr. Suhana Mohd. Said and Assoc. Prof. Dr. Kazi Md. Salim Newaz who provided me an opportunity to join their team, and who gave access to the laboratory and research facilities. Without their precious support, it would not be possible to conduct this research. My deepest gratitude is extended to the government of Malaysia through its Ministry of Higher Education for awarding the scholarship (MyBrain-MyPhD) along with the essential financial support throughout my research journey. Besides, this research has been made possible through the financial aid from the University of Malaya IPPP postgraduate grant (PG029-2015A) that I am highly indebted to. I would like to thank my fellow lab members for the stimulating discussions while were working together before deadlines, and all the fun we had.

My heartiest thanks are also dedicated to my friends whom I have benefited from in terms of valuable technical and academic assistance throughout the demanding research period. Last but not the least, I would like to thank my family: my parents (Shazali bin Kamaruzzaman & Siti Mariam binti A Wahab), my sister and my husband for supporting me spiritually throughout my research study, while writing this thesis, and in my life generally.

TABLE OF CONTENTS

LIST OF FIGURES

LIST OF TABLES

LIST OF SYMBOLS AND ABBREVIATIONS

GNPs	:	Graphene nanoplatelets
rGO	:	Reduced graphene oxide
GNP-OH	:	Hydroxylated GNPs
TFPEG	:	Tetrahydrofurfuryl polyethylene glycol
HEG	:	Hydrogen exfoliated graphene
GNS	:	Graphene nanosheets
CNT	:	Carbon nanotube
SWNT	:	Single-walled carbon nanotube
MWCNT	:	Multi-walled carbon nanotube
DI	:	Deionised water
PEG	:	Polyethylene glycol
PPG	:	Polypropylene glycol
P-123	:	Pluronic P-123
PEO	:	Polyethylene oxide
PPO	:	Polypropylene oxide
EG	:	Ethylene glycol
$NaBH_4$	:	Sodium borohydride
Bi_2Te_3	:	Bismuth telluride
$K_3Fe(CN)_6$	:	Potassium ferricyanide
$K_4Fe(CN)_6$	:	Potassium ferrocyanide
Fe_3O_4	:	Iron (II,III) oxide
ZnO	:	Zinc oxide
$ZnSO_4$	:	Zinc sulfate
fPEG	:	Phenyl-terminated functionalized polyethylene glycols

GNR	:	Graphene nanoribbons
CTAB	:	Cetyltrimethylammonium bromide
PPy/CGN	:	PPy/CTAB-intercalated graphene sheet nanocomposites
PDDA	:	Poly(diallyldimethylammonium chloride)
H_2SO_4	:	Sulfuric acid
$KMnO_4$	:	Potassium manganate
$NaNO_3$	:	Sodium nitrate
HNO_3	:	Nitric acid
HCl	:	Hydrochloric acid
PPy	:	Polypyrrole
APTES	:	Aminopropyltriethoxysilane
NMMOm	:	N-oxide monohydrate
eGPNc	:	Water-dispersible graphene
VTMS	:	Vinyltrimethoxysilane
PI	:	Polyimide
FGNS	:	Functionalized graphene nanosheets
Si	:	Silicone rubber
APTSi-GO	:	3-aminopropyltriethoxysilane functionalized graphene oxide
PVA	:	Poly(vinyl alcohol)
THF	:	Tetrahydrofuran
DCC	:	N,N′-dicyclohexylcarbodiimide
H_2O_2	:	Hydrogen peroxide
NH_4OH	:	Ammonium solution
PTFE	:	Polytetrafluoroethylene
KBr	:	Potassium bromide

$AlCl_3$	:	Aluminum chloride
I^-/I_3^-	:	Iodide/triiodide
mL	:	Milliliter
L	:	Liter
rpm	:	Rotation per minute
COOH	:	Carboxylic group
OH	:	Hydroxyl group
g	:	Gram
m	:	Mass flow rate, $kg.s^{-1}$
hr(s)	:	Hour(s)
°C	:	Degree Celsius
T (θ)	:	Absolute temperature, K
ZT	:	Figure of merit, Ω^{-1}
min(s)	:	Minute(s)
m^2/g	:	Meter square per gram
%	:	Percentage
π	:	Pi
mV	:	Millivolt
S_c	:	Seebeck coefficient, V/K
k	:	Thermal conductivity, W/mK
W	:	Watt, J/s
kW	:	Kilowatt
kHz	:	Kilohertz
wt.%	:	Weight percentage
nm	:	Nanometer
μm	:	Micrometer

mm	:	Millimeter
inch	:	Inch
cm^{-1}	:	Per centimeter
s^{-1}	:	Per second
s	:	Second
$m^2.g^{-1}$	:	Surface area
ΔE_p	:	Peak to peak separation (in cyclic voltammetry)
FPSC	:	Flat-plate solar collector
FTIR	:	Fourier transform infrared spectroscopy
AFM	:	Atomic force microscope
HRTEM	:	High-resolution transmission electron microscopy
IR	:	Infrared
UV-Vis	:	Ultraviolet-visible
XPS	:	X-ray photoelectron spectroscopy
CVD	:	Chemical vapor deposition
eV	:	Binding energy
DC	:	Direct current
Pt	:	Platinum
B	:	Boron
N	:	Nitrogen
O	:	Oxygen
h	:	Heat transfer coefficient, W/m^2K
q	:	Heat flux, $W.m^{-2}$
Nu	:	Nusselt number
Re	:	Reynolds number
x	:	Axial distance

ΔP	:	Pressure drop, Pa/m
ϕ	:	Nanoparticle volumetric fraction
μ	:	viscosity, Pa.s
ε	:	Turbulent dissipation, J/(kg.s) = m^2/s^3
ρ	:	Density, kg/m^3
η	:	Thermal performance factor
σ	:	Electrical conductivity, S/m

CHAPTER 1: INTRODUCTION

1.1 Background

Currently, the functionalization of graphene or graphene nanoplatelets (GNPs) has become the main attraction by many researchers around the world. This is due to its excellent properties in mechanical strength, thermal and electrical properties, and other properties that make GNPs as one of the versatile materials for various applications. Graphene is categorized in the carbon nanomaterial group, which obviously means that the main background of the structure is made of carbon and the difference is based on the layers and/or shapes of each material. For example, carbon nanotube is also made of carbon element. However, it has a rod-shaped structure and could differ in size. Meanwhile, graphene is a stack of layers with a honeycomb lattice structure and it can also consist of only one layer.

Compared to carbon nanotube, graphene is much less costly but still has the properties as good as carbon nanotube. Meanwhile, GNPs are much cheaper than graphene. Therefore, GNPs have been considered as favorable nanomaterials that can be used in various applications due to their desired balance of properties and cost. Current researchers are focusing for the material that can give good physicochemical properties; thus, they are also looking forward to finding an environmentally friendly material as well. However, GNPs tend to aggregate in different polar solvents due to strong Van der Waals forces (McAllister et al., 2007). Thus, GNPs need to be modified in order to enhance the properties to give better performance in particular applications. Therefore, the need to functionalize GNPs material using a greener and simple method is essential and highly demanded. Consequently, the effectiveness of functionalization process on GNPs should be investigated based on colloidal stability (Islam, Rojas, Bergey, Johnson, & Yodh, 2003). In relation to this, numerous efforts have been done to functionalize

graphene/GNPs where it becomes an important area of nanomaterials nowadays and plays an important role in modern science and technology (S. Stankovich et al., 2006).

These strategies can be roughly divided into two categories: the introduction of functional groups directly onto graphitic surface and the use of surfactants via direct attachment to enhance dispersion. Both strategies are known as covalent and non-covalent methods, respectively (Sarsam, Amiri, Kazi, & Badarudin, 2016; Sarsam, Amiri, Zubir, et al., 2016; Sun, Fu, Lin, & Huang, 2002; Xue et al., 2008). Non-covalent method involves polar-polar interactions by wrapping graphene surface with, for example surfactants or polymers, to stabilize GNPs dispersion in a solution (Georgakilas et al., 2016; Ji, Wu, Ma, & Yang, 2015; Kaur et al., 2015; Taha et al., 2016; W. Yang, Akhtar, Leifer, & Grennberg, 2013). On the other hand, covalent functionalization involves the attachment of hydrophilic functional groups such as carboxyl, hydroxyl, and sulfonate groups on the graphitic surface (D. Cai & M. Song, 2010; Craciun, Khrapach, Barnes, & Russo, 2013; Huang, Qi, Boey, & Zhang, 2012; Shan et al., 2009). In addition, the modification of graphene surface also involves rich solution chemistry with high dispersibility in polymers and solvents, with some new properties are introduced to graphene (B. Chen, Zhao, Liu, Xu, & Pan, 2015; J. C. Wei, R. Atif, T. Vo, & F. Inam, 2015; S. K. Yadav & Cho, 2013). Nevertheless, the functionalization of GNPs through chemical oxidation-reduction reactions requires the use of dangerous chemicals such as strong acids that are harmful to humans. High safety protection is also required in order to avoid hazardous effects (Xue et al., 2008).

Thus, in this research, the hazard for the preparation of functionalized GNPs is minimized through a green and a simple method that is suitable for mass production of highly stable GNPs. Moreover, the approaches used also comprise less toxic materials and are safer for humans. At the same time, the objectives to achieve functionalized GNPs

with highly stable properties in aqueous media and solvents, as well as available to be used in heat-based applications can be reached. At the end of this study, benefits in terms of knowledge and experiences in modification of nanomaterials can be obtained. Successful utilization of GNPs can contribute to a wide range of applications. The environmentally friendly and facile techniques may result in a breakthrough and the material can also be obtained through natural resources, thus receives more attention nowadays. This research is an interdisciplinary research in nanotechnology, which is in line with Malaysia's progress in this field. Furthermore, this research can give contributions and improve competitiveness in the field of material engineering.

1.2 Problem statement

Recently, GNPs nanomaterial is receiving attention from many researchers due to their good properties and high performance in different types of applications. However, the ability in terms of dispersion and stability in most of the common solvents is one of their biggest limitations. Due to this matter, many researchers are trying to find the best method to functionalize GNPs nanomaterial. However, the methods used by most of the previous researchers usually involved complex reactions and hazardous processes that require stringent safety measures during experimental works. Different types of functionalization methods (i.e., covalent and non-covalent) might also lead to different qualities in terms of stability and thermophysical properties, which need further investigation. In addition, it will affect performance when applied to specific applications. Therefore, the need to functionalize GNPs material using a greener and cost-effective method is essential and highly demanded. In this work, more convenient and environmentally friendly methods were applied to fill this gap and to simultaneously optimize their properties in different fields.

1.3 Objectives of the present research

The main objective of this study is to enhance the stability and properties of GNPs and study their potential in different types of heat-based applications. Due to their limitations (poor dispersion and stability in solution), different types of modifications were used for the GNPs nanomaterial.

In order to achieve the main objective, four sub-objectives are designed as follows:

1. To functionalize GNPs material and synthesize the material through covalent and non-covalent methods using green approaches.
2. To evaluate the stability of covalent and non-covalent functionalized GNPs in distilled water and different types of solvents (methanol, ethanol, ethylene glycol, and 1-hexanol).
3. To investigate the thermophysical properties based on thermal conductivity and viscosity of the functionalized GNPs in aqueous media.
4. To investigate experimentally the potential of each functionalized GNPs based on different parameters in different types of applications, which include heat transfer and thermoelectrochemistry.

1.4 Outline of the thesis

This thesis reports the study of the functionalization of GNPs using different modification approaches: covalent and non-covalent processes. The procedures involved characterizations that were carried out using different instruments for the study of morphological structure, colloidal stability, and thermophysical properties. In addition, this thesis also focuses on the potential of all the prepared treated-GNPs materials toward heat transfer and thermoelectrochemistry applications. The thesis is outlined as follows.

Chapter 1 provides the general introduction about the research in this thesis. It gives an overview on the current limitations regarding the functionalization of GNPs nanomaterial. This chapter also presents the problem statements and the targeted objectives to be achieved at the end of the study. The literature review about graphene/GNPs and their properties is discussed in Chapter 2. The fundamentals behind the functionalization process based on covalent and non-covalent techniques are also included this chapter. In addition, this chapter encompasses the contributions of graphene/GNPs in different types of fields according to their performances and effects based on different types of materials.

In Chapter 3, the details on the methodology for the functionalization of GNPs materials by using different synthesis methods are explained. Furthermore, this chapter gives an introduction regarding the functional groups introduced to GNPs and a brief comparison with previous research for each treated-GNPs sample. This chapter also consists of the techniques to conduct the tests on morphological structure, stability performance based on photometric results, zeta potential and particle size distributions, and thermophysical properties (i.e., viscosity and thermal conductivity). Furthermore, the procedures related to the experimental setup for each of the application are described in detail.

Meanwhile, the details regarding the results and discussion for each characterization test are discussed in Chapter 4. This chapter also explains the performances based on the different parameters investigated for the functionalized GNPs material in different fields as mentioned previously. Lastly, in Chapter 5, all of the outcomes in this study that are discussed in the previous chapters are summarized as a conclusion. The possibilities and recommendations for future works are also presented in this chapter.

CHAPTER 2: LITERATURE REVIEW

2.1 Introduction to graphene

The history of graphene started around 160 years ago, when Sir Benjamin Collins Brodie exposed graphite to a strong acid and introduced graphene oxide (GO) as early as 1859 (Geim, 2012). In 1916, the structure of graphite was first explored using related powder diffraction method and its properties were studied in detail by Kohlschütter and Haenni in 1918 (Gupta, 2017). Later in 1947, P.R. Wallace came out with a theoretical study of graphene (Wallace, 1947). Then, G. Ruess and F. Vogt captured the first images of a few layers of graphite in 1948 using electron microscopy, followed by the observation of single graphene layers (Brink, 2014). The study of graphene was continued until the early 2000s and became prominent after Novoselov, Geim, and co-workers used a very simple method called "scotch-tape method" to synthesize graphene in 2004. Their breakthrough has awarded them the Nobel Prize in Physics in 2010 (Geim & Novoselov, 2007; Gong, Liu, Li, Yu, & Teoh, 2016).

Generally, it is known as a two-dimensional (2D) nanomaterial comprising of sp^2-hybridization carbon atoms ordered in a flat honeycomb lattice pattern with one-atom thick (T. Zhang et al., 2017). Thus, it makes this material as one of the thinnest materials ever known. It is also a basic element that is made up of other carbon allotropes such as fullerenes (zero-dimensional) that can be formed through a complete sphere, whereas carbon nanotube (one-dimensional) can be formed by rolling up the sheet (Tiwari et al., 2016). In addition, graphene in multiple layers is made up of a building block of graphite (three-dimensional) that is weakly bound between each other (Y. Hu & Sun, 2013; Mostofizadeh, Li, Song, & Huang, 2011). The schematic figure of graphitic formation can be seen in Figure 2.1.

Since the discovery of graphene, this material has drawn great interest among scientists in the field of advanced materials (J. G. Wang, Ma, Liang, & Sun, 2017). This is due to the amazing properties in terms of thermal conductivity (5,000 W/mK), electrical, mechanical (Young's modulus of 1 TPa), and high chemical stability (Migkovic-Stankovic, Jevremovic, Jung, & Rhee, 2014). Other than that, graphene also possesses other unique properties such as high specific surface area, extraordinary electron transport capabilities, and good optical transparency (Singh et al., 2011; J. Wei, R. Atif, T. Vo, & F. Inam, 2015). These features have made graphene as an ideal material by many researchers for the use in various applications such as energy storage, corrosion, heat transfer, solar cells, biomaterials, and many more (Liao, Zhang, Qiao, & Zhang, 2017; Renteria, Nika, & Balandin, 2014).

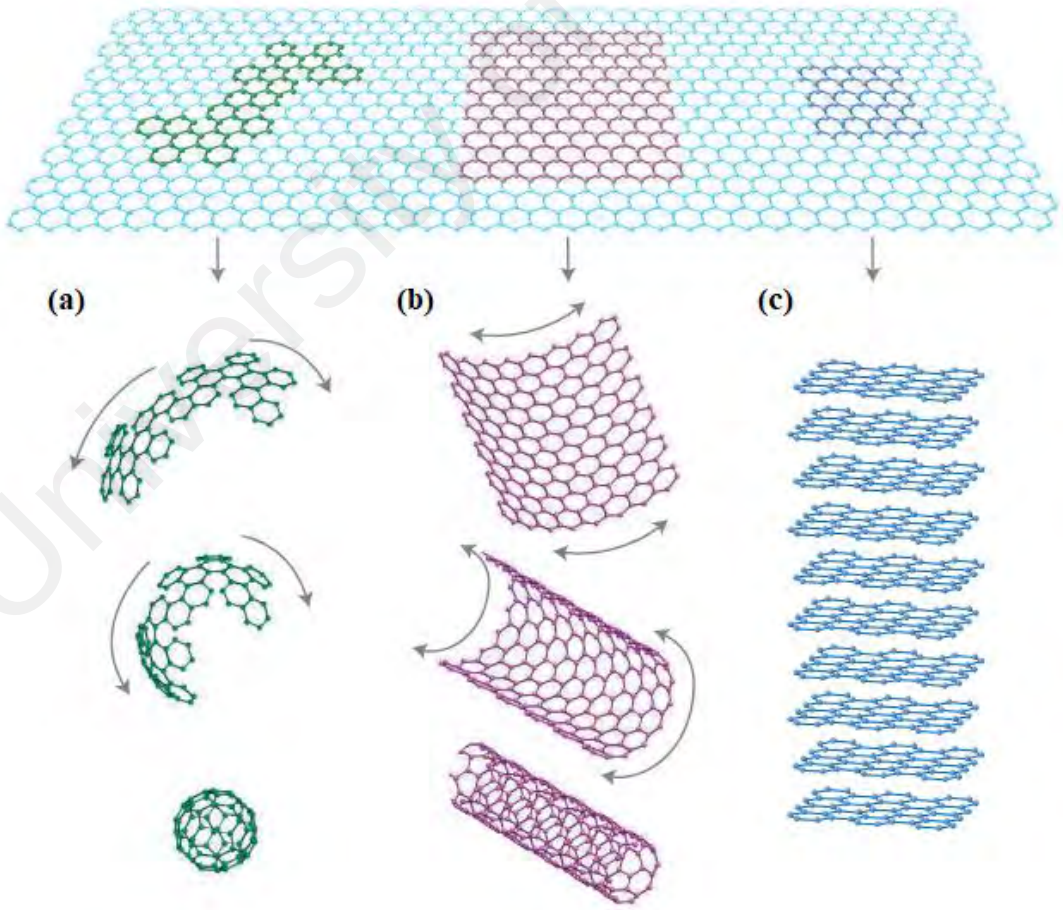

Figure 2.1: Graphitic forms of (a) fullerenes, (b) carbon nanotube, and (c) graphite (Geim & Novoselov, 2007).

2.2 Properties of graphene

2.2.1 Surface properties

Graphene is known as a material with a large surface-to-volume ratio and it is optically transparent (G. Zhu et al., 2011). It has carbon-carbon distance length of 0.14 nm with the atomic thickness of 0.35 nm (Gong et al., 2016). The arrangement between each carbon atom is 120° as can be seen in Figure 2.2 (de Andres, Ramirez, & Verges, 2008; Heyrovska, 2008). Besides, each carbon atom in the graphene honeycomb lattice is sp^2 hybridized, which has the ability to contribute an electron and form π orbital that forms a delocalized electron network (Fuhrer, Lau, & MacDonald, 2010).

Theoretically, the surface area of graphene is 2,630 $m^2.g^{-1}$; however, the surface area of treated or modified graphene has typical experimental values within the range of approximately 100–1,000 $m^2.g^{-1}$ when measured by Brunauer-Emmett-Teller (BET) method (S. Stankovich et al., 2006; Stoller, Park, Zhu, An, & Ruoff, 2008; Thommes, Kohn, & Froba, 2000). The values of surface area typically depend on their layers and structure that are usually influenced by the method of production (Tang, Zhou, & Chen, 2013). Usually, chemical functionalization and manufacturing process at specific conditions will influence the layers and structure of graphene (Y. Hu & Sun, 2013; Puangbuppha, Limsuwan, & Asanithi, 2012). The large surface area of graphene will give more advantage in terms of more surface interaction between graphene and the polymer or chemical molecule to be interacted with (Chieng, Ibrahim, & Yunus, 2012; J. F. Dai, Wang, Ma, & Wu, 2015; Q. H. Liu et al., 2012). Besides, the modification of graphene structure that can make the graphene surface rough has also been demonstrated to provide better practical adhesion by previous researchers (S. Stankovich et al., 2006).

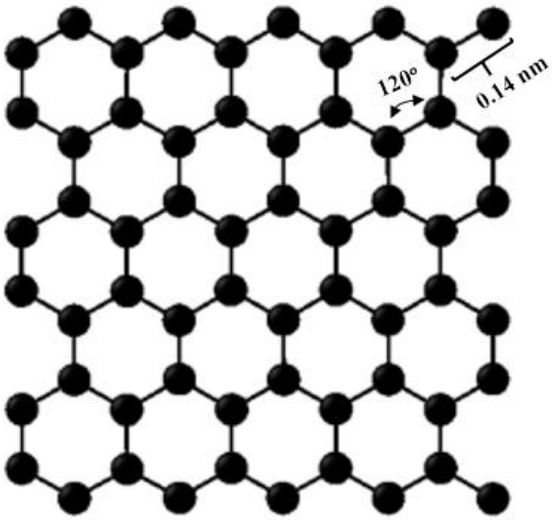

Figure 2.2: Schematic diagram of graphene structure (Ghasemi & Rajabpour, 2017).

2.2.2 Electrical properties

The electrical conductivity of graphene is approximately 64 $Sm.cm^{-1}$ and this value is higher than the conductivity of a single-walled carbon nanotube (SWCNT) (X. Wang, Zhi, & Mullen, 2008). The conductivity of graphene at different ranges of temperatures usually remain stable, even at very low temperature, which makes this material useful to be used in many fields such as energy conversion or storage applications (Geim & Novoselov, 2007). The 2D structure of graphene has remarkable electrical properties, where graphene possesses high mobility and transport of electrons in a medium at room temperature (J. G. Wang et al., 2017). The electrical properties can be determined through the bonding of π orbitals in the graphitic structure of graphene (Radadiya, 2015). However, the properties such as carrier concentration and doping type should be well designed and controlled in order to fulfill the requirements for device applications (Y. J. Kim, Kim, Novoselov, & Hong, 2015). This is because graphene only consists of a monolayer with one-atom thickness, which made all the surfaces of graphene are in contact with the environment. Thus, the electrical properties of graphene are highly sensitive and affected when introduced to foreign atoms or molecules, unlike bulk materials (Schedin et al., 2007). Therefore, a proper chemical modification for the

graphene structure is needed to modulate the electrical properties parameters in terms of carrier concentrations, types of doping, and band gap of graphene. Besides, the distribution of foreign atoms or molecules on the graphene surface also plays a part in improving electrical performances for practical applications (Britnell et al., 2012; Georgiou et al., 2013; Withers et al., 2015).

2.2.3 Thermal properties

Graphene is considered as a highly potential material for thermal management applications due to its high thermal transport properties, which have driven many researchers to focus on graphene (Ghasemi & Rajabpour, 2017; Shahil & Balandin, 2012). The thermal conductivity of graphene is within the range of 3,000–5,000 W/mK at room temperature, which makes graphene as the best heat conductor or high thermal conductivity material compared to other known materials (e.g., copper and silicon) (D. Nika, Ghosh, Pokatilov, & Balandin, 2009; Steinhögl, Schindler, Steinlesberger, Traving, & Engelhardt, 2005). Another comparison can be made with diamond, which has the approximate thermal conductivity of 2,000 W/mK at room temperature (Sukhadolau et al., 2005; Tohei, Kuwabara, Oba, & Tanaka, 2006). Despite the size of graphene, several researchers conducted a number of experiments regarding thermal conductivity and it was discovered that the material had high absorption of heat (Fugallo et al., 2014). In addition, some studies also showed that graphene with a larger surface area could enhance heat transportation (S. Kang et al., 2017). The doping of graphene with a material or solvent usually enhances thermal properties due to the stable bonding between carbon-carbon atoms in the lattice structure (Tessy Theres Baby & Ramaprabhu, 2010; Shahil & Balandin, 2012). However, when chemical treatment is carried out on graphene, its thermal conductivity usually decreases depending on the deformity that occurs (Pop, Varshney, & Roy, 2012). This is due to the roughness that occurs on the edge or surface that causes phonons to be scattered within the boundaries as mentioned by previous

researchers (D. L. Nika, Pokatilov, Askerov, & Balandin, 2009; Yan Wang, Qiu, & Ruan, 2012). Nonetheless, the ability of modified graphene can give benefit for energy storage and thermal management applications (Renteria et al., 2014). Further details on the research of thermal conductivity by previous researchers can be seen in Table 2.1.

Table 2.1: Summary of experimental results on thermal conductivity of graphene and functionalized graphene-based nanofluids.

Authors	Particle Type	Particle Concentration	Enhancement	Temperatures
(Tessy Theres Baby & Ramaprabhu, 2010)	Exfoliated graphene	0.005–0.056 vol.%	14%–64%	25–50°C
(X. Li, Chen, Mo, Jia, & Shao, 2014)	SiO_2-coated graphene	0.1 wt.%	Up to 20%	15–65°C
(S. S. Park & Kim, 2014)	Graphene	0.001–0.01 vol.%	6.2%–14%	25°C
(J. Liu, Wang, Zhang, Fang, & Zhang, 2014)	Graphene	0.01–0.03 wt.%	3%–22.9%	25–200°C
(Sen Gupta et al., 2011)	Graphene nanosheets	0.05–0.2 vol.%	Up to 27%	30–50°C

2.2.4 Mechanical properties

The outstanding mechanical properties of graphene have drawn the interest of many researchers to utilize it as a reinforcing agent in nanocomposites (Young, Kinloch, Gong, & Novoselov, 2012). The impressive properties lie in the ideal crystal lattice geometry made of highly stable sp^2 bonds (Kun, Tapaszto, Weber, & Balazsi, 2012). Besides, the mechanical properties also depend on the structural defects that can be caused by grain boundaries and dislocations (Koch, 2007). Graphene is not only known to be extraordinarily strong (~1 TPa), but it also has elastic properties, which made this material

particularly special (Z. Q. Shen, Ye, Zhou, Kroger, & Li, 2018). The first experimental analysis that examined the mechanical properties exhibited by monolayer graphene using atomic force microscopy (AFM) was done by Papageorgiou and co-workers (Papageorgiou, Kinloch, & Young, 2017). In their study, the strength properties were measured through mechanical experimental works by depositing the graphene membrane onto a substrate. Next, AFM nanoindentation was applied to measure the as-mentioned properties. It was found that the intrinsic strength of the monolayer graphene membrane was 42 N/m or 130 GPa (C. Lee, Wei, Kysar, & Hone, 2008). Experimentally, this value has made graphene to be considered as the strongest material ever discovered compared to other materials (Kotakoski & Meyer, 2012). In the other study by Li et al., they investigated the effect of adding graphene nanoplatelets (GNPs) to natural rubber. Interestingly, GNPs produced an effective result in increasing the stiffness of natural rubber compared to other carbon allotropes (S. H. Li et al., 2017).

2.3 Synthesis of graphene

Numerous efforts have been made to produce or synthesize graphene materials and its derivatives with high quality and high production yield (Huang et al., 2012). Graphene can be prepared using four different methods (Li et al., 2007). The first method is chemical vapor deposition (CVD) and epitaxial growth, for instance, the decomposition of ethylene on nickel surfaces. The second method is the micromechanical exfoliation of graphite, which is also known as the “scotch-tape” or “peel-off” method (Aizawa et al., 1990). The third method is epitaxial growth on electrically insulated surfaces and the fourth method is the solution-based reduction of GO (Berger et al., 2006).

2.3.1 Chemical vapor deposition (CVD)

Chemical vapor deposition (CVD) is one of the most well-established methods to synthesize carbon-based nanomaterials, namely graphene with large area, high structural

quality monolayer, and few-layered graphene sheets (Xuesong Li et al., 2009). There are several types of CVD methods such as hot/cold wall CVD, thermal CVD, plasma-enhanced CVD, and others. Basically, CVD involves three main parameters: temperature, catalyst, and reactants (Y. Hu & Sun, 2013). Different types of chemicals such as methane, hexane, and pentane have been used as the main sources of hydrocarbons other than ethylene and liquid precursors (Dong et al., 2011; Srivastava et al., 2010). Generally, in CVD, thermal decomposition of hydrocarbon is carried out to provide the source of carbon. Then, the production mechanisms of graphene on the growth substrate are initiated with the growth of carbon atoms that nucleate on the metal and grow into large domains (Y. J. Kim et al., 2015). Some difficulties might occur due to the chemical inertness of graphene, which can contribute to the defect of material structure. Other than that, the stability of the grown material can also be affected by thermal fluctuations during the process (K. Novoselov, Mishchenko, Carvalho, & Neto, 2016). However, despite the complexity of CVD, it is still the most preferred method to synthesize graphene due to the high chance of producing large area of graphene with no contamination (J. Kang, Shin, Bae, & Hong, 2012; J. Song et al., 2013).

Many researchers have reported the use of CVD in graphene processing. One of the reported research is by Bae and co-workers that used roll-to-roll (RTR) process to produce 30-inch graphene film using CVD, as can be seen in Figure 2.3 (Bae et al., 2010). More interestingly, the RTR technique has been employed by other researchers as well with some adjustments and modifications such as Polsen et al. that used the same RTR process but with a concentric tube CVD (Polsen, McNerny, Viswanath, Pattinson, & Hart, 2015). Moreover, a promising technique was introduced by Bointon et al. that used resistive heating cold-wall CVD that is faster than the conventional method. Additionally, this technique has been known to successfully produce monolayer graphene with high quality (Bointon, Barnes, Russo, & Craciun, 2015).

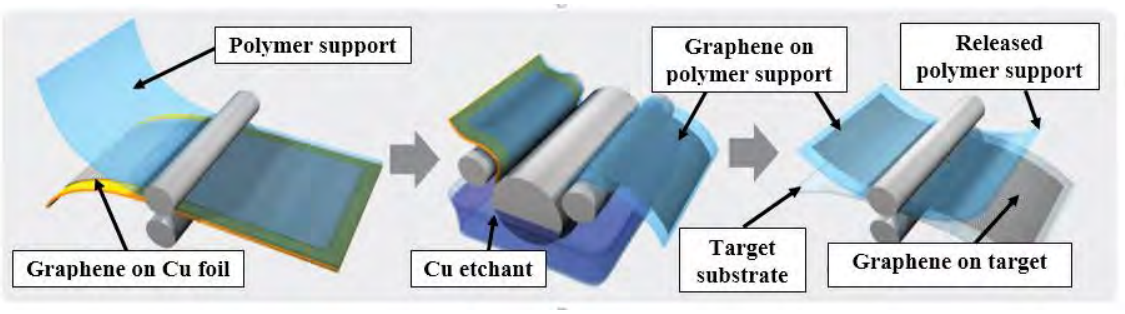

Figure 2.3: Schematic of the roll-to-roll process in the production of graphene films grown on a copper foil (Bae et al., 2010).

2.3.2 Mechanical exfoliation of graphite

Graphite is made of many layers of graphene sheets stacked together and bonded by weak Van der Waals forces. Mechanical exfoliation is the first isolation method of producing free-standing graphene using high-purity pyrolytic graphite or good-quality natural graphite (K. S. Novoselov et al., 2004). This method is known to be the simplest preparation method often known as the "scotch-tape" or "peel-off" process. In this technique, graphite flakes are mechanically exfoliated using a scotch tape repeatedly to separate it into a few layers of graphene (Lu, Yu, Huang, & Ruoff, 1999; Ni et al., 2007). This exfoliation technique is able to provide high-quality graphene crystals and electronic quality without introducing mechanical damage and structural defects (Kostya S Novoselov et al., 2005; Konstantin S Novoselov et al., 2007). The obtained graphene flakes are usually evaluated using different types of methods such as AFM, optical microscopy, and Raman spectroscopy (Papageorgiou et al., 2017). Although this method is simple and easy, it is not suitable for large-quantity production. This is due to the difficulties in controlling the mechanical cleavage of graphite materials that leads to randomly placed graphene sheets (Fuhrer et al., 2010). Besides, there is a possibility of impurities in the graphene sheets produced from the adhesive tape (Rümmeli et al., 2011). However, the simplicity of this method can be well used in laboratory-scale experiment for the fundamental studies of physical properties of graphene (C. Lee et al., 2008; Nair et al., 2008).

2.3.3 Liquid phase exfoliation

Another type of exfoliation process usually carried out to fabricate graphene is liquid phase exfoliation. Basically, this process involves different steps including dispersion in solvents, sonication, and purification in order to obtain a graphene product without contamination (Niu et al., 2016). In detail, a variety of solvents or surfactants can be used to disperse graphene. However, in order to promote exfoliation, organic solvents particularly those with high energy of adsorption towards the graphitic surface of graphene should be chosen (Conti et al., 2016; Haar et al., 2015). Meanwhile, sonication process is considered as a crucial step in determining the amount of graphene product that can be achieved. Furthermore, to remove impurities, centrifugation will take place to purify the sample afterward. The parameters with important roles for these three steps are the amount of graphite, sonication time, and rotational speed of centrifuge (Ciesielski & Samori, 2014, 2016; J. N. Coleman, 2013). It should be noted that the solvents must be carefully chosen as some solvents are harmful to the environment and using a large amount of these solvents may be hazardous to humans. In addition, the cost for using specific solvents will also increase if the solvents are highly reactive (Y. Wei & Sun, 2015). However, this production method is facile and appears to be promising routes for mass production of graphene (Cui, Zhang, Hao, & Hou, 2011). In the previous research by Hernandez et al., they carried out ultrasonication treatment in a liquid phase using certain organic solvents and it was proven that this route could produce high-quality graphene with high yield (Hernandez et al., 2008).

2.3.4 Chemically converted graphene

This technique involves the oxidation of graphite to synthesize graphite oxide first, followed by exfoliation process to produce dispersible GO, which is later reduced to generate chemically converted graphene (CCG) (Figure 2.4) (S. Bai & Shen, 2012; S. Park & Ruoff, 2009). The method was developed by Hummers and co-workers, which

was used to obtain GO product. This method is usually referred by most of the researchers due to its high efficiency to produce high yield (J. Chen, Yao, Li, & Shi, 2013). In this technique, graphite is oxidized by a treatment using both solvents of potassium manganite ($KMnO_4$) and sodium nitrate ($NaNO_3$) in a strong acid medium, i.e., sulfuric acid (H_2SO_4) (Hummers Jr & Offeman, 1958). As a result, the deformity or structural defects will be introduced with a large amount of hydrophilic oxygenated groups on the structure (Guerrero-Contreras & Caballero-Briones, 2015). Further exfoliation process to obtain highly stable and purified GO dispersion can be done through ultrasonication and also centrifugation (H. Bai, Li, & Shi, 2011).

Various reducing agents such as sodium borohydride, hydrazine monohydrate, hydroquinone, strong alkaline solutions, and others can be used to reduce GO (X. Fan et al., 2008; J. Shen et al., 2009; Shin et al., 2009). Among these reducing agents, hydrazine monohydrate is the most common agent for reduction process (Stankovich et al., 2007). It is the most widely used reducing agent by researchers due to its strong reduction ability to eliminate the oxygen-containing groups from GO (D. Li, Müller, Gilje, Kaner, & Wallace, 2008). However, hydrazine monohydrate is highly hazardous to human health. Therefore, more environmentally-friendly approaches have been developed for the reduction of GO to avoid the use of strong and toxic chemicals, such as L-ascorbic acid, tea, and lysozyme (Yan Wang, Shi, & Yin, 2011; F. Yang, Liu, Gao, & Sun, 2010; Jiali Zhang et al., 2010). Other techniques, for example thermal reduction method (solvothermal and hydrothermal), have also been employed for the reduction of GO. This method is performed in a solution with moderate temperatures of 100–300 °C (Murugan, Muraliganth, & Manthiram, 2009; Y. Zhu et al., 2010). Overall, the production of CCG material using this method has the potential to be scaled up, which is beneficial for researchers.

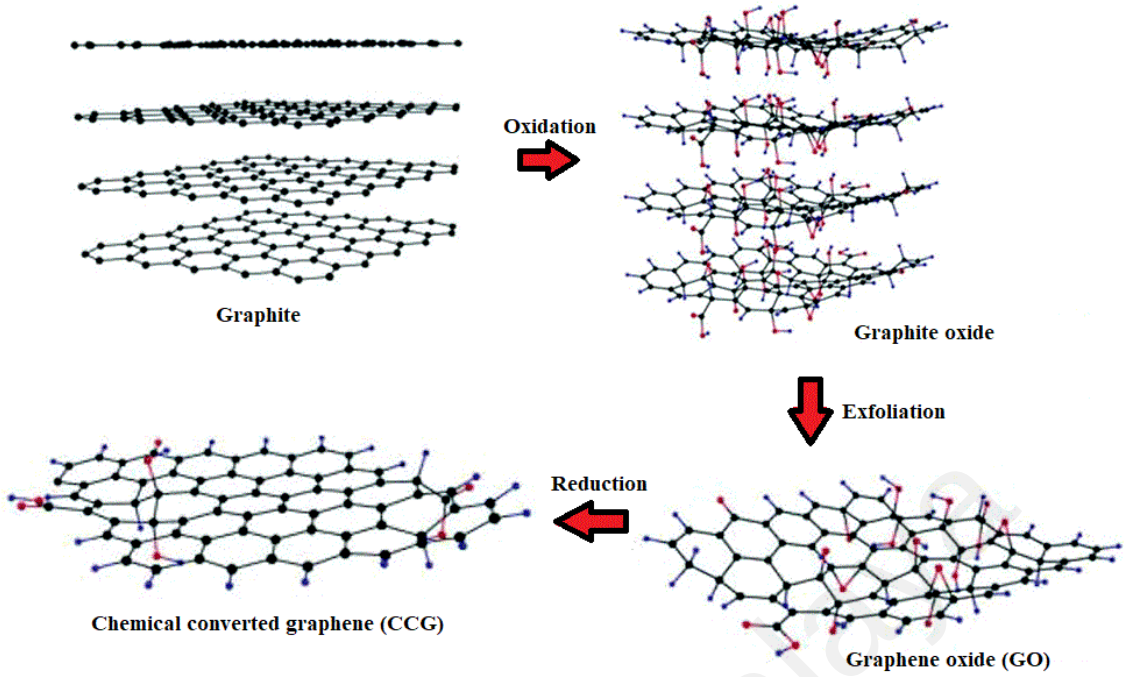

Figure 2.4: Oxidation, exfoliation, and reduction processes involved in the preparation of chemically converted graphene (CCG) (H. Bai et al., 2011).

2.4 Graphene nanoplatelets (GNPs)

Graphene nanoplatelets (GNPs) refer to a new generation of carbon-based nanomaterials (King, Klimek, Miskioglu, & Odegard, 2013). GNPs are promising materials for a wide range of applications including nanocomposite structures, phase change systems, supercapacitors, and thermal management (Agromayor et al., 2016; Bafana, 2016; Han et al., 2013; H. B. Yang, Memon, Bao, Cui, & Li, 2017; Y. W. Zhu et al., 2010) due to the extraordinary properties of GNPs. For instance, the mechanical strength of GNPs is higher than that of steel by two orders of magnitude, with theoretical Young's modulus of ~1 TPa. In addition, GNPs have high electron mobility and thermal conductivity, with the values of ~2.5 (10^5) $cm^2/V^{-1}S^{-1}$ and ~3000 $W\ m^{-1}\ K^{-1}$, respectively. More importantly, GNPs have a large surface-to-volume ratio, which provides large contact surface area with polymer (Antunes, Gedler, Abbasi, & Velasco, 2016; Lin et al., 2015; Scaffaro, Botta, Maio, Mistretta, & La Mantia, 2016; Yi Wang et al., 2015). In addition to excellent intrinsic mechanical and electrical properties, as well as high thermal

conductivity of GNPs on a weight basis, these nanomaterials are more cost-effective for industrial applications compared to carbon nanotubes (Ahmadi-Moghadam, Sharafimasooleh, Shadlou, & Taheri, 2015; Strankowski, Piszczyk, Kosmela, & Korzeniewski, 2015).

2.5 Functionalization of graphene/GNPs

Pristine graphene or GNPs materials are known to be hydrophobic in nature, which make them difficult to be dispersed in most of the polar solvents. Thus, it is important to functionalize graphene sheets for use in future applications.

2.5.1 Functionalization of graphene using covalent process

The covalent functionalization of graphene structure usually takes place at the edge of the sheets and/or on the plane of the surface (can be seen in Figure 2.5). This process is associated with rehybridization into sp^3 carbon network configuration from sp^2 carbon atoms (M. J. Park et al., 2006). In other words, covalent functionalization involves chemical reactions between carbon in the main structures and other functional groups, producing new functionalized materials with different properties (S. P. Zhang, Xiong, Yang, & Wang, 2011). Due to several objectives to be achieved by researchers, the functionalization of pristine graphene/GNPs has been developed over years. One of the main objectives is to enhance the dispersibility of graphene in aqueous media or common organic solvents. This can be achieved through some modification of graphene structure with certain organic groups (Niyogi et al., 2010).

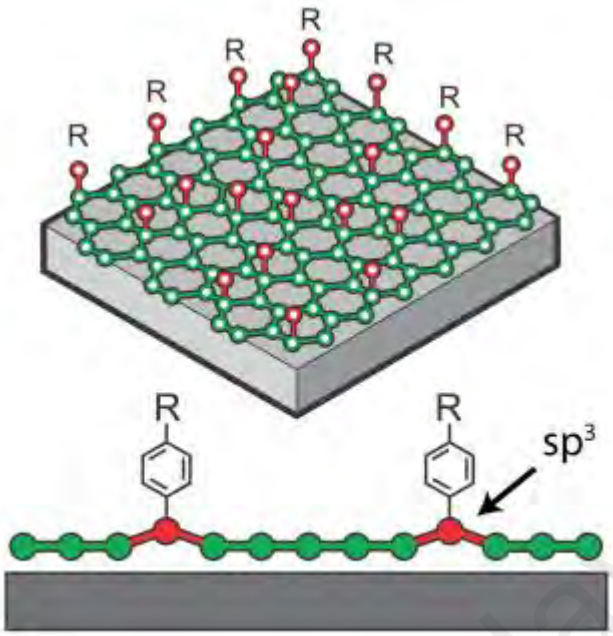

Figure 2.5: Schematic illustration of covalent modification of the graphene lattice ("Research: Projects: Graphene Chemistry," 2018).

Through covalent functionalization, it is expected that stronger bonds can be formed between the graphene and the polymers. However, due to the lack of functional groups on the graphene sheet to be conjugated with, this condition is hardly realized. Thus, further disruption on the graphene structure by introducing hydroxyl groups onto the structure is one of the strategies to increase the possibility of polymer attachment (V. Coleman et al., 2008). This combination will obviously combine the properties as well; graphene will offer its good properties, whereas polymers will contribute in terms of dispersibility (M. Song, 2013; Zheng, Shen, & Zhai, 2013). Salavagione et al. reported a direct esterification approach to functionalize GO with hydroxyl groups of poly(vinyl alcohol) (PVA) in the presence of N,N′-dicyclohexylcarbodiimide (DCC) and also 4-dimethylaminopyridine (DMAP) catalysts. The functionalized graphene product was later reduced using hydrazine hydrate to produce reduced graphene hybrid (see Figure 2.6). Through this method, the modified graphene could be solubilized in water and dimethyl sulfoxide (DMSO) (Salavagione, Gomez, & Martinez, 2009). The same researchers reported several techniques in preparing nanocomposites of reduced graphene

oxide (rGO) with poly(vinyl chloride) (PVC). Through their observation, the covalent attachment of rGO with the modified PVC improves mechanical and thermal properties (Salavagione & Martínez, 2011).

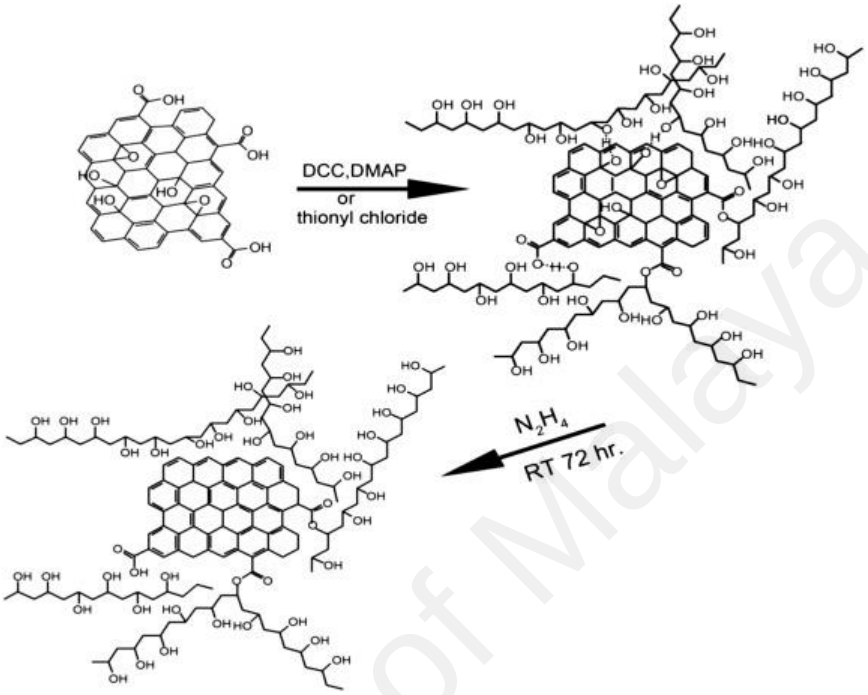

Figure 2.6: Schematic diagram of the esterification of graphite oxide with PVA and end product after reduction with hydrazine hydrate (Salavagione et al., 2009).

Qian et al. demonstrated that high-performance polyimide (PI)-based nanocomposites can be fabricated using 3-aminopropyltriethoxysilane functionalized graphene oxide (APTSi-GO) as the reinforcing filler. APTSi-GO nanosheets were highly dispersed with the polymer matrix due to the strong covalent interaction between both materials. The technique involves in-situ polymerization and thermal imidization of PI-based nanocomposites and functionalized graphene nanosheets (FGNS). A prominent reinforcement effect was demonstrated, showing 79% and 132% improvement in the tensile strength and tensile modulus, respectively. In addition, it also improved the glass-transition temperature and thermal stability (Qian et al., 2015). Zhang et al. studied the effect of covalently functionalized GNPs toward the thermal and mechanical properties of silicone rubber (SR) composite. The covalent modification of graphene structure was

carried out by reacting aminopropyltriethoxysilane (APTES) and vinyltrimethoxysilane (VTMS) with the hydroxyl groups on the surface of GNPs. Based on the comparison with pristine GNPs/SR composite, the composite with functionalized GNPs provides better improvement in thermal conductivity and tensile strength. This is due to the high dispersion of modified GNPs, which gives better interfacial interaction with the matrix (G. Zhang, Wang, Dai, & Huang, 2016).

The formation of scalable water-dispersible graphene (eGPNc) powders that were initially prepared with consecutive chlorosulfonic acid (CSA)/hydrogen peroxide (H_2O_2) and methylmorpholine N-oxide monohydrate (NMMOm) treatments has been reported by Jo et al. (see Figure 2.7) (Jo et al., 2017). The produced eGPNc film was dispersed in water and the obtained solution was used as a reaction medium for in-situ polymerization of pyrrole to obtain covalently bonded polypyrrole (PPy)/graphene nanocomposite. By loading eGPNc onto the nanocomposite, there was an improvement in the capacitance of PPy from 54.0% to 91.0%.

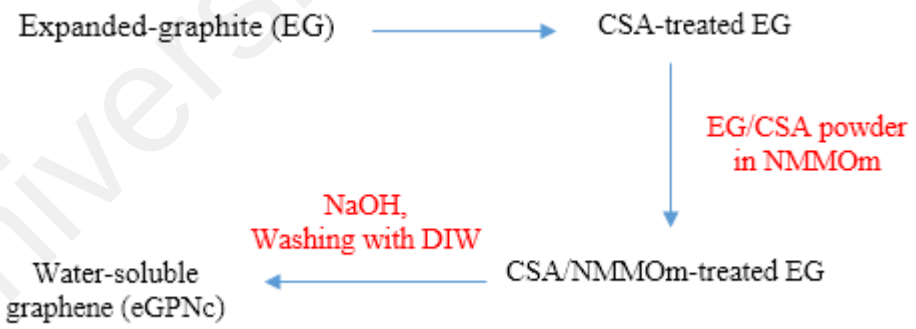

Figure 2.7: Steps in the preparation of water-soluble graphene (eGPNc) (Jo et al., 2017).

2.5.2 Functionalization of graphene using non-covalent process

Non-covalent process is a well-known technique that is primarily based on Van der Waals, hydrophobic, and electrostatic forces interactions between the molecules and the surface of graphene/GNPs. This type of functionalization acts in a manner where

graphene is wrapped with long-chain stabilizers such as surfactants or polymers (E. Y. Choi et al., 2010; Y. C. Li et al., 2015). The main mechanism underlying this method is π-π stacking interactions between the functional groups and the surface of the graphene sheets (see Figure 2.8), which minimize the impact on the surface of GNPs and prevent the disruption of electron conjugation. On the other hand, it can be said that the important properties of graphene such as mechanical strength, as well as thermal and electrical conductivity are unaffected (H. Bai, Y. X. Xu, L. Zhao, C. Li, & G. Q. Shi, 2009; D. Y. Cai & M. Song, 2010). For some researchers, it is very important for the main graphenic nanostructures to remain intact without being interrupted, depending on their objectives.

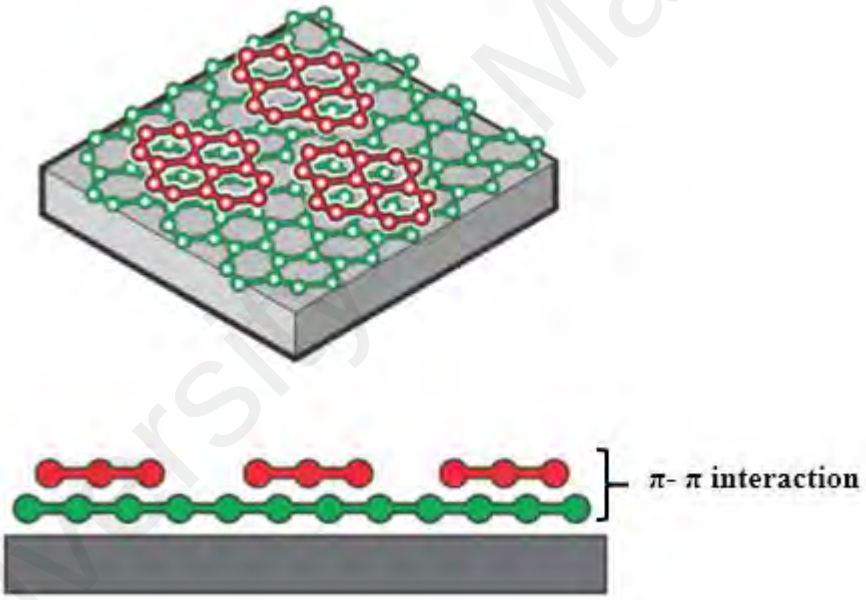

Figure 2.8: Schematic illustration of non-covalent modification through weak interactions ("Research: Projects: Graphene Chemistry," 2018).

There are many reports about the preparation of non-covalent modified graphene using polymer composites that produced a variety of different polymer matrices. A simple way to create the interaction between these components is through non-covalent process. There are some examples of π-π interactions between the graphitic structures and polymers containing aromatic rings. Polymers with repeating units of aromatic structure

can provide a strong binding with graphenic layers and produce highly homogeneous polymer composites that can enhance stability properties (Lian, Fan, Shi, Li, & Yin, 2014; Sasha Stankovich et al., 2006; Jizhen Zhang et al., 2015). The sulfonated derivative of polyaniline containing a series of aromatic polymers (refer to Figure 2.9) can interact strongly with graphene nanosheets through π-π stacking connections (H. Bai, Y. Xu, L. Zhao, C. Li, & G. Shi, 2009).

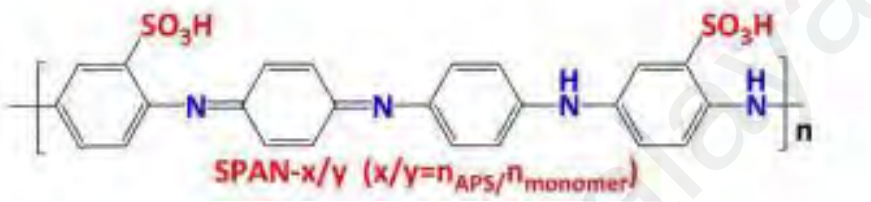

Figure 2.9: Schematic structure of sulfonated polyaniline (J. Dai et al., 2017).

Zhang et al. carried out the functionalization of rGO using a series of pyrene- or phenyl-terminated functionalized polyethylene glycols (f-PEG). The procedure involves the attachment of pyrene groups onto the graphene surface, whereas ethylene glycol chains provide the interconnection of the nanocomponents. The authors also studied the effects of the two joined components based on electrical conductivity. It was found that the functionalized graphene was able to conduct electricity as a result of the mixture between the non-conductive polymer and graphene as the highly conductive material (Jizhen Zhang et al., 2015). In addition, other researchers (Lian et al.) functionalized graphene nanoribbons (GNR) with Kevlar in order to reinforce polyvinyl chloride (PVC). Kevlar is known as a polymer with aromatic rings and sulfonated polyaniline that can provide strong interaction with the structure of graphene by π-π stacking as can be seen in Figure 2.10. The combination of Kevlar, graphene, and PVC demonstrated an excellent increase of yield strength and Young's modulus by 106% and 72.3%, respectively (Lian et al., 2014).

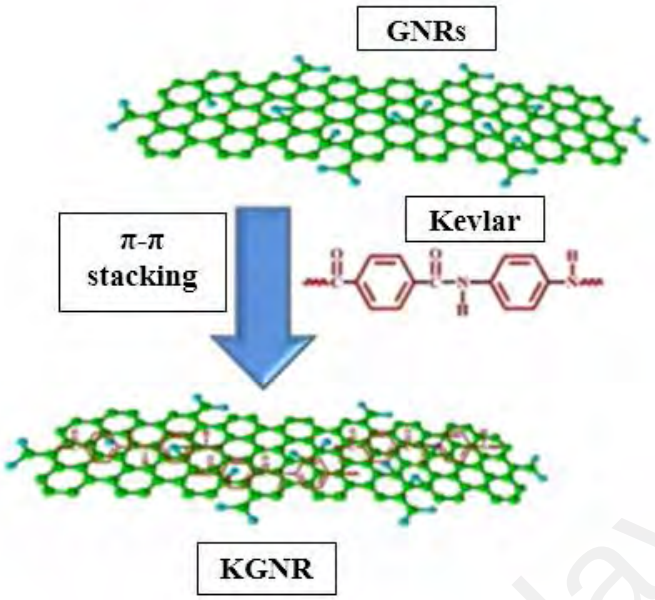

Figure 2.10: Interaction between Kevlar and graphene nanoribbons (GNR) (Lian et al., 2014).

Graphene nanosheets are also reinforced with polymers without the aromatic part. For instance, cetyltrimethylammonium bromide (CTAB), which is a stabilizer (surfactant), can be used to disperse graphene nanosheets in aqueous media (Talat, Awasthi, & Srivastava, 2014). Another example is the preparation of PPy/CTAB-intercalated graphene sheet nanocomposites (PPy/CGN) by using oxidative polymerization of pyrrole in the presence of CTAB-intercalated graphene (Y. Fan, Liu, Cai, Liu, & Zhang, 2012). Besides, Kaur et al. reported the non-covalent functionalization of graphene in combination with poly(diallyldimethylammonium chloride) (PDDA), a polyelectrolyte containing nitrogen using an easy method. Triton X-100, which is a non-ionic surfactant, was used during functionalization to enhance the non-covalent modification of graphene with PDDA. The results also showed great thermal stability for the graphene functionalized with PDDA in their study (Kaur et al., 2015). Furthermore, Figure 2.11 shows surfactant-assisted mixing was applied for rGO functionalized with a surfactant in order to achieve homogeneous dispersion in water-soluble polyurethane (WPU, polyurethane functionalized by sulfonate groups) (Hsiao et al., 2013).

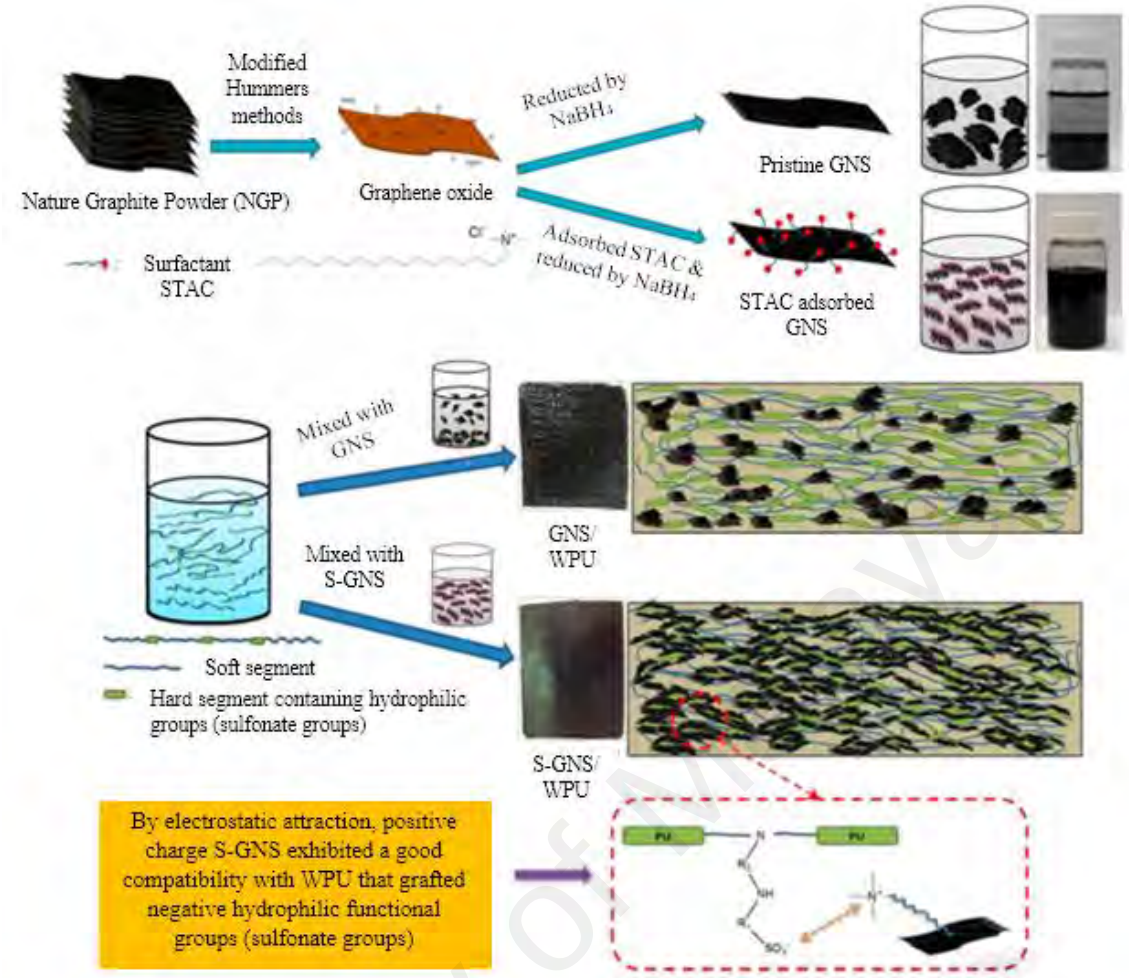

Figure 2.11: Synthesis of a composite material with waterborne polyurethane and surfactant-covered rGO (Hsiao et al., 2013).

2.5.3 Functionalization of graphene using doping process

As graphene can be applied in different applications, doping is known as one of the efficient ways to functionalize graphene and alter its properties. Many researchers especially in the material science field have extensively investigated graphene doping methods via various processes (Oh, Kim, & Yeom, 2014). Doping usually involves the substitution of carbon atoms from the graphitic structure of graphene with other foreign atoms, and the process is also known as heteroatom doping. Nitrogen or boron atoms are the natural candidates for doping of graphene due to their similar atomic size as carbon with specific electron donor and hole acceptor properties (Guo, Fang, Zhang, & Gong, 2011). By controlling the degree of doping, the electrical properties of graphene can be

potentially tailored depending on the study. Thus, this method is widely used for the application of graphene in semiconductor and nanoelectronics fields (M. Kim et al., 2016). The behavior of doped graphene sheets, whether it is n- or p-type, depends on the electrophilic properties of the replacement atoms on the graphene structure.

Several research groups reported the synthesis of B- and N-doping of graphene. For instance, Panchakarla et al. used arc-discharge method to prepare B- and N-doped graphene in the presence of H_2+B_2H_6 and H_2+NH_3 using high current between the graphite electrodes (Panchakarla et al., 2009). By using CVD, Liu et al. managed to synthesize N-doped graphene using a copper film on a silicon substrate as the catalyst under hydrogen atmosphere, with methane and ammonia as the C and N sources, respectively (D. Wei et al., 2009). Partially nitrogen-doped rGO produced via hydrothermal technique in the presence of ammonia and hydrazine by Long et al. is presented in Figure 2.12. The resulting structure and surface chemistry of the treated GO strongly depend on the temperature applied during the hydrothermal treatment (D. Long et al., 2010). Wang et al. investigated the synthesis of N-doped GNRs by using high-power electrical joule heating in ammonia gas atmosphere and from the investigation, the formation of C-N bonds was observed at the edge of graphene sheets (where chemical reactivity is high) (X. Wang, 2010).

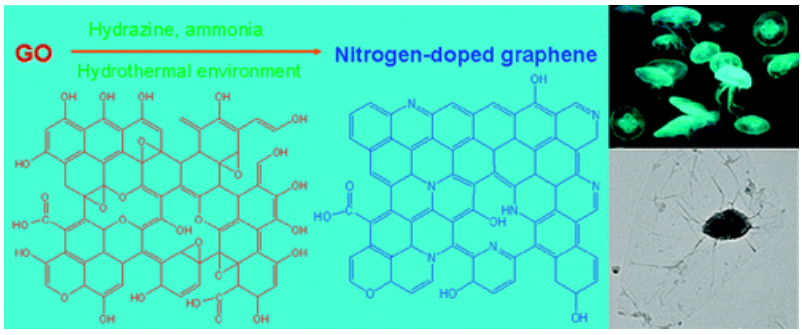

Figure 2.12: Schematic structure of GO and N-doped GO produced by hydrothermal reduction (D. Long et al., 2010).

Xiong and co-workers reported nitrogen-doped graphene (N-G) prepared via thermal annealing. The process was carried out by using GO as a starting material, which was later annealed in ammonia at specific temperatures. The resultant N-G was used as a conductive support for Pt nanoparticles in the subsequent step. The reduction process involved hexachloroplatinic acid and either ethylene glycol (EG) or sodium borohydride ($NaBH_4$). From their study, they were able to demonstrate the synthesis of Pt-loaded N-G catalysts through a series of routes (refer to Figure 2.13) (Xiong et al., 2013). Recently, zinc oxide (ZnO) nanoparticles/N-doped rGO nanocomposites (ZnONPs/N-rGO) was synthesized using hydrothermal method. The process started with the injection of an appropriate amount of zinc sulfate ($ZnSO_4$) into GO suspension. Ammonia solution was then added dropwise before it was transferred into a high-pressure reactor to proceed with hydrothermal treatment (S. Yang, Li, Qu, Wang, & Wang, 2017). The authors used the obtained nanocomposite for further test in sensor application.

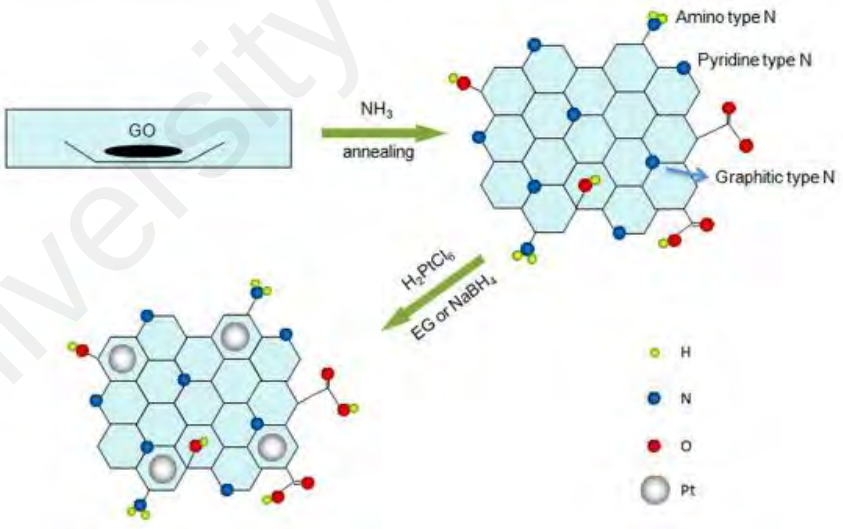

Figure 2.13: Schematic diagram of the synthesis of N-doped graphene (N-G) loaded with Pt nanoparticles (Xiong et al., 2013).

2.6 Green materials for GNPs functionalization

2.6.1 Tetrahydrofurfuryl-terminated polyethyleneglycol (TFPEG)

Polyethylene glycol (PEG) is one of the common polymers used to functionalize nanomaterials (Prencipe et al., 2009). PEG can easily disperse in organic solvents and therefore, it is an ideal candidate to increase the solubility of GNPs. With covalent functionalization, PEG can improve the solubility of GNPs in water or other common solvents (Xu et al., 2014). However, since PEG is a straight-chain polymer, PEG may lead to the aggregation of GNPs due to cross-linking between the GNPs (Kalinina et al., 2011). Interestingly, monofunctional oligomers such as monofunctional tetrahydrofurfuryl-terminated polyethylene glycol (TFPEG) can prevent cross-linking of the adjacent GNPs sheets. Functionalization with monofunctional groups can enhance the colloidal stability of GNPs in distilled water and common organic solvents such as ethylene glycol (EG) (Amiri, Sadri, et al., 2015).

In order to prepare organic solvent-based GNP nanofluids, the GNPs need to fulfil the following criteria: (1) long-term colloidal stability, (2) ability to disperse well in a variety of organic solvents, and (3) reversible particle aggregation (Amiri, Kazi, et al., 2015; Johnson, Dobson, & Coleman, 2015). A number of studies have been carried out to enhance the dispersibility of GNPs with TFPEG. Arzani et al. (Arzani, Amiri, Kazi, Badarudin, & Chew, 2016) synthesized TFPEG-functionalized GNPs for use in heat transfer applications. However, they used a high amount of aluminum chloride ($AlCl_3$), which is rather costly and impractical to functionalize GNPs with TFPEG in bulk quantities. In addition, it is undesirable to use high amount of $AlCl_3$ to functionalize GNPs because $AlCl_3$ is toxic to humans and therefore, one needs to adhere to a stringent safety procedure when handling this chemical (Mandriota, Tenan, Ferrari, & Sappino, 2016).

A strategy was proposed to significantly enhance the dispersibility of GNPs in organic solvents by covalent functionalization of GNPs with TFPEG using a facile, green, and cost-effective approach. The carboxylated GNPs with TFPEG was functionalized using zirconium (IV) oxychloride octahydrate, which serves as an effective catalyst for direct esterification. In addition, this catalyst is non-toxic and inexpensive (Nikoofar & Khademi, 2015). The catalyst forms a cationic cluster structure in which ester condensation takes place through a series of protonation of –COOH ligands in the GNPs, forming carbocations. This process facilitates the TFPEG molecules to complete the reaction, where water is formed as a by-product after the process (Nakayama, Sato, Ishihara, & Yamamoto, 2004).

2.6.2 Nitrogen atom

In recent years, many scientists have improved the GNPs applications by altering their physical and chemical properties (Fu, Jiao, & Zhao, 2013; Khodabakhshi, Arab, Svec, & Gerlich, 2017). These may include producing GNPs in different layers with and without defects through novel synthesis techniques (Compton & Nguyen, 2010), mass production of functionalized GNPs by chemical-mechanical procedures (Loh, Bao, Ang, & Yang, 2010), and doping with foreign atoms, e.g., nitrogen and sulfur (L. L. Zhang et al., 2012). Among these methods, an efficient way to modulate their properties is through doping heteroatoms into pristine GNPs structure (Q. L. Wei et al., 2015). Substituent heteroatoms such as nitrogen (N) atom could lead to an increase in the electron mobility, thermal stability, electrical property, and magnetic property of GNPs (Z. Xing et al., 2016). This is due to the atomic size and strong valence bonds with carbon atoms that affect the properties of doping materials (Usachov et al., 2011; Yue et al.). In addition, doping N atoms into graphitic carbon network has been considered as an effective approach to enrich free charge-carrier density (Xin et al., 2012). Besides, it can also strengthen the metal-based graphene interaction by becoming the active site for metal particles to be

anchored (Yuan, Chen, & Yan, 2012). Due to all these factors, the potential of using nitrogen-doped GNPs can be expanded into many applications such as transistors, supercapacitors, conductive materials, and electrochemical catalysts (K. R. Lee, Lee, Lee, Ahn, & Woo, 2010; Mahalingam, Ramasamy, & Ahn, 2017; Y. Mao et al., 2012).

Several approaches have been introduced for the synthesis of nitrogen-doped graphene such as arc discharge, chemical vapor deposition (CVD), thermal annealing, plasma, and others (Panchokarla et al., 2009; X. R. Wang et al., 2009; D. C. Wei et al., 2009). CVD is the most common method used by researchers, which involves hydrocarbon in the presence of organic NH_3 (as the nitrogen source) to produce nitrogen-doped graphene (Qu, Liu, Baek, & Dai, 2010). For N_2 plasma or arc discharge method, special instruments and attentive practical conditions are needed to conduct the experiment (Panchokarla et al., 2009). All of these methods are costly for practical applications and for production in a large quantity. In comparison to these methods, hydrothermal only needs a mild condition for operation. Besides, nitrogen-doped GNPs can also be mass produced efficiently through this technique (P. Chen et al., 2013). There are previous studies of nitrogen-doped graphene that used hydrazine along with ammonia in a hydrothermal reaction (D. H. Long et al., 2010). However, hydrazine is considered as a highly toxic reagent (Zhou, Bao, Tang, Zhong, & Loh, 2009). Most previous studies involved with the oxidation of GNPs used Hummer's method to produce the starting materials for further functionalization with nitrogen atom (M. S. Lee, Choi, Baek, & Chang, 2017; Yeom et al., 2015). This method requires many chemicals to reach high oxidation of carbon structure in GNPs. Thus, the development of a low-cost and facile method to produce high yield and stable nitrogen-doped GNPs is still a challenge.

2.6.3 Xylitol and citric acid cross-linking

Sugar alcohols are known for their structure that is rich in hydroxyl groups, which becomes one of the main attractions as this compound will enhance the dispersibility of GNPs in a solution. Xylitol as a sugar alcohol is one of the best candidates to be used in the functionalization of GNPs based on its natural properties and safe to humans (Liang & Jiang, 2013). Meanwhile, citric acid is also known as a non-toxic and low-cost compound, which becomes a great choice to be cross-linked with xylitol (Ge, Wang, Liu, & Huang, 2016; Gyawali et al., 2010; Rahman & Mieno, 2014). Cross-linking between citric acid and xylitol is readily generated through renewable raw materials, which is a major advantage for these materials. Also, it has high potential for economical mass production in the future (J. Liu et al., 2016). To the best of our knowledge, there is not much literature reporting on the functionalization of GNPs using sugar alcohols to date.

2.6.4 Pluronic-P123 surfactant

Some previous studies concentrated on the effects of surfactants on the thermal and rheological properties of graphene/GNPs solutions (Sarsam, Amiri, Kazi, et al., 2016; J. Wei & Inam, 2017). However, there is still lack of research on the stability of water-based and organic-based GNPs nanofluids using Pluronic-P123 surfactant. This surfactant consists of Polyethylene glycol (PEG) and polypropylene glycol (PPG) monomers linked in sequential arrangement to form a triblock PEG-PPG-PEG copolymer. In this study, Pluronic-P123 surfactant (P123) was chosen primarily due to its green properties, which are biodegradable, non-toxic, and economical to be used in a bulk quantity (Alexandridis & Tsianou, 2011; T. T. Xing, Lou, Bao, & Chen, 2014). In addition, the chain length of hydrophilic polyethylene oxide (PEO) chain in Pluronic copolymer plays an important part in producing a stable, aqueous, homogeneous graphene solution. Furthermore, the unique characteristics of polypropylene oxide (PPO) compensate GNPs hydrophobicity, leading to an improved solubility of GNPs colloid. With the hydrophobic PPO chain (30

units of propylene oxide) that is much longer than short alkyl chain in other surfactants, e.g., Triton X-100 ($CH_3C(CH_3)_2CH_2C(CH_3)_2C_6H_4$-$(OCH_2CH_2)_{10}OH$), the interaction between the PPO segments and conjugated graphene structure is strong compared to other polymers/surfactants. Therefore, this interaction can lead to Pluronic copolymer-functionalized GNPs (P-GNPs), which is highly stable in many organic solvents (Zu & Han, 2009).

2.7 Graphene/graphene nanoplatelets in engineering applications

2.7.1 The use of graphene/graphene nanoplatelets in heat transfer applications

Over the past years, nanofluid researchers have mainly concentrated on preparing stable nanofluids with enhanced heat transfer properties (Kwon et al., 2013). Many industries have used conventional working fluids such as water, engine oil, EG, and others as the heat transfer fluids (T. T. Baby & Ramaprabhu, 2011). There is a need for working fluids with high efficiency as the productivity and lifespan of equipment depend on how good the heat transfer fluid works (Duangthongsuk & Wongwises, 2010). Conventional working fluids have poor heat transfer performance due to their low thermal conductivity compared to solid particles such as metals or metal oxides (Wen, Lin, Vafaei, & Zhang, 2009). Thus, nanoscale particles with high thermal properties are suspended in working fluids to produce nanofluids (Agromayor et al., 2016; Emami-Meibodi et al., 2010; Zyla, Fal, Traciak, Gizowska, & Perkowski, 2016). The term “nanofluid” was first used by Choi in 1995 (Heris, Etemad, & Esfahany, 2006; H. F. Jiang, Li, Xu, & Shi, 2014). Choi et al. successfully proved that the thermal conductivity increased significantly with a small addition of nanoparticles in base fluids (S. Choi, Zhang, Yu, Lockwood, & Grulke, 2001).

Nanofluid is known as a suspension where ultrafine particles are suspended in a conventional base fluid in order to enhance the thermal properties of the base liquid

(Ghozatloo, Rashidi, & Shariaty-Niassar, 2014; S. Li & Eastman, 1999; W. H. Yu, France, Routbort, & Choi, 2008). It has been proven that nanofluids are able to improve the thermal conductivity and heat transfer coefficients (Daungthongsuk & Wongwises, 2007; Heris et al., 2006; Kakac & Pramuanjaroenkij, 2009; Wen & Ding, 2004). Due to its advantages, many studies have been conducted to evaluate the performance of convective heat transfer nanofluids (E. Sadeghinezhad et al., 2014; Sadeghinezhad et al., 2015; Y. Yang, Zhang, Grulke, Anderson, & Wu, 2005). In order to produce nanofluids, solid nanoparticles need to be mixed well with the base fluids. Low colloidal stability of nanoparticles in base fluids can be considered as the main difficulty. To make the matter worse, the stability usually causes blockage of flow channels, which can reduce the effectiveness of the heat transfer system (Abu-Nada, 2008). Therefore, the discovery of suitable nanofluids that are able to enhance the thermal conductivity and heat transfer properties with high stability is still a challenge. Many researchers have conducted extensive research on the heat transfer capability of nanofluids using carbon-based nanomaterials such as graphene/GNPs over the past years (Azizi, Hosseini, Zafarnak, Shanbedi, & Amiri, 2013; Cabaleiro et al., 2017; Ma et al., 2013; Mehrali et al., 2016).

Tessy Theres Baby and Sundara Ramaprabhu in 2011 developed hydrogen exfoliated graphene (HEG) dispersed deionized (DI) water, and ethylene glycol (EG)-based nanofluids (labelled as f-HEG). They studied the thermal conductivity and heat transfer properties of these nanofluids at different volume fractions and temperatures. The enhancement in the thermal conductivity of f-HEG at 0.05% volume fraction was approximately 16% at 25 °C and 75% at 50 °C. Moreover, their results suggested that a considerable improvement in heat transfer for the samples was observed when compared to its base fluid (T. T. Baby & Ramaprabhu, 2011). Another researchers, Sadeghinezhad et al. published the works related with the study of heat transfer using GNPs. The samples were prepared at different concentrations (0.025, 0.05, 0.075, and 0.1 wt.%) using

ultrasonication method. They revealed that the heat transfer coefficient of GNPs nanofluids was higher than the base fluid (distilled water) by approximately 13%–160%. Moreover, when the flow rate and heat flux increased, the heat transfer coefficient of GNPs nanofluid also increased (Emad Sadeghinezhad et al., 2014). In 2016, Agromayor and his team synthesized sulfonic acid-functionalized GNPs water-based nanofluids in their work. The experimental setup was designed to study the nanofluids at different concentrations under several operational conditions. Their analysis showed a noticeable improvement in the convection heat transfer coefficient by 32% for the concentration of 0.5 wt.% when compared with pure water. Similarly, these coefficients increased with the increase of flow rate and temperature of the fluid (Agromayor et al., 2016).

Later in 2017, Wang et al. prepared graphene nanosheets (GNS)-ethanol nanofluids from the exfoliated graphite with different volume fractions between 0.02 and 0.1 vol.%. They reported an enhancement in thermal conductivity of approximately 10% with 0.1 vol.% of GNS suspension. For the enhancement of convective heat transfer, GNS nanofluids showed higher values compared to the base fluids by approximately 12% (Xinzhi Wang, Hu, Li, & He, 2017). In the same year, Houman et al. examined the heat transfer performance of GNPs-platinum (Pt) hybrid nanofluids. They conducted the analysis with different concentrations of nanofluids ranging from 0.02 to 0.1 wt.%. The effects of nanoparticle loading, Reynolds number, and temperature were evaluated in order to assess the heat transfer abilities. From the reported values, all nanofluids samples showed high ability of heat transfer. All samples also showed a significant improvement compared to water with the maximum values around 30% for the highest weight concentration and Reynolds number (Yarmand et al., 2017). A study by Askari et al. reported the work on iron (II, III) oxide (Fe_3O_4)/graphene nanohybrid synthesized for the application in water-based nanofluid. The nanohybrid was prepared by dispersing Fe_3O_4 over the graphene sheets uniformly. Further experimental works were carried out for the

investigation of thermal characteristics of nanofluids including thermal conductivity and convective heat transfer coefficient. The results suggested that the addition of Fe_3O_4/graphene nanofluid improved the thermal conductivity by 14%–32% for the mass fraction of 1 wt.%. In addition, the convective heat transfer coefficient increased significantly by 14.5% compared to the base fluid (Askari, Koolivand, Pourkhalil, Lotfi, & Rashidi, 2017). Therefore, based on all the studies reviewed, it can be concluded that the enhancement in convection heat transfer is affected by the improvement of thermophysical properties and excellent thermal performance of graphene-based nanofluids, which highlights the great potential in heat transfer applications. However, there has been lack of information on the actual improvement should the base liquid and the colloids are allowed to operate at the same velocity to reflect the actual role of additive in improving heat transfer. Further, a side by side comparison between the colloids and water performance over the laminar and turbulent flows under constant mean velocity mode is by far unavailable within the literature. This would motivate more exploration in this topic to provide an insight into the actual performance by discounting the role of velocity increment within the analysis.

2.7.2 The use of graphene/graphene nanoplatelets in thermoelectrochemistry field

Thermoelectricity involves the conversion from the temperature gradient to electrical voltage by the chosen thermoelectric material (Anno, Imakita, Takei, Akita, & Arie, 2017). This process requires a good understanding of heat conduction in materials in order to control the thermal management for energy recycling. Besides, the specific thermoelectric material must have good thermal and mechanical properties, as well as the ability to generate thermoelectric effect (Mahmoud et al., 2015). In addition, thermal energy recycling requires materials with specific requirements such as high Seebeck coefficient, good electrical conductivity, and low thermal conductivity (Amollo, Mola,

Kirui, & Nyamori, 2018). The energy conversion efficiency of a material can be defined by the figure of merit (ZT) through the following equation (1):

$$ZT = \frac{S^2\sigma}{\kappa}T \qquad \text{eq. 1}$$

Where *S* is the Seebeck coefficient (V/K), σ is the electrical conductivity (S/m), κ is the thermal conductivity, and T is the absolute temperature (J. M. Yang, Yan, Wang, & Yang, 2014). Most of the thermoelectric systems proposed by researchers today depend on the semiconductor components that are fragile and costly. The components in a semiconductor are usually rare metalloids such as bismuth telluride (Bi_2Te_3) (Rowe, 2005). Other than that, antimony-doped skudderites, zintl phases, and complex nanofabricated BiTe alloys are also materials that are used in thermoelectric devices (Kauzlarich, Brown, & Snyder, 2007). These devices always suffer from certain drawbacks such as high cost, low efficiencies, and susceptible to damage due to the impacts that can be contributed by drops, large thermal gradient, or thermal cycling (Mark S Romano et al., 2013).

Thermoelectrochemistry has almost similar meaning as thermoelectricity but differ in terms of the electrochemistry process involves during the reaction. A thermoelectrochemical cell that basically consists of a solid or liquid electrolyte with suitable redox active species can overcome some of the main issues for the semiconductor devices as mentioned previously. The advantages of using a thermoelectrochemical cell are high flexibility that allows the cell to conform to irregular shapes, redox couples in which low maintenance is expected and the cell can be made from any abundant materials (Abraham, MacFarlane, & Pringle, 2011, 2013; Black, Murphy, Atkin, Dolan, & Aldous, 2016). In addition, the power and efficiency performance for a thermoelectrochemical cell can be significantly affected by the nanostructuring and geometry area of parallel electrodes (R. Hu et al., 2010; Mark S Romano, Razal, Antiohos, Wallace, & Chen, 2015).

Electrocatalysts are also one of the factors affecting the performance of a thermoelectrochemical cell. Among various electrocatalysts, researchers are mostly interested with the materials from carbon-based nanomaterials, especially graphene (Shearer, Cherevan, & Eder, 2014). This is because graphene possesses powerful properties such as large surface area and high electrical conductivity due to the fully conjugated network of sp^2-hybridized carbon atoms compared to other nanomaterials. Both properties make graphene as a great option of 2D electrocatalysts (X. W. Mao, Rutledge, & Hatton, 2014). For example, in 2008, Hong's group reported the use of graphene-based nanostructures as the counter electrode materials for dye-sensitized solar cells. They prepared a composite film containing 1 wt.% of graphene-coated indium tin oxide (ITO) electrode and demonstrated high electrocatalytic activity (Hong, Xu, Lu, Li, & Shi, 2008). Later in 2012, Kang et al. compared the power generation using nanocarbon-based thermogalvanic cells. The experimental work was carried out using aqueous potassium ferro/ferricyanide electrolyte for thermal energy harvesting. This work included rGO composite as one of the materials for the study. In general, they concluded that a nanocarbon electrode with high surface area has high potential to provide high power generation for the nanocarbon electrode thermocells (T. J. Kang et al., 2012).

In the same year, Romano et al. attempted to optimize the electrolyte and utilize rGO as the electrode in order to increase the power conversion efficiency of thermogalvanic cells. The mass power density obtained using rGO electrodes was comparable with platinum when tested at a specific temperature with certain concentrations of potassium ferricyanide/potassium ferrocyanide ($K_3Fe(CN)_6/K_4Fe(CN)_6$)solution (M. S. Romano et al., 2012). Besides that, other research group reported about the reaction activities of graphene nanoplatelet aggregates (GNAs) and graphene nanoplatelets (GNPs), which have different surface areas towards iodide/triiodide redox reaction. The evaluation was based on cyclic voltammetry and electrochemical electrochemical impedance

spectroscopy (EIS). This study showed that the activity of the I_3^-/I^- electrolyte reaction was depend on the edge plane area of the graphene aggregates. Besides, high activity for the electrolyte reaction can be observed due the large surface of graphene itself and its high ability for electrolyte application (Ohtani & Hoshi, 2018). The study of graphene/GNPs that is based on electrochemistry concepts shows that the potential applications of graphene/GNPs nanomaterials can be broadened, and also represent a potential class as electrocatalysts for future use in thermoelectrochemistry application. However, the study on the effect of chemically modified GNPs when mixed with electrolyte is less discussed. Thus, a further study on their potential values can lead to a better understanding and good exploration.

2.8 Green approaches towards functionalization of graphene nanoplatelets (GNPs)

Functionalization and dispersion of graphene nanoplatelets are very crucial and important for their end applications. Chemical functionalization of GNPs will prevents the agglomeration from occur and at the same time able to maintains the inherent properties of GNPs. In general, the functionalization of GNPs can be performed by different routes either by covalent or non-covalent modification techniques. It has been known that both of these techniques are very effective in the preparation of treated GNPs.

Recently, functionalization of graphene nanoplatelets (GNPs) by using green approaches have become very demanding among the researchers. Also, significant research efforts have been carried out towards environmental friendly, green technology process and also reagentless steps. One of the reasons is due to the detected drawbacks from the used of harsh chemicals and/or materials that have been introduced in most of the studies which the researchers have been aware of it. As GNPs itself is considered as one of green materials due to its source which can be obtained from nature, the use of

green methods/techniques to functionalize it will become a great combination. Green chemical and green chemistry reaction have attracted wide attentions around the globe due to their process that does not involve harmful materials to the environment. Also, this kind of approach may lead to even better results when compare with hazardous conventional options.

To achieve green chemistry process, some considerations such as elimination of chemical waste, reduction of hazardous process, use of renewable source and use of safer/less toxic chemicals should be put into account. However, green materials that want to be functionalized together with GNPs must be a suitable candidate that able to deliver the results that want to be achieved based on different applications. The so-called green approach have been the most favorable ways to functionalize GNPs and will become a priority to explore more in future.

CHAPTER 3: METHODOLOGY

In this chapter, the methods of preparation, characterization, and evaluation of the stability and thermophysical properties of the functionalized graphene nanoplatelets (GNPs) materials are described. In addition, the details regarding the experimental setup of heat-based applications are also presented in this section. The graphical chart of an overview for all experimental works carried out in this study is presented in Figure 3.1.

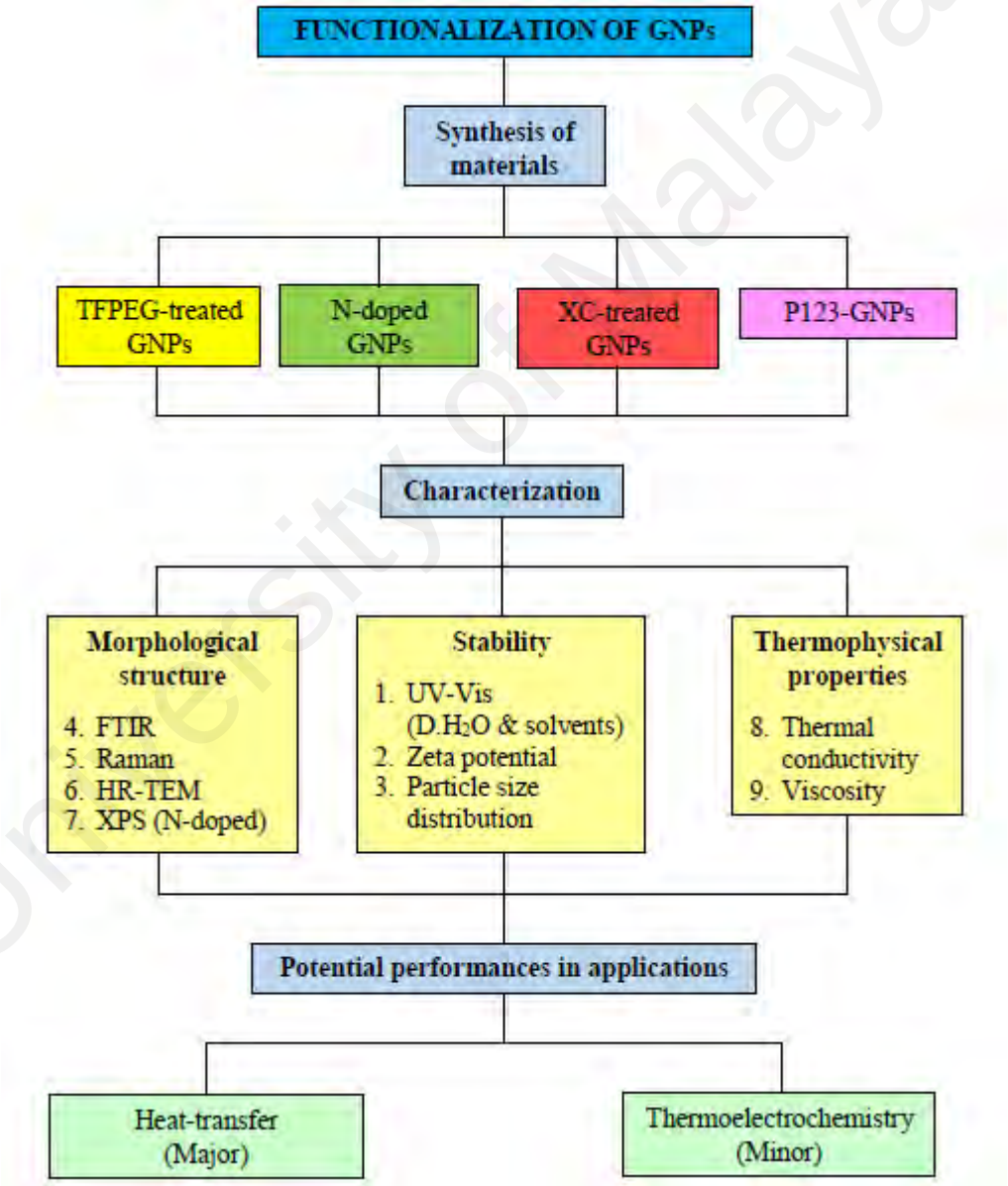

Figure 3.1: General overview of experimental works in this research.

3.1 Modification of graphene nanoplatelets (GNPs)

3.1.1 Preparation of TFPEG-treated GNPs

3.1.1.1 Materials

The GNPs (specific surface area = 750 m^2/g) were purchased from XG Sciences, Inc., USA, whereas TFPEG (molecular formula: $C_5H_9O(C_2H_4O)nOH$, (n = 1–5)), molecular weight = ~200 g mol^{-1}) and zirconium (IV) oxychloride octahydrate ($ZrOCl_2.8H_2O$) were purchased from Sigma-Aldrich (M) Sdn. Bhd., Malaysia. Sulfuric acid (H_2SO_4, purity = 95%–97%), nitric acid (HNO_3, purity = 65%), and tetrahydrofuran (THF) were sourced from Friendemann Schmidt Pty. Ltd., Australia.

3.1.1.2 Preparation of carboxylated graphene nanoplatelet (GNP-COOH)

The as-received GNPs (12 g) without any purification were poured into H_2SO_4 (300 mL) and the solution mixture was shook for 30 s. Next, the container was transferred into an ice bath and nitric acid (100 mL) was added dropwise into the solution mixture. A sulfuric acid to nitric acid ratio of 3:1 was used because this is the suitable ratio for acid treatment (Kanakia et al., 2013), which results in the formation of carboxylic groups on the surface of GNPs (Figure 3.2). The solution mixture was stirred at ~55°C for 5 hr and the solution was subsequently cooled to 25 °C. The resultant black solution was diluted with distilled water (6 L) and HCl (3 wt.%) and the solution was centrifuged at 4,000 rpm to remove excess acid.

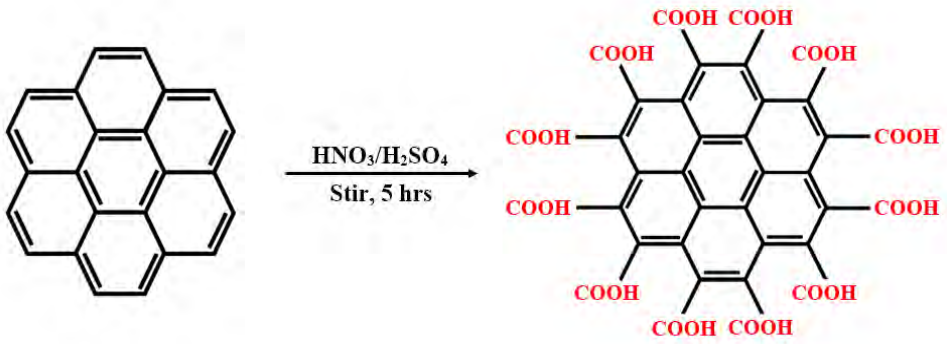

Figure 3.2: Schematic diagram of the acid treatment of pristine GNPs.

3.1.1.3 Synthesis of TFPEG-treated GNPs

In order to synthesize the TFPEG-treated GNPs (Figure 3.3), zirconium (IV) oxychloride octahydrate (0.6 g, molecular formula: $ZrOCl_2.8H_2O$) was mixed with TFPEG (12 g) through continuous stirring for 30 min. Next, THF (500 mL) was added into the solution mixture. Following this, GNP-COOH was poured into the solution mixture and the mixture was stirred for 24 hr at 80 °C. Once the reaction was complete, the solution mixture was centrifuged at 7,500 rpm for 15 min. Lastly, the resultant solution was washed with distilled water and ethanol a few times and then dried in an oven at 60 °C for 48 hr.

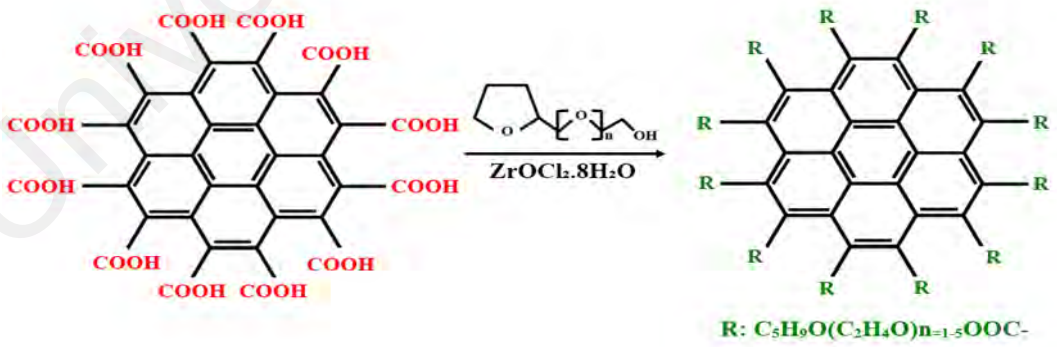

Figure 3.3: Schematic diagram of the covalent functionalization of GNP-COOH with TFPEG.

3.1.2 Preparation of N-doped GNPs

3.1.2.1 Materials

GNPs with the specific surface area of 750 m^2/g were purchased from XG Sciences, Inc. Other chemicals such as hydrogen peroxide (30%) (H_2O_2) and ammonia solution (28%–30%) (NH_4OH) were purchased from Merck.

3.1.2.2 Preparation of hydroxylated graphene nanoplatelets (GNP-OH)

GNPs (6 g) were poured into a vessel including 30 mL of H_2O_2 and the solution was stirred for 5 min at room temperature. Then, the mixture was further sonicated using an ultrasonic bath for 1 hr at 30 °C. After completing the sonication procedure, the sample mixture was refluxed with continuous stirring for 5 hr at ~110 °C. To eliminate all the unreacted H_2O_2, the resulting hydroxylated GNPs (GNP-OH) was centrifuged at 7,000 rpm for 15 min. The supernatant was pipetted off, followed by washing with distilled water and ethanol three times. The final product was dried at 60 °C for 12 hr in a vacuum oven.

3.1.2.3 Synthesis of N-doped GNPs

Briefly, 5 g of GNP-OH was dispersed in 150 mL of distilled water and sonicated for 15 min to produce a homogeneous water-based GNP-OH solution. 4 mL of ammonia (28%) was added gradually into the solution while the mixture was stirred. Upon the increase of ammonia, the pH of solution was increased to almost 10. Then, the resultant dispersion was transferred into a Teflon autoclave with a polytetrafluoroethylene (PTFE) vessel of 250 mL capacity. The chemical reaction further took place in a furnace chamber at 180 °C for 12 hr. This temperature was found to be the optimum temperature to yield more nitrogen-doped graphene product by previous researchers (B. J. Jiang et al., 2012). After being subsequently cooled down to room temperature, the sample was centrifuged at 7,000 rpm, washed with distilled water and ethanol, and dried in a vacuum oven at 60

°C for 24 hr. The possible types of nitrogen species that will be inserted in the GNPs structure are shown in Figure 3.4.

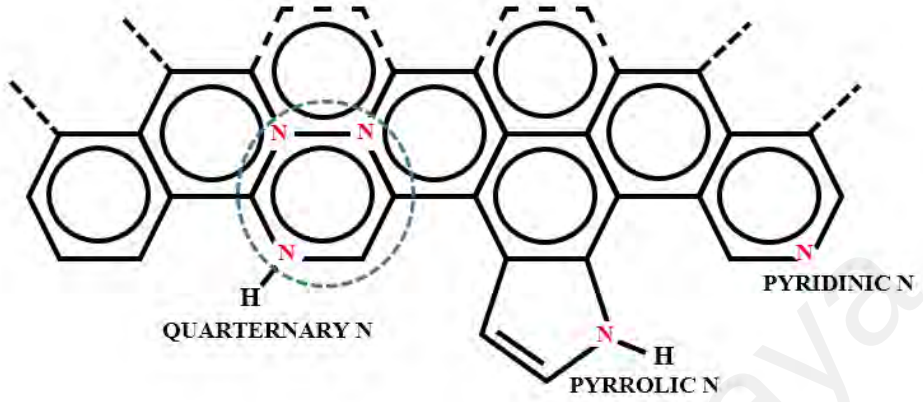

Figure 3.4: Possible types of nitrogen species inserted in the honeycomb lattice of graphene nanoplatelets.

3.1.3 Preparation of XC-treated GNPs

3.1.3.1 Materials

GNPs with specific surface area of 750 m^2/g were used as the pristine materials and purchased from XG Sciences, Inc. Other chemicals such as H_2O_2 (30%) were purchased from Merck. Citric acid and xylitol were purchased from Biobasic, Canada.

3.1.3.2 Preparation of hydroxylated graphene nanoplatelet (GNP-OH)

The synthesis of GNP-OH was similar to the preparation of GNP-OH material in Section 3.1.2.3.

3.1.3.3 Synthesis of XC-treated GNPs

An approximate amount of GNP-OH (5 g) was mixed together with the desired amount of xylitol and citric acid at the ratio of 1:5. The mixture was ground first in a mortar until it homogeneously mixed before the mixture was transferred into a beaker. Next, the polymerization was conducted at 150 °C for 3 hr inside a vacuum oven. During the reaction, bubbles were formed, which were caused by the release of water. After that, the

obtained solid sample was redispersed in distilled water and sonicated for 10 min. In order to remove free xylitol and citric acid, washing process using a centrifuge was carried out three times at 7,000 rpm for 15 min using distilled water and ethanol. The decant was pipetted out and the remaining residue was dried under vacuum in an oven for 12 hr at 60 °C. Figure 3.5 shows the possible reactions that occur during the process.

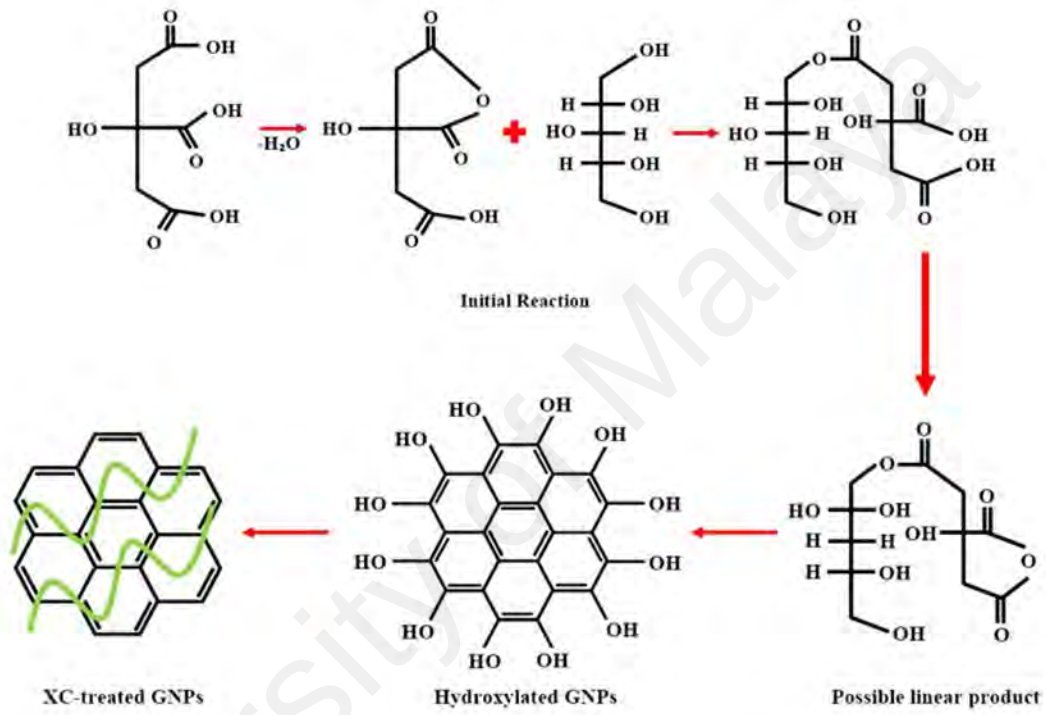

Figure 3.5: Schematic illustration of the covalent functionalization of hydroxylated GNPs with polymer linkage between xylitol and citric acid.

3.1.4 Preparation of P123-GNPs

3.1.4.1 Materials

GNPs with specific surface area of 750 m^2/g were used as the pristine materials and purchased from XG Sciences, Inc. Pluronic-P123 was purchased from VCN Materials Co., Ltd.

3.1.4.2 Synthesis of P123-GNPs

Non-covalent functionalization was employed in the presence of P123. Different ratios of surfactant:GNPs were used to optimize the concentration of surfactants. The ratios of

P123 to GNPs were 1:1, 1:2, 1:3, and 1:4. During sonication procedure, a water bath was used to maintain the temperature of the sample.

3.2 Characterizations of morphological, stability, and thermophysical properties

The main structure of the functionalized GNPs was analyzed using Fourier transform infrared spectroscopy (FTIR), Raman spectroscopy, high-resolution transmission electron microscopy (HRTEM), and X-ray photoelectron spectroscopy (XPS). Meanwhile, the stability of each sample was analyzed with an ultraviolet-visible (UV-Vis) spectrophotometer and Zetasizer Nano ZS. In addition, the thermophysical properties were evaluated using a thermal conductivity probe and a rheometer. Further details are discussed in the following subsections.

3.2.1 Fourier transform infrared spectroscopy (FTIR)

FTIR technique is useful in the identification and characterization of chemical structures. This is due to its function that is able to reveal the types of functional groups attached to the carbon of GNPs. It involves the interaction between IR radiations and the analyzed sample. During the process, the infrared radiation will hit the target material and some of the radiation will be absorbed whereas the others will be transmitted, leading to the spectrum results. For FTIR, the process was carried out using the FTIR instrument (Thermo-Scientific) where potassium bromide (KBr) pellets were prepared by incorporating the treated GNPs and pristine GNPs, and the FTIR spectra were evaluated within a wavenumber range of 400–4000 cm^{-1}.

3.2.2 Raman spectroscopy

Raman spectroscopy plays an important role in the characterization of geometric structure for graphitic materials and it has been used by many researchers (Malard, Pimenta, Dresselhaus, & Dresselhaus, 2009). This technique is very sensitive to the

changes that occur on the chemical structure of the matter even with small differences. Thus, it is very useful for the study of functionalized GNPs where it involves the modification of the pristine structure. During the analysis, the sample is illuminated with the source of laser beam and the scattered lights produced will be based on the interaction with the sample. The difference between the scattered light and incident light will produce the Raman spectrum. The Raman spectra of the treated GNPs and pristine GNPs were evaluated using a Renishaw spectrometer and a wavenumber range was set at 500–3200 cm^{-1} at 25 °C.

3.2.3 High-resolution transmission electron microscopy (HRTEM)

The changes of the GNPs macroscopic structure can be observed from the analysis using HRTEM. The method works through the electron beams that will interact with the matter and form an image. Meanwhile, the magnification can be adjusted by using the electromagnetic lenses. HRTEM samples were prepared by sonicating the treated GNPs and pristine GNPs in deionized water for 15 min. Then, a drop of each sample was placed on a lacey carbon grid and left to dry for a few minutes. After that, the sample was examined under different magnifications of the microscope using E.A. Fischione Instruments, Inc.

3.2.4 X-ray photoelectron spectroscopy (XPS)

XPS is known as a quantitative analysis to study the effect of nitrogen doping in carbon nanomaterials such as graphene (Z. Xing et al., 2016; R. Yadav & Dixit, 2017). The nitrogen composition that is doped in graphene will be based on the peak intensity between C1s and N1s. From the N1s spectrum obtained, further determination of nitrogen configurations will be carried out. This spectrum can be deconvoluted into different or several individual peaks located at different binding energies (eV), which can be possible

peaks of pyrrolic-N, pyridinic-N, and quaternary-N. The elemental analysis for a specific sample (N-doped GNPs) was performed using XPS (Axis Ultra DLD).

3.2.5 Colloidal stability of water-based and organic solvent-based functionalized GNP nanofluids

3.2.5.1 Types of solvents

Methanol, ethylene glycol, and 1-hexanol were obtained from Emsure®. Meanwhile, ethanol solvent was purchased from J. Kollin Chemicals, John Kollin Corporation.

3.2.5.2 Preparation of nanofluids

GNPs sheets were dispersed in aqueous media and solvents using an ultrasonication probe (Sonics Vibra-Cell, VC 750, Sonics & Materials, Inc., USA) with 750 W (output power) and 20 kHz frequency (power supply). Carbon-based nanomaterials are commonly hydrophobic, where they cannot create stable colloidal samples in most polar solvents, such as water, without functionalization or the presence of a surfactant (Z. Zhang & Lockwood, 2009). Water-based samples were prepared with the concentration of 0.0025, 0.0050, 0.0075, and 0.0100 wt.%. Meanwhile, for methanol-based, ethanol-based, ethylene glycol-based, and 1-hexanol-based treated GNP nanofluids, the particle concentration was chosen based on the highest stability observed in distilled water. All samples were prepared through sonication process for 15 min.

3.2.5.3 Analysis of UV-Vis spectrum and photometric study

By using UV-Vis spectrophotometry, the colloidal stability of the samples could be determined based on the light absorbance of the suspensions. A Shimadzu UV-spectrophotometer (Model: UV-1800, Shimadzu Corporation, Japan) was used and the spectrophotometric analysis was conducted within a wavelength range of 190–1100 nm. A dilution ratio of 1:20 with respect to the solvent was used to ensure that UV-Vis radiation passes through the samples and the degree of absorption is detected within the

range of wavelength investigated in this study. Special quartz glass cuvettes suitable for use in the UV-Vis wavelength region were used. The samples were measured at different time intervals over a period of 15 days.

3.2.5.4 Measurements of zeta potential and particle size distributions

Zeta potential determination involves the measurement of the magnitude of electrostatic/charge, which can be either repulsion or attraction between the particles. On the other hand, particle size distributions are related with the measurement of the size of particles present in a certain proportion to be measured. Both zeta potential and particle size distributions were measured using a two-angle particle and molecular size analyzer based on dynamic light scattering (Model: Zetasizer Nano ZS, Malvern Instruments Ltd., UK) to evaluate the colloidal stability of the samples (Sarsam, Amiri, Kazi, et al., 2016). The readings of measurement were taken for all samples with the highest stability in distilled water on the 1st day and 15th day of dispersion.

3.2.6 Thermophysical properties measurements of treated-GNPs material

The thermophysical properties of interest in this study are viscosity and thermal conductivity. For the measurement, the samples of water-based treated GNP nanofluids at different particle concentrations (0.100, 0.075, 0.05, and 0.025 wt.%) were prepared through sonication process for 15 min.

3.2.6.1 Measurement of thermal conductivity

The thermal conductivity of the water-based treated GNP nanofluids was measured using a fully portable field and laboratory thermal property analyzer (Model: KD2-Pro, Decagon Devices, Inc., USA) and the measurements were conducted within the fluid temperature range of 20–60 °C. The hot-wire method using the KS-1 probe was used, which consists of a single needle sensor with a length and diameter of 60 and 1.3 mm, respectively. A WiseCircu® WCR digital precision refrigerated bath circulator (Model:

WCR-P6, DAIHAN Scientific Co., Ltd., South Korea) was used with a total power consumption of 1.4 kW and an accuracy of 0.1 °C to maintain the temperature of the samples during the measurements. The measurements were taken for 15 min in between successive readings in order to allow the sample temperature to reach a steady-state condition.

3.2.6.2 Measurement of viscosity

The measurement of steady-shear viscosity of the water-based treated GNP nanofluids was conducted using a rotational rheometer (Model: Physica MCR 301, Anton Paar GmbH, Austria). The dynamic viscosity measurement or also known as a measurement of fluid internal resistivity toward the flow was carried out within a set of temperature range and shear rate. The temperature and shear rate were set between 20 and 50°C, and 20 and 200 s^{-1}, respectively, for all samples. The viscosity measurement will enable the evaluation of the behavior of all treated-GNPs samples, whether it will be Newtonian or non-Newtonian nanofluid. A Newtonian fluid means that the viscosity of a particular fluid remains unchanged even though the shear stress is applied at constant temperature. On the other hand, a non-Newtonian fluid means that the viscosity of a specific fluid tends to change when shear is applied at the same temperature.

3.3 Experimental setup for heat-based applications

3.3.1 Heat transfer experimental setup

Two separate experimental setups were built which operate under laminar and turbulent regimes. The first establishment is a typical pipe flow based convective heat transfer set-up which uses tape heater to provide the constant heat flux into the test section. On the other hand the second set-up was designed to simulate solar thermal collector which consist of a flat plate and series of tubes containing heat transfer liquid welded underneath the plate to absorb and transport the heat. While the principle of both

set-ups is relatively similar, the first set-up was designed to operate under turbulent regime while the later is to run under laminar and transition flow. In this manner, the performance under both flow regimes can be obtained. The study involved collecting the raw data necessary to perform heat transfer analysis and subsequent explanation of the findings.

3.3.1.1 Turbulent convective heat transfer experimental setup

For the evaluation of heat transfer performance, the weight concentration of nanofluids for each sample was 0.1 wt.%. The nanofluids was prepared through sonication methods for 15 mins. The experimental setup for convective heat transfer study was built, and the image of the setup is illustrated in Figure 3.6. The setup includes a tank (for nanofluids), a test section, a cooling unit, a pump, a flow-measuring unit, a DC power supply, a data logger, a pressure controller, a differential pressure transducer, and a heater. The test section was made of a stainless steel tube with the length of 1.45 m and width of 10 mm that was wrapped with glass wool to create the insulation layer. Two thermocouples were installed at the inlet and outlet of the test section in order to measure the temperature at each point, respectively. To measure the surface temperature, five thermocouples were applied onto the tube at 0.3 m from the entrance of the nanofluid sample and the distance between each thermocouple was 0.2 m. The tube was wrapped uniformly by two thick thermal insulation layers (i.e., glass wool) to ensure the readings taken are valid and the heat loss from the tube line is reduced. A pump with two valves was installed to circulate and adjust the flow rate of the samples during the test. In addition, the pressure drop of the fluids was measured by a differential pressure transducer. Meanwhile, a power supply and a transformer were used to supply uniform heat flux toward a circular stainless steel tube.

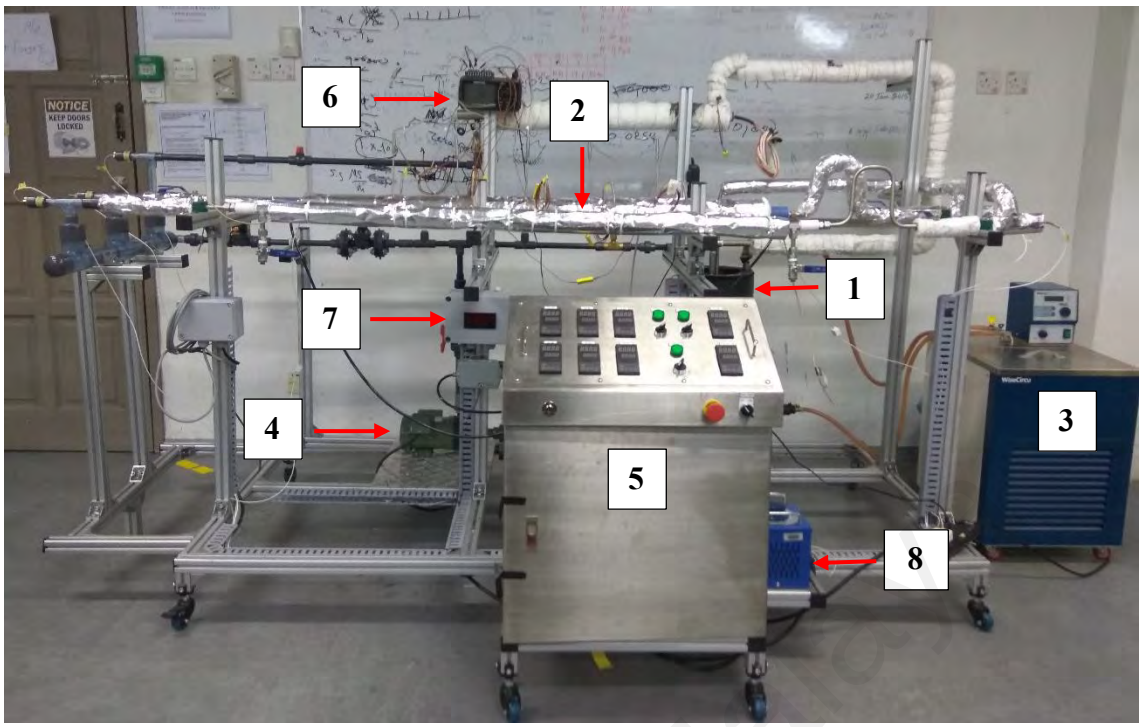

Figure 3.6: Experimental setup for the evaluation of all functionalized GNPs samples in heat transfer performance. The numbers represent: 1- storage tank, 2- test section, 3- cooling unit, 4- pump, 5- power supply, 6- data logger, 7- differential pressure transducer, and 8- transformer.

3.3.1.2 Laminar convective heat transfer experimental setup

Figure 3.7 shows the test rig used to study the thermal performance of functionalized GNPs using a flat-plate solar collector (FPSC). All functionalized GNPs nanofluids samples were fixed at 0.1 wt.% concentration for the solar performance test. The setup for this experiment consisted of two sections: the FPSC section and the flow loop section. In this study, copper was used for the fabrication of FPSC setup. The flow loop section consists of a jacketed tank with an overhead stirrer, a stainless steel tube with a thermal insulator, a centrifugal pump, a digital flow meter, a refrigerated water bath, a digital flow meter, a main electrical control box, and a data logger. A stainless steel jacketed tank was installed to store the working fluid. The insulated jacketed tank was used for absorbing heat from the FPSC section. In order to increase the blending of the working fluid and improve the heat exchange of the fluid inside the tank, an overhead stirrer was also installed. A heat exchanger was connected with a refrigerated water bath to maintain the

fluid temperature at the inlet of the FPSC. Meanwhile, a magnetic-drive centrifugal electric pump was utilized to control the flow rate during the process. A digital flow rate meter was installed to measure the flow rate of the working fluid. In addition, the temperatures of the bulk fluid inside the tank and during the process were measured and displayed by a data logger located at the FPSC section of the setup.

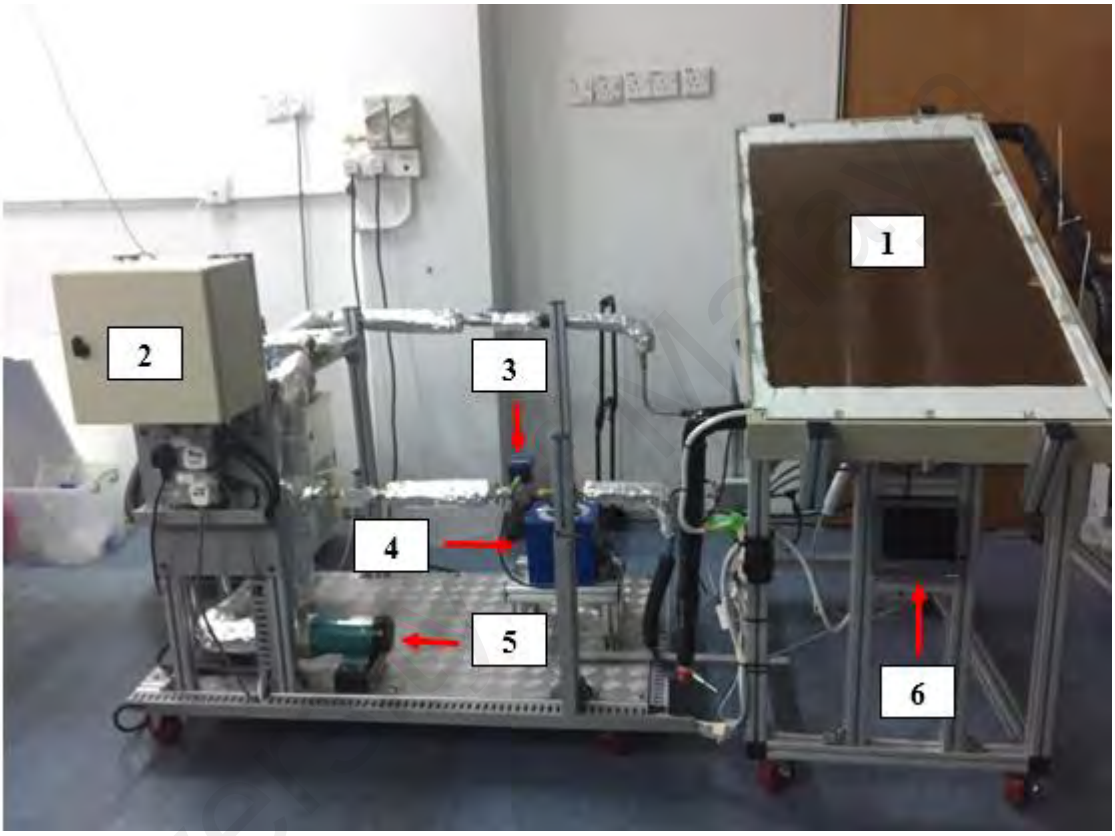

Figure 3.7: An experimental setup for the evaluation of all chemically modified GNPs samples in FSPC setup. The numbers represent: 1- flat plate solar collector, 2- electrical control box, 3- flow meter, 4- voltage transformer, 5- electric pump and 6- data logger.

3.3.2 Thermoelectrochemistry experimental setup

The redox solution of iodide/triiodide (I^-/I_3^-) was prepared at the molarity of 0.4 M by dissolving iodine (2.67 g, R&M Chemicals) and potassium iodide (2.03 g, R&M Chemicals) in 50 ml of distilled water. In order to ensure proper solubility, the mixed solution was stirred and heated up to 50 °C on a hotplate until all the chemicals were dissolved. The reactions that occurred during the process are as follows:

$$2\ KI + I_2 \longrightarrow KI + I_3$$

For the treated-GNPs sample, a similar concentration of 0.1 wt.% was also used to evaluate the performance in thermoelectrochemistry application. A specific concentration of treated-GNPs samples was mixed with the I^-/I_3^- solution. The compartments (Pyrex glass beakers and glass vials) to carry out the test for all samples were set up as shown in Figure 3.8. The glass beakers were filled with distilled water before the vials were placed inside the beakers. First, the prepared I^-/I_3^- aqueous redox solution was used as a control in the experiment. Then, the test was further carried out for the redox solution mixed with each functionalized GNPs sample. Pt wires were used as an electrode and inserted in each vial containing the solution and the samples. Each time the sample in the vials was changed, the Pt electrodes were cleaned using acetone and rinsed with chloroform three times. In this experimental setup, a salt bridge containing the same solution was used to link the two compartments together in order to establish the physical exchange of the solution during the process. To create a thermal gradient condition, heat was applied at one side of the compartment using a hotplate at 0.2 °C/min rate in which the temperature was set at 30, 35, 40, 45, 50, 55, and 60 °C. Meanwhile, on the other side of the compartment, the temperature was maintained at 30 °C (room temperature) during the test.

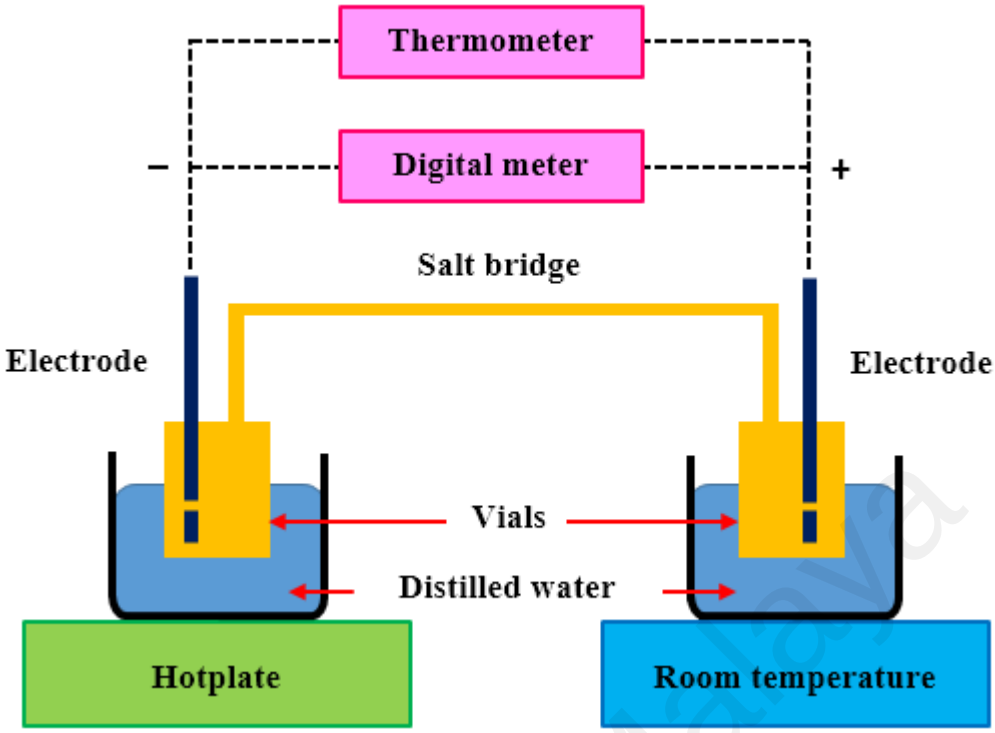

Figure 3.8: Schematic illustration of the thermoelectrochemistry experimental setup.

CHAPTER 4: RESULTS AND DISCUSSION

In this chapter, the discussion is based on the results of functionalized GNPs materials obtained from the analysis using particular instruments as mentioned in Chapter 3. Furthermore, the evaluation of the performances for different parameters in each application is discussed in this chapter.

4.1 Morphological structure, stability, and thermophysical properties of functionalized GNPs material

4.1.1 Fourier transform infrared spectroscopy (FTIR)

In this section, the FTIR spectra of pristine GNPs, TFPEG-treated GNPs, N-doped GNPs, and XC-treated GNPs samples are presented. Based on Figure 4.1, pristine GNPs sample shows a featureless peak as they are only polyaromatic layers of carbon. After the functionalization using covalent techniques, some defects occur on the pristine structure of GNPs. These defects cause a loss in the symmetry of the honeycomb lattice of GNPs due to some absorption in the IR spectrum; thus, the peaks are observed.

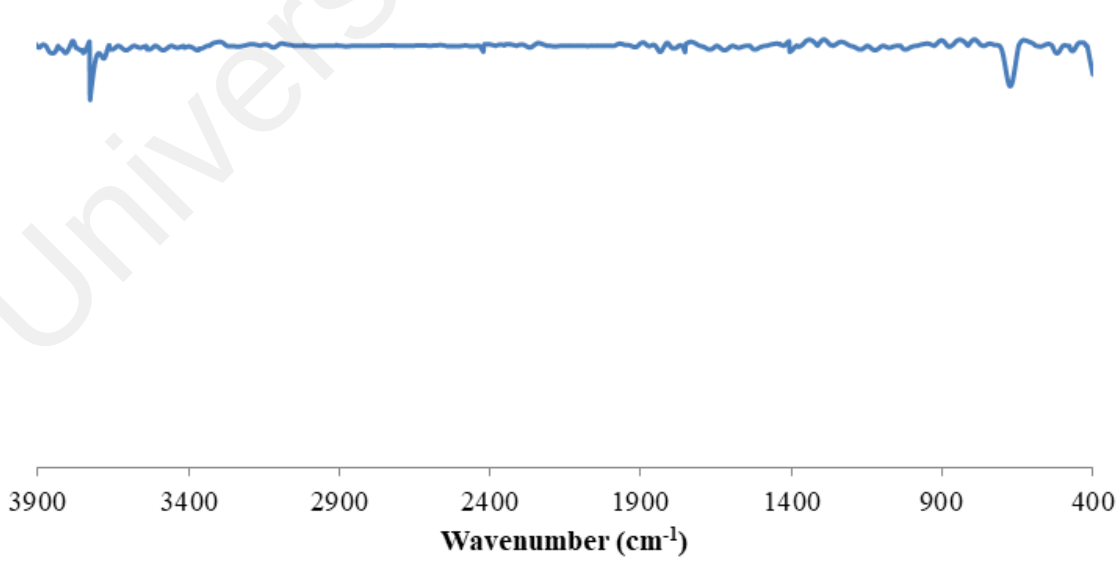

Figure 4.1: FTIR spectrum of pristine GNPs.

4.1.1.1 TFPEG-treated GNPs material

Figure 4.2 shows the FTIR spectra of TFPEG-treated GNPs. The main IR peaks and the assigned bonds interpreted from the FTIR spectrum of the TFPEG-treated GNPs are summarized in Table 4.1. It can be observed from Figure 4.2 that the TFPEG-treated GNPs show the absorbance peaks at 2922, 1635, and 1380 cm^{-1}, which represent C–H, C=O, and C–O bonds, respectively. These bonds are present due to the attachment of TFPEG molecules on the edge and surface of the GNP sheets. The existence of C=O and C–O bonds indicates that the direct esterification reaction is successful. In addition, the TFPEG-treated GNPs show a broad absorbance peak within a wavenumber range of 3000–3500 cm^{-1}, which is ascribed to the –OH chains of the TFPEG. The appearance of these peaks in the FTIR spectrum for the TFPEG-treated GNPs qualitatively proves the success of the covalent functionalization procedure.

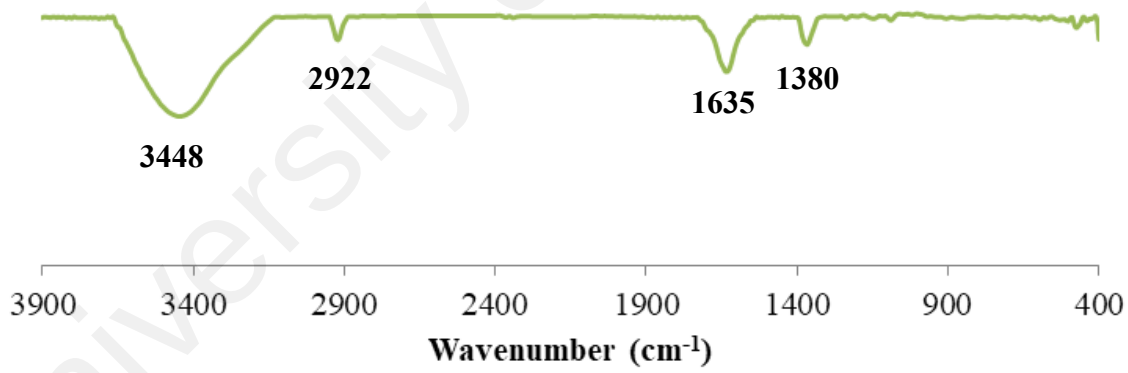

Figure 4.2: FTIR spectrum of TFPEG-treated GNPs.

Table 4.1: Interpretation of the IR peaks for TFPEG-treated GNPs.

Peak (cm^{-1})	Interpretation
3448	–OH stretching vibration
2922	C–H stretching vibration
1635	C=O stretching vibration
1380	C–O stretching vibration

4.1.1.2 N-doped GNPs material

Figure 4.3 displays the IR spectra of hydroxylated GNPs and nitrogen-doped GNPs. A list of the main peaks present with the assigned bonds are shown in Table 4.2. In the spectrum of GNP-OH, the peaks located at the range of 3400 cm^{-1} is attributed to hydroxyl groups. Also, the peaks at the range of 2800-2930 cm^{-1} are related to the structural vibration of C–H groups. The peaks at 1697 and 1634 cm^{-1} are assigned to the C=O and C=C stretching vibrations, respectively. The presence of these peaks confirms successful oxidation procedure. The spectrum of N-doped GNPs shows the reduction of oxygen-containing groups after N-doping process, where the intensity of the peaks at the range of 3400 cm^{-1} drops significantly. More importantly, the decreasing intensity of the C=O and C=C bands are in a good agreement with nitrogen-doping procedure, showing successful doping.

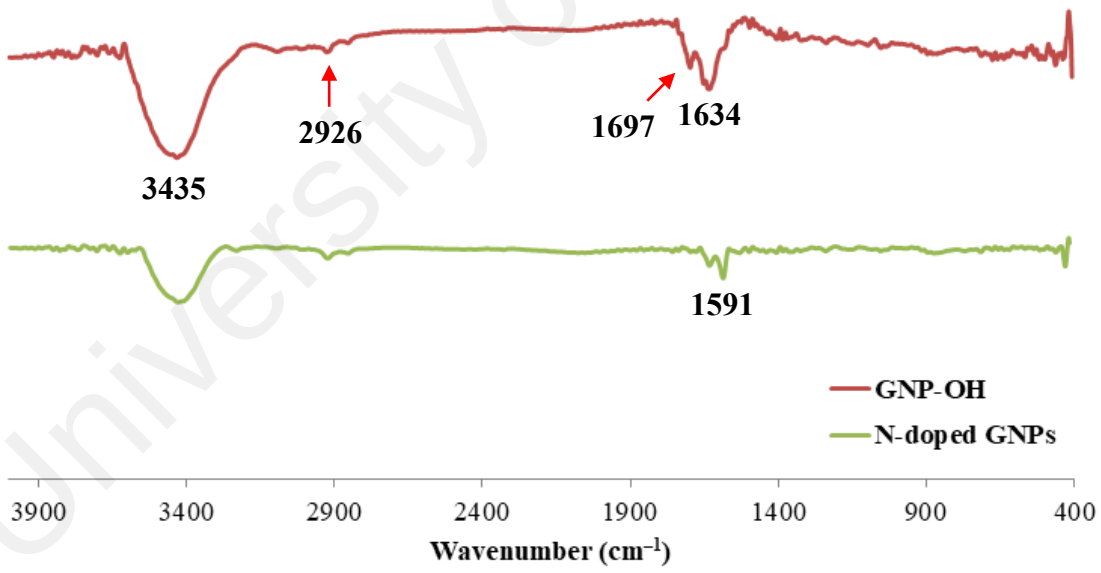

Figure 4.3: FTIR spectra of GNP-OH and N-doped GNPs.

Table 4.2: Interpretation of the IR peaks for N-doped GNPs.

Peak (cm^{-1})	Interpretation
3435	–OH stretching vibration
2926	C–H stretching vibration
1697	C=O stretching vibration
1634	C=C stretching vibration
1591	C=N stretching vibration

4.1.1.3 XC-treated GNPs material

FTIR was also conducted in order to confirm the modification of GNPs with copolymers of citric acid and xylitol as illustrated in Figure 4.4. A more detailed list of the main infrared peaks together with the assigned bonds are shown in Table 4.3. Based on the spectra (Figure 4.4), the characteristic peak at 1741 cm^{-1} appears clearly, which is assigned to C=O stretching of –COOH and esters. The peaks at 1628 and 1375 cm^{-1} are assigned to the stretching of –COO–. Meanwhile, the peak absorption at 1155 cm^{-1} is assigned to the C–O in –C–OH. The stretch absorption bands of C–H bond at 2924 cm^{-1} was also observed in the spectra. The XC-treated GNPs sample shows broad peaks within the range of 3000–3500 cm^{-1}, which are attributed to the –OH chains from the absorption of alcohol. Based on the presence of the previous mentioned peaks as compared to the pristine sample, it shows that successful modification procedure is achieved in this study.

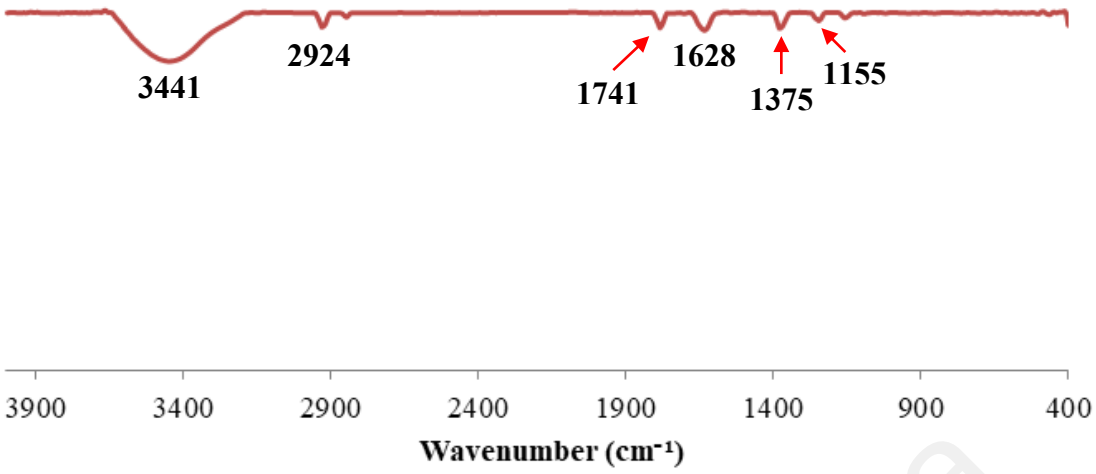

Figure 4.4: FTIR spectrum of XC-treated GNPs.

Table 4.3: Interpretation of the IR peaks for XC-treated GNPs.

Peak (cm^{-1})	Interpretation
3441	–OH stretching vibration
2924	C–H stretching vibration
1741	C=O stretching vibration
1628	–COO– stretching vibration
1375	–COO– stretching vibration
1155	C–O stretching vibration

4.1.2 Raman spectrometry

From Raman spectra we can estimate the number of layers for graphene based on the I_G/I_{2D} ratio (Wall, 2011). If the ratio is exceed 0.4, it indicates the presence of multilayers graphene (Fesenko et al., 2015). In this case, the ratio calculated is 18.07 which means that the GNPs product that use in this study fall into multilayers graphene/GNPs categories. Besides, Raman analysis was used to provide more evidence on the success of the covalent functionalization procedure. In Raman spectrum, the presence of a G-band is due to the presence of sp^2 carbon network whereas the presence of a D-band is due to the defects that occur on the chemical structure (S. K. Yadav & Cho, 2013). Meanwhile, the intensities of D- and G-bands are related to the vibration mode of sp^3 and sp^2 carbon network, respectively (J. F. Dai et al., 2015). In this section, the integral intensity ratio of

D-band to G-band (I_D/I_G) that usually measures the rate of sp^2-hybridized carbon to sp^3-hybridized carbon was also calculated and summarized in Table 4.4. Figure 4.5 shows the Raman spectra of pristine GNPs with the I_D/I_G ratio of 0.508. The obtained ratio was compared with TFPEG-treated GNPs, XC-treated GNPs and N-doped GNPs samples that involved in this research study.

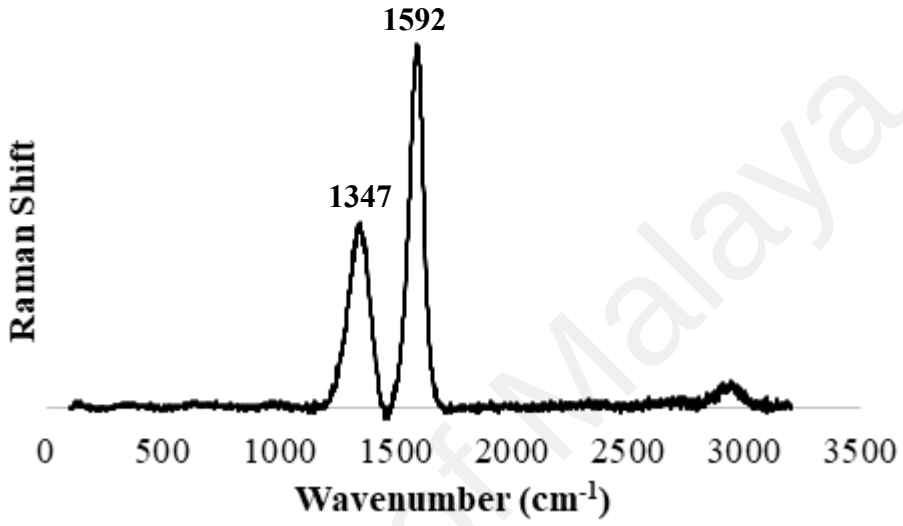

Figure 4.5: Raman spectra of pristine GNPs.

Table 4.4: Displacement and intensity ratios for GNPs and treated-GNPs through Raman spectroscopy.

Sample ID	D-band (cm^{-1})	G-band (cm^{-1})	I_D/I_G Ratio
Pristine GNPs	1347	1592	0.508
TFPEG-treated GNPs	1353	1599	0.757
N-doped GNPs	1348	1578	0.712
XC-treated GNPs	1349	1583	0.867

4.1.2.1 TFPEG-treated GNPs material

Figure 4.6 shows the Raman spectra of TFPEG-treated GNPs. The peaks are present at the wavenumber of 1353 and 1599 cm^{-1}.The I_D/I_G ratio of the TFPEG-treated GNPs is 0.757 as shown in Table 4.4. The I_D/I_G ratio is higher for the TFPEG-treated GNPs compared to the pristine GNPs due to the formation of covalent bonds on the graphene sheets resulting from covalent functionalization.

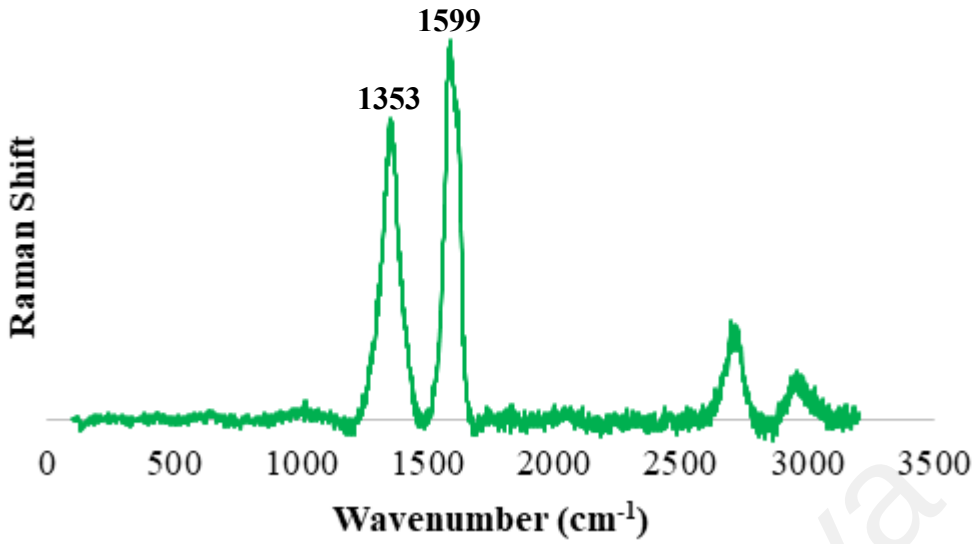

Figure 4.6: Raman spectra of TFPEG-treated GNPs.

4.1.2.2 N-doped GNPs material

Figure 4.7 displays the Raman spectra of N-doped GNPs. The spectra reveal that the D-band and G-band of pristine GNPs appear at 1347 and 1592 cm^{-1}, respectively. The I_D/I_G of N-doped GNPs is 0.712, which is higher than that of pristine GNPs. This confirms N-doping of GNPs, which could be produced by high capability of nitrogen heteroatoms that can cause some disordered bonding in graphene lattice.

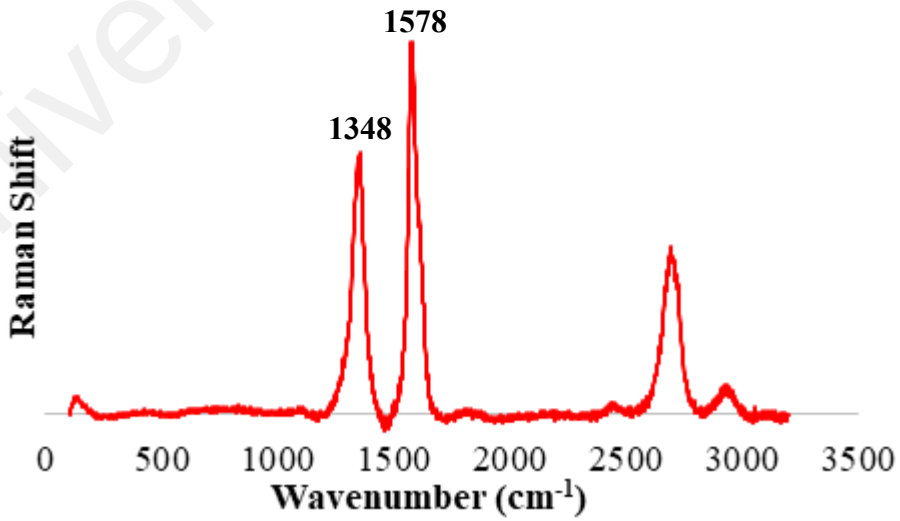

Figure 4.7: Raman spectra of N-doped GNPs.

4.1.2.3 XC-treated GNPs

The spectra for Figure 4.8 shows the I_D/I_G ratio of XC-treated GNPs of 0.867. It can be seen that, the peaks of the spectra are observed at 1349 and 1583 cm^{-1}. The I_D/I_G ratio of XC-treated GNPs is higher than pristine GNPs, which implies the addition of the functional groups on the graphene sheets through successful covalent bond formation in the procedure.

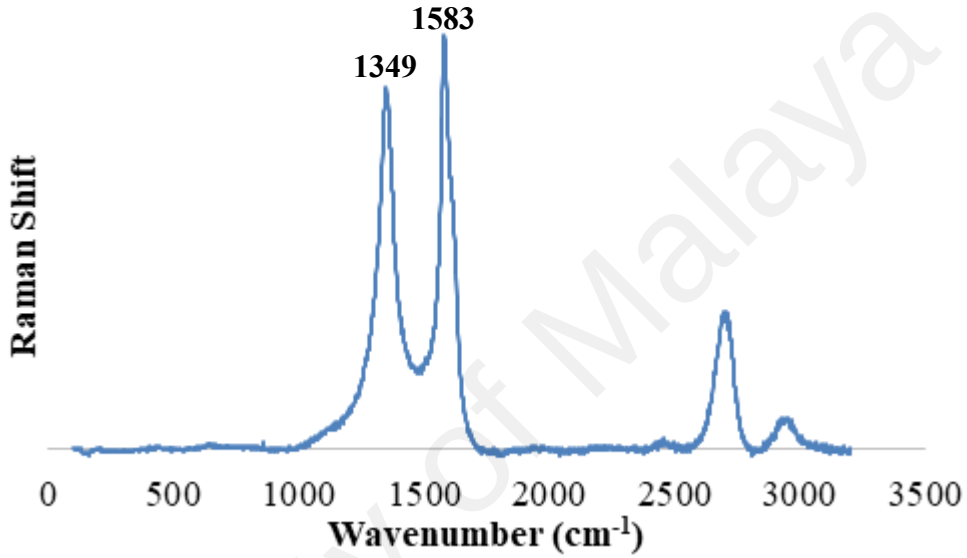

Figure 4.8: Raman spectra of XC-treated GNPs.

4.1.3 High-resolution transmission electron microscopy (HRTEM)

The morphologies of the pristine GNPs and all functionalized GNPs samples were observed using HRTEM and the results are shown in this section. It can be seen from Figure 4.9(a) and (b) that the pristine GNPs consist of sheets with fairly transparent structures and smooth surfaces, and the edges are clearly intact.

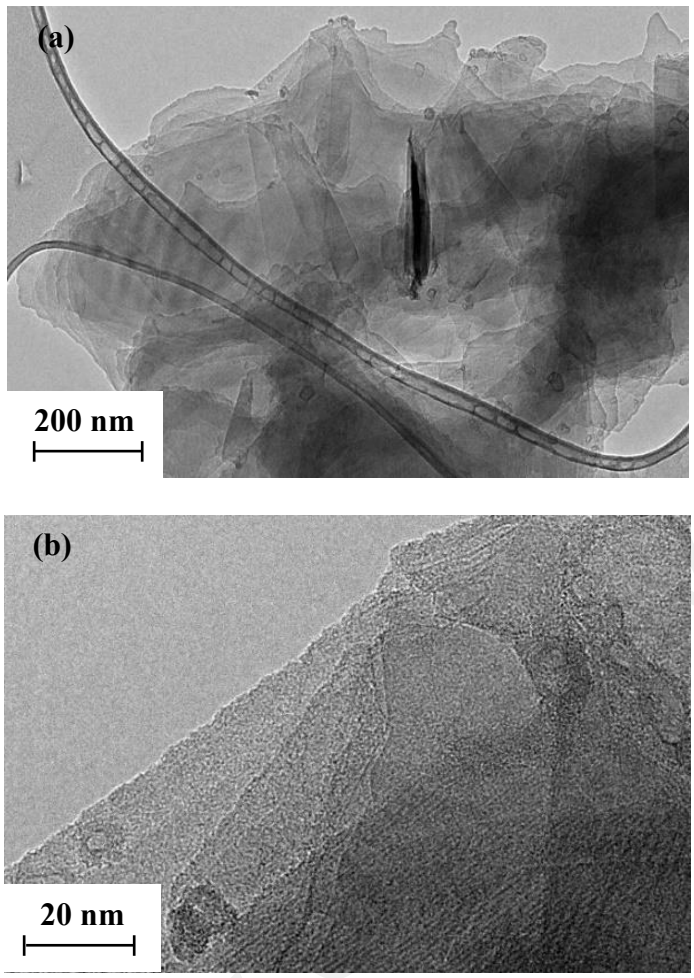

Figure 4.9: HRTEM images of pristine GNPs at (a) 200 nm and (b) 20 nm resolutions.

4.1.3.1 TFPEG-treated GNPs material

After functionalization, the addition of TFPEG and carboxyl groups onto the surfaces and edges of the GNPs makes the sheets appear slightly blur with loads of crumples and wrinkles, as shown in Figure 4.10(a). The changes in the morphology along with analysis of the functional groups indicate that the reaction between the GNP-COOH and TFPEG is indeed successful. The presence of folded flakes with defects and roughness at the edges (Figure 4.10(b) and (c)) also indicates that the covalent functionalization procedure is successful.

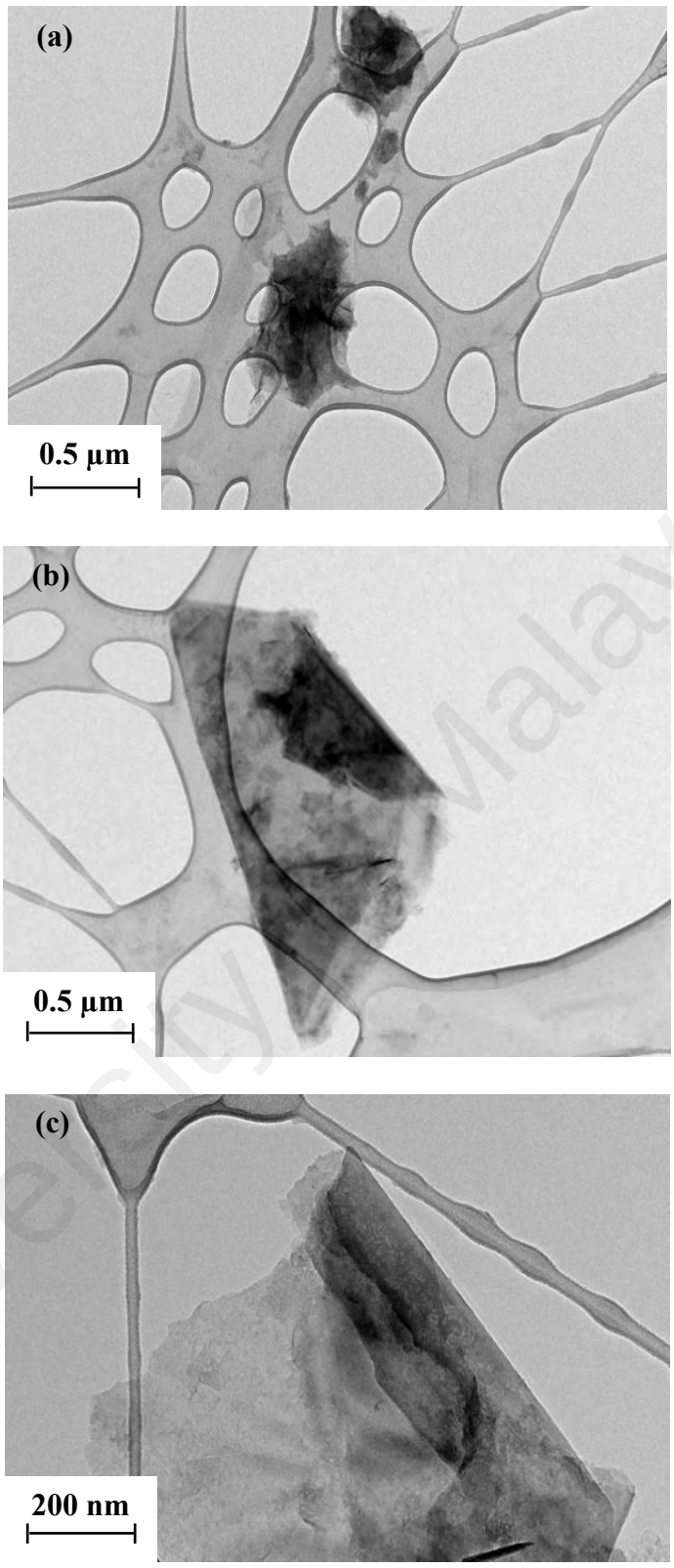

Figure 4.10: HRTEM images of TFPEG treated-GNPs at (a) 0.5 µm and (b) 0.5 µm and (c) 200 nm resolutions.

4.1.3.2 N-doped GNPs material

The microstructural characteristics of N-doped GNPs were investigated and the results are shown in Figure 4.11. After nitrogen-doping process, the sheets exhibit more entangled and wrinkled-like morphology, as can be seen in Figure 4.11(a) and (b). The change in morphology indicates that the rate of disorderly in the main carbon structure increased, implying successful nitrogen doping.

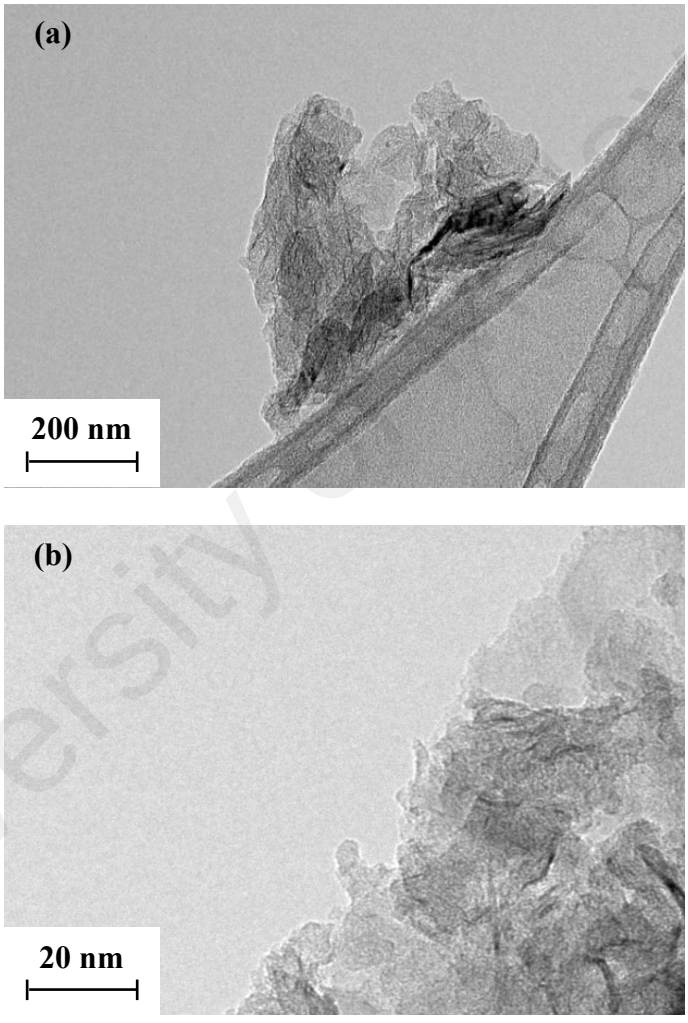

Figure 4.11: HRTEM images of N-doped GNPs at (a) 200 nm and (b) 20 nm resolutions.

4.1.3.3 XC-treated GNPs material

The modification of XC-treated GNPs was verified by HRTEM imaging as shown in Figure 4.12. Modified GNPs exhibit loads of crumples almost similar to the previously prepared materials as can be seen in Figure 4.12(a). Figure 4.12(b) shows that the edge

of the XC-treated GNPs yields wrinkled-like morphology, which indicates successful functionalization.

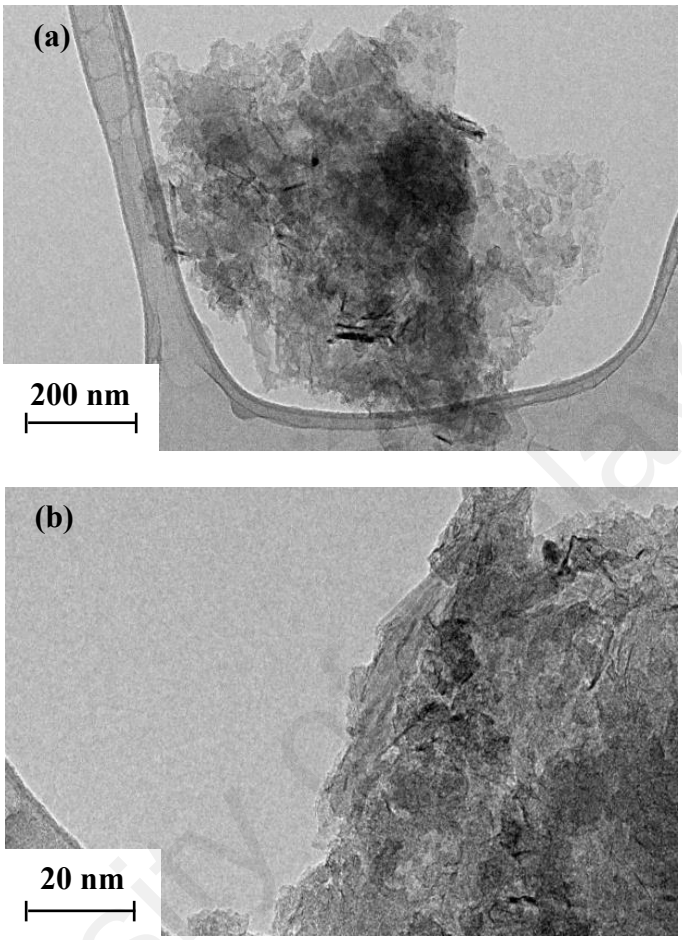

Figure 4.12: HRTEM images of XC-treated GNPs at (a) 200 nm and (b) 20 nm resolutions.

4.1.3.4 P123-GNPs material

Figure 4.13(a) and (b) display the sheets structure with more wrinkles after non-covalent functionalization process. The changes in the images are due to the two-dimensional (2D) structures distorted during the ultrasonication process, which resulted from the flexibility of graphene sheets after treatment.

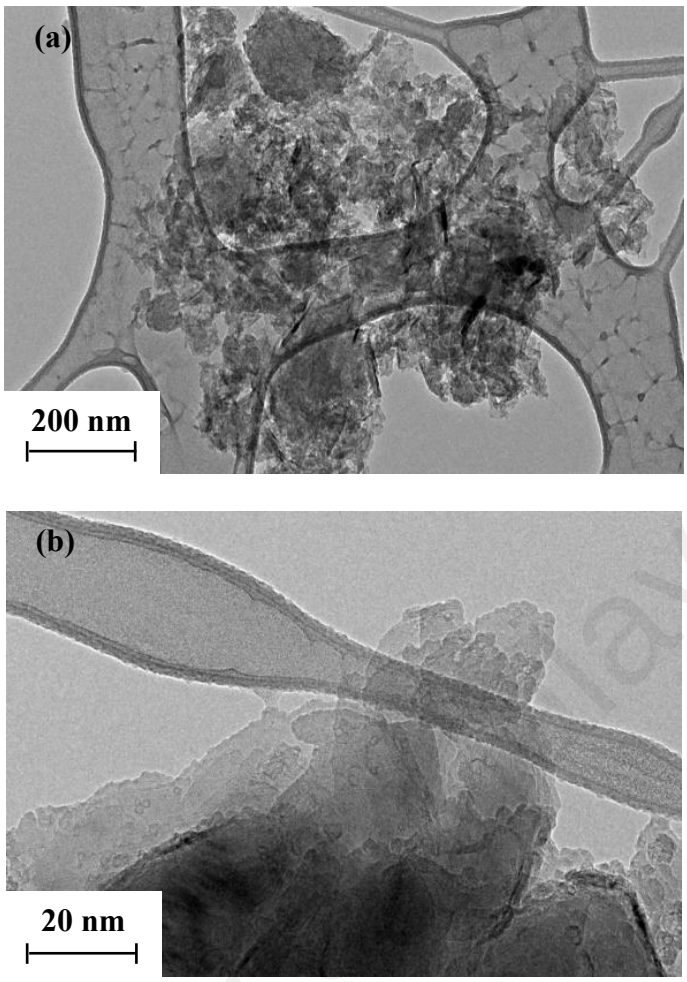

Figure 4.13: HRTEM images of P123-GNPs at (a) 200 nm and (b) 20 nm resolutions.

4.1.4 Analysis of X-ray photoelectron spectroscopy (XPS)

Further functional component analysis for the N-doped GNPs was carried out by XPS analysis and is shown in Figure 4.14. As shown in panel (a), the wide-scan spectrum shows the presence of three elements: C, N, and O atoms with atomic percentage of 87.13%, 5.34%, and 7.53%, respectively. To present the results quantitatively, Table 4.5 shows the atomic percentage of N-doped GNPs sample. The high-resolution C1s spectrum in Figure 4.14(b) consists of a sharp peak positioned at 284.6 eV that corresponds to sp^2-hybridized/graphitic carbon. Also, other main components at 284.2, 285.1, and 287.5 eV are originated from the carbon atom bonded to carbon atoms by a single band, C-O/C=O, and C-N/O-C=O bonds, respectively. The N1s spectrum of N-doped GNPs (Figure 4.14(c)) illustrates an asymmetric N1s spectrum, which composed

of three peaks, i.e., pyrrolic-N (~ 398.1 eV), graphitic-N (~399.8 eV), and N-oxides of pyridinic-N (~401.8 eV). The presence of thermally-stable graphitic-N after annealing in N-doped GNPs confirmed that the suggested method is successful. Also, the high-resolution O1s spectrum in Figure 4.14(d) exhibits two subpeaks that are attributed to oxygen atoms in carboxylic groups (529.3 eV) and non-carbonyl oxygen atoms (531.3 eV).

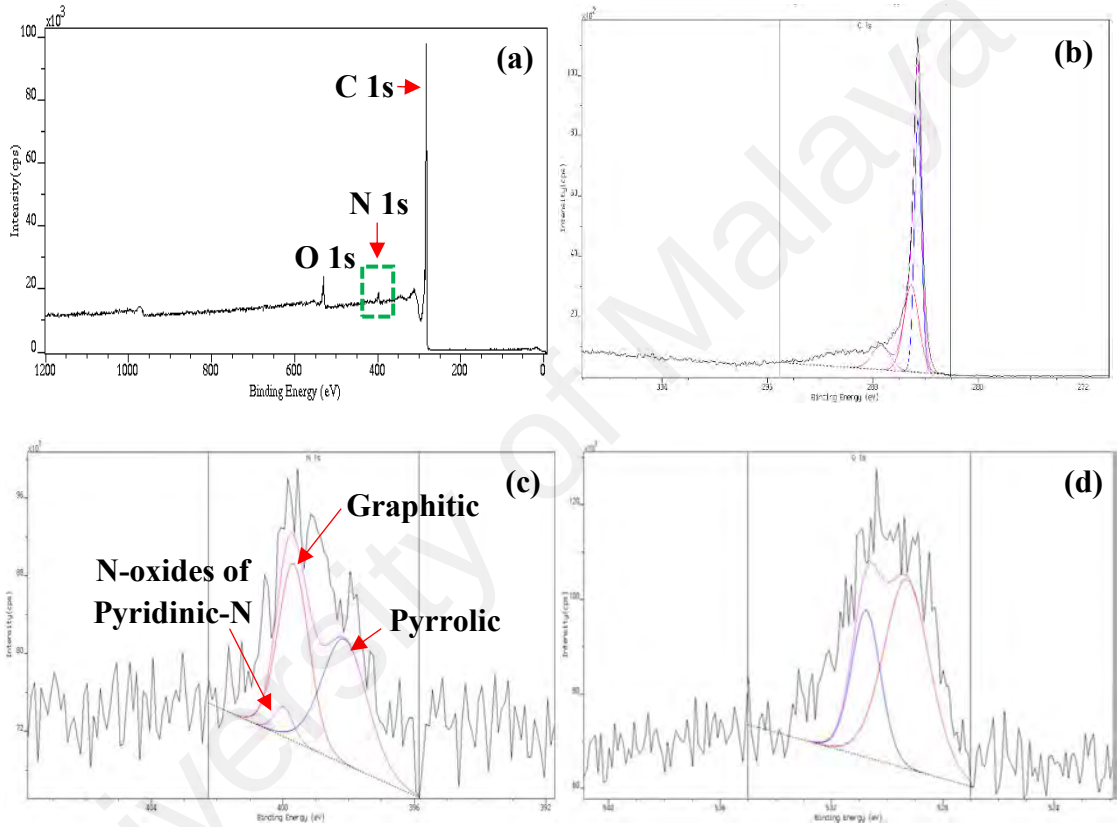

Figure 4.14: (a) X-ray photoelectron spectroscopy (XPS) images of N-doped GNPs material, (b) high-resolution C1s spectrum of N-doped GNPs, (c) high-resolution N1s spectrum of N-doped GNPs, and (d) high-resolution O1s spectrum of N-doped GNPs.

Table 4.5: Elemental analysis of wide-scan area for N-doped GNPs material.

Peak	Position (eV)	Atomic Concentration (%)
C1s	284.6	87.13
N1s	398.0	5.34
O1s	532.0	7.53

4.1.5 Colloidal stability for water-based treated GNP nanofluids

The photographs of comparison between the stability of pristine GNPs and all functionalized GNPs samples were captured and the images are presented in Figure 4.15. From the observation, the pristine GNPs were unable to stabilize in distilled water for more than 24 hr, and sediments formed at the bottom of the sample vial. This is due to the Van der Waals forces of the GNPs, which leads to the agglomeration of the GNPs in distilled water. In contrast, the treated-GNPs materials (TFPEG-treated GNPs, N-doped GNPs, XC-treated GNPs, and P123-GNPs) show remarkable colloidal stability in distilled water after 24 hr.

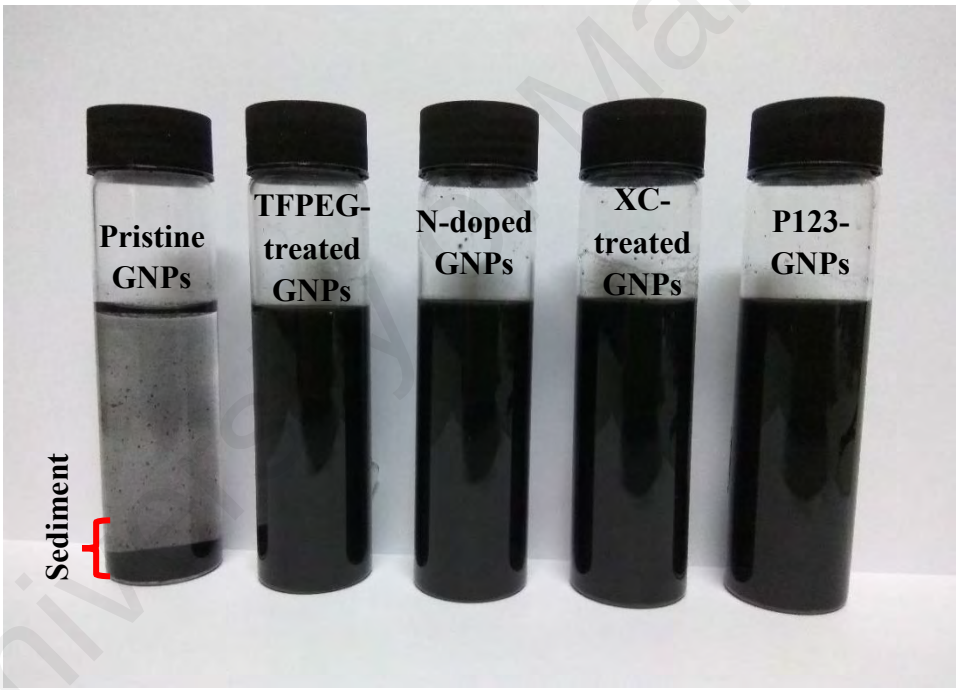

Figure 4.15: Photographs of water-based pristine GNPs dispersion and water-based TFPEG treated-GNPs, water-based N-doped GNPs, water-based XC-treated-GNPs, and water-based P123-GNPs after 24 hr of preparation.

Figure 4.16 shows the UV-Vis spectra for all water-based TFPEG-treated GNPs, N-doped GNPs, and XC-treated GNP nanofluid samples prepared at different particle concentrations (0.0025, 0.0050, 0.0075, and 0.0100 wt%). Meanwhile, the sample of P123-GNPs was prepared according to the ratio of surfactant:GNPs from 1:1 to 1:4. It can be observed that there is a single peak within a wavelength range of 260–270 nm.

The sharp absorption peak at ~265 nm is likely due to the π→π* transition of C=C bond of the GNPs. This correspond to the sample solutions that consisted of treated GNPs which dispersed well in base fluid. It is also evident that the peak intensity increases with an increase in particle concentration, in accordance with the Beer-Lambert law (Amiri, Kazi, et al., 2015).

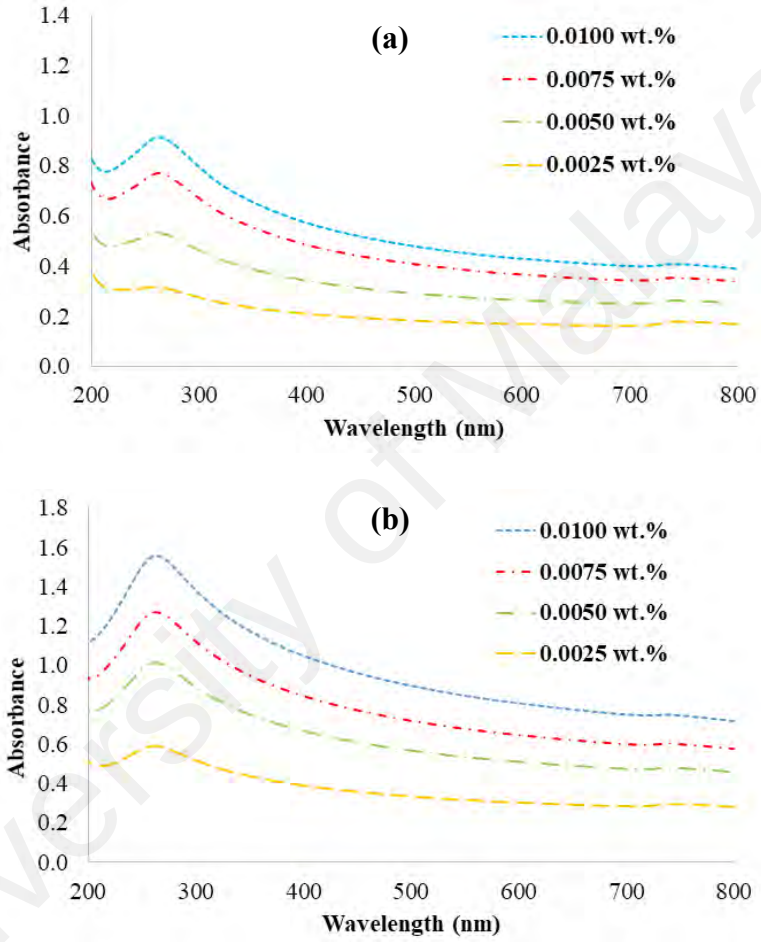

Figure 4.16: UV-Vis spectra of water-based (a) TFPEG-treated GNP and (b) N-doped GNPs nanofluids at different particle concentrations.

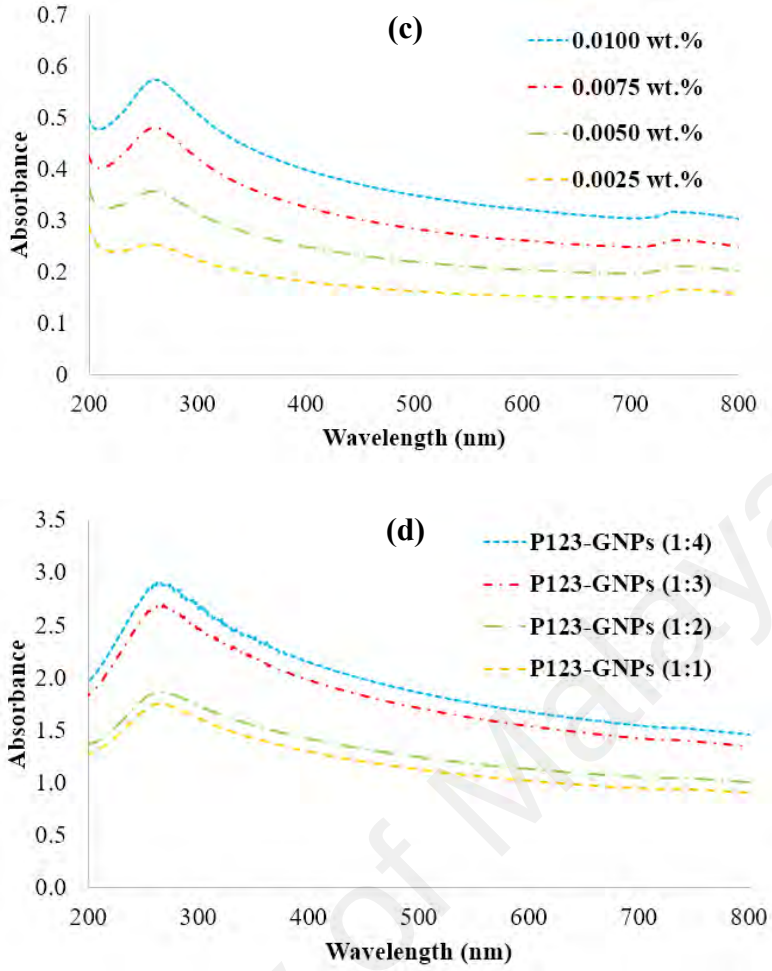

Figure 4.16 (continued): UV-Vis spectra of water-based (c) XC-treated GNPs and (d) P123-GNPs nanofluids at different particle concentrations.

Figure 4.17 shows the colloidal stability of all water-based treated GNP nanofluids over a 15-day period. The results are indeed encouraging because the water-based treated GNP nanofluids have excellent colloidal stability within the period of investigation, judging from the high relative particle concentrations. Thus, it is deduced that TFPEG polymer, nitrogen doped, Pluronic P-123 surfactant, and the polymer of sugar alcohol (xylitol with citric acid) are superior candidates to achieve highly stable water-based GNP nanofluids. In addition, it is discovered that the percentage of sediment formed in the nanofluids is insignificant, where the remaining relative particle concentrations after 15 days are 89%, 85%, 79%, and 78% for TFPEG-treated GNPs nanofluids; 83%, 80%, 78%, and 77% for N-doped GNPs nanofluids; and 89%, 83%, 82%, and 80% for XC-treated GNPs nanofluids containing 0.0100, 0.0075, 0.0050, and 0.0025 wt.% of related

nanoparticles, respectively. Meanwhile, the lowest sedimentation rate for P123-GNPs is only 12% with the ratio of 1:1 within the period. The relative particle concentration is based on the percentage ratio of the current concentration to the concentration of a fresh sample. It is found that the highest and lowest percentages of sediment formed for the water-based treated GNPs are approximately 23% and 11%, respectively. It is apparent from the results that all water-based treated-GNP nanofluids show remarkable colloidal stability with an average percentage of sediment of less than 25% after 15 days. The summary for all of the values obtained, can be referred to Table 4.6.

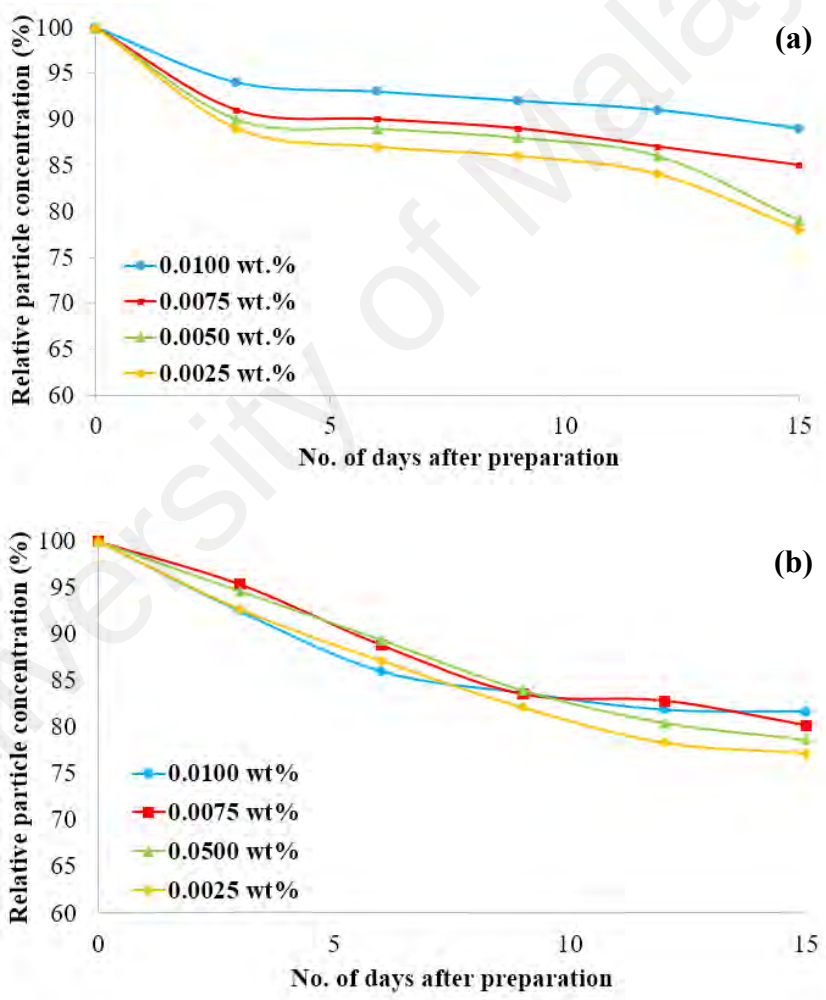

Figure 4.17: Relative particle concentration versus the number of days after preparation for water-based (a) TFPEG-treated GNP and (b) N-doped GNPs nanofluids at different particle concentrations.

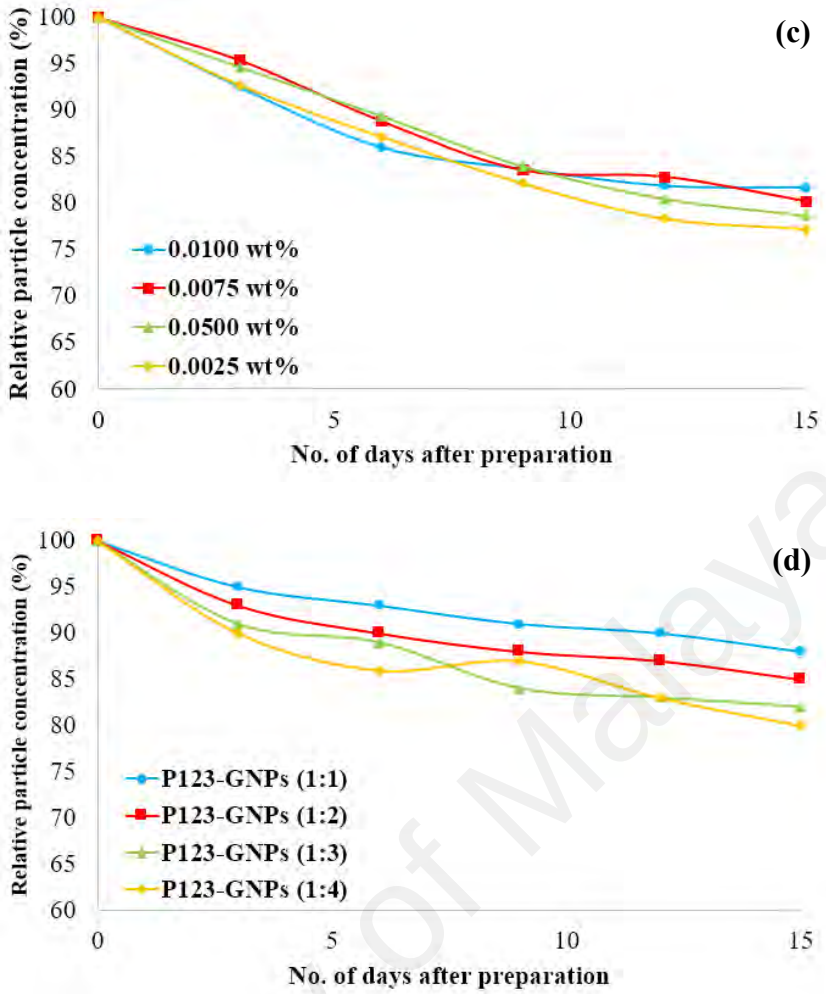

Figure 4.17 (continued): Relative particle concentration versus the number of days after preparation for water-based (c) XC-treated GNPs and (d) P123-GNP nanofluids at different particle concentrations.

Table 4.6: Shows the relative particle concentration that still remained after 15 days for each modified GNPs samples.

Samples name	Relative particle concentration (%)			
	0.0100/1:1	0.0075/1:2	0.0050/1:3	0.0025/1:4
TFPEG-treated GNPs	89	85	79	78
N-doped GNPs	83	80	78	77
XC-treated GNPs	89	83	82	80
P123-GNPs	88	85	81	79

4.1.6 Colloidal stability for organic solvent-based treated GNP nanofluids

The colloidal stability of the TFPEG-treated GNPs, N-doped GNPs, XC-treated GNPs, and P123-GNPs were also determined in different solvents (ethanol, methanol, 1-hexanol,

and ethylene glycol) within a-24 hr period and the results are shown in Figure 4.18. It is apparent that all the functionalized GNPs materials show good colloidal stability regardless of the type of solvent used as the aqueous medium. There is no sedimentation in the samples even after 24 hr, which indicates that the TFPEG-treated GNPs, N-doped GNPs, XC-treated GNPs, and P123-GNPs have the potential to remain stable over extended periods.

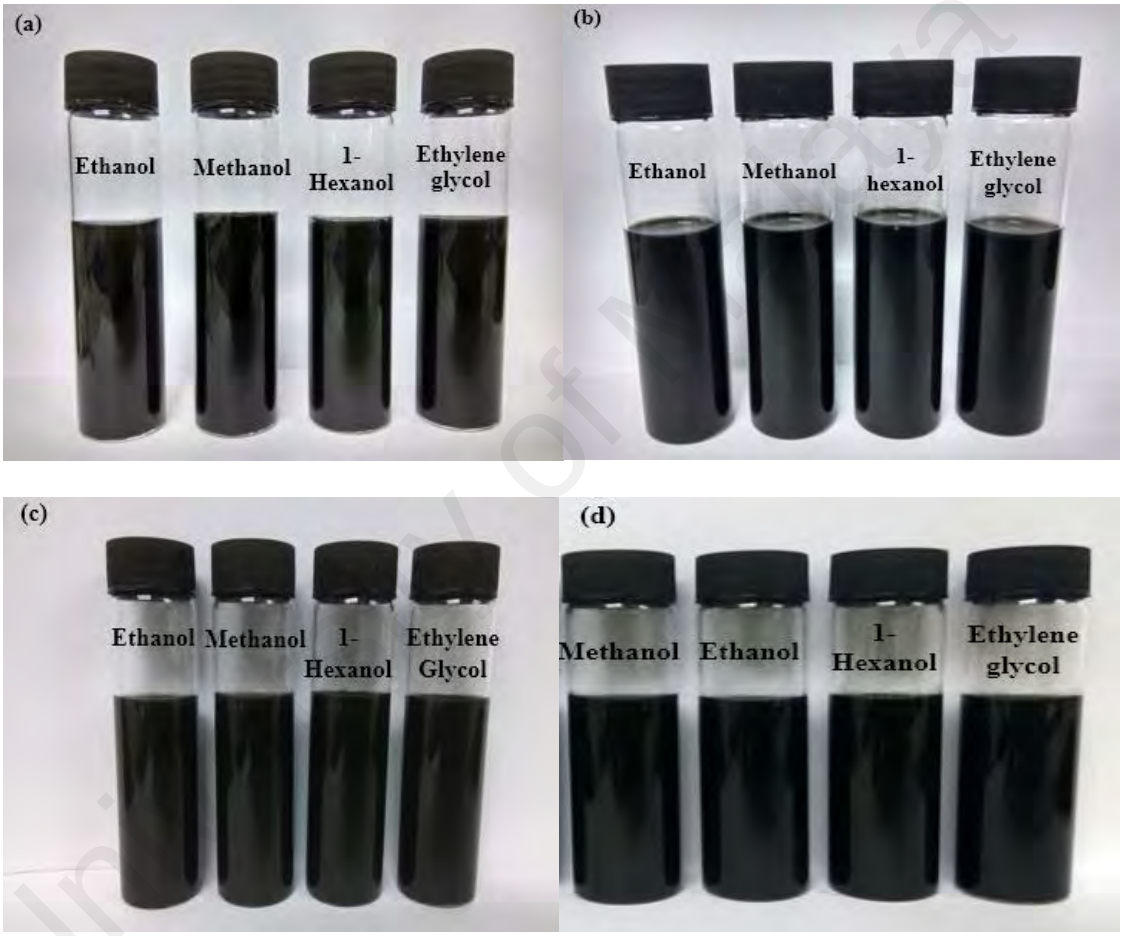

Figure 4.18: Photographs of (a) TFPEG treated-GNPs (b) N-doped GNPs, (c) P123-GNPs and (d) XC-treated GNPs in methanol-based, ethanol-based, 1-hexanol-based, and ethylene glycol-based of after 24 hr of preparation.

Further spectrophotometric measurements were conducted using UV-Vis spectroscopy in order to determine the colloidal stability of the organic solvent-based treated GNP nanofluids over a period of 15 days and the results are shown in Figure 4.19. The particle concentration of 0.01 wt.% was used for all samples. It can be seen from

Figure 4.19 that there is a broad absorbance peak within a wavelength range of 250–270 nm for all samples, which corresponds to π→π* transition of C=C bond of the GNPs. It can be observed that the trend of the UV-Vis spectra is similar to that of the water-based nanofluid containing 0.01 wt% of treated GNPs nanoparticles as previously shown in Figure 4.16 under section 4.1.5.

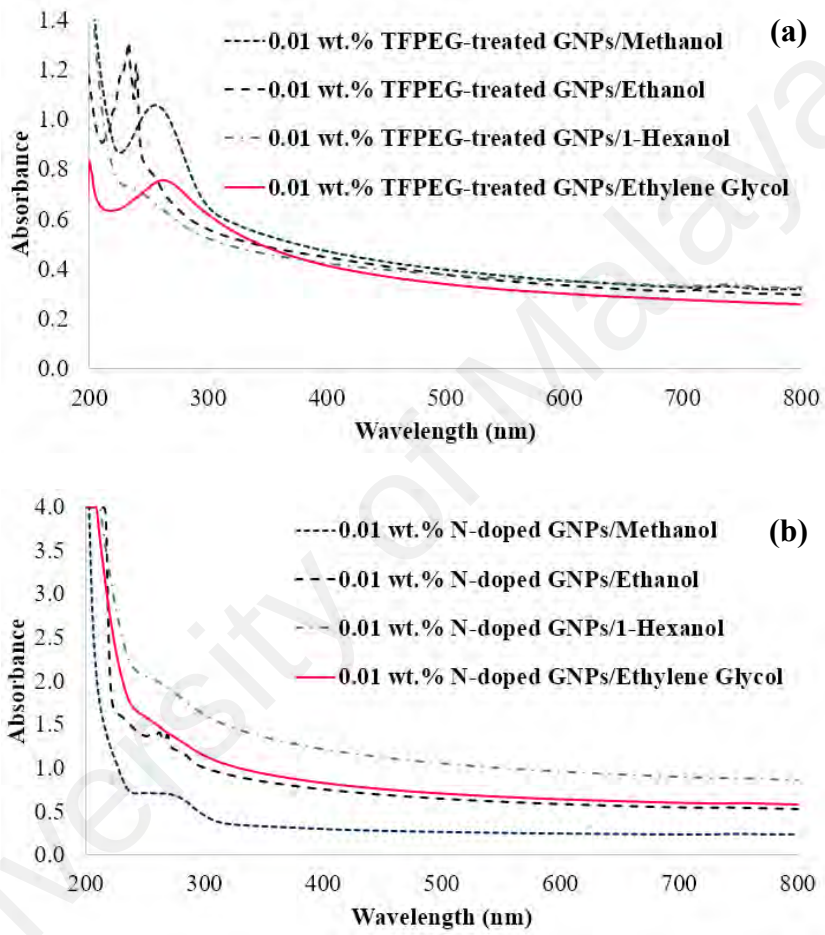

Figure 4.19: UV-Vis spectra of the methanol-based, ethanol-based, 1-hexanol-based, and ethylene glycol-based of (a) TFPEG-treated GNPs and (b) N-doped GNPs nanofluids.

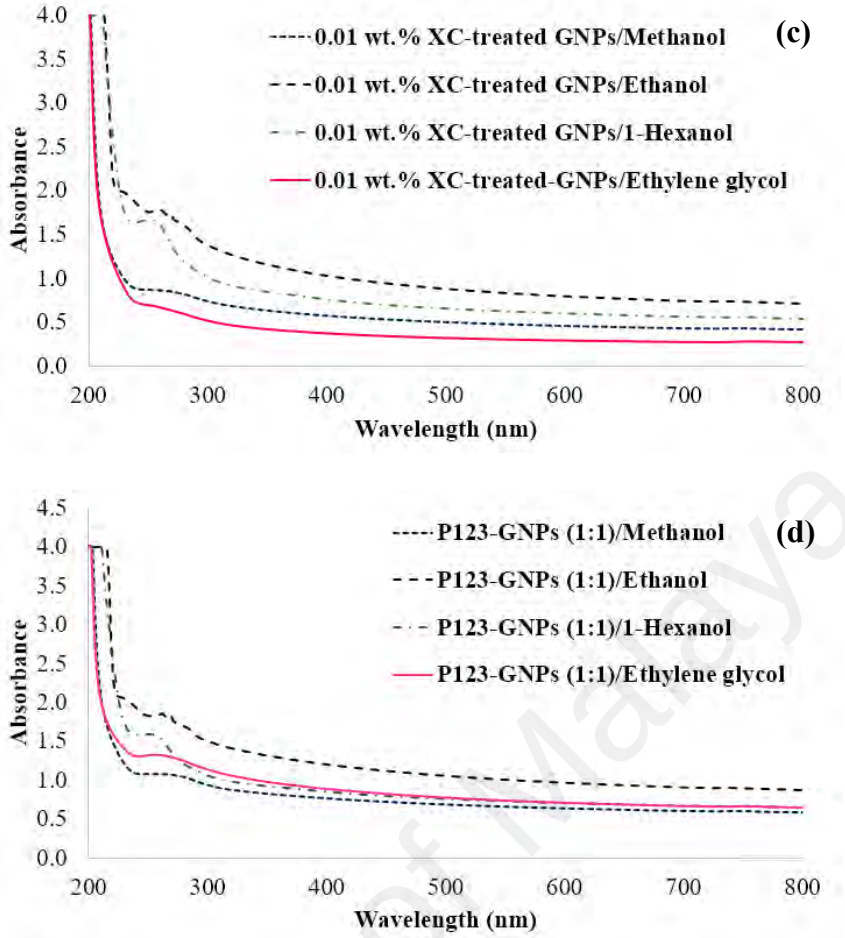

Figure 4.19 (continued): UV-Vis spectra of the methanol-based, ethanol-based, 1-hexanol-based, and ethylene glycol-based of (c) XC-treated GNPs and (d) P123-GNPs nanofluids.

In addition, the relative particle concentrations of the samples were determined over a 15-day period and the results are shown in Figure 4.20 and all the results are summarized in Table 4.7. It is found that the percentage of sediment values for the ethylene glycol-based, methanol-based, ethanol-based, and 1-hexanol-based TFPEG-treated GNP nanofluids, N-doped GNPs nanofluids, P123-GNPs nanofluids, and XC-treated nanofluids are 18%, 25%, 36%, and 47%; 18%, 29%, 33%, and 43%; 13%, 17%, 26%, and 34%; and 18%, 25%, 28%, and 36%, respectively. Interestingly, it is found that all treated GNPs samples have superior stability in EG and methanol, judging from the low percentage of sediment values. The high dispersibility of the TFPEG-treated GNPs and XC-treated GNPs may be due to the miscible functional groups attached on the structure

of GNPs. Meanwhile, the presence of functional groups containing oxygen and nitrogen attached to the N-doped GNPs structure has increased the hydrophilicity of the N-doped GNPs. It also explains the affinity of the sample to be more stable in high-polarity solvents. It is also interesting to note that the rate of stability of GNPs in the presence of P123 is different in different solvents. This could be due to the polar head group in non-ionic surfactants of Pluronic P-123 that helps GNPs to be more stable in higher polar solvents (Hayyan, Abo-Hamad, AlSaadi, & Hashim, 2015; Su, Wang, & Liu, 2002; T. P. Zhang, Liu, Sheng, Duan, & Zhang, 2014). Based on the overall stability performances for all samples, it can be concluded that the sequence of stability in different solvents is as follows:

Ethylene glycol > methanol > ethanol > 1-hexanol

Therefore, based on this unique property, all functionalized GNPs samples can be a good alternative in preparing stable graphene-based dispersions in different types of organic solvents for further applications.

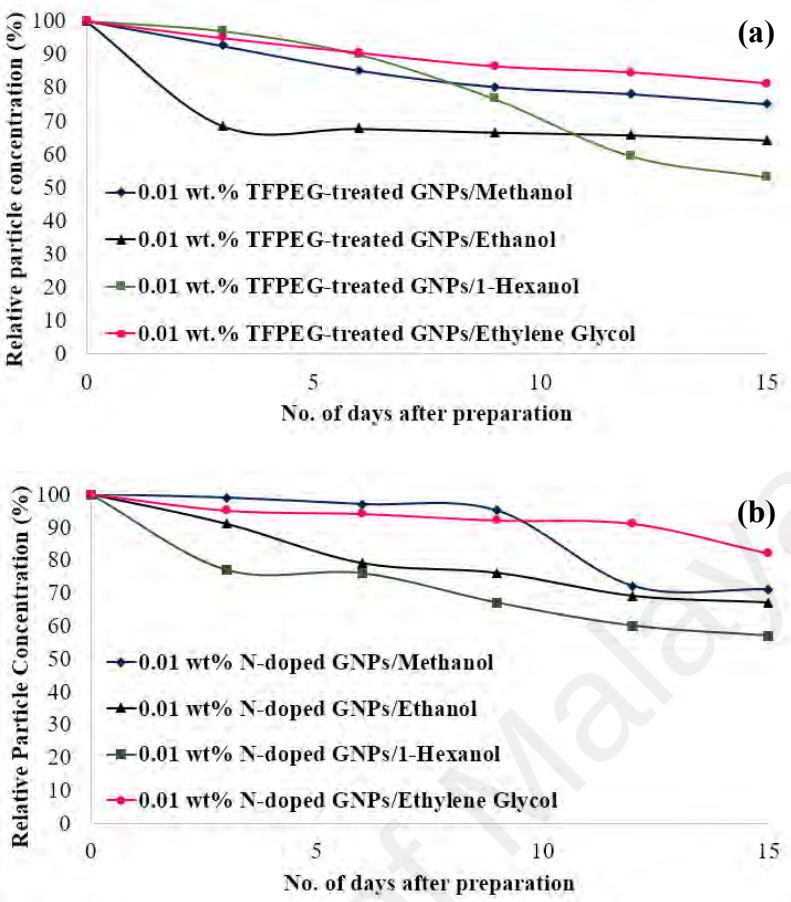

Figure 4.20: Relative particle concentration versus the number of days after the preparation of methanol-based, ethanol-based, 1-hexanol-based, and ethylene glycol-based of (a) TFPEG-treated GNPs and (b) N-doped GNPs nanofluids.

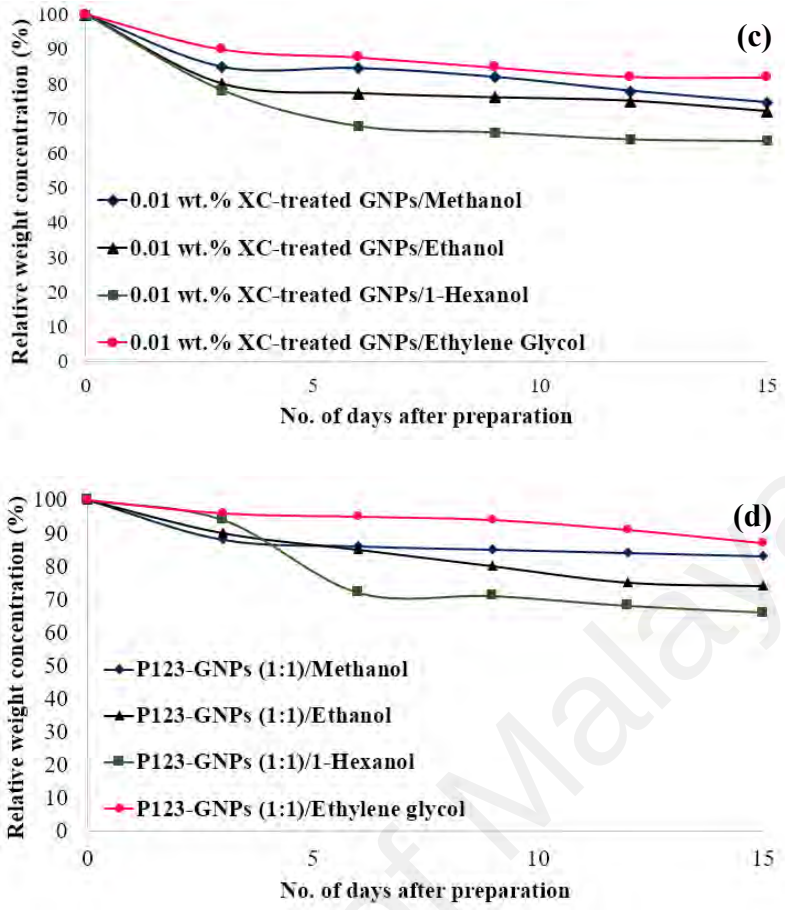

Figure 4.20 (continued): Relative particle concentration versus the number of days after the preparation of methanol-based, ethanol-based, 1-hexanol-based, and ethylene glycol-based of (c) XC-treated GNPs and (d) P123-GNPs nanofluids.

Table 4.7: Shows the remained relative weight concentration (%) for each prepared functionalized GNPs sample after 15 days.

Samples	Types of solvents & Relative weight concentrations (%)			
	Ethylene glycol	Methanol	Ethanol	1-hexanol
TFPEG-treated GNPs	82	75	64	53
N-doped GNPs	82	71	67	57
P123-GNPs	87	83	74	66
XC-treated GNPs	84	75	72	64

4.1.7 Analysis of particle size distributions

The particle size distributions of pristine GNPs and all treated GNPs dispersed in distilled water were analyzed after 15 days and the results are shown in Figure 4.21. It shall be noted that the particle concentration used during the measurements is 0.01 wt.%.

It is found that the relative particle concentration of the water-based treated GNP nanofluids conforms well to the particle size distributions. The average particle size of the water-based pristine GNP nanofluid and water-based treated GNP nanofluid on Day 1 and Day 15 after sample preparation are summarized as shown in Table 4.8. It is evident that the average particle size is very large (more than 1,000 nm) for pristine GNPs after 15 days. In contrast, the average particle size is significantly smaller for all the treated GNPs samples (less than ~270 nm). This indicates that the treated GNPs are stable colloids in water.

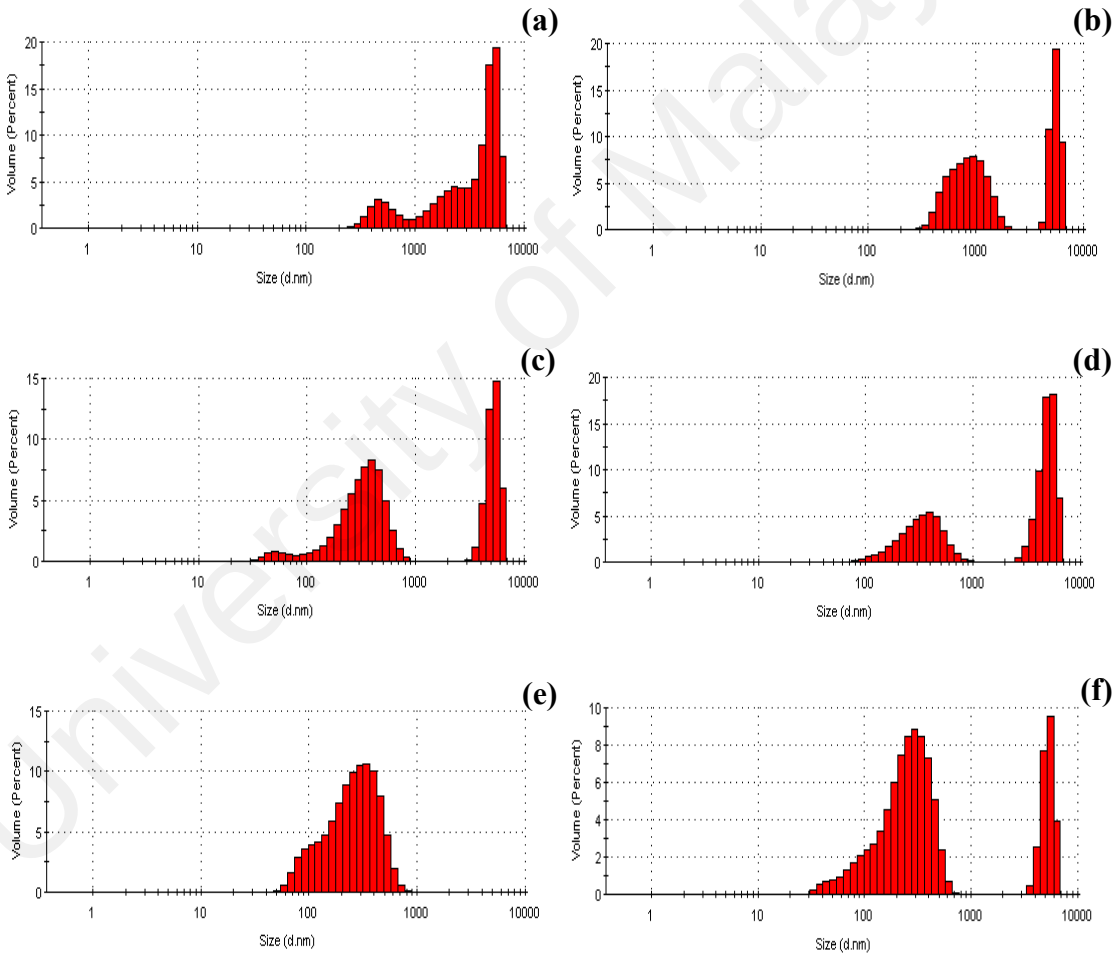

Figure 4.21: Particle size distributions of pristine GNPs on (a) Day 1 and (b) Day 15, TFPEG-treated GNPs on (c) Day 1 and (d) Day 15, and N-doped GNPs on (e) Day 1 and (f) Day 15.

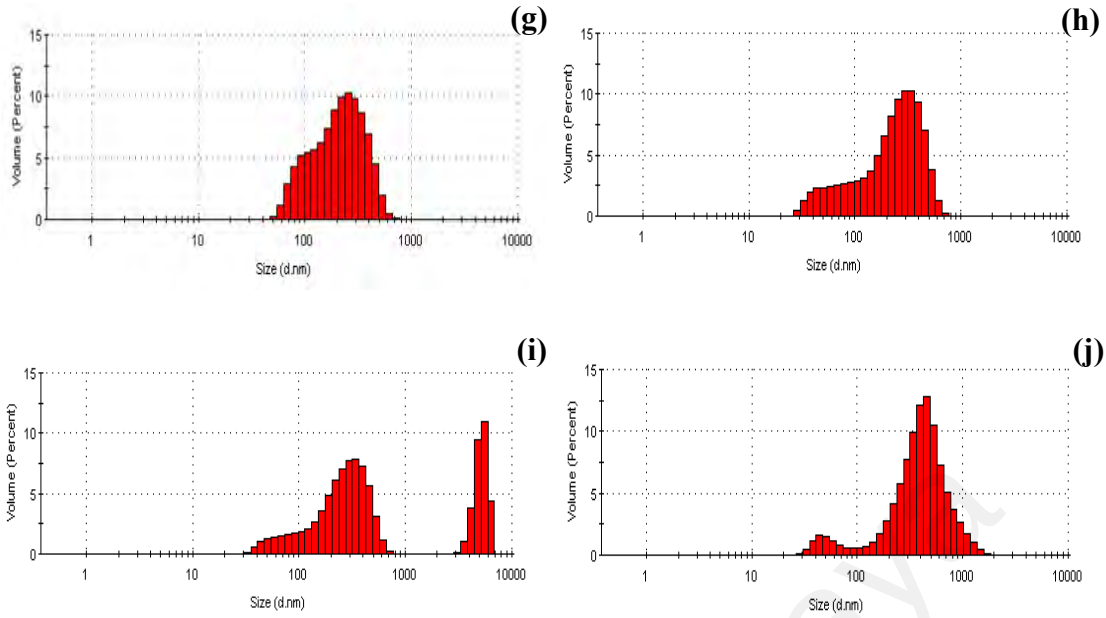

Figure 4.21 (continued): Particle size distributions of XC-treated GNPs on (g) Day 1 and (h) Day 15 and P123-GNPs on (i) Day 1 and (j) Day 15.

Table 4.8: Average particle size values of pristine GNPs, TFPEG-treated GNPs, N-doped GNPs, XC-treated GNPs, and P123-GNPs in water after 1 day and 15 days of preparation. Note that the particle concentration is 0.01 wt.%.

Day(s)	Particle Size Distribution (nm)				
	Pristine GNPs	TFPEG-treated GNPs	N-doped GNPs	XC-treated GNPs	P123-GNPs
1	1060	239.8	175.9	156.4	183.3
15	1133	247.1	180.0	165.1	267.0

4.1.8 Analysis of zeta potential

The zeta potential as another test for the evaluation of colloidal stability was also applied to check the stability of the best samples (Ghadimi, Saidur, & Metselaar, 2011). The value of zeta potential is directly related to the stability of the dispersed nanofluid (Amrollahi, Rashidi, Meibodi, & Kashefi, 2009; H. T. Zhu et al., 2007). The repulsion that rises between the particles of the same charge determines the stability of the dispersion. Therefore, the particles with high surface charge will have low possibility to agglomerate (J. H. Lee et al., 2008). In addition, the measured zeta potential value for the nanofluids with the range of < -30 mV and > +30 mV is also considered to have physically

stable colloids (W. Yu & Xie, 2012). Figure 4.22 shows the zeta potential values measured by Zetasizer Nano ZS for pristine GNPs, TFPEG-treated GNPs, N-doped GNPs, XC-treated GNPs, and P123-GNPs samples after 1 day and 15 days. The details can be seen in Table 4.9. The zeta potential is -24.7 mV for the water-based pristine GNP nanofluid on Day 1, which indicates that the dispersion is less stable. The pristine GNP dispersion becomes more unstable after 15 days, which is evident from the increase in zeta potential (-14.2 mV). This indicates that the pristine GNPs are unstable in water. Meanwhile, all treated-GNPs samples show high colloidal stability in water, where the zeta potential is more than -30 mV on Day 1 and there is only a slight increase in the zeta potential after 15 days. This proves that all of the treated GNPs samples are stable in water after 15 days of preparation.

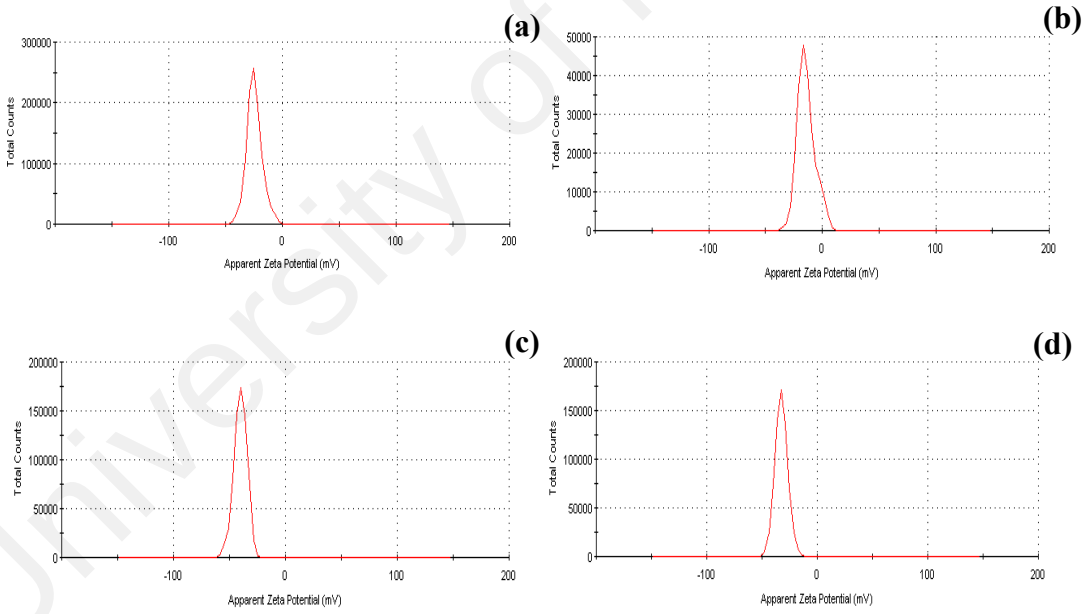

Figure 4.22: Zeta potential of pristine GNPs on (a) Day 1 and (b) Day 15 and TFPEG-treated GNPs on (c) Day 1 and (d) Day 15.

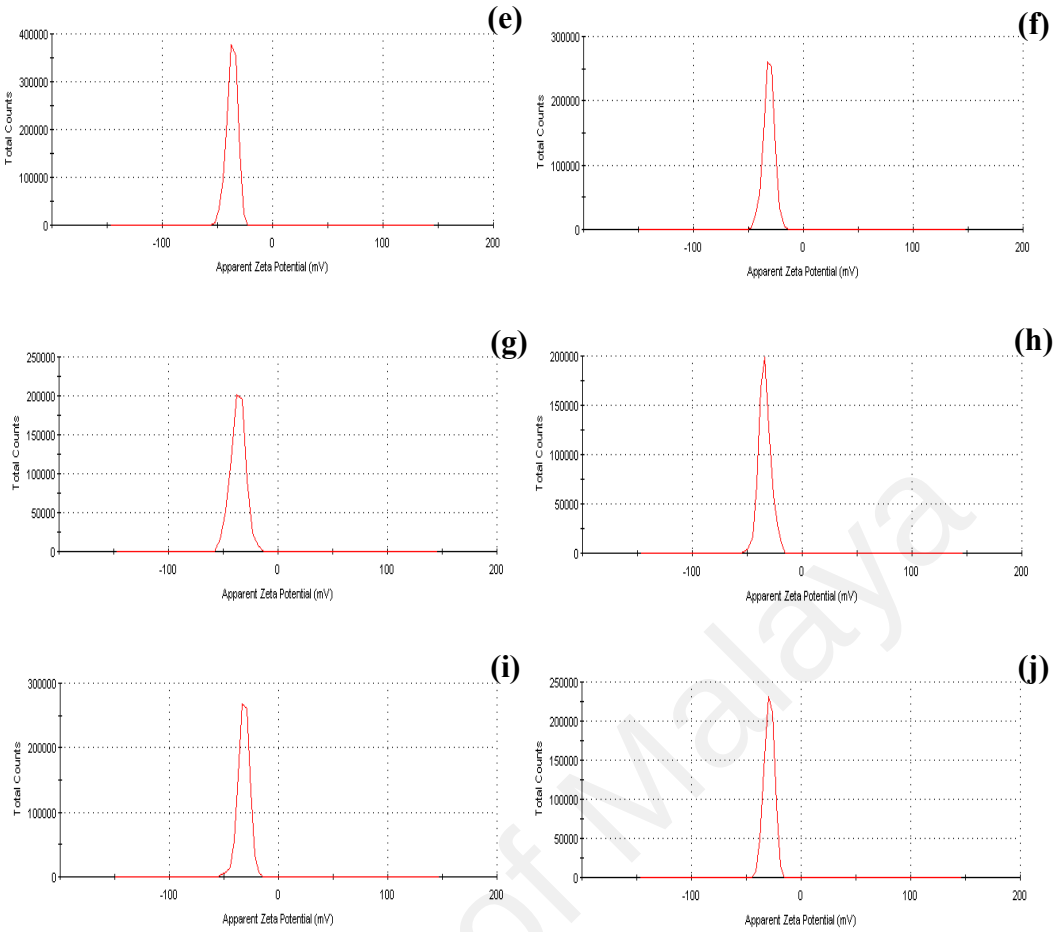

Figure 4.22 (continued): Zeta potential of N-doped GNPs on (e) Day 1 and (f) Day 15, XC-treated GNPs on (g) Day 1 and (h) Day 15, and P123-GNPs on (i) Day 1 and (j) Day 15.

Table 4.9: Zeta potential values of pristine GNPs, TFPEG-treated GNPs, N-doped GNPs, XC-treated GNPs, and P123-GNPs in water after 1 day and 15 days of preparation. Note that the particle concentration is 0.01 wt.%.

Day(s)	Zeta Potential (mV)				
	Pristine GNPs	TFPEG-treated GNPs	N-doped GNPs	XC-treated GNPs	P123-GNPs
1	-24.7	-40.3	-36.8	-36.3	-31.9
15	-14.2	-32.5	-31.4	-34.0	-30.1

4.1.9 Evaluation of thermal conductivity

Thermal conductivity at different temperatures between 20 and 60 °C was measured for all treated GNPs samples using KD2-Pro thermal properties analyzer. In order to validate the analyzer (KD2-Pro), the data for the distilled water were compared with the standard data of (Ramires et al., 1995) as shown in Figure 4.23. As expected, the

measured thermal conductivity for distilled water increased when the temperature increased. The average error obtained is ±0.9%, which is still below the satisfied value to work with the KD2-Pro analyzer. Thus, it can be concluded that KD2-Pro works with satisfactory condition and the data obtained from the measurement using this analyzer are considered reliable.

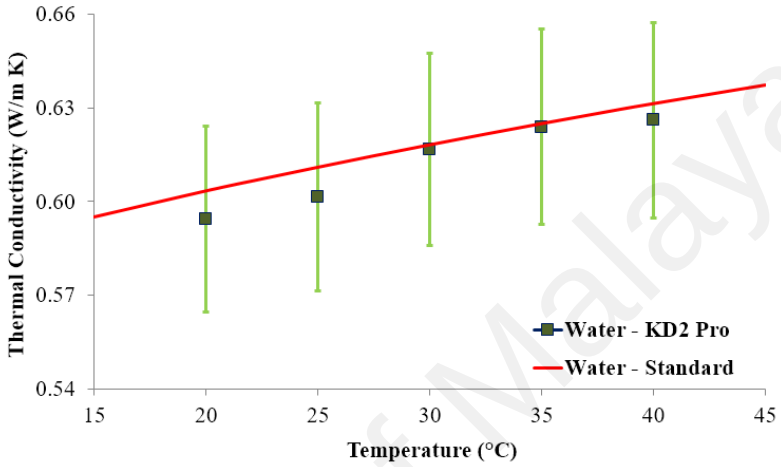

Figure 4.23: Comparison of thermal conductivity values of distilled water between NIST standard (Ramires et al., 1995) and KD2-Pro thermal property analyzer measurements. The error bars indicate an average error of ±0.9%.

The measured thermal conductivity values for 0.025, 0.05, 0.075, and 0.1 wt.% of water-based TFPEG-treated GNPs, N-doped GNPs, XC-treated GNPs, and P123-GNPs are plotted versus temperature and shown in Figure 4.24(a) until Figure 4.24(d). It can be seen that the thermal conductivity increases when the temperature increases, which is in a good agreement with the trend of the data obtained for distilled water. Within the range of the temperatures studied, the enhancement of the thermal conductivity values at the temperature of 20–60 °C for all concentrations of water-based TFPEG-treated GNPs, N-doped GNPs, XC-treated GNPs, and P123-GNPs dispersions is in the range of 2.4%–31.7%, 0.84%–13.0%, 3.2%–34.0%, and 2.5%–24.5%, respectively, when compared to distilled water. This shows that the prepared water-based functionalized GNPs nanofluids

have significantly higher thermal conductivity than that of distilled water without GNPs nanoparticles.

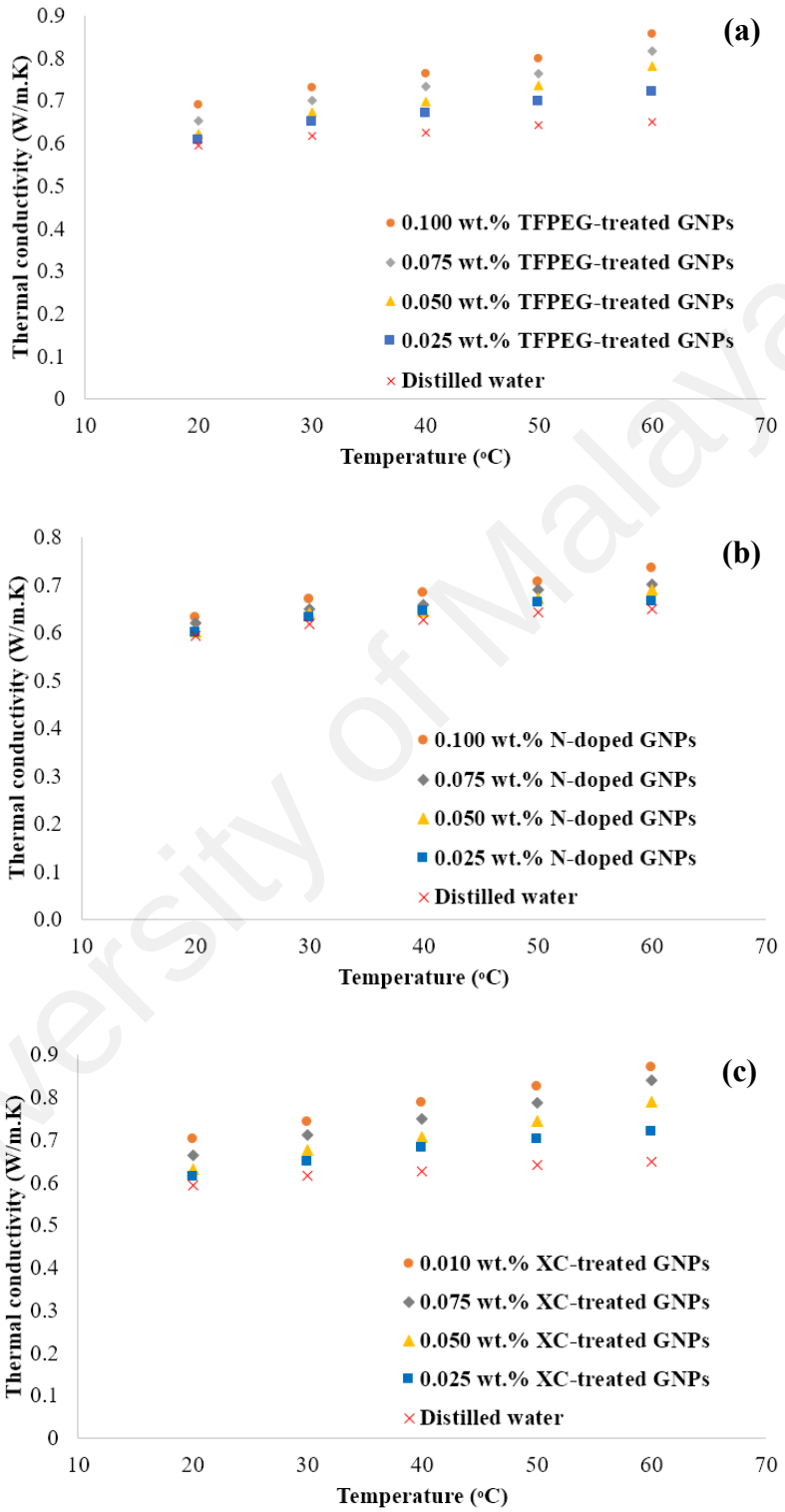

Figure 4.24: Thermal conductivity versus temperature for water-based (a) TFPEG-treated GNPs, (b) N-doped GNPs, and (c) XC-treated GNPs nanofluids at all concentrations.

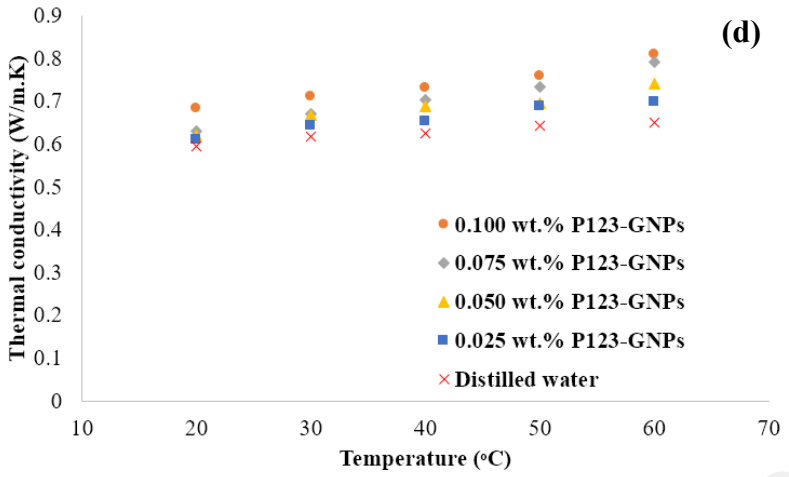

Figure 4.24 (continued): Thermal conductivity versus temperature for water-based (d) P123-GNPs nanofluids at all concentrations.

4.1.10 Evaluation of viscosity

In order to validate the reliability of viscosity measurements made using the rotational rheometer, the viscosities of distilled water were measured at different temperatures and the results were compared with the standard data published by the National Institute of Standards and Technology (NIST). The obtained results are shown in Figure 4.25. It is found that the average error in the viscosity for distilled water is ±2.47% at different temperatures. This indicates that the difference in the viscosity values measured using the experimental setup in this study and the values given in the NIST standard data is pretty small. Hence, it is deduced that the rotational rheometer is reliable to measure the viscosities of the nanofluids and the results can be taken with confidence.

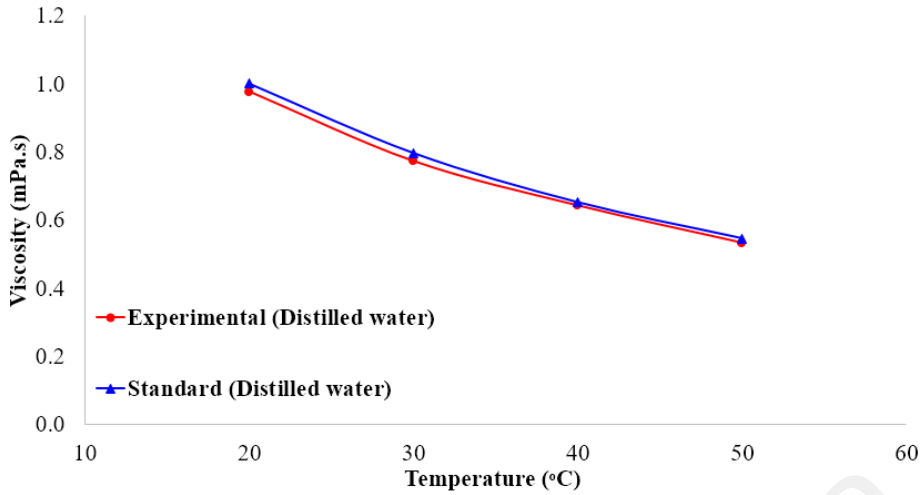

Figure 4.25: Viscosity versus temperature for distilled water (experiments and NIST standard).

The viscosity of the water-based TFPEG-treated GNPs, N-doped GNPs, XC-treated GNPs, P123-GNPs nanofluids (at different particle concentrations of 0.025, 0.05, 0.075, and 0.1 wt.%), and distilled water as a function of temperature is shown in Figure 4.26(a) until Figure 4.26(d). The viscosity measurements were performed within the fluid temperature range of 20–50 °C. It can be seen from the results that the viscosity decreases with an increase in temperature for both water-based treated-GNP nanofluids and distilled water. It is believed that this is due to the weakened intermolecular forces of the nanofluids as the fluid temperature is increased. However, it is apparent that there is no significant difference in the viscosities between the water-based treated-GNP nanofluids and distilled water, and there is only a slight increment in the viscosities for the nanofluids. This slight increment is certainly an advantage of all water-based treated-GNP nanofluids because this will reduce the pumping power required if these nanofluids are used as working fluids in heat transfer systems (Sarsam, Amiri, Kazi, et al., 2016; Sarsam, Amiri, Zubir, et al., 2016).

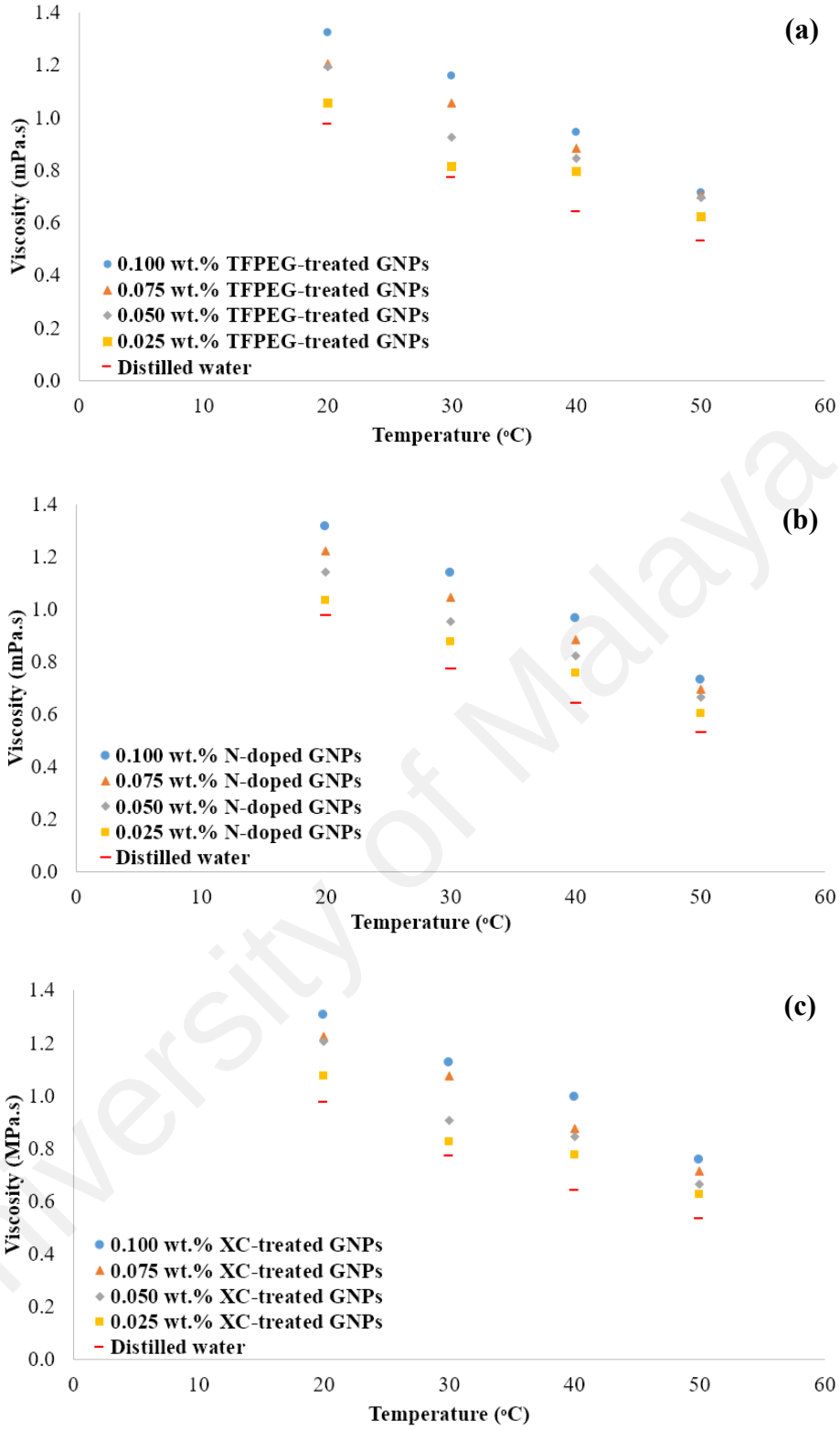

Figure 4.26: Viscosity versus temperature for water-based (a) TFPEG-treated GNPs, (b) N-doped GNPs, (c) XC-treated GNPs nanofluids at all concentrations, and distilled water.

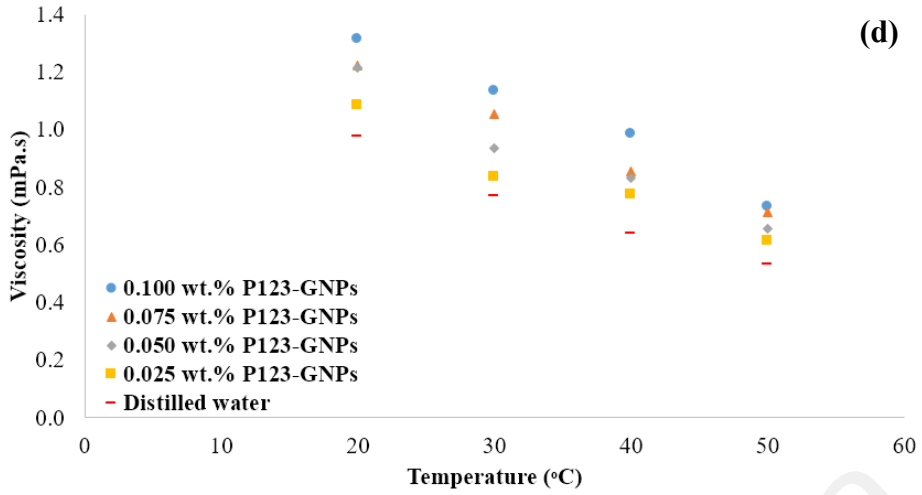

Figure 4.26 (continued): Viscosity versus temperature for water-based of (d) P123-GNPs nanofluids at all concentrations and distilled water.

Figure 4.27(a) shows the viscosity behavior of distilled water with Newtonian behavior within the whole range of shear rate for the temperature range from 20 to 50 °C. The Newtonian behavior means that the viscosity of a particular nanofluid is less viscous. Less viscosity will give better performance, which will reduce the pumping power and pressure loss when used in heat transfer fields. The same behavior could be observed once TFPEG-treated GNPs, N-doped GNPs, XC-treated GNPs, and P123-GNPs nanofluids are applied, which showed almost constant viscosity within the tested range. The results can be seen in Figure 4.27(b) until Figure 4.27(d). The measurement was carried out for all water-based treated-GNPs nanofluids and 0.1 wt.% particle concentration was selected as the concentration for further performance analysis in heat-based applications. Thus, it can be said that all of the prepared samples (TFPEG-treated GNPs, N-doped GNPs, XC-treated GNPs, and P123-GNPs) have low increment in viscosity with Newtonian behavior, which can be concluded as a good material for future use.

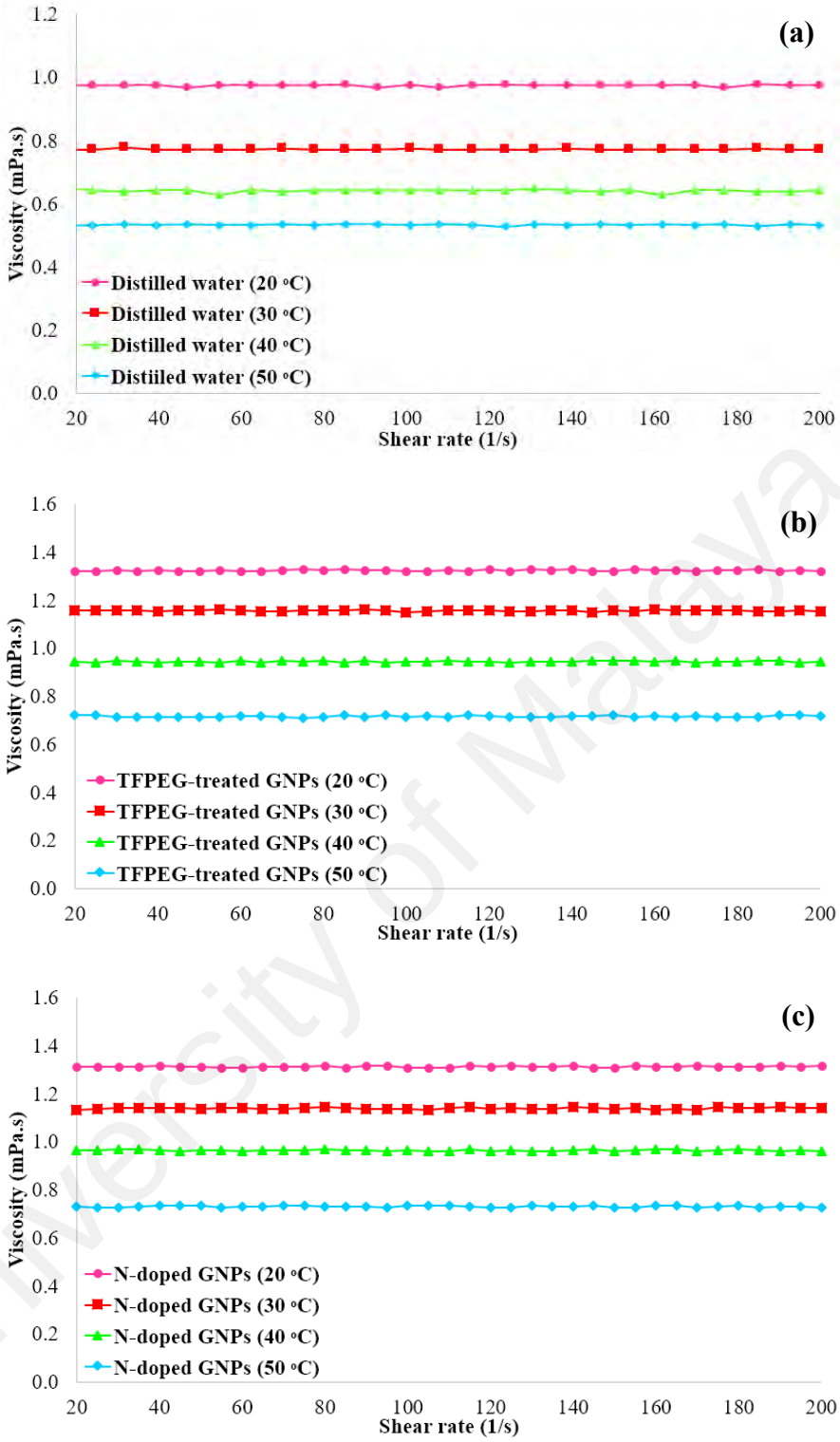

Figure 4.27: Viscosity versus shear rate at different temperatures for (a) distilled water, water-based (b) TFPEG-treated GNPs, and (c) N-doped GNPs nanofluids.

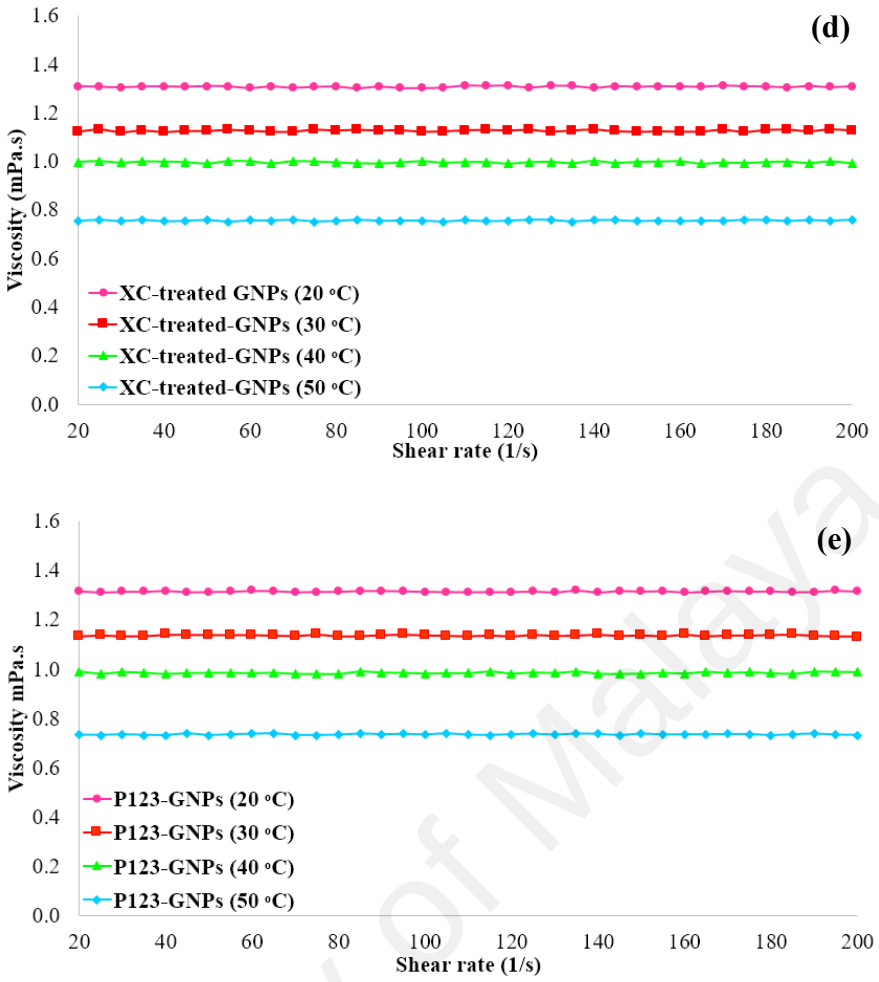

Figure 4.27 (continued): Viscosity versus shear rate at different temperatures for water-based (d) XC-treated GNPs and (e) P123-GNPs nanofluids.

4.2 Investigation on the performances of the functionalized GNPs toward heat-based applications

4.2.1 Heat-transfer field

4.2.1.1 Experiment on turbulent convective heat transfer

Figure 4.28 provides the plot of Re for water and nanocolloids undergoing forced internal flow under constant mean velocity approach. As highlighted previously, the main cause of Re drop lies on the increase in viscosity of the colloids which is more dominant compare to density increase in Re calculation. By keeping the velocity constant, a more realistic results will manifest to account only the role of colloids in affecting the thermal transport performance. It has been reported that as high as 50% to 200% of viscosity

increase manifest with the use of colloidal solution, far greater than the thermal conductivity rise which experience 2-10 folds less in magnitude (Chon, Kihm, Lee, & Choi, 2005; Das, Putra, Thiesen, & Roetzel, 2003; Prasher, Song, Wang, & Phelan, 2006; Timofeeva, Routbort, & Singh, 2009).

This strongly implies that maintaining constant Re for colloids in convective heat transfer study may hold ineffective outcome since the velocity and pumping power has to be increased and the projected heat transfer performance should the water is run under the same condition could simply overcast if not offset the improvement made by the colloids. Timofeeva and others (Timofeeva et al., 2009) emphasized this point in her report suggesting that exponential increase in viscosity will profoundly mask any benefit of thermal conductivity increment and led to the negative improvement in thermal transport application. This issue has been demonstrated previously by Pak and Cho (Pak & Cho, 1998) who recorded significant drop in heat transfer performance for metal oxide based nanocolloids at increasing particle loading running under constant velocity mode. Due to this adverse effect, much of the investigations on internal convective heat transfer have been conducted under low concentration to contain the nonlinear trend in viscosity increase (Aravind et al., 2011; Sundar, Singh, & Sousa, 2014). Nevertheless, for graphene and CNT based colloids, the morphology aspect of the material structure implies that the increase in viscosity is greater compare to metal oxide nanoparticles which is mostly synthesized in much smaller size and mostly in spherical shapes. This will eventually impact the flow and performance of heat transfer in convective mode at high concentration. Further, it is evident that most of the viscosity measurement were conducted at high starting shear rate, indicating the inadequacy in profiling the true nature of the colloids at laminar sublayer region where most of the hydrodynamic and thermal transport manifest.

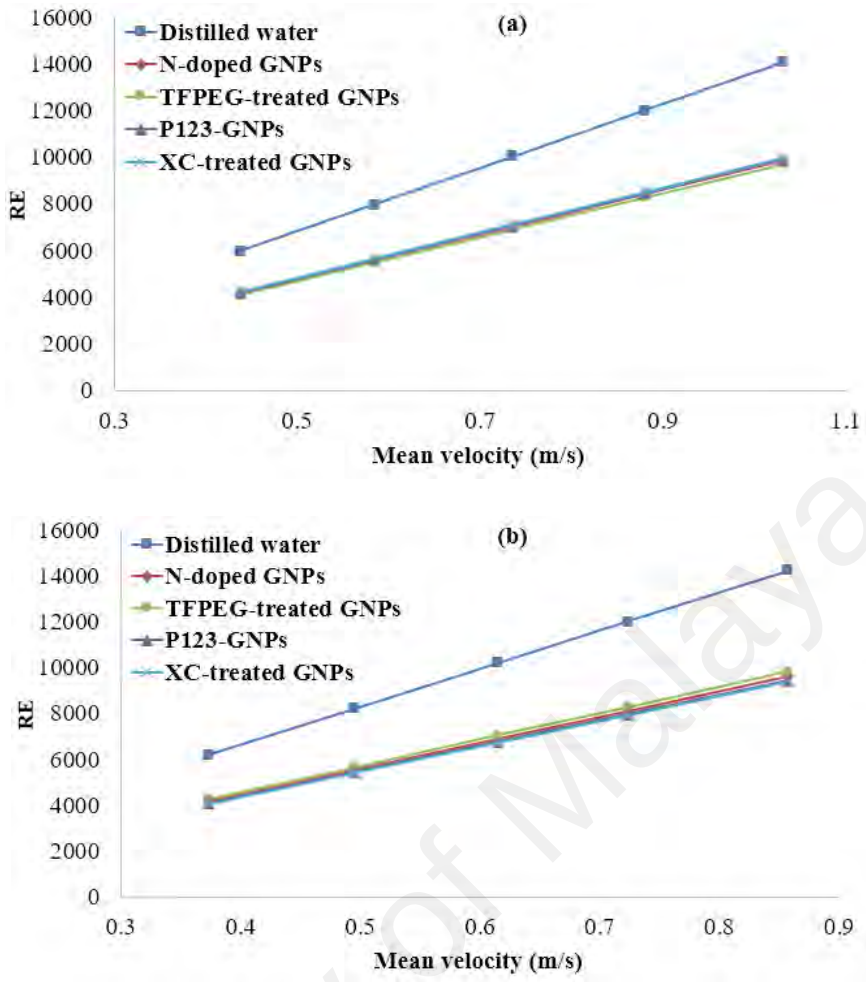

Figure 4.28: Comparison of Re at specific mean velocity between different colloids (0.1w %) and water at (a) 30°C and (b) 40°C. The heat flux for both conditions was set at 13429w/m^2.

Figure 4.29 to Figure 4.32 provide the average Nusselt number and friction factor plots for the water run experiment at different temperature. Using Gnielinski correlation as reference (Gnielinski, 1976), as low as 5% and 9% deviation was determined between the lowest and the high velocities at 30°C bulk temperature for high heat flux (i.e. 13429W/m^2) while 2% to 8% difference was calculated at 40°C. On the other hand for low heat flux condition (6731W/m^2), a much lower deviation of less than 2% was evident at 30°C while the similar trend of deviation to the high heat flux condition was established (i.e. 4% to 8% difference). On similar note, comparison between the current results with established correlations (i.e. (Petukhov, 1970) and (Dittus & Boelter, 1930) also revealed close agreement. The results verified the test rig capability to perform further

investigation on convective heat transfer based on high conformity results with the well-establish correlation. In addition, the friction factor calculation for water based on the pressure drop measurement was found to be in similar range to the established empirical correlation and largely insensitive to the bulk temperature difference. The highest difference (11%) was recorded at the highest velocity for 30°C, 6731W/m^2 combination while the lowest (1%) was recorded for 40°C, 13429W/m^2 combination. It is interesting to note that due to the constant mean velocity approach adopted in the present study, a relatively negligible increase in friction factor was expected to manifest. By substituting the friction factor in Darcy-weisbach expression with blassius (Blasius, 1913) explicit approximation, the pressure drop for a turbulent flow in smooth circular conduit can be described by the following formula:

$$\Delta p = 0.074 L \rho^{3/4} V^{7/4} \mu^{1/4} D^{5/4} \qquad \text{eq. 2}$$

The expression underlines the impact of various parameters within the calculation of pressure drop. It is evident that a slight change in velocity will significantly affect pressure drop calculation due to the power factor associated to its term. Thus, by maintaining the velocity similar to the controlled experiment (i.e. water run), the change in pressure drop will be minimal, unlike when a constant Re was chosen whereby the corresponding increase in velocity is to be powered by almost two magnitude. Therefore, in this context, further investigation on the effect of nanocolloids in friction factor was not conducted.

In order to provide the reliability factor on the raw data measurement and derived parameters calculation such as Nu, friction factor and heat transfer coefficient, an uncertainty analysis was performed on the data based on error propagation principle underlined by Kline and McClintock (S. Kline & F. McClintock, 1953) as well as Taylor and Thompson (J. Taylor, 1997). Table 4.10 provides the parameters involved within the

present heat transfer analysis along with their uncertainty values. The procedure and formula to conduct the above analysis is given in the appendix.

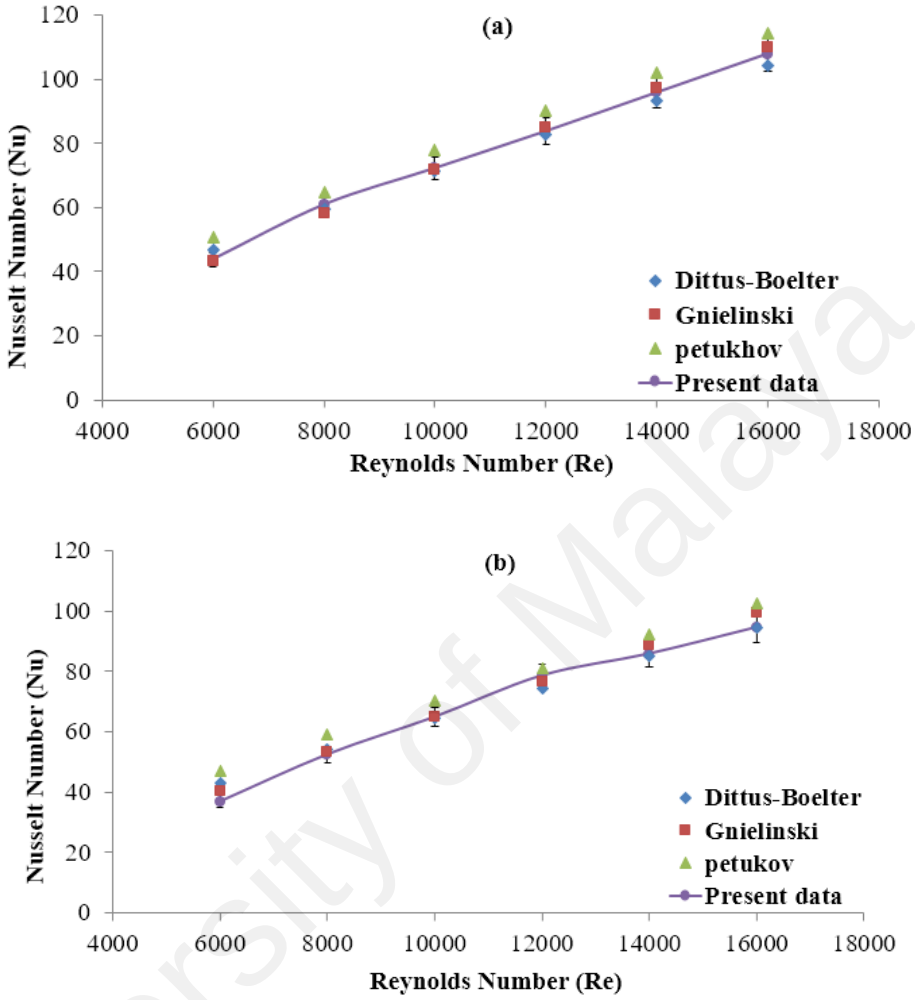

Figure 4.29: Comparison of average Nusselt number at increasing Re between present measurement and literature for (a) 30°C and (b) 40°C. The heat flux for both conditions was set at 6731w/m^2.

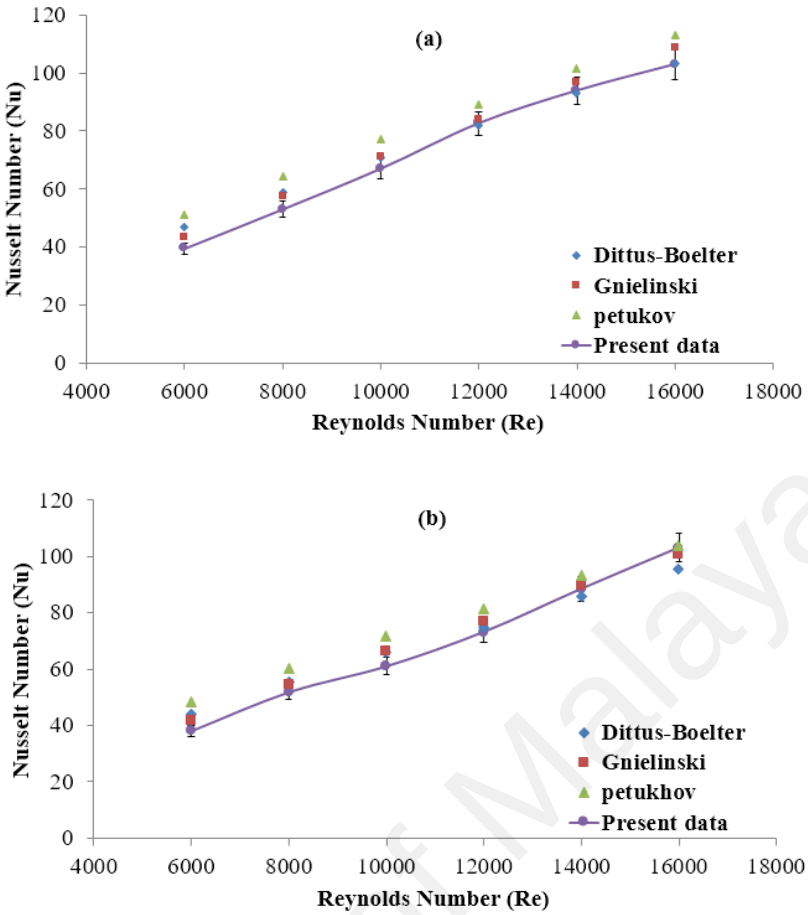

Figure 4.30: Comparison of average Nusselt number at increasing Re between present measurement and literature for (a) 30°C and (b) 40°C. The heat flux for both conditions was set at 13429w/m^2.

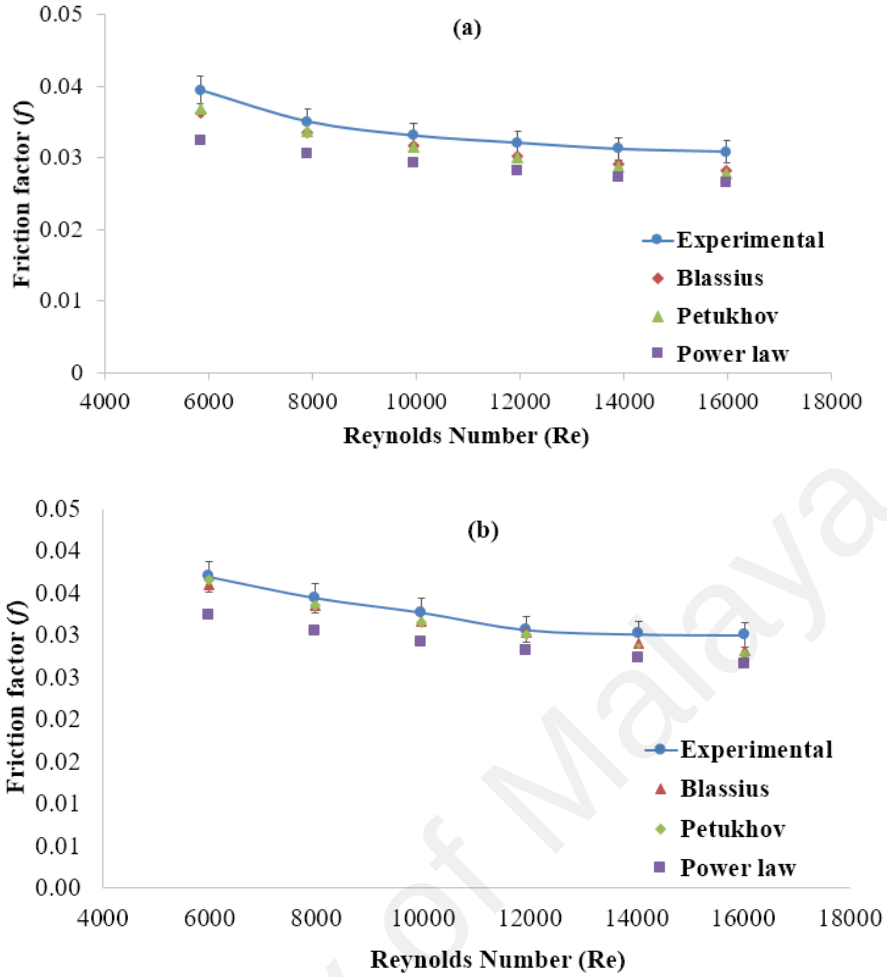

Figure 4.31: Plot of friction factor against Reynolds number at (a) 30°C and (b) 40°C for water and its comparison to existing correlation. The heat flux for both conditions was set at 6731W/m².

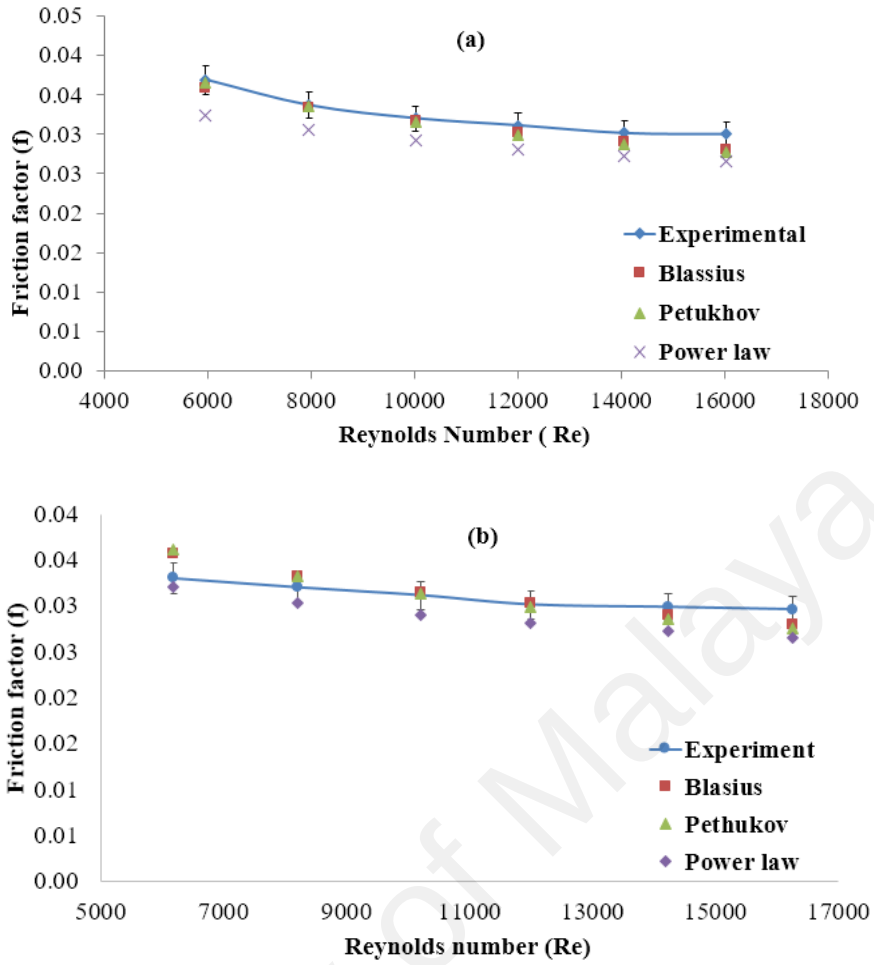

Figure 4.32: Plot of friction factor against Reynolds number at (a) 30°C and (b) 40°C for water and its comparison to existing correlation. The heat flux for both conditions was set at 13429W/m^2.

Table 4.10: List of uncertainty for different parameters governing the present heat transfer experiment.

Parameter	Uncertainty (%)
Heat flux (q)	1.7
Heat transfer coefficient (h)	1.8
Nusselt Number (Nu)	5.2
Mass flow rate (m)	0.8
Reynolds Number (Re)	1.5
Friction factor	6.4

Figure 4.33 until Figure 4.36 provide the plot of both local Nusselt number (Nu) and local heat transfer coefficient (h) for water run. The results showed that both parameters experienced relatively similar magnitude along the axial position from the upstream. This

shows that the flow was under thermally and hydrodynamically developed state when it reached the first measurement point and remain unchanged thereafter. Also both parameters undergo linear increase with respect to increasing Re, which of the similar trend to the existing convective heat transfer process found in the literature. These results follows the well-established convention in the study of close conduit heat transfer, particularly on the thermal boundary length identification (Deissler, 1954).

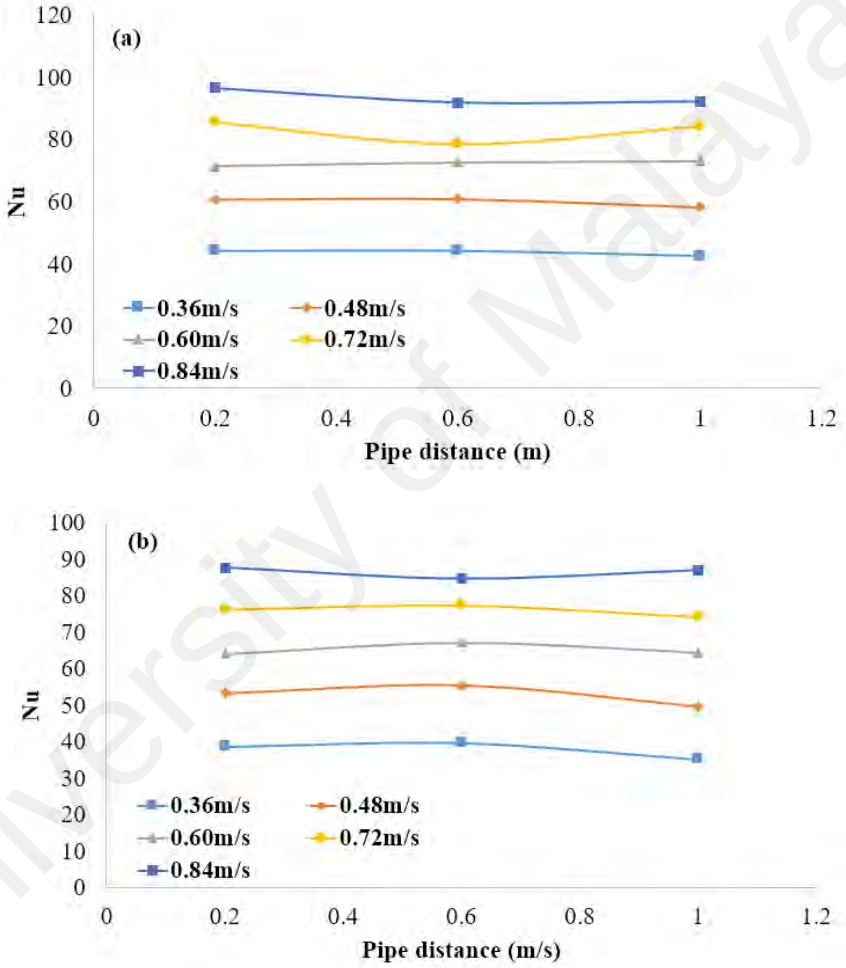

Figure 4.33: Plot of local Nusselt number along axial dimension for water test run at (a) 30°C and (b) 40°C. The heat flux for both conditions was set at 6731W/m^2.

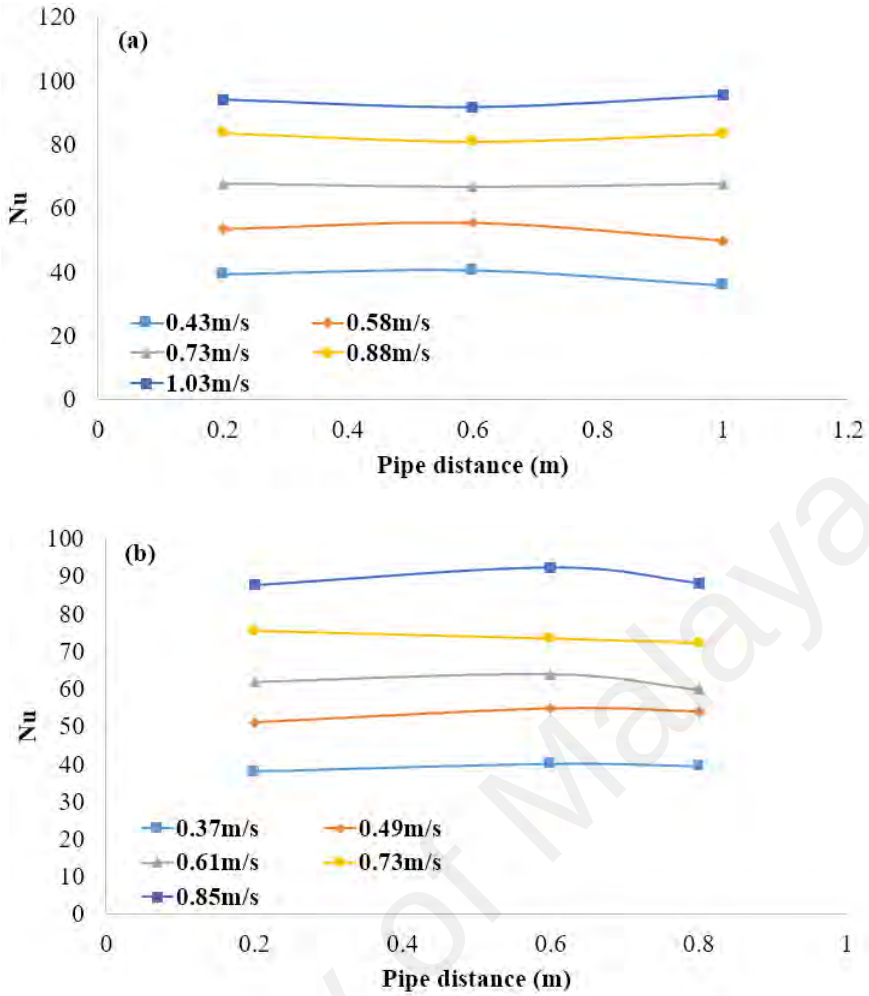

Figure 4.34: Plot of local Nusselt number along axial dimension for water test run at (a) 30°C and (b) 40°C. The heat flux for both conditions was set at 13429W/m^2.

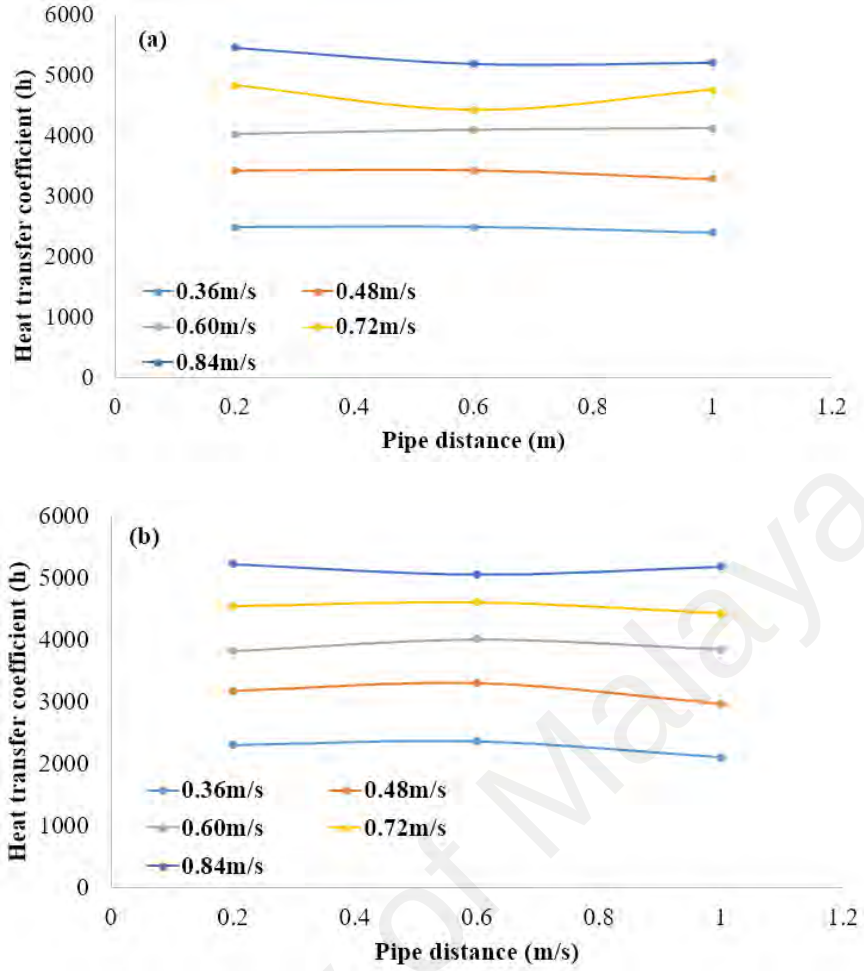

Figure 4.35: Plot of local heat transfer coefficient number along axial dimension for water test run at (a) 30°C and (b) 40°C. The heat flux for both conditions was set at 6731W/m^2.

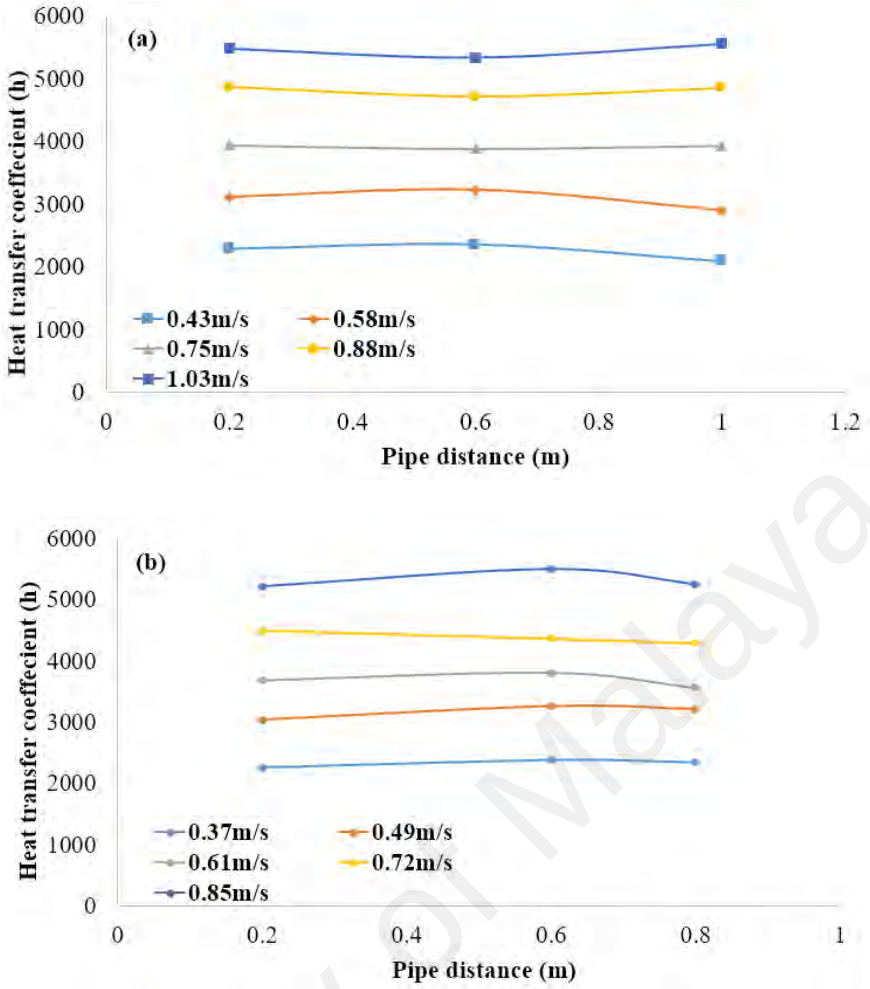

Figure 4.36: Plot of local heat transfer coefficient along axial dimension for water test run at (a) 30°C and (b) 40°C. The heat flux for both conditions was set at 13429W/m^2.

Investigation was extended by evaluating the effect of adding different functionalized GNPs on the present water base fluid under convective mode heat transfer as shown in Figure 4.37 until 4.40. The results highlighted that all materials showed positive impact on the heat transfer based on the improvement in both Nu and h with respect to water. Further, the increment was more pronounced for h since the Nu requires the inclusion of thermal conductivity value, k into the formula that offset the impact of in convective mode in contributing to the improvement of heat transfer. It is worthy to highlight that the use of bulk thermal conductivity in heat transfer analysis has been critically argued by several researchers (Bianco, Manca, & Nardini, 2011; Buongiorno, 2006). They emphasized on the need to employ much more realistic approach in conducting the analysis, particularly

by varying the particle concentration from the maximum at free flow region to zero at the wall. They added that based on this approach, the increment in k will not induce pronounced conduction effect relative to water at the near wall and the resultant Nu increment will match the h which is insensitive of the k variation. Based on the above argument, it is suggested that the increment in heat transfer in dominated by the particle behavior at the boundary layer region which is the active site of heat transfer. Some researchers have suggested that transport behavior of the particles at this region induces micro-convection phenomenon which allow the heat to be carried to the mainstream region (Eapen et al., 2007; Prasher et al., 2006). This concept of heat transfer enhancement has been practiced using fiber and bubbles which have shown significant increase (Kazi, Duffy, & Chen, 2014; Kitagawa & Murai, 2013). Uniquely, the enhancement was also reported for natural fiber which is known to possess much lower thermal conductivity relative to water, further reinforcing the idea of the role of particle interaction within the active layer to contribute to the improvement in heat transfer. In the present circumstance, it is believed that the above phenomenon is coupled with the inherently high thermal conductivity of the particles to give synergistic effect that may explain the significant improvement.

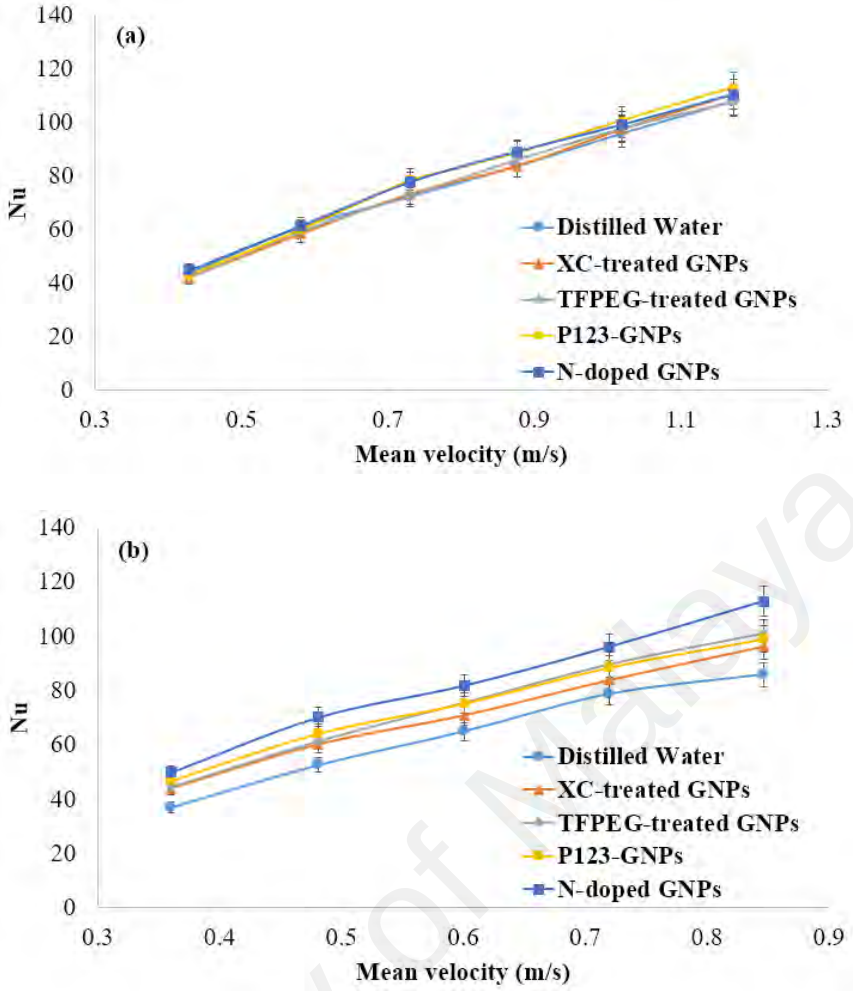

Figure 4.37: Plot of average Nusselt number versus mean velocity at (a) 30°C and (b) 40°C. The heat flux for both conditions was set at 6731W/m^2.

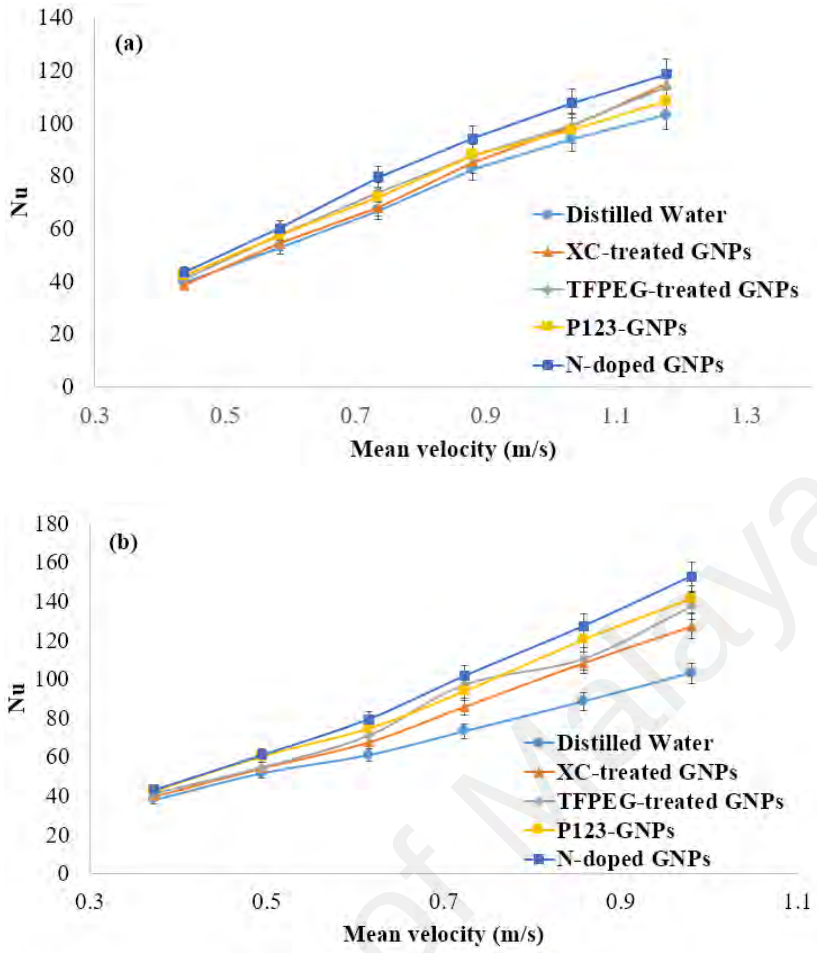

Figure 4.38: Plot of average Nusselt number versus mean velocity at (a) 30°C and (b) 40°C. The heat flux for both conditions was set at 13429W/m^2.

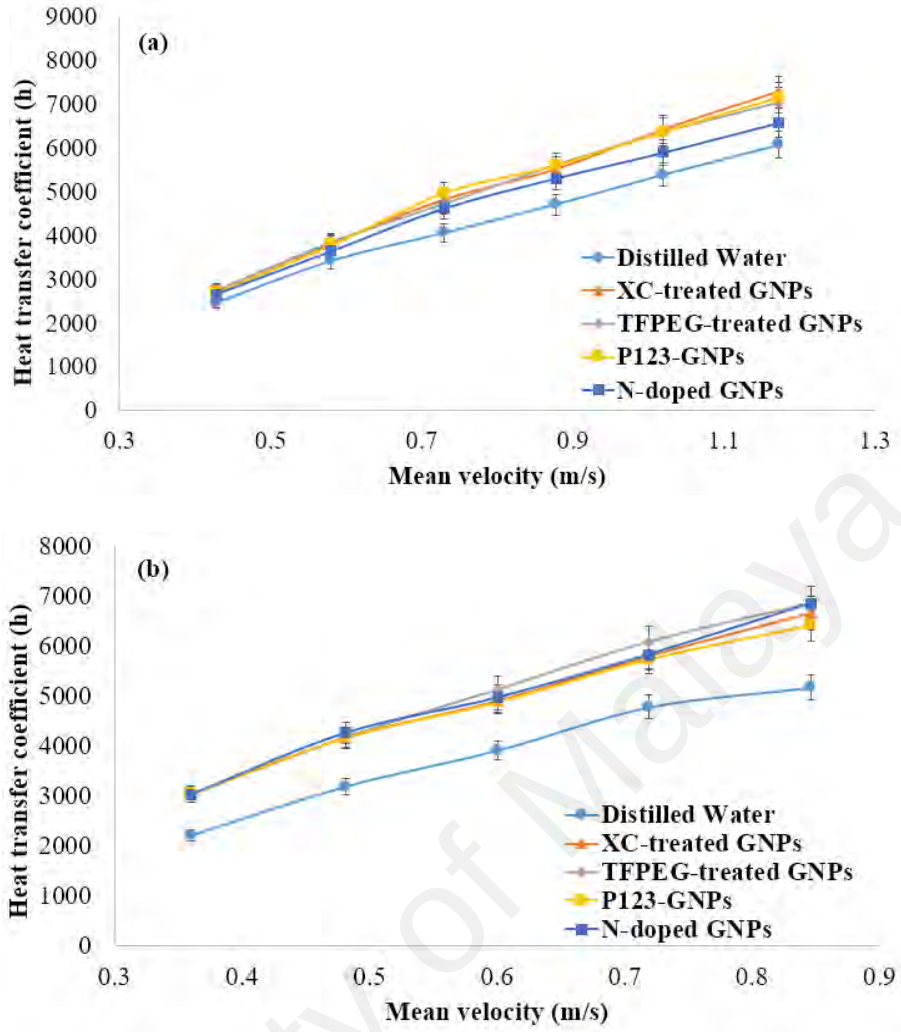

Figure 4.39: Plot of average heat transfer coefficient versus mean velocity at (a) 30°C and (b) 40°C. The heat flux for both conditions was set at 6731W/m^2.

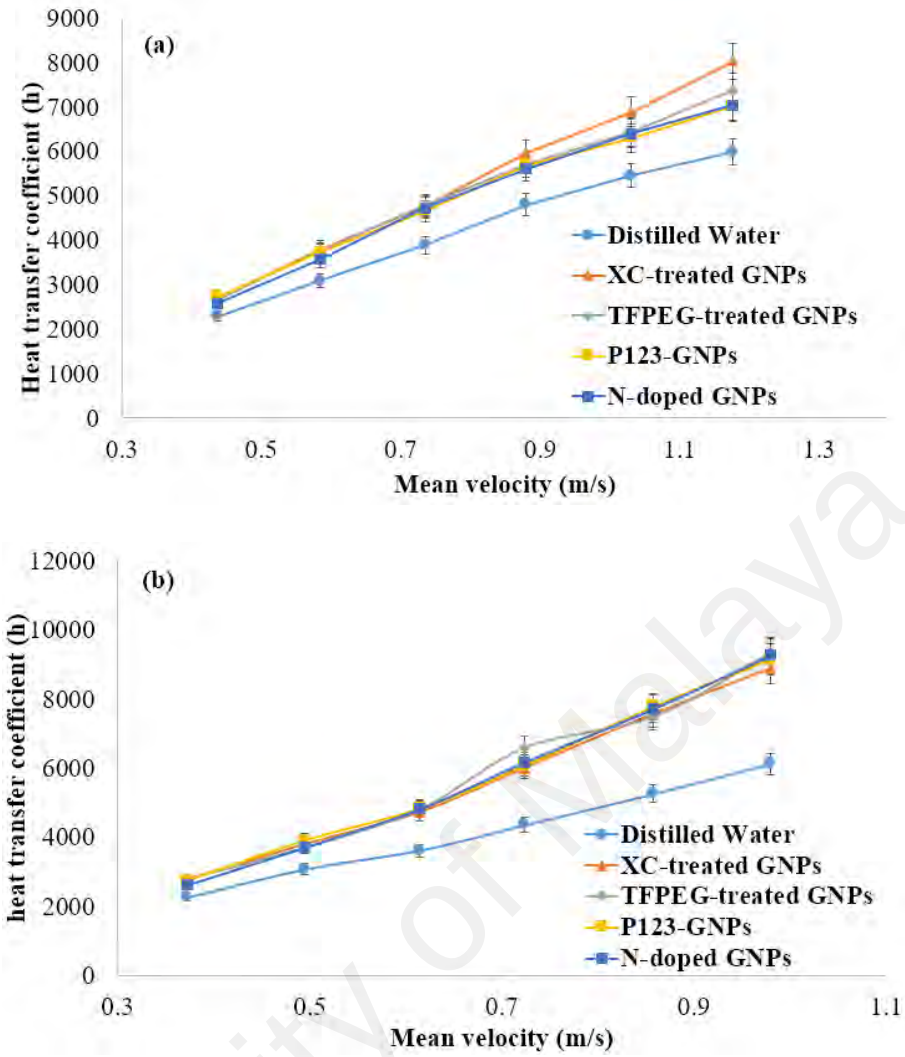

Figure 4.40: Plot of average heat transfer coefficient versus mean velocity at (a) 30°C and (b) 40°C. The heat flux both air conditions was set at 13429W/m^2.

Further assessment on the heat transfer improvement was conducted by monitoring the local heat transfer parameter along the axial length of the test section as highlighted in Figure 4.41 until Figure 4.48. In this exercise, N-doped GNPs, XC-treated GNPs and TPEG-treated GNPs were selected as the material to demonstrate the trend of heat transfer increment under different controlling parameters. The selection was based on the recorded high and low magnitude of average heat transfer parameter whereby N-doped GNPs attained the highest for both temperature and heat flux while XC-treated GNPs and TPEG-treated GNPs were among the lowest. In essence, the results showed much pronounced improvement in h in comparison to Nu. Further, the improvement shows an

increasing trend as the bulk temperature was increased from 30°C to 40°C. The increment is less dominated by the velocity increase at low temperature while at high temperature, the increment is more sensitive to change in flow. Interestingly, the role of heat flux on improving the heat transfer was minimal, judging by the relatively similar trend on improvement for both investigated heat flux conditions. Also, the above trends were found to manifest for all the material selected for the current investigation.

Further detail classification of the level of improvement for the above material is provided by Table 4.11 and Table 4.12. As highlighted previously, increasing the heat flux imposed modest to moderate level improvement to the heat transfer performance, particularly at 30^{o}C as evident by two folds increase and approximately similar magnitude for 40^{o}C. On the other hand, the level of improvement for all the material rise drastically from 30^{o}C to 40^{o}C for each of the selected flux, particularly at high Reynolds number which registered about three folds and five folds increment at Re = 10000. In addition, for each heat flux, increasing Re rendered small to insignificant increment of the heat transfer improvement, further suggested that the trend of improvement in heat transfer performance is dominated by the bulk temperature of the fluid rather than the heat flux and Reynolds number. By invoking the previous argument on heat transport phenomena of multiphase flow, it is suggested that, as a result of reduced viscosity with increasing temperature, much vigorous interaction between particles and the fluid occurs near the wall and this turbulent mixing is enhanced due to less resistance in travelling path. This trend was also captured in bubble enhanced heat transfer where the increase in bulk temperature results in increase in heat transfer quality. These results pave an insight into finding the appropriate combination of fluid parameters to obtain the best heat transfer performance that can be suited to the restriction in heat exchanger dimension and range of operating variables.

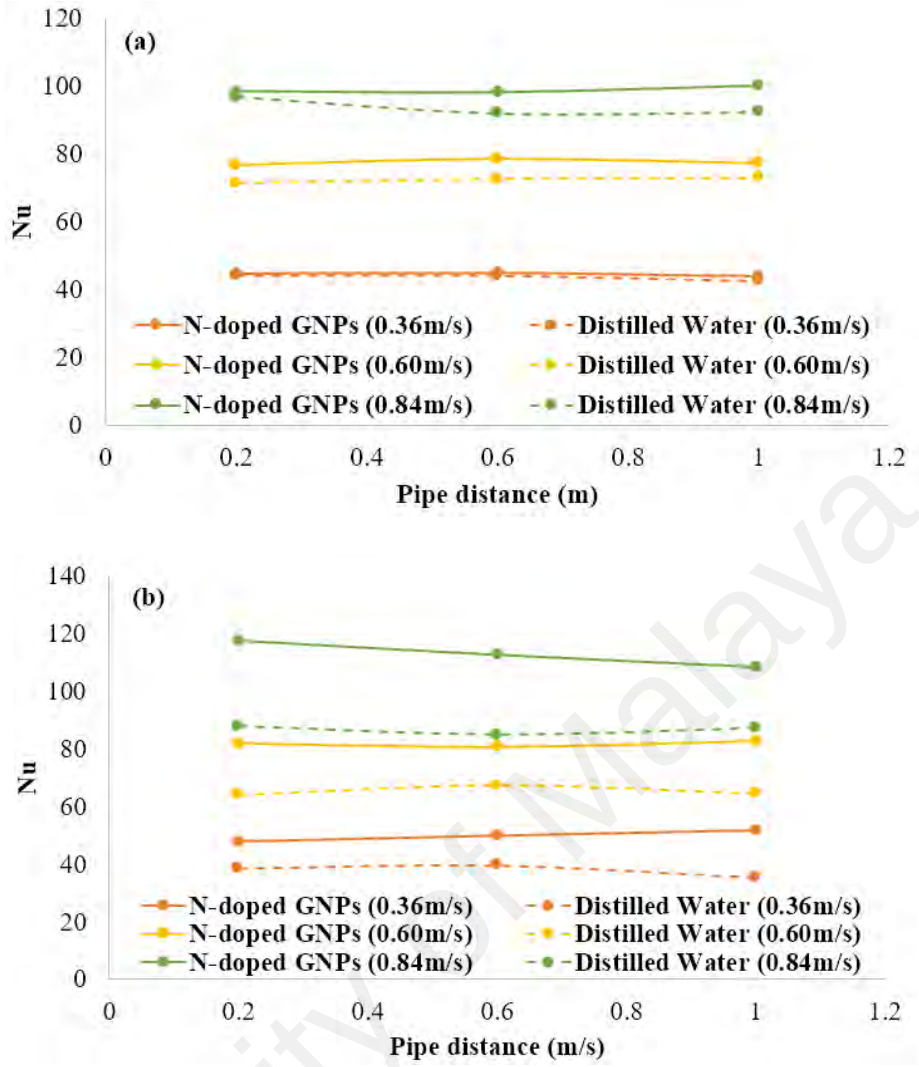

Figure 4.41: Plot of local Nusselt number along axial distance for N-doped GNPs colloid at (a) 30°C and (b) 40°C. The heat flux was set at 6731W/m^2.

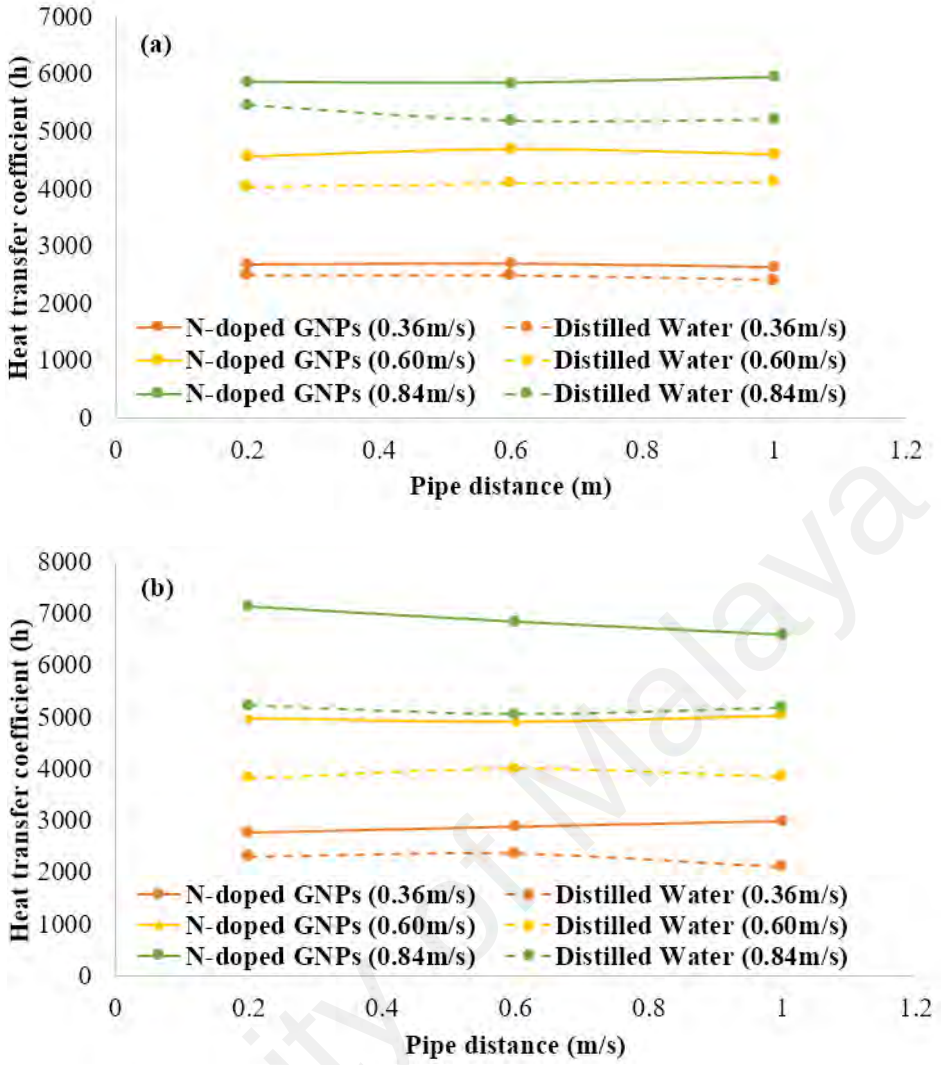

Figure 4.42: Plot of local heat transfer coefficient along axial distance for N-doped GNPs colloid at (a) 30°C and (b) 40°C. The heat flux was set at 6731W/m^2.

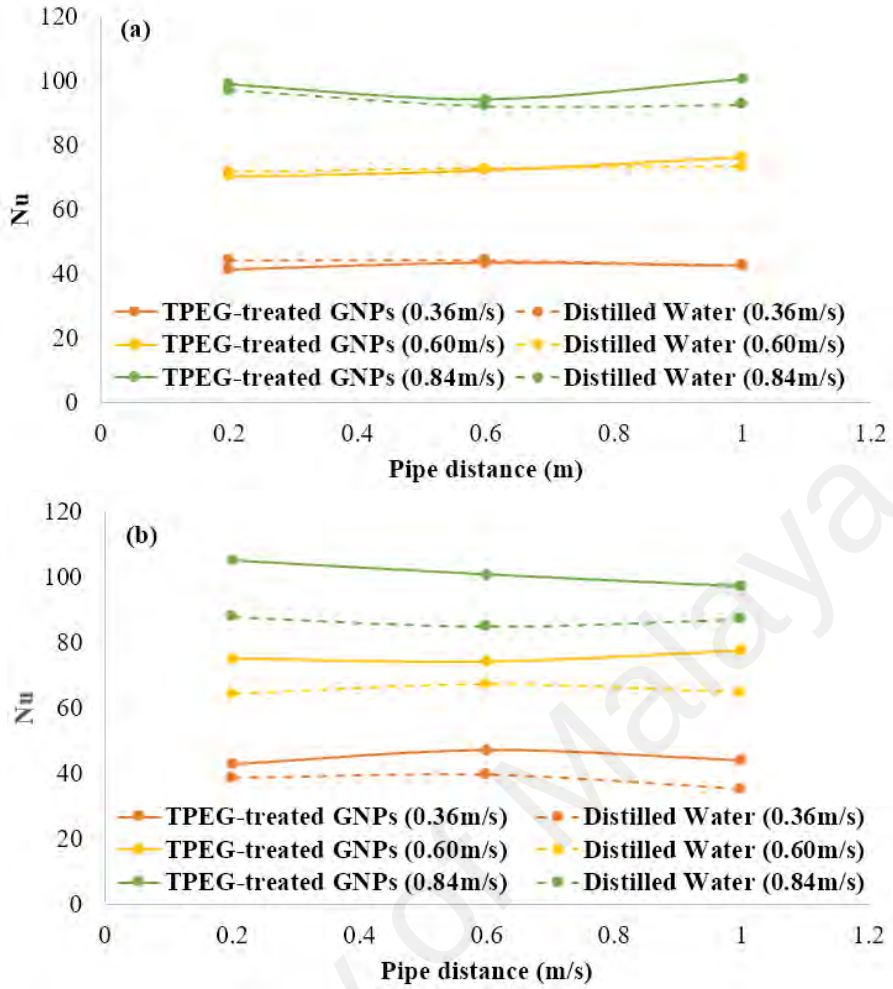

Figure 4.43: Plot of local Nusselt number along axial distance for TFPEG-treated GNPs colloid at (a) 30°C and (b) 40°C. The heat flux was set at 6731W/m².

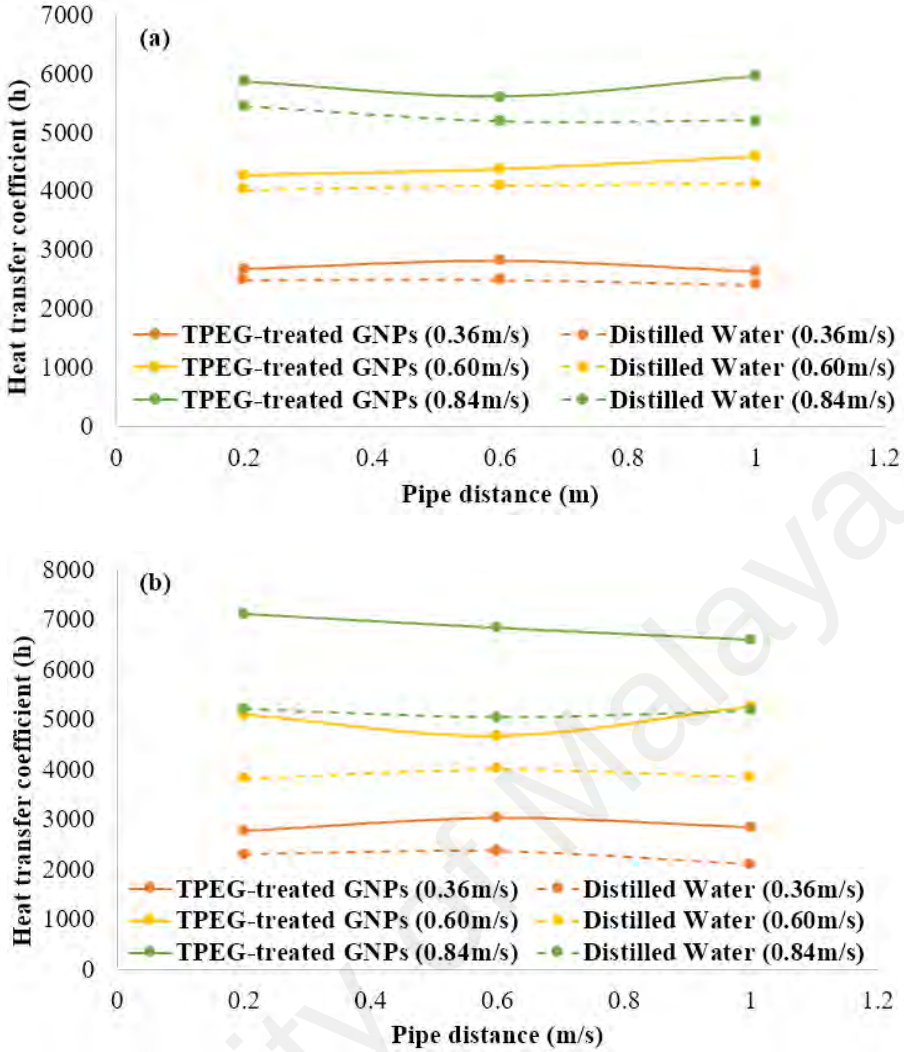

Figure 4.44: Plot of local heat transfer coefficient along axial distance for TFPEG-treated GNPs colloid at (a) 30^{o}C and (b) 40^{o}C. The heat flux was set at 6731W/m^{2}.

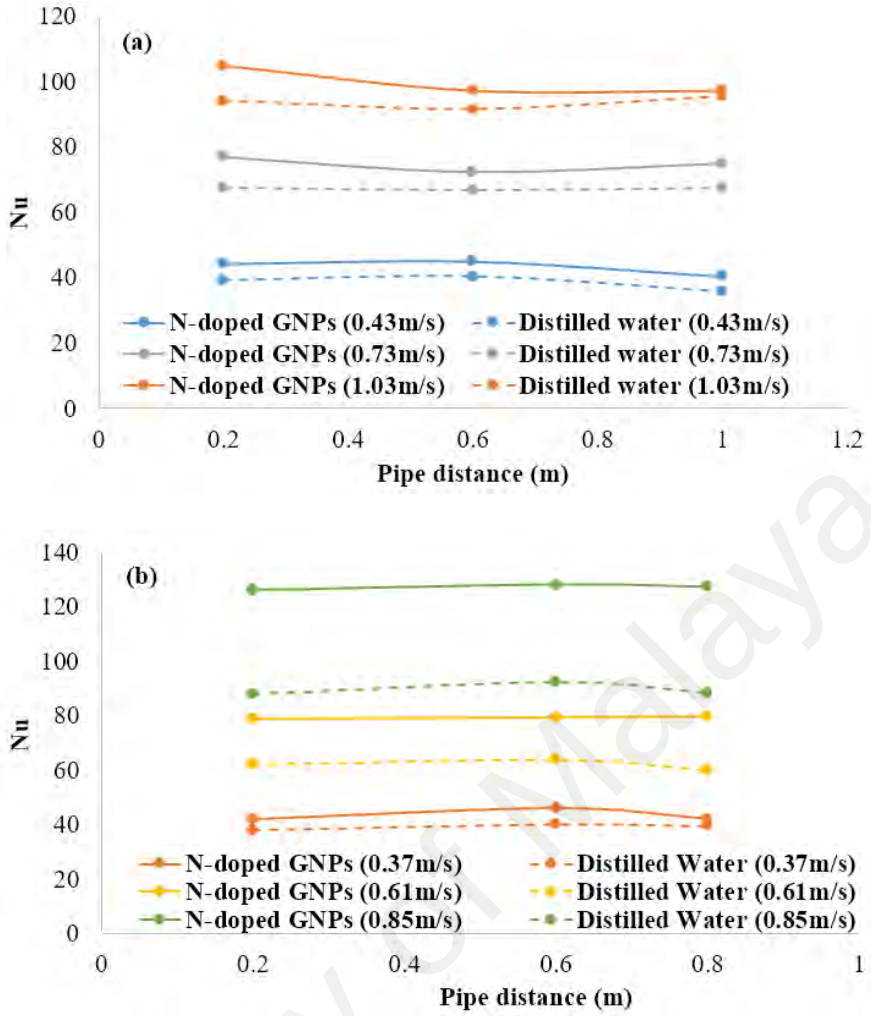

Figure 4.45: Plot of local Nusselt number along axial distance for N-doped GNPs colloid at (a) 30°C and (b) 40°C. The heat flux was set at 13429W/m².

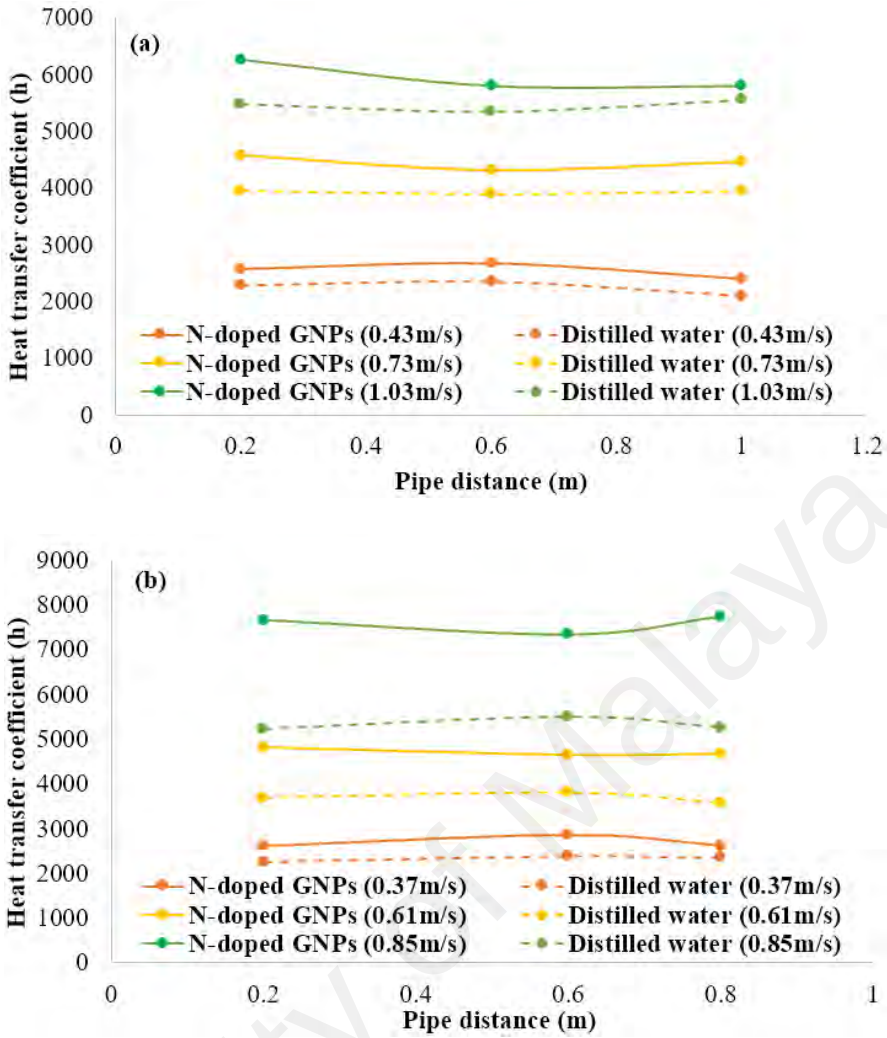

Figure 4.46: Plot of local heat transfer coefficient along axial distance for N-doped GNPs colloid at (a) 30°C and (b) 40°C. The heat flux was set at 13429W/m^2.

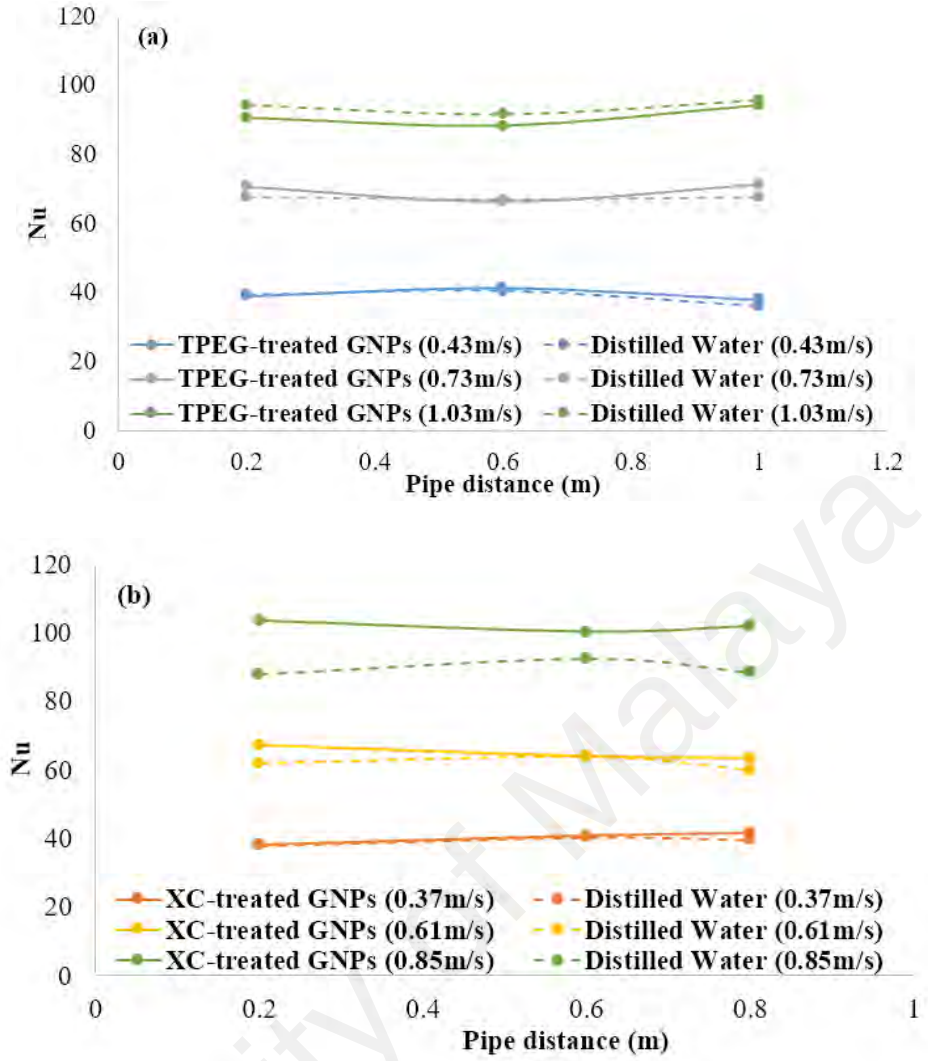

Figure 4.47: Plot of local Nusselt number along axial distance for (a)TFPEG-treated GNPs colloid at 30°C and (b) XC-treated GNPs colloid at 40°C. The heat flux was set to 13429W/m^2.

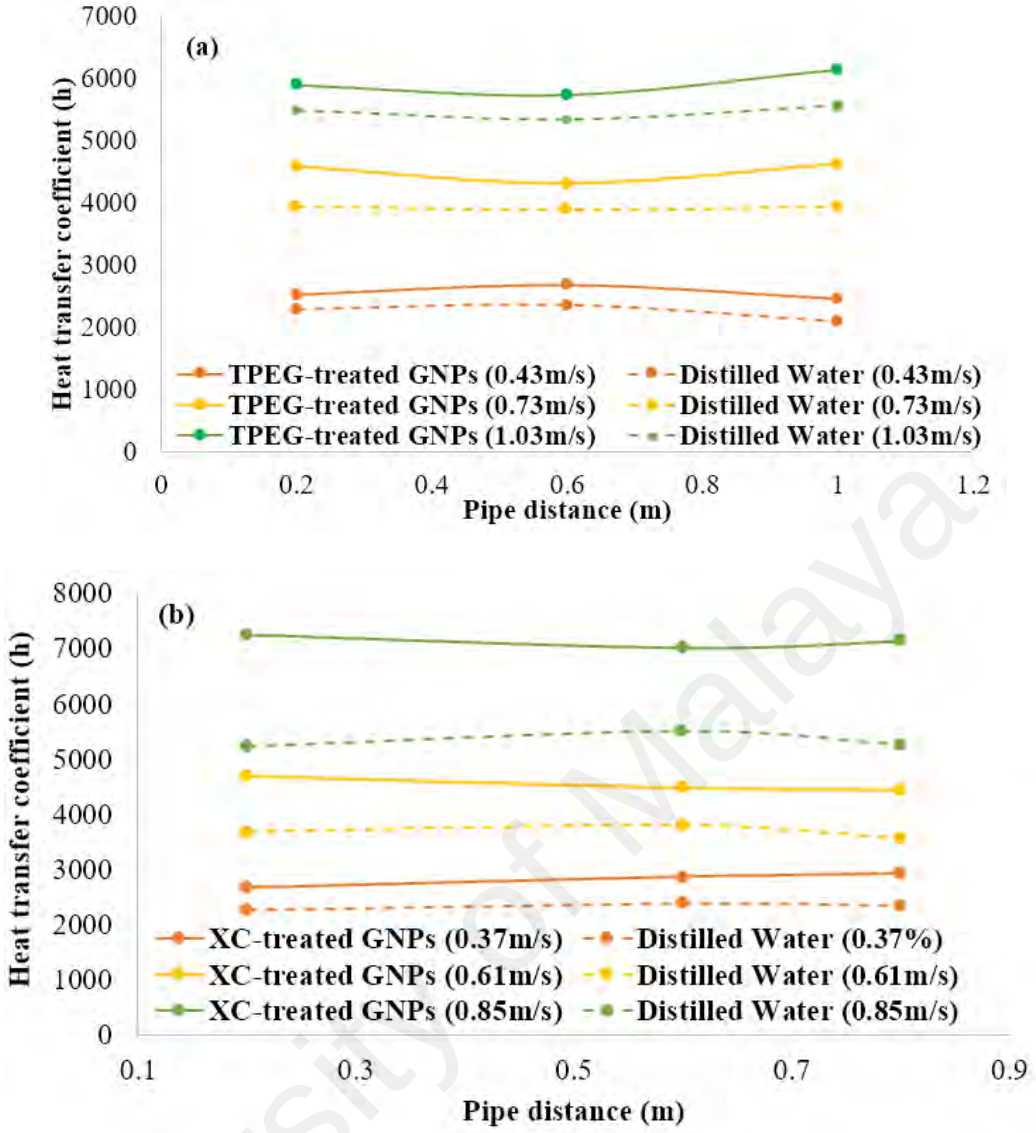

Figure 4.48: Plot of local heat transfer coefficient along axial distance for (a) TFPEG-treated GNPs colloid at 30°C and (b) XC-treated GNPs colloid at 40°C. The heat flux was set at 13429W/m^2.

Table 4.11: List of percentage improvement of heat transfer coefficient for different colloids at specific temperature. The heat flux was set at 6731W/m^2.

Re	30°C		40°C	
	N-doped GNPs	TPEG-treated GNPs	N-doped GNPs	TPEG-treated GNPs
4000	7.4	7.4	20.5	20.4
10000	7.6	7.6	36.5	36.5

Table 4.12: List of percentage improvement of heat transfer coefficient for different colloids at specific temperature. The heat flux was set at 13429W/m^2.

Re	30^{o}C		40^{o}C	
	N-doped GNPs	XC-treated GNPs	N-doped GNPs	XC-treated GNPs
4000	13.0	13.0	15.5	18.1
10000	14.1	14.1	46.7	39.0

Further assessment was conducted on the perspective of surface temperature measurement that represents a useful raw data interpretation to relate to the heat transfer enhancement. In general, Figure 4.49 until Figure 4.52 indicated that a lower surface temperature was recorded for the nanocolloids based experiment in comparison to water value which forms the basis toward the improvement of heat transfer performance. The improvement however was more significant at high temperature rather than heat flux and velocity, substantiating the previous finding on the role of bulk temperature in contributing to the overall heat transfer improvement. In all the circumstances, The N-doped GNPs based nanocolloid registered much lower surface temperature compared the other two materials (i.e. XC-treated GNPs and TPEG-treated GNPs). This may be attributed to the sample preparation procedure which is less defective toward the GNPs structure in comparison to others. As evident in the literature the use of strong acid alkaline to induce oxygen functional groups on carbon based material results in structural defect particularly on the basal plane, followed by the conversion sp2 bond to sp3 networks that compromise the ballistic heat transport property inherent within the pristine graphene. It is therefore a grand challenge for the researcher to find a less severe alternative route to functionalized graphene without sacrificing the critical structure. This can be done by attacking specific site, particularly at the edge of graphene whereby working around this sites ensure that the basal plane structure of the graphene remain uninterrupted. In the current study, XC-treated GNPs undergo oxidation process added with the attachment of long chain crosslinked sugar polymer, meanwhile TPEG

underwent acid exfoliation prior to chemical derivatization which increases the potential of uncontrolled structural defect. On the other hand the N-doped GNPs functionalization relied only on mild oxidizing agent (H_2O_2) and intermediate chemical to introduce the N-doped GNPs molecules on to the GNPs structure. Also based on the characterization results, more N-doped GNPs were found under pyrindic and pyrrolic arrangement rather than graphitic in nature which shows that most of the functionalization occurred at the edge of GNPs.

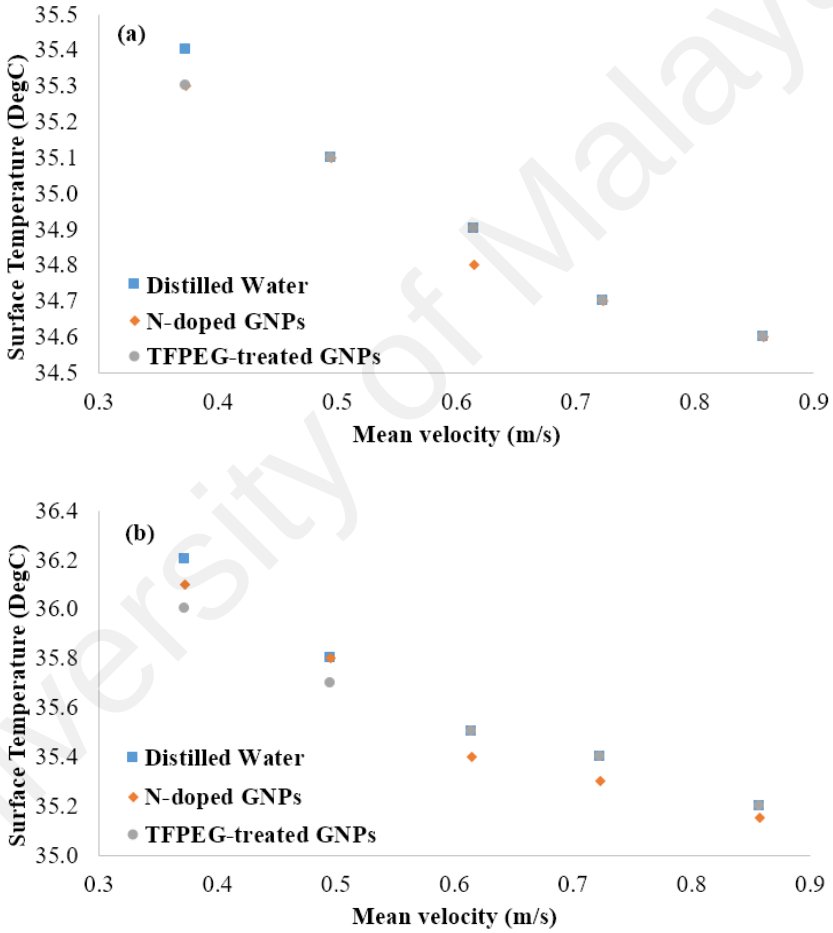

Figure 4.49: Plot of surface temperature against mean velocity for different functionalized GNPs colloids at (a) X=20D and (b) X=60D. The bulk temperature and heat flux were set at 30°C and 6731W/m², respectively.

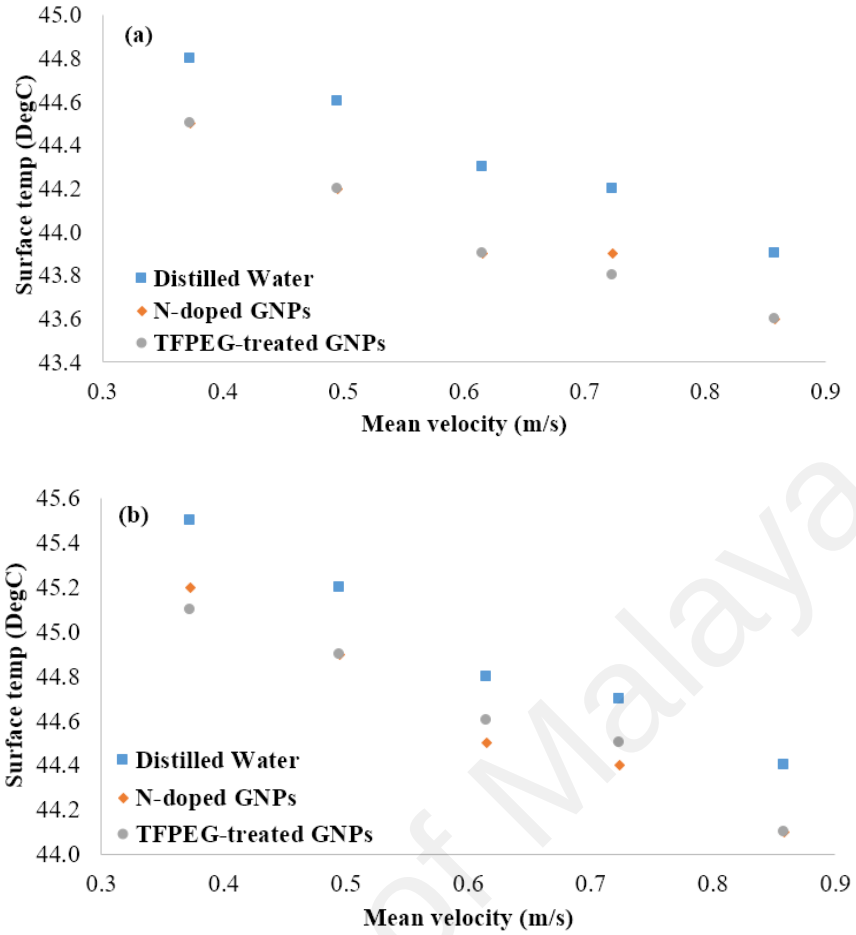

Figure 4.50: Plot of surface temperature against mean velocity for different functionalized GNPs colloids at (a) X=20D and (b) X=60D. The bulk temperature and heat flux were set at 40°C and 6731W/m^2, respectively.

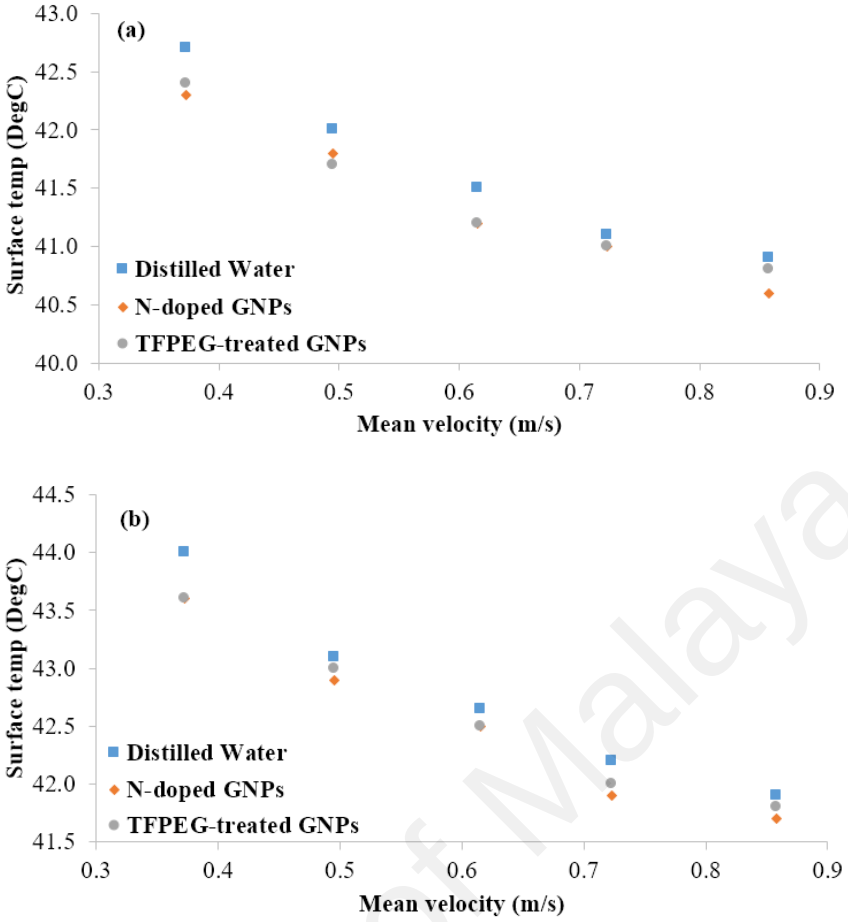

Figure 4.51: Plot of surface temperature against mean velocity for different functionalized GNPs colloids at (a) X=20D and (b) X=60D. The bulk temperature and heat flux for were set at 30°C and 13429W/m^2, respectively.

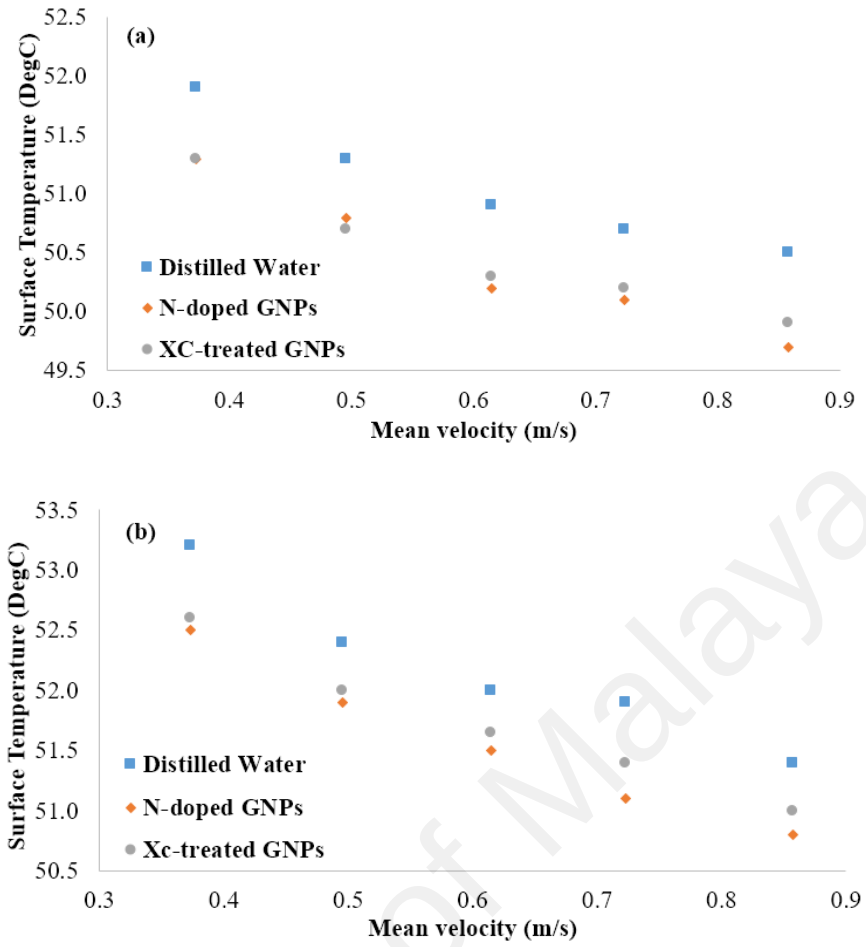

Figure 4.52: Plot of surface temperature against mean velocity for different functionalized GNPs colloids at (a) X=20D and (b) X=60D. The bulk temperature and heat flux for were set at 40°C and 13429W/m^2, respectively.

4.2.1.2 Experiment on laminar convective heat transfer

Investigation was extended to look into the effect of nanocolloids in convective heat transfer under laminar regime. As mentioned previously, a plate solar heat exchanger was used whereby the heating on the plate was provided by a silicone rubber heater. Figure 4.53 until Figure 4.56 provide the results of local Nu and h for water run at different axial position, heat flux and bulk temperatures. The results indicate that both heat transfer parameters experience a downward trend from the upstream region where the heating starts and along the axial position. A validity check on the result with the existing correlation by Petukhov revealed close agreement, particularly at the downstream section with the highest difference reached 6% for (40°C, 8902W/m^2) combination while the lowest was recorded at 3% for (40°C, 16295W/m^2). Further, it was shown that the

magnitude at the entrance region increases with increasing Re, indicating similar trend of internal convective heat transfer that requires longer entry length for higher velocity. The mean velocity for each temperature is given in Table 4.13. These velocity was used in nanocolloids experiment to assess their performance under constant mean velocity mode.

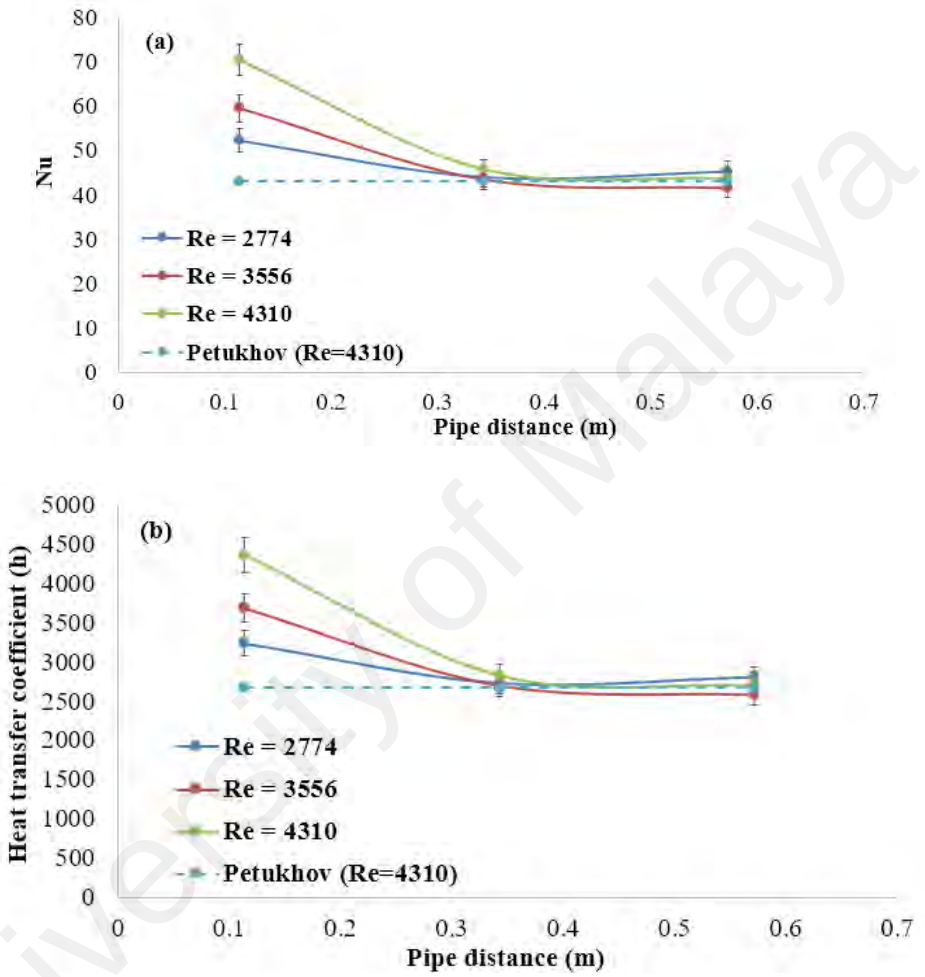

Figure 4.53: Comparison of (a) local Nusselt number and (b) local heat transfer coefficient for water run along the axial dimension between present measurement and literature. The bulk temperature and heat flux were set at 30°C and 8902W/m^2.

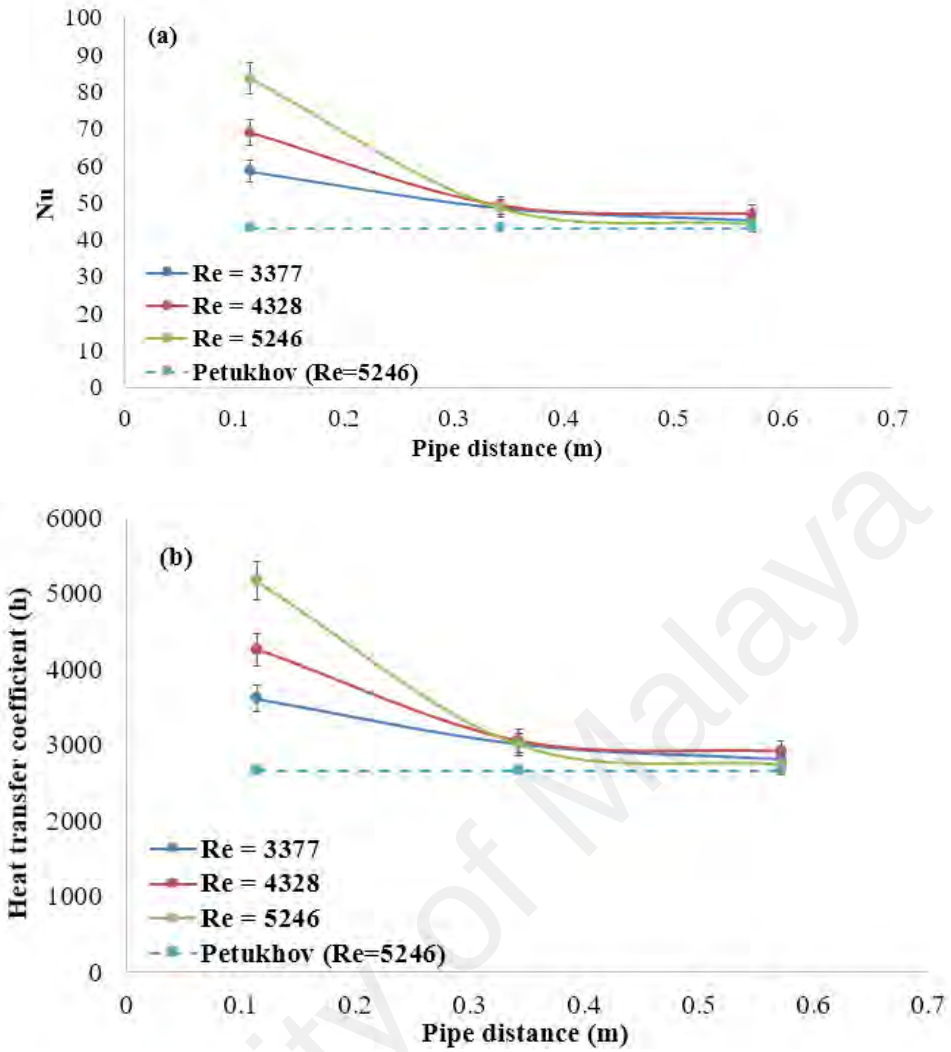

Figure 4.54: Comparison of (a) local Nusselt number and (b) local heat transfer coefficient for water run along the axial dimension between present measurement and literature. The bulk temperature and heat flux were set at 40°C and 8902W/m².

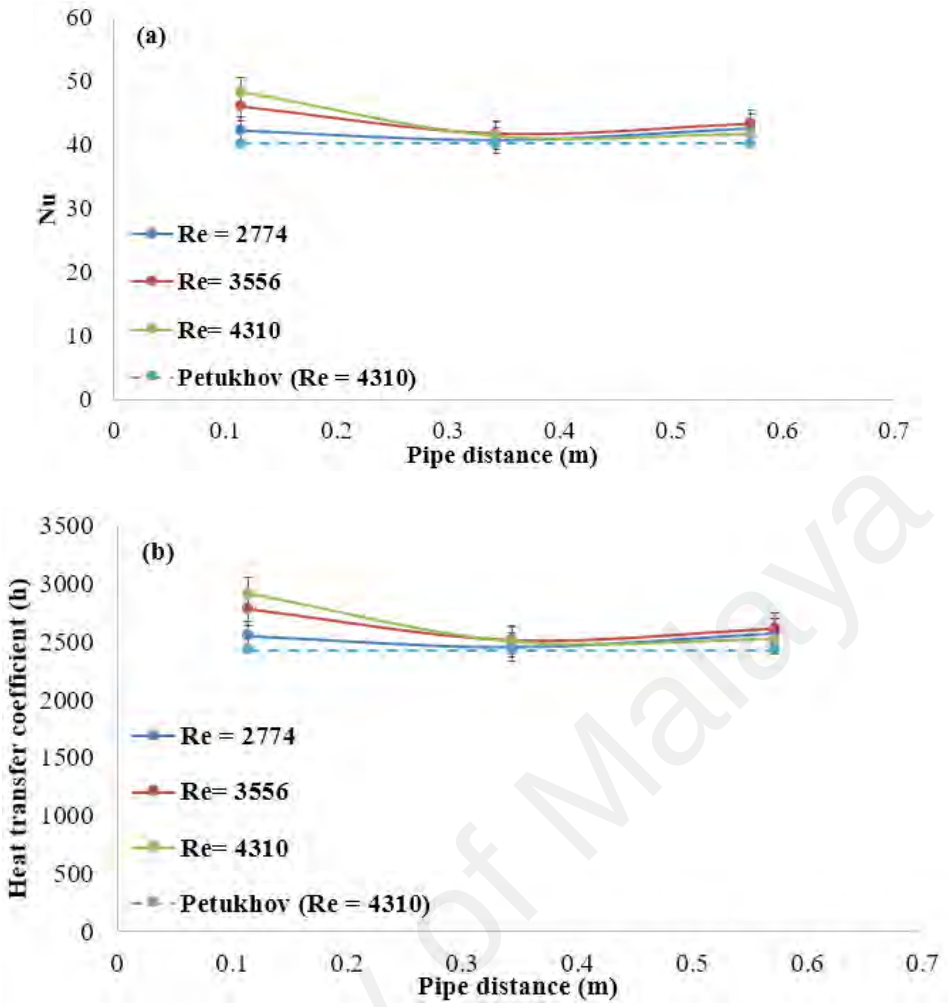

Figure 4.55: Comparison of (a) local Nusselt number and (b) local heat transfer coefficient for water run along the axial dimension between present measurement and literature. The bulk temperature and heat flux were set at 30°C and 16295W/m^2.

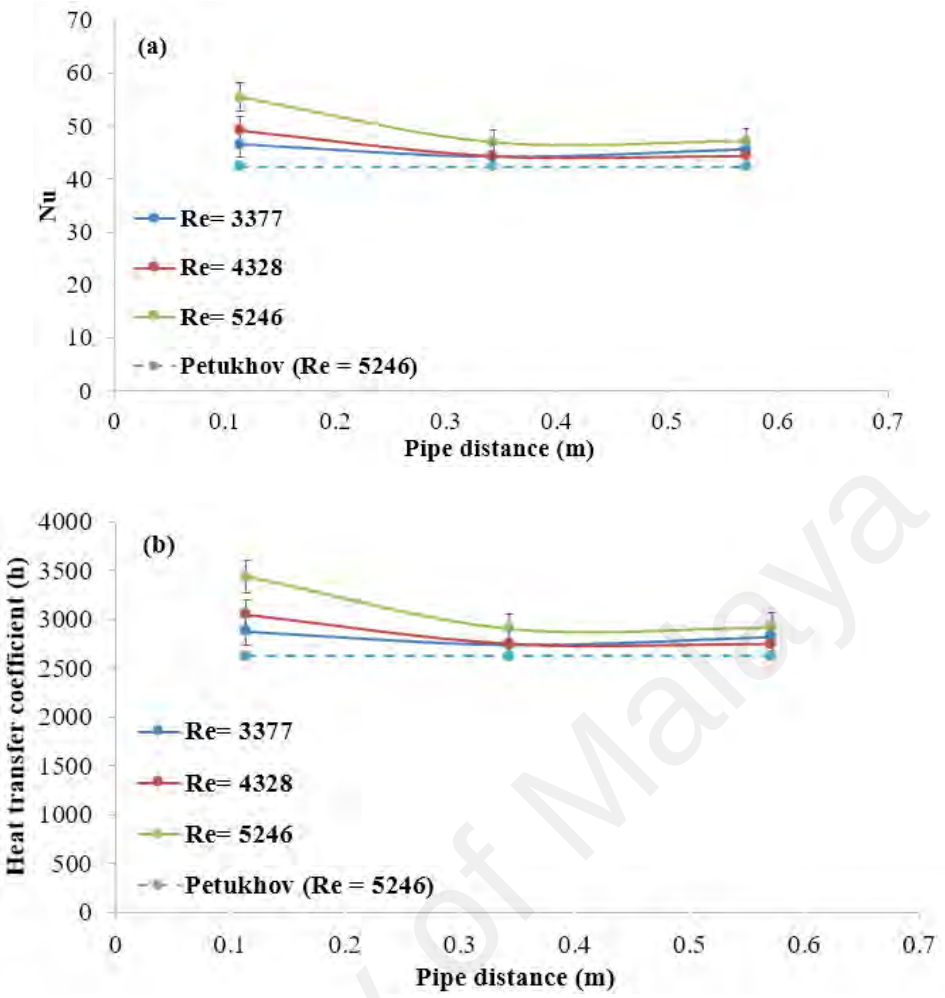

Figure 4.56: Comparison of (a) local Nusselt number and (b) local heat transfer coefficient for water run along the axial dimension between present measurement and literature. The bulk temperature and heat flux were set at 40°C and 16295W/m^2.

Table 4.13: List of Re along with the corresponding mean velocity for water.

Re/Temperature		U_{mean} (m/s)
30°C	40°C	
2774	3377	0.21
3556	4328	0.27
4310	5246	0.32

Figure 4.57 illustrates the Re magnitude difference between water an nanocolloids at constant mean velocity. Similar to the earlier study on turbulent convective heat transfer, the use of solid particles resulted in a drop of Re to the point where the flow transforms from transition to laminar regime for 30°C bulk temperature and from turbulent to laminar

for 40ºC. This allows investigation to be conducted in laminar region. It is also interesting to look into how degradation of flow quality from water to nanocolloids affect convective heat transfer performance. The evaluation will be compared against water value which is set as benchmark to gauge the level of performance for each of the material used in the study.

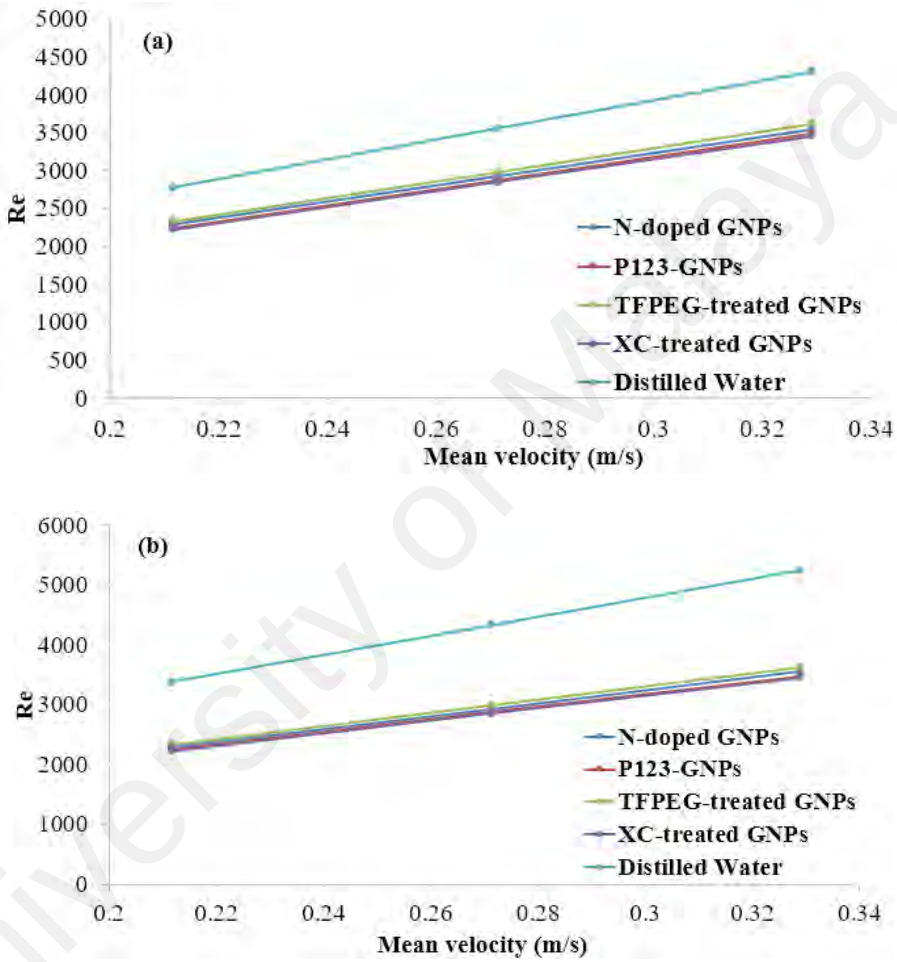

Figure 4.57: Comparison of Re at specific bulk velocity between different colloids and water at (a) 30ºC and (b) 40ºC for heat flux 8902W/m^2.

Figure 4.58 until 4.65 illustrate the plot of Nu and h for each of the material used in present study. It is interesting to note that the results indicate a drop in heat transfer performance in comparison to water based on much lower h and Nu registered. This shows that by maintaining the flow velocity, the increase in thermal conductivity was inadequate to compensate the loss in flow quality to absorb and transport the heat. As

evident form the figure, the drop in h is less for each of the configuration in comparison to Nu due to the involvement of k. Further, similar to earlier study the trend heat transfer performance improvement moves toward higher bulk temperature, further suggesting that nanocolloids are suitable to be used at high temperature under laminar flow. This findings fortify the previous argument by Yu et al, 2010 and Timofeeva, et al., 2009 that performance evaluation of heat transfer should not solely rely on constant Re condition as this will bring to negative enhancement as exemplify in the current study (Timofeeva et al., 2009; W Yu, France, Timofeeva, Singh, & Routbort, 2010).

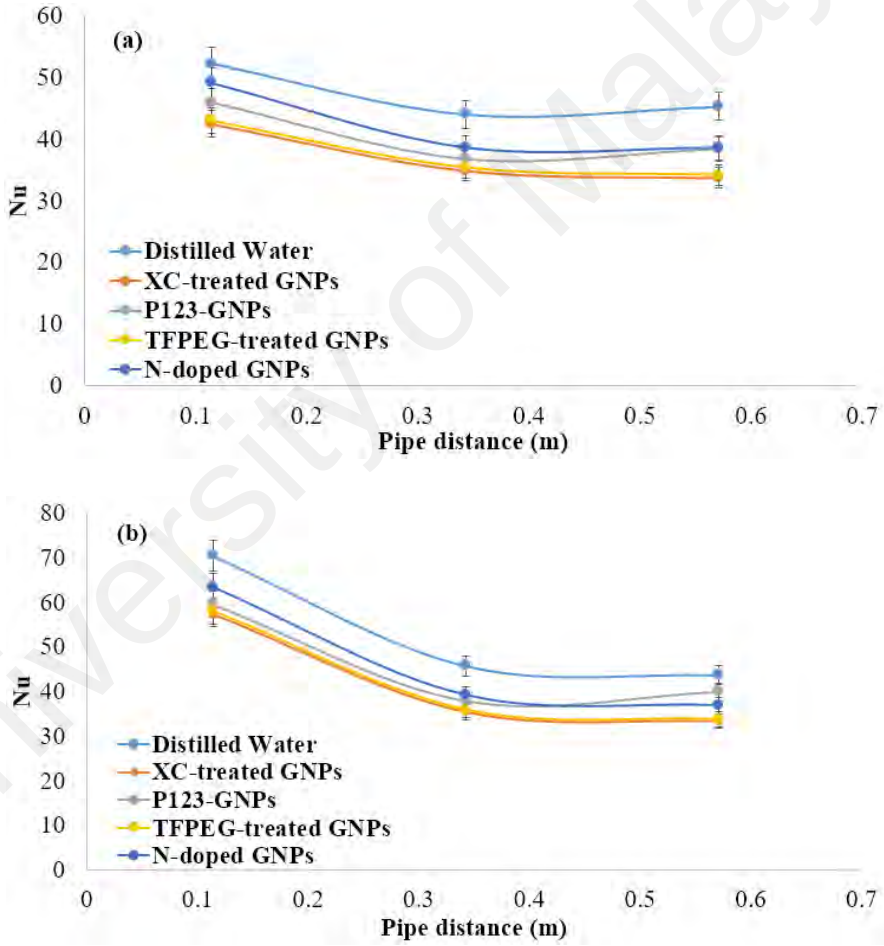

Figure 4.58: Comparison of local Nusselt number along the axial position between different functionalized GNPs at (a) U_{mean} = 0.21m/s and (b) U_{mean} = 0.32m/s. The bulk temperature and heat flux for were set to 30°C and 8902W/m^2, respectively.

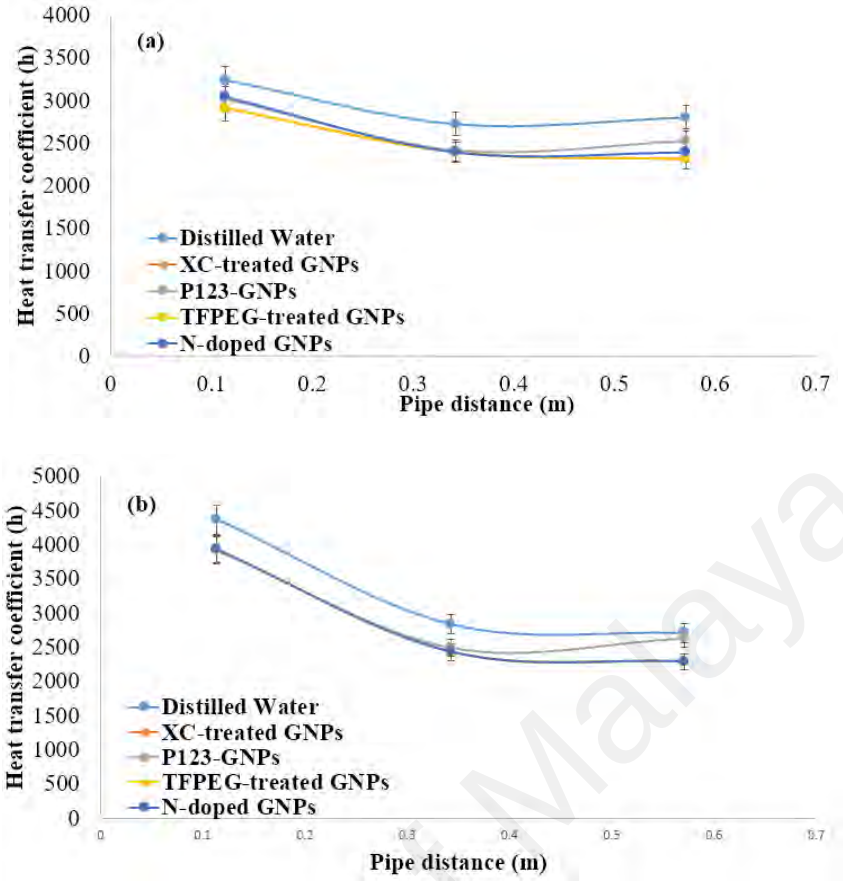

Figure 4.59: Comparison of local heat transfer coefficient along the axial position between different functionalized GNPs at (a) U_{mean} = 0.21m/s and (b) U_{mean} = 0.32m/s. The bulk temperature and heat flux for were set to 30°C and 8902W/m^2, respectively.

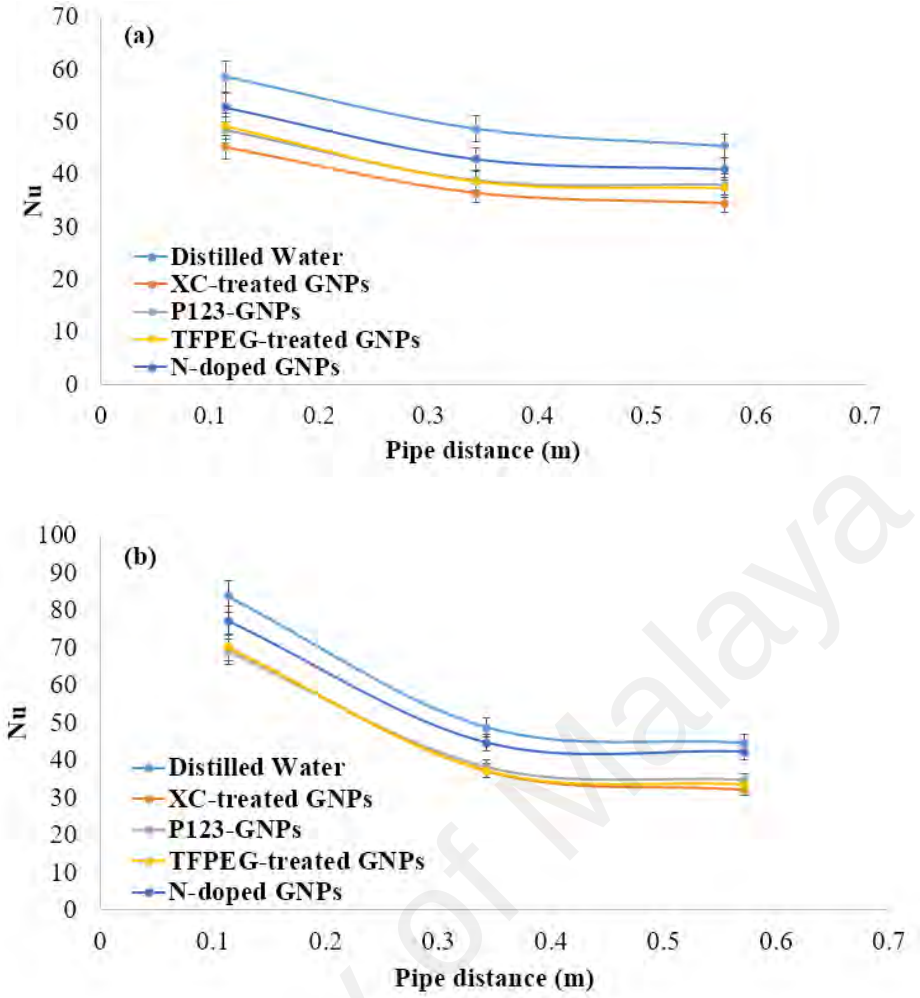

Figure 4.60: Comparison of local Nusselt number along the axial position between different functionalized GNPs at (a) U_{mean} = 0.21m/s and (b) U_{mean} = 0.32m/s. The bulk temperature and heat flux were set at 40°C and 8902W/m^2.

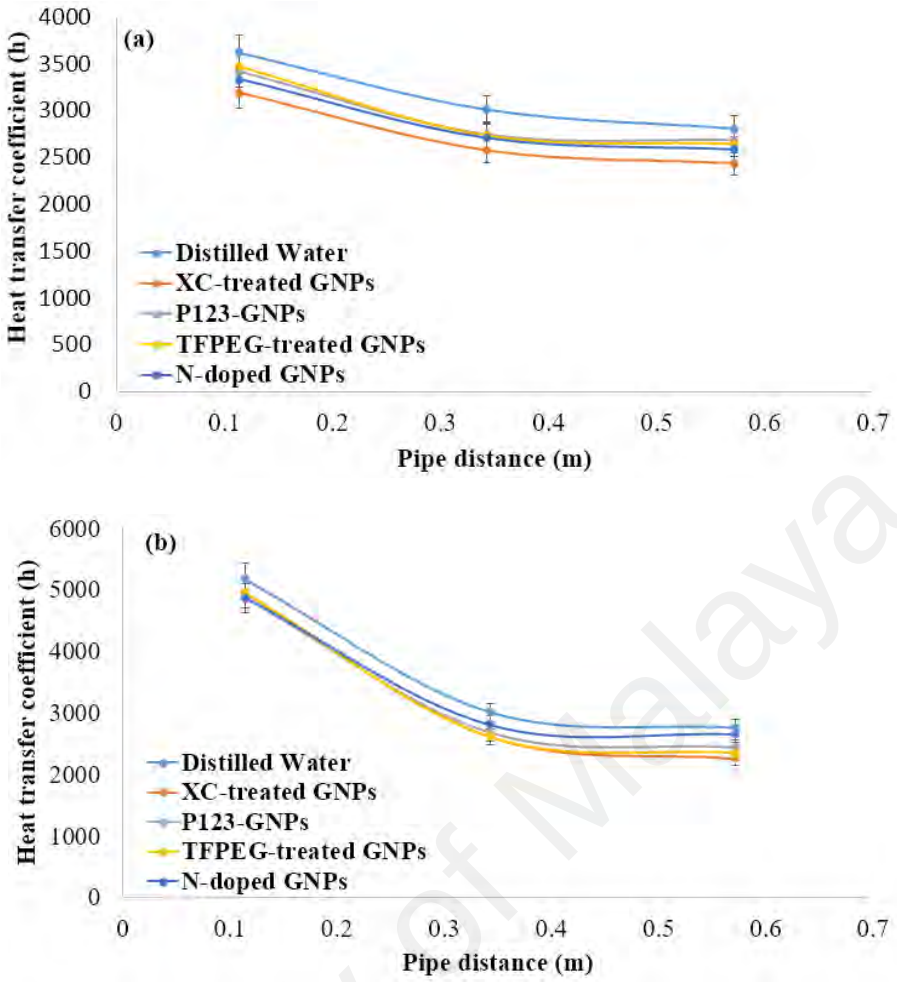

Figure 4.61: Comparison of local heat transfer coefficient along the axial position between different functionalized GNPs at (a) U_{mean} = 0.21m/s and (b) U_{mean} = 0.32m/s. The bulk temperature and heat flux were set at 40°C and 8902W/m^2.

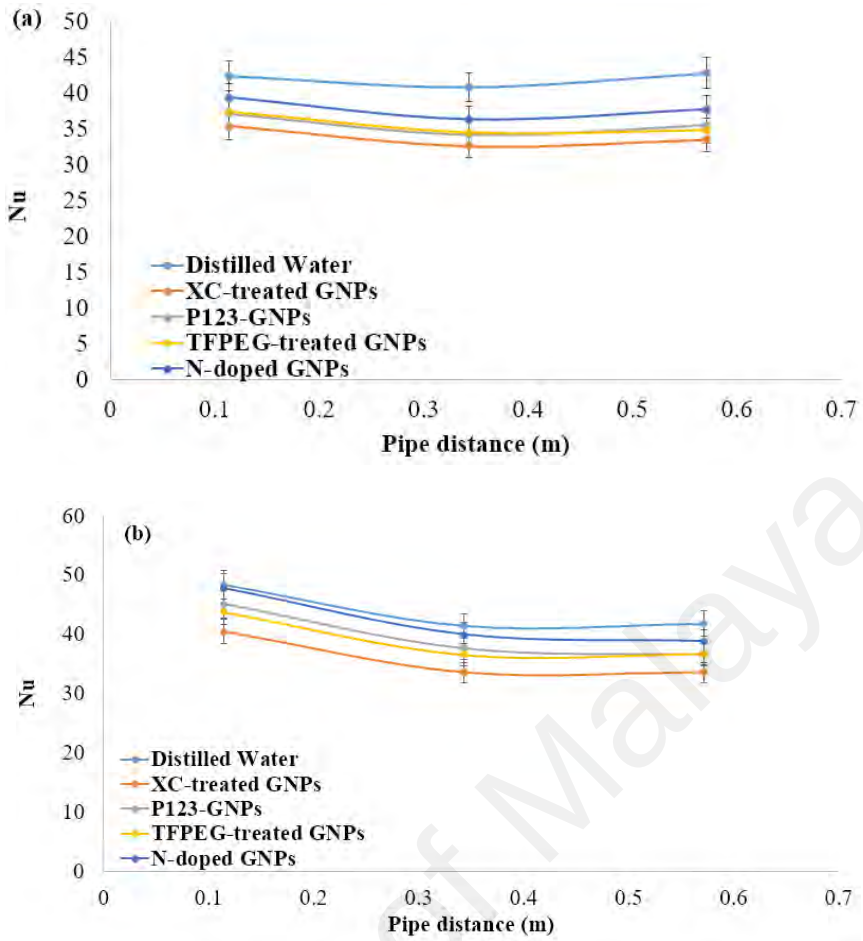

Figure 4.62: Comparison of local Nusselt number along the axial position between different functionalized GNPs at (a) U_{mean} = 0.21m/s and (b) U_{mean} = 0.32m/s. The bulk temperature and heat flux were set at 30°C and 16295W/m^2.

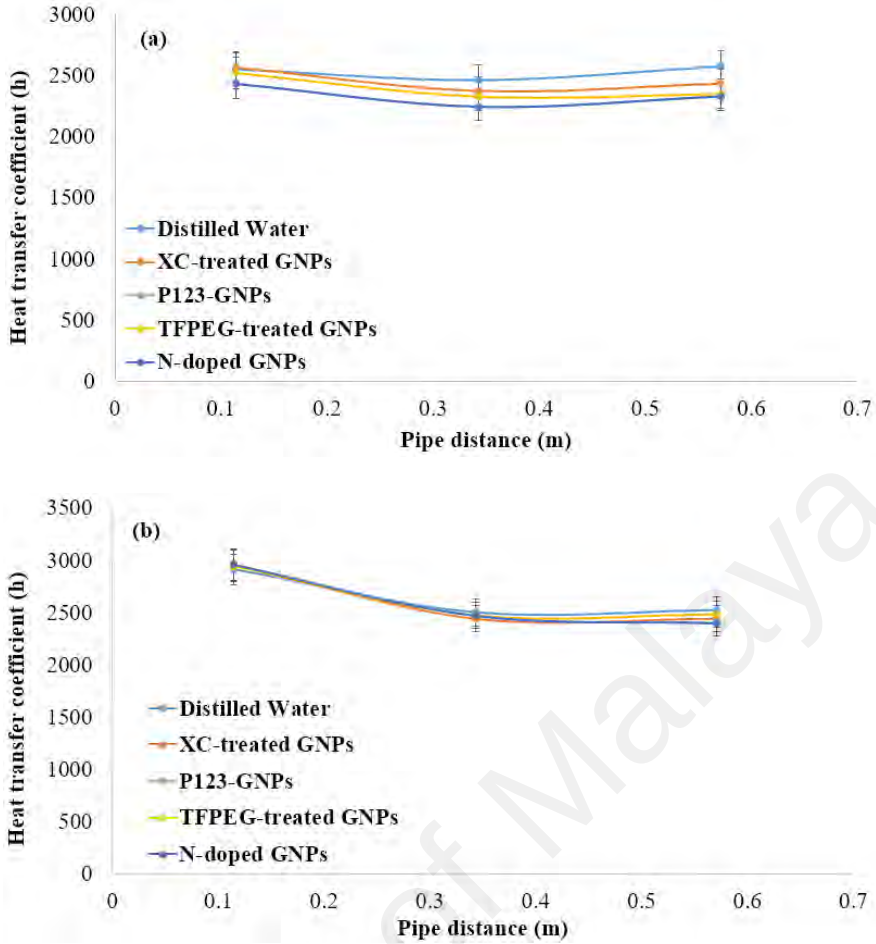

Figure 4.63: Comparison of local heat transfer coefficient along the axial position between different functionalized GNPs at (a) U_{mean} = 0.21m/s and (b) U_{mean} = 0.32m/s. The bulk temperature and heat flux were set at 30°C and 16295W/m^2.

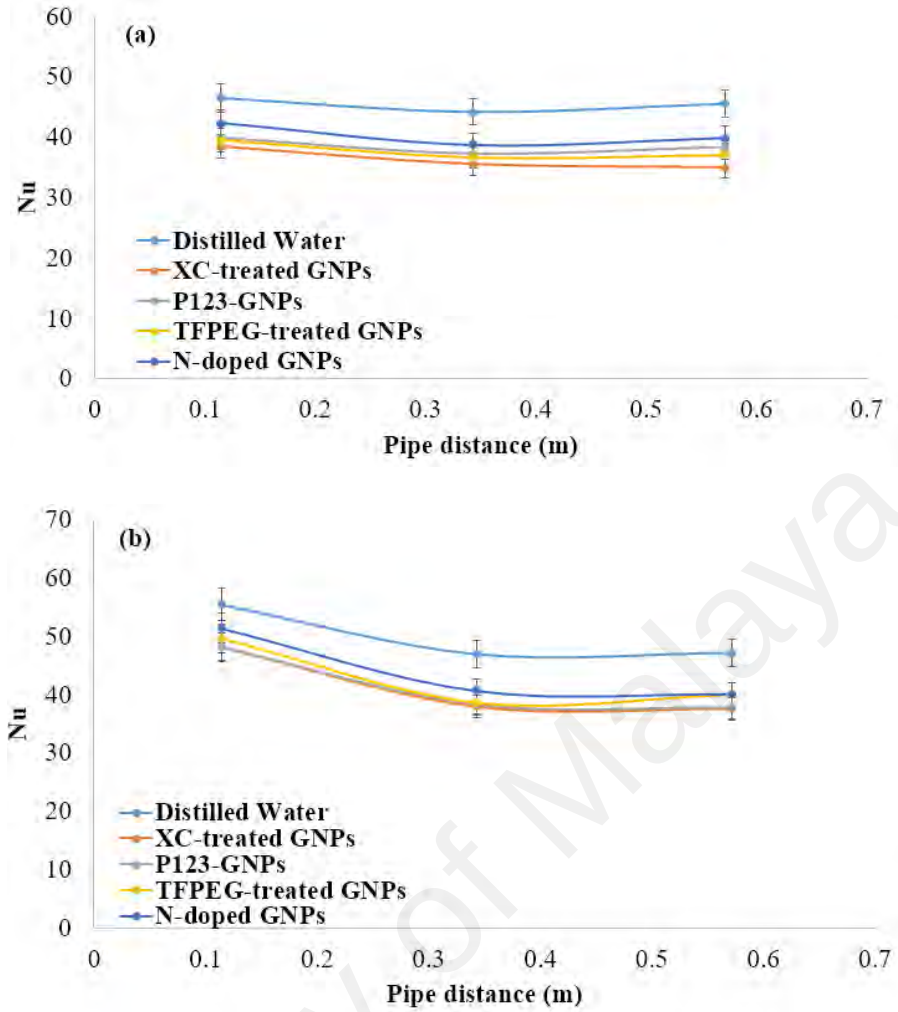

Figure 4.64: Comparison of local Nusselt number along the axial position between different functionalized GNPs at (a) U_{mean} = 0.21m/s and (b) U_{mean} = 0.32m/s. The bulk temperature and heat flux were set at 40°C and 16295W/m^2.

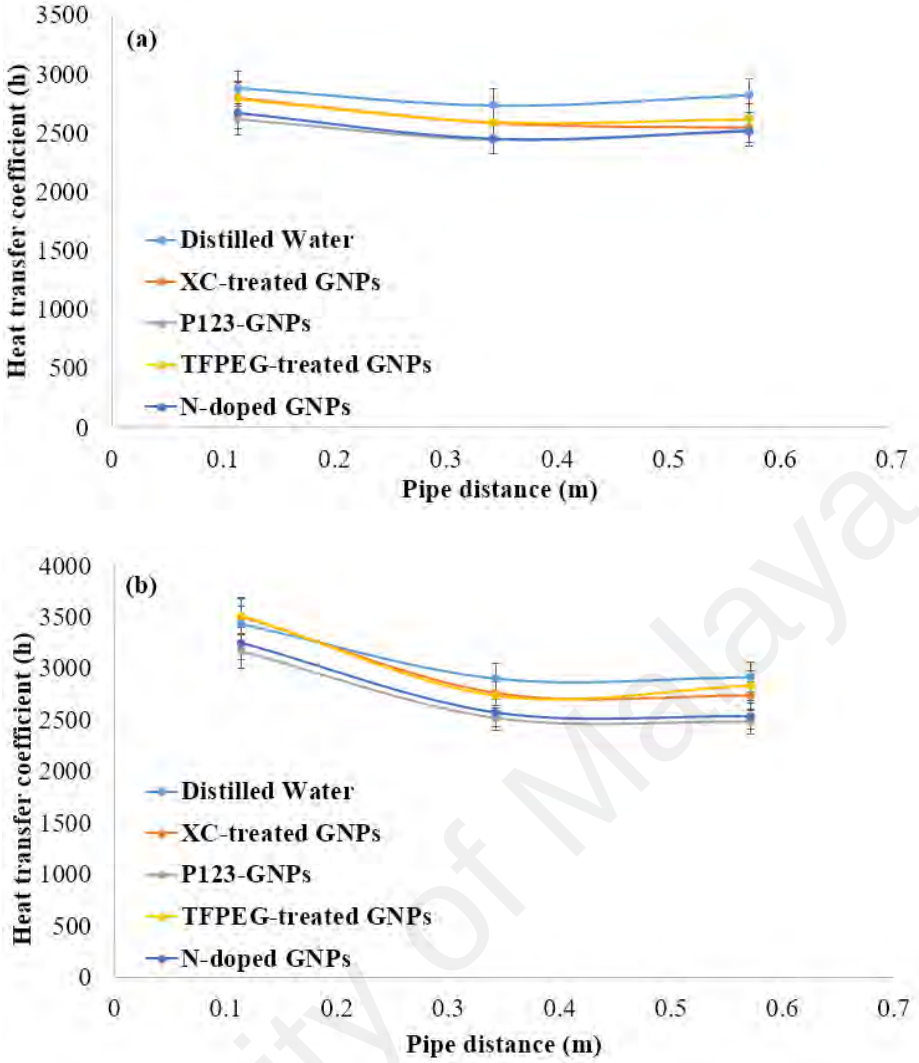

Figure 4.65: Comparison of local heat transfer coefficient along the axial position between different functionalized GNPs at (a) U_{mean} = 0.21m/s and (b) U_{mean} = 0.32m/s. The bulk temperature and heat flux were set at 40°C and 16295W/m^2.

In order to provide better view on the scope of heat transfer performance drop under laminar flow condition, series of plots representing heat transfer coefficient at specific heat flux, velocity and temperature were established as given in Figure 4.66 until Figure 4.69 while Table 4.14 and Table 4.15 summarized the level of depreciation of N-doped GNPs and TPEG-treated GNPs under the investigated temperatures. The plots revealed, in general that the majority of the nanocolloids used in the present study produced negative improvement in heat transfer, both at low and high mean velocity. Further, the role of velocity to increase h was not pronounced as elucidated by Table 4.14 and Table 4.15 where both velocities registered relatively similar depreciation level. Further, in

contrast to turbulent heat transfer, the role of bulk temperature in improving the h was not clearly seen. The drop was also relatively unchanged both at the upstream and downstream sections of the heat transfer section, mainly due to the thermal entry effect where the boundary layer is developing and the particles are mostly in unsettling form. However the performance drop showed a trend of improvement as the heat flux increases from lower to the higher level as highlighted in the tables. It should be noted that for laminar flow heat transfer, the temperature rise from the wall to the free stream region escalates in comparison to turbulent flow for a given heat flux. The heat transfer by conduction becomes more dominant and results in less temperature difference between the above two sites (i.e. wall and free stream). This sharp increase in temperature may play a role in improving the heat transfer which explain the reduction in performance drop at higher heat flux. This results shed light on the importance of devising a strategy to use solid additive at much higher flow regime to take advantage of the turbulent mixing and microconvection that would reinforce the heat transfer process.

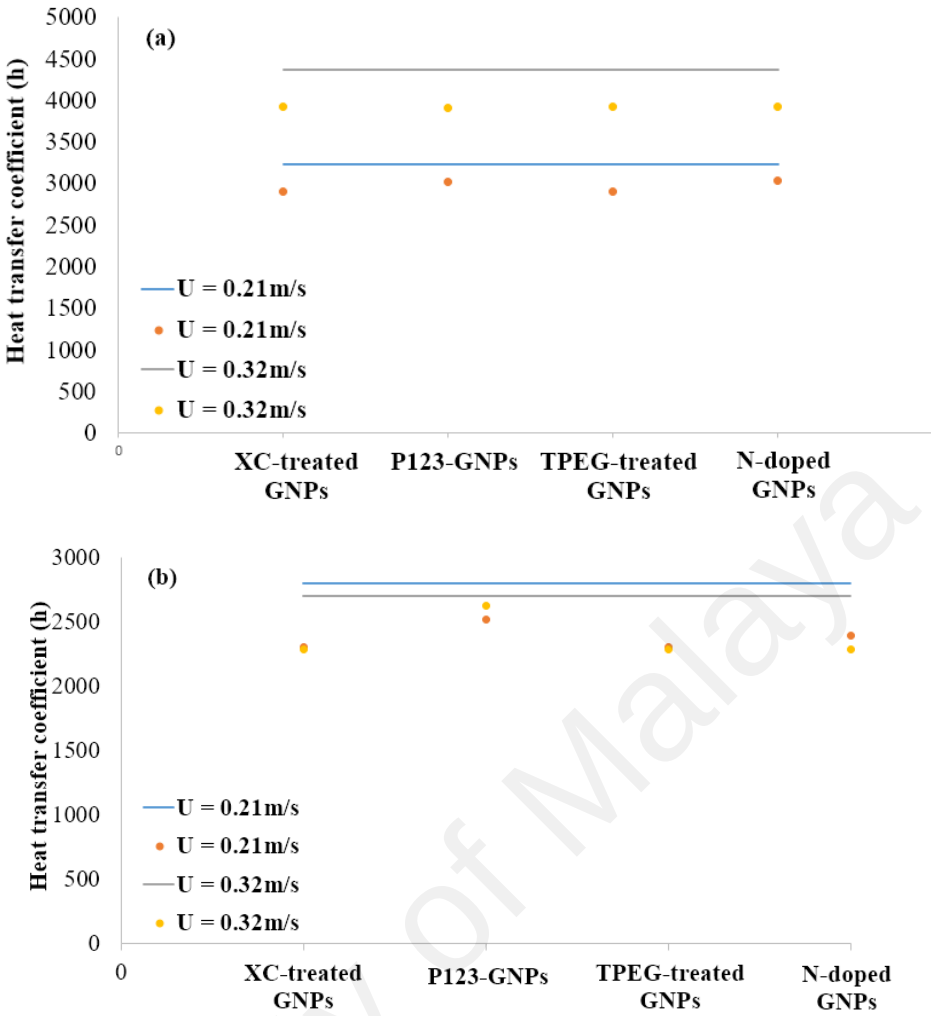

Figure 4.66: Comparison of local heat transfer coefficient, h between different functionalized GNPs at (a) X = 10D and (b) X = 52D. The baselines represent h for water at specific mean velocity. The bulk temperature and heat flux for air conditions was set at 30°C and 8902W/m^2.

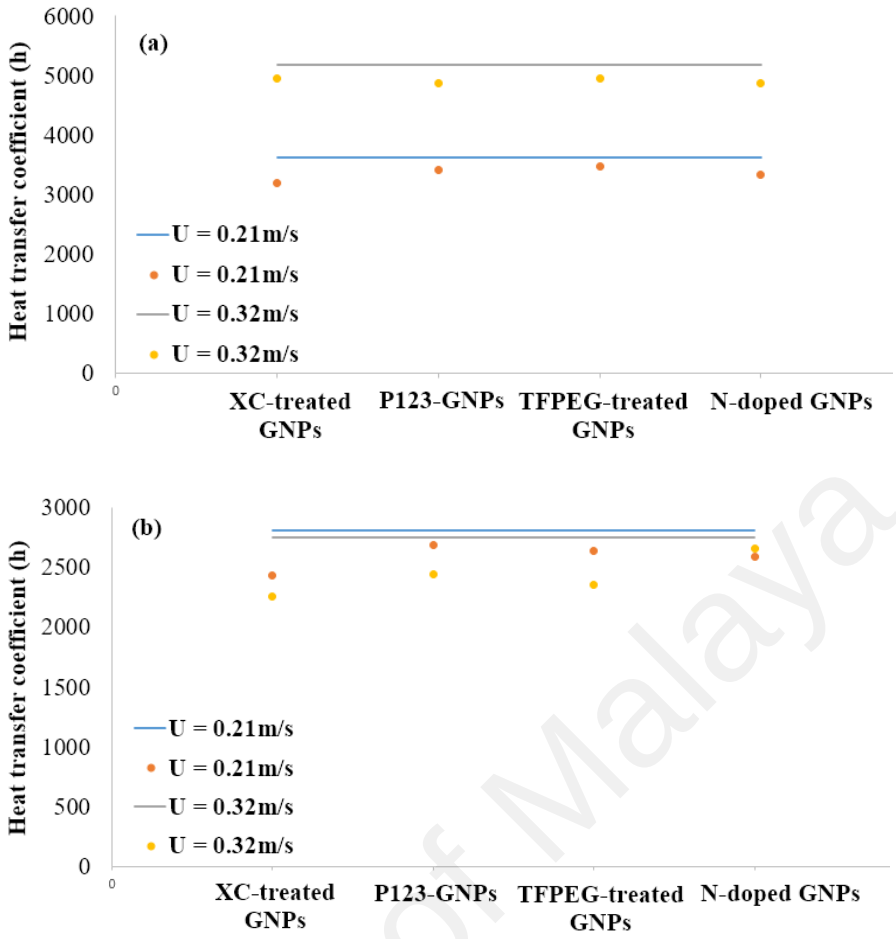

Figure 4.67: Comparison of local heat transfer coefficient, h between different functionalized GNPs at (a) X = 10D and (b) X = 52D. The baselines represent h for water at specific mean velocity. The bulk temperature and heat flux for air conditions was set at 40°C and 8902W/m^2.

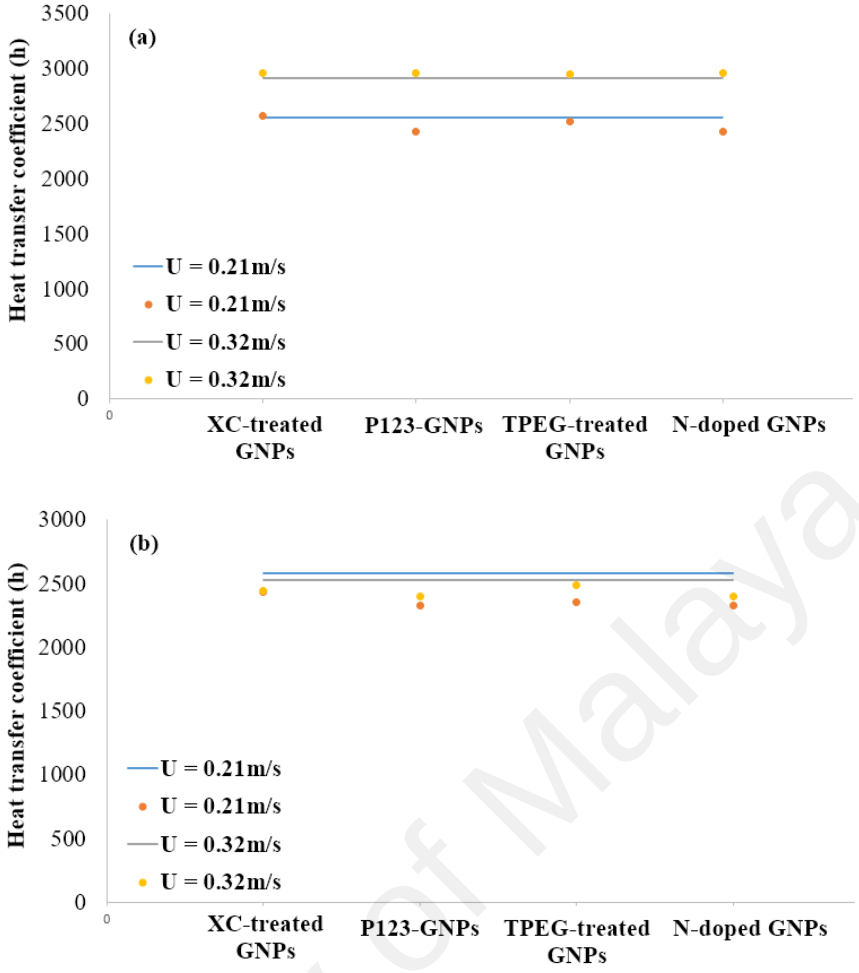

Figure 4.68: Comparison of local heat transfer coefficient, h between different functionalized GNPs at (a) X = 10D and (b) X = 52D. The baselines represent h for water at specific mean velocity. The bulk temperature and heat flux for air conditions was set at 30°C and 16295W/m^2.

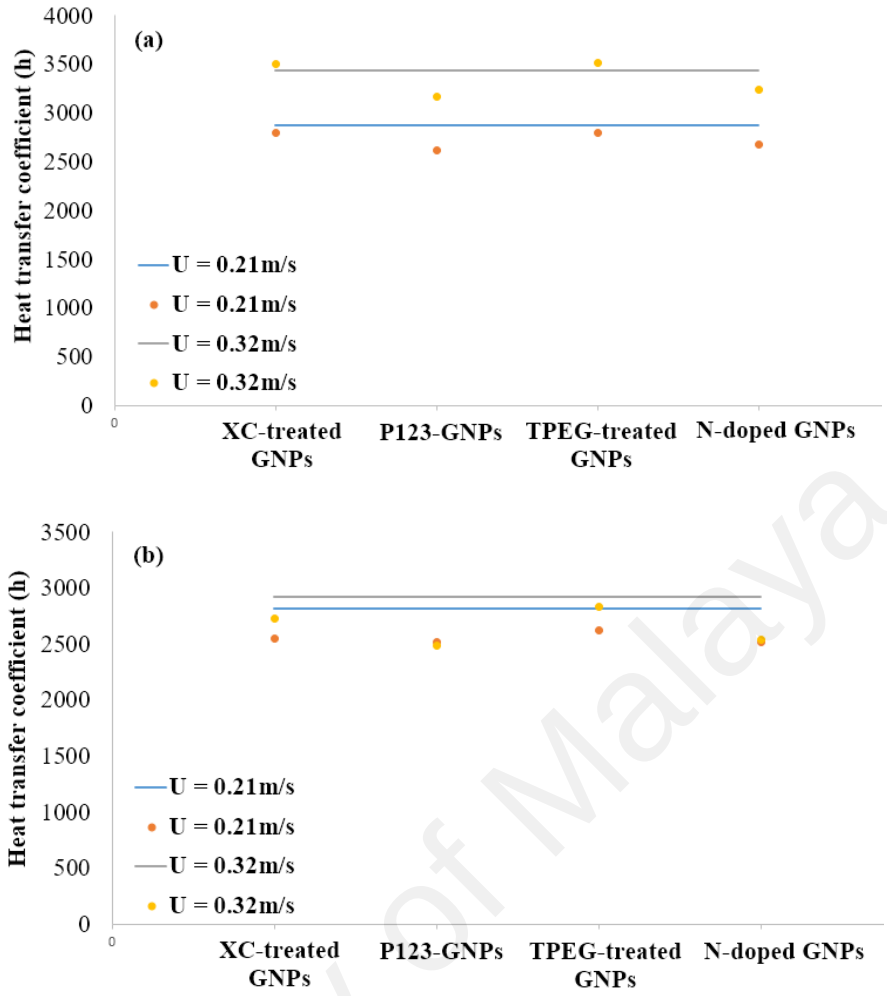

Figure 4.69: Comparison of local heat transfer coefficient, h between different functionalized GNPs at (a) X = 10D and (b) X = 52D. The baselines represent h for water at specific mean velocity. The bulk temperature and heat flux for air conditions was set at 40°C and 16295W/m^2.

Table 4.14: List of percentage improvement of heat transfer coefficient for different colloids at specific temperature and velocity. The data was evaluated at X/D=52 and heat flux was set at 8902W/m^2.

U_{mean}	30°C		40°C	
	N-doped GNPs	TPEG-treated GNPs	N-doped GNPs	TPEG-treated GNPs
U = 0.21m/s	-14.7	-10.0	-7.7	-6.0
U = 0.32m/s	-15.6	-10.0	-3.5	-14.5

Table 4.15: List of percentage improvement of heat transfer coefficient for different colloids at specific temperature. The data was evaluated at X/D=52 and the heat flux was set at 16295W/m^2.

U_{mean}	30°C		40°C	
	N-doped GNPs	TPEG-treated GNPs	N-doped GNPs	TPEG-treated GNPs
U = 0.21m/s	-9.6	-9.6	-10.6	-7.0
U = 0.32m/s	-4.7	-4.7	-13.2	-3.0

The earlier findings on contradictory performance of nanocolloids relative to water at different flow regimes has shed light on the need to conduct rigorous analysis on the heat exchanger system, particularly on the material thermophysical properties and regime of flow operation, bulk temperature and heat flux prior to resort in using solid additive to improve the heat transfer performance. The previous results indicate that the increase in viscosity of the nanocolloilds should be as minimal as possible for any increment of heat transfer to manifest. Further, operating the heat exchanger at turbulent region provide positive trend of heat transfer performance in comparison to laminar flow heat transfer. Figure 4.70 until Figure 4.73 summarized the above nanocolloidal heat transfer performance in close conduit in terms of operating regime. The figures highlighted the shift from negative to positive improvement relative to water as the flow changes from laminar to turbulent (Re > 4000) under constant velocity approach. The above Re was selected as the interface separating the negative to positive improvement of the current convective heat transfer study due to the fact that this value signifies the formation of complete turbulent after the transitional flow between the laminar and turbulent regimes. This explains more on the role of nanoparticles on altering the turbulent characteristic that lead to the improvement in heat transfer. This value is also indicated in most references as well as the moody diagram. This happened for all the materials under present investigation and the trend follows both at different heat fluxes and bulk temperatures. This study paves an avenue to relook at the notion of positive impact

generated by the nanocolloid particularly at the laminar regime. Also the extremely high improvement obtained under the previous studies of turbulent heat transfer need to be normalized under constant velocity to provide much realistic improvement that warrant the use of solid additive in heat transfer process. Further, a study where nanoparticles and microbubbles are to be compared of their performance seems to be lacking and future work on this subject will provide more insight onto the approach that brings more benefit from the other. Since the heat and hydrodynamic transport occurs at the boundary layer, a fundamental study on the turbulent behavior and interaction of the particles with the bulk fluid will be an interesting aspect to inspect. An existing instrument such as laser Doppler and interferometer as well as magnetic sensor can be used to resolve the velocity profile of the particles similar to the previous study on multiphase system.

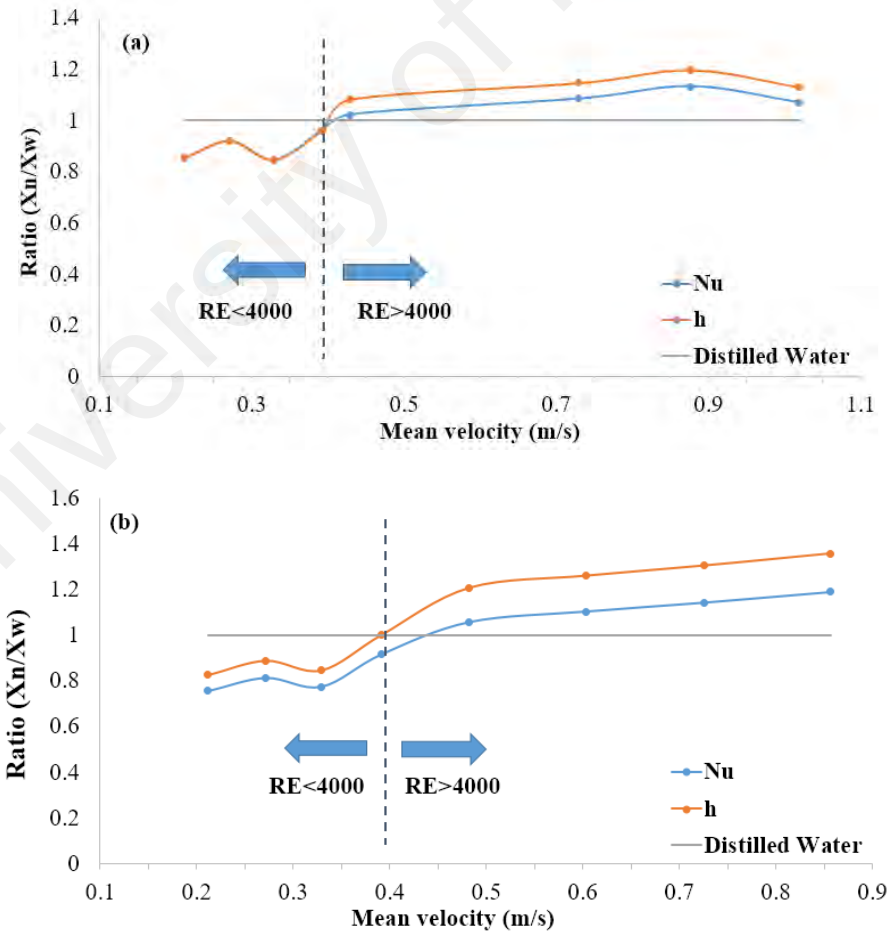

Figure 4.70: Plot of Nu and h ratio for (a) N-doped GNPs and (b) TPEG-treated GNPs colloids against water at increasing velocity. The results were taken at X =

52D and X=60D for laminar and turbulent flow, respectively. The bulk temperature and heat flux was set to 30°C and 8902W/m².

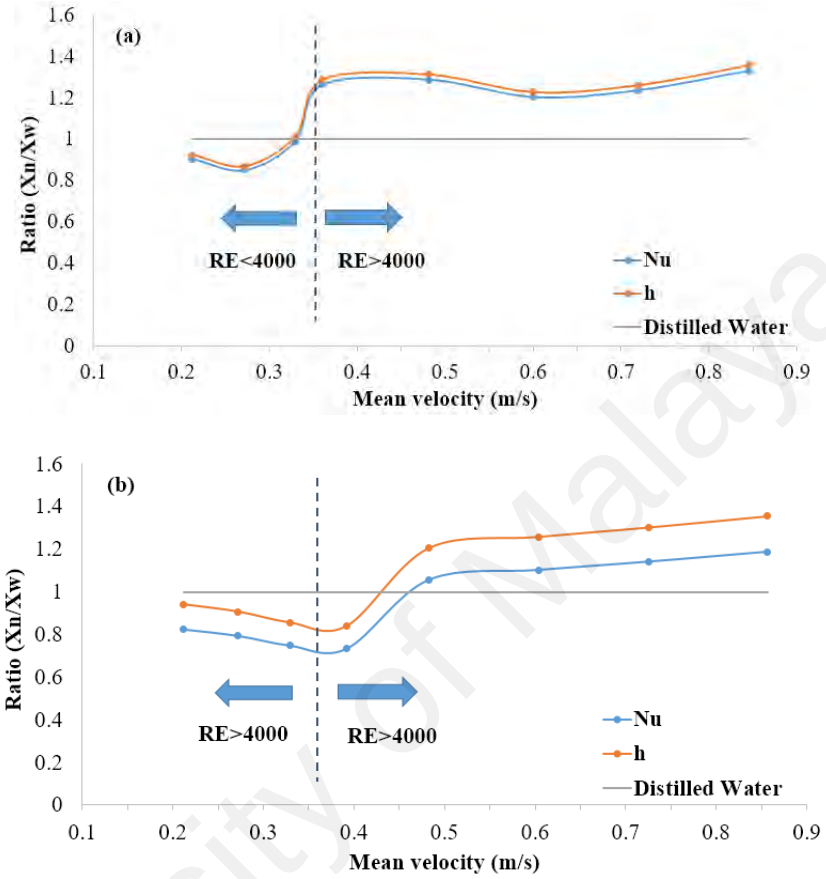

Figure 4.71: Plot of Nu and h ratio for (a) N-doped GNPs and (b) TFPEG-treated GNPs colloids against water at increasing velocity. The results were taken at X = 52D and X=60D for laminar and turbulent flow, respectively. The bulk temperature and heat flux was set to 40°C and 8902W/m².

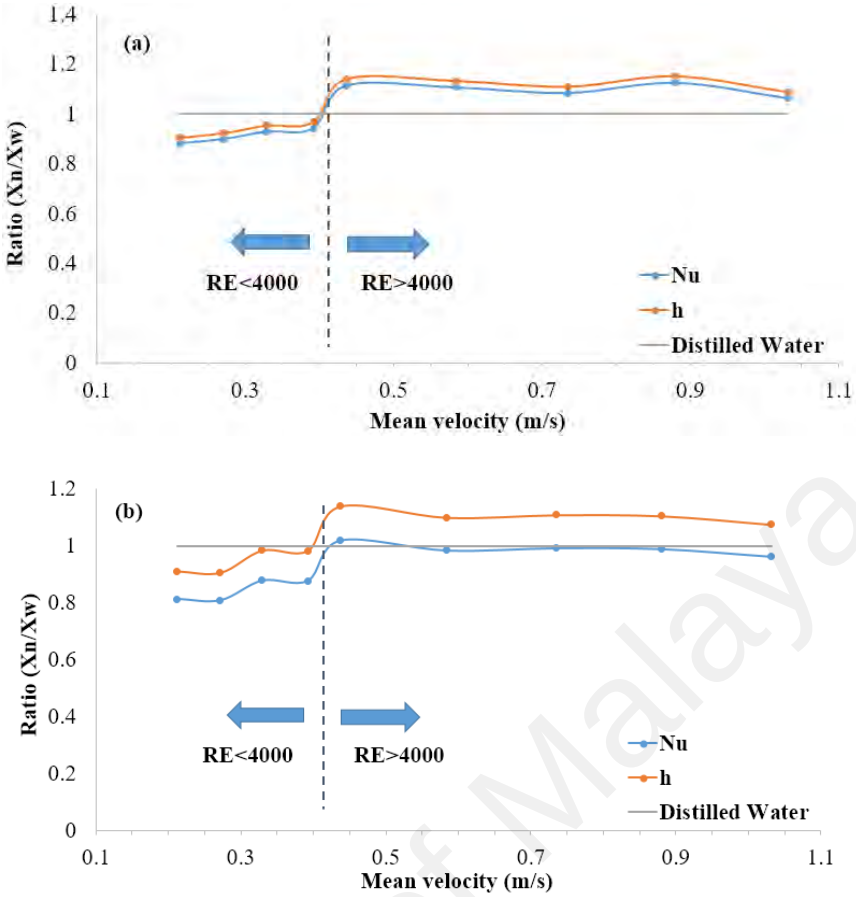

Figure 4.72: Plot of Nu and h ratio for (a) N-doped GNPs and (b) TFPEG-treated GNPs colloids against water at increasing velocity. The results were taken at X = 52D and X=60D for laminar and turbulent flow, respectively. The bulk temperature and heat flux was set to 30°C and 16295W/m^2.

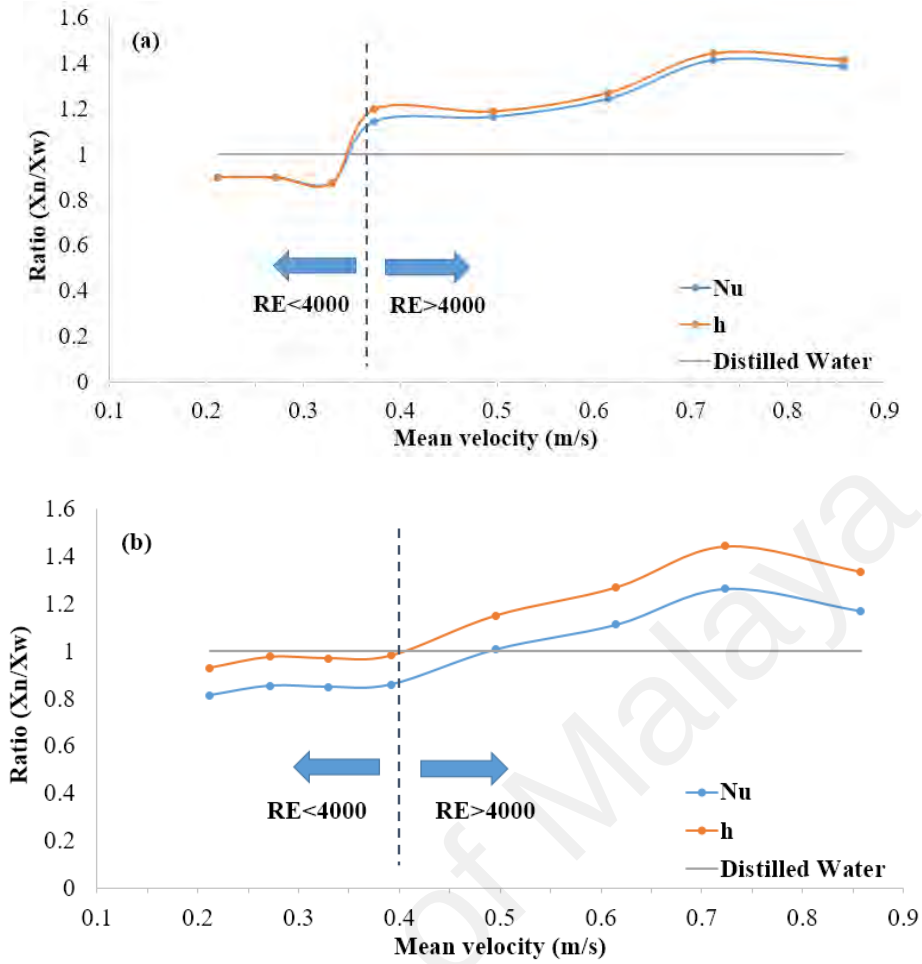

Figure 4.73: Plot of Nu and h ratio for (a) N-doped GNPs and (b) TFPEG-treated GNPs colloids against water at increasing velocity. The results were taken at X = 52D and X=60D for laminar and turbulent flow, respectively. The bulk temperature and heat flux was set to 40°C and 16295W/m².

4.2.2 Thermoelectrochemistry field

4.2.2.1 Seebeck coefficient

The Seebeck coefficient (S_c) obtained for the 0.4 M I^-/I_3^- (aq) redox couple (i.e., control sample) from the electrochemical analysis was 0.49 mV/K. This value is within the range of the reported value by previous researchers (i.e., 0.53 ± 0.04 mV/K) for a 0.4 M solution (Abraham et al., 2011). From this, it can be ensured that the experimental setup gives an acceptable value and the readings for all samples are reliable. After the addition of each sample of TFPEG-treated GNPs, N-doped GNPs, XC-treated GNPs, and P123-GNPs in I^-/I_3^- solution, the measured Seebeck coefficient values are 0.66, 0.69, 0.63, and 0.62 mV/K respectively. Figure 4.74 shows the different values between the solutions

of only I^-/I_3^- and with the addition of the treated GNPs samples, and more details are available in Table 4.16.

It can be seen that all Seebeck values show a significant enhancement compared to the intrinsic value for I^-/I_3^- solution. The increment is approximately 35%, 41%, 29%, and 27% for TFPEG-treated GNPs, N-doped GNPs, XC-treated GNPs, and P123-GNPs samples, respectively. The results obtained could be due to the nitrogen and oxygen functional group containing sites on the graphitic structure of GNPs. These two functional groups are responsible in providing high catalytic activity of graphene toward I^-/I_3^- solution, which could help in iodine reduction reaction (Denaro et al., 2009; Trancik, Barton, & Hone, 2008). The increase in liquid viscosity when added with a particular amount of sample can increase reverse peak on potential axis (ΔE_p) values. As the values of ΔE_p increase, it could indicate the presence of electrochemical irreversibility. However, as the temperature increases, the decrease in viscosity can reduce the values of ΔE_p. The decrease in ΔE_p values could be due to an increased rate in electron transfer through the electrode interface as the temperature increases (Ejigu, Lovelock, Licence, & Walsh, 2011).

In addition, the measured value for the specific sample of mixed N-doped GNPs with I^-/I_3^- solution is higher than other mentioned samples. The reason could be due to the capability of nitrogen to enhance the electrochemical activity of graphene by providing higher energy electrons and promoting reducing ability compared to oxygen-doped graphene (H. Wang, Maiyalagan, & Wang, 2012). Besides, based on the results of the stability test from UV-Vis analysis, it provides the evidence of agglomeration that occurred at a certain time. This may also cause the tendency to increase the Seebeck coefficient as there is a probability for the increment of elastic interaction, thus increases the entropy of the system (Hasnan et al., 2017).

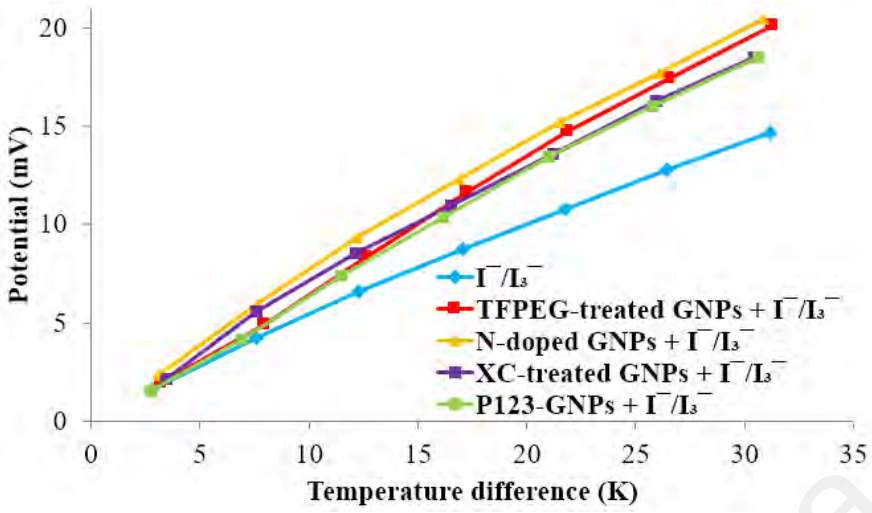

Figure 4.74: Seebeck coeeficient measurement of iodide/triiodide liquid solution and other functionalized GNPs samples.

Table 4.16: Details of specific value of Seebeck coefficient for all tested samples.

Name of sample	Seebeck coefficient value (mV/K)
I^-/I_3^-	0.49
TFPEG-treated GNPs + I^-/I_3^-	0.66
N-doped GNPs + I^-/I_3^-	0.69
XC-treated GNPs + I^-/I_3^-	0.63
P123-GNPs + I^-/I_3^-	0.62

4.2.2.2 Electrical conductivity

The values of electrical conductivity for TFPEG-treated GNPs, N-doped GNPs, XC-treated GNPs, and P123-GNPs samples with I^-/I_3^- solution are presented in Figure 4.75 and tabulated in Table 4.17. Based on the table, it can be observed that there is an obvious increment in conductivity when the temperature increased from 30 until 60 °C for all samples. This is because of the increase in the mobility of ions in the solutions, which is related with the decrease of the viscosity of the solutions as the temperature increases. As the viscosity decreases, it means that there is a dissociation of molecules, which can also lead to the increment of ions, therefore increases the conductivity (An et al., 2014; Sarojini, Manoj, Singh, Pradeep, & Das, 2013; Shoghl, Jamali, & Moraveji, 2016). Although there is better performance in terms of the Seebeck measurement, but all

of the mixed samples show significantly less conductivity values compared to I^-/I_3^- solution.

One of the reasons is probably due to higher viscosity that can hinder the capability of the conducting species to diffuse in an electrolyte (Cho, Yoon, Sekhon, & Han, 2011). Another reason could be from the deformity of the conductive carbon structure (Roy-Mayhew, Bozym, Punckt, & Aksay, 2010). In addition, agglomeration could also reduce the conductivity for all measured samples (Al-Saleh, Al-Anid, & Hussain, 2013). The sample of N-doped GNPs shows the lowest electrical conductivity probably because it is less stable in aqueous media (refer to Section 4.1.5) compared to other materials.

Besides, I^-/I_3^- solution is generally known as an electrolyte solution that obviously has the ability to generate more current and can give high electrical conductivity (Wu et al., 2015). Furthermore, the value of Seebeck coefficient is inversely proportional to the charge carrier transport, which is directly connected with conductivity (Gibbs, Kim, Wang, & Snyder, 2015). Thus, the increment in Seebeck coefficient is normally observed with the decrement of electrical conductivity, which can also be one of the reasons. However, all functionalized GNPs materials show good performance with a significant increment for Seebeck coefficient. Thus, it can be said that all functionalized graphene materials have the potentials to provide better performance in the thermoelectrochemistry application.

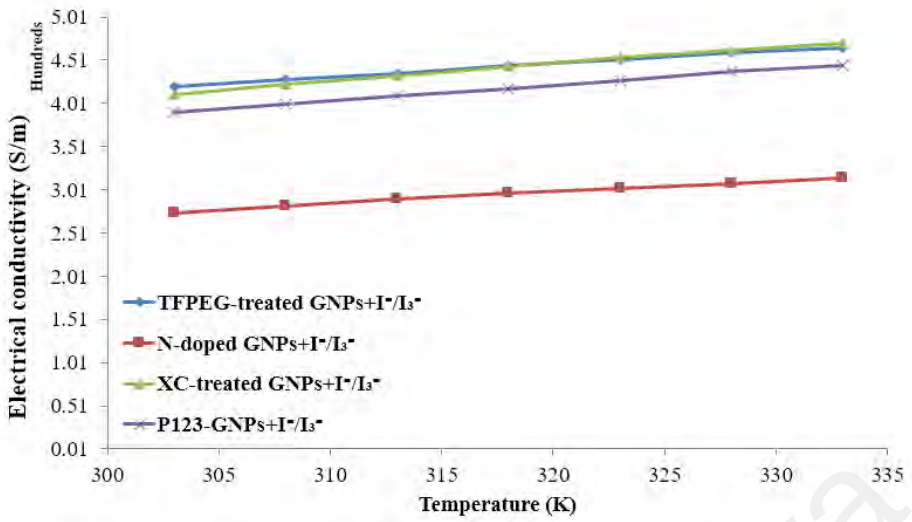

Figure 4.75: Electrical conductivity measurement of functionalized GNPs with the addition of iodide/triiodide liquid solution.

Table 4.17: Details of specific value of electrical conductivity for all tested samples.

Electrical conductivity (S/m)					
Temperature (K)	**I^-/I_3^-**	**TFPEG-treated GNPs + I^-/I_3^-**	**N-doped GNPs + I^-/I_3^-**	**XC-treated GNPs + I^-/I_3^-**	**P123-GNPs + I^-/I_3^-**
303	7661.26	421.12	274.25	410.54	390.74
308	7805.30	428.92	281.63	423.47	400.28
313	7981.08	435.77	289.98	433.12	410.23
318	8145.73	445.01	296.65	443.75	417.33
323	8300.21	452.04	303.14	454.84	427.71
328	8439.05	459.22	308.42	462.02	437.94
333	8562.37	465.29	314.46	470.43	445.24

CHAPTER 5: CONCLUSIONS AND RECOMMENDATIONS

5.1 Conclusion

This chapter discusses conclusions based on the experimental works that focus on the functionalization of GNPs material and their potential in heat transfer and thermoelectric applications. In addition, recommendations for further experiments or procedures in the future, which could be carried out depending on the availability of instruments and time factor, are also discussed. The major findings are summarized by focusing on the morphology, stability, and thermophysical properties of functionalized GNPs, as well as their influence in heat-based applications.

In short, many variables need to be considered in the modification of GNPs nanomaterials. The experimental works are discussed in detail in Chapter 4, where the results start with the analysis of morphological properties for each functionalized GNPs sample (TFPEG-treated GNPs, N-doped GNPs, P123-GNPs, and XC-treated GNPs). Next, the stability test has been carried for all samples and it can be concluded that all samples show good stability, especially in higher polar solvents (i.e., water, ethylene glycol, and methanol) within 15-day period. This is due to the functional groups attached on the surface of GNPs, which aid the dispersion of the nanomaterials in the solvents. The stability results are supported by the analysis of particle size and zeta potential, which lead to better understanding of nanofluid properties and their behavior. In addition, both covalent and non-covalent functionalization shows that the material with higher weight percentage and balance ratio of functionalize material gives better colloidal stability. Further investigation in thermophysical properties based on viscosity and thermal conductivity analysis has been carried out at selected range of temperature. For thermal conductivity, an enhancement has been observed for all samples compared to water at the investigated temperatures of 20, 30, 40, 50, and 60 °C. Meanwhile, TFPEG-treated GNPs,

N-doped GNPs, P123-GNPs, and XC-treated GNPs show Newtonian behavior with small difference of viscosity values when compared to the base fluid (water).

The final objective is also elaborated in Chapter 4, where the results are reported based on heat transfer and thermoelectrochemistry. The evaluation on convective heat transfer for the performance of nanofluids is based on turbulent regime, as well as laminar and transition flow. From the findings, it can be concluded that there is a significant improvement of heat transfer coefficient for each prepared nanocolloid at the selected temperatures. Parameters such as temperature play a significant role in improving heat transfer performance, especially at higher temperature. Besides, sample preparation is also important in affecting heat transfer behavior. Meanwhile, Seebeck coefficient and electrical conductivity are highlighted in the study of thermoelectrochemistry. From the results, there is an increment in Seebeck values but a decrease in electrical conductivity after the addition of iodide/triiodide solution for each functionalized sample. This is due to different influences that are affected by the types of functional group, stability, and viscosity. Although the significance of the conclusion in this field is less supported by the results, it is still possible to reach some conclusions on how the functionalized samples affect the mentioned parameters. Furthermore, chemically modified GNPs samples used in this study can be considered to have a potential value in above mentioned applications.

5.2 Recommendations for Future Works

At present, several new insights of greener and facile approaches on attaining functionalized nanomaterials with good stability using different base fluids are observed. The knowledge gained from the practical study based on their chemical and morphological structures would become a good platform to have a better understanding in developing a better strategy to achieve excellent colloidal stability. Moreover, the use of GNPs in convective heat transfer and thermoelectrochemistry fields provides

information regarding its potential in both applications. In the literature, different techniques have been used by researchers to functionalize graphene/GNPs material.

Both heat transfer and thermoelectrochemistry applications are dependent on many parameters such as base fluid type, range of temperature, and volume fraction of particles. At present, a detailed experimental investigation on the effect of these parameters on the mentioned applications has not been performed yet. After completing this study, there are some aspects that could not be covered in detail and some of the aspects are still in questions. Therefore, future works are recommended as follows:

1. The preparation of functionalized GNPs is the most critical part, as the morphological, thermophysical, and stability properties of GNPs will affect the performance of heat transfer and thermoelectric applications. Poor preparation of nanoparticles can lead to suspension, which can affect stability due to the agglomeration of nanoparticles. Most of the procedures or methods to increase the stability of GNPs found in the literature require a huge amount of hazardous chemicals. In addition, some of the techniques are costly and require longer time.

Hence, intensive studies using various techniques and methods can be carried out in the future to enhance the stability and thermophysical properties with a greener, simple, and cost-effective method. Several main parameters such as concentration, ratio of the material used for functionalization, pH, sonication time, and temperature during preparation should be considered and further studied to observe their effects after functionalization process. These parameters are critical as they influence particle size distribution, stability, and thermophysical properties of the nanomaterials.

2. The stability of functionalized nanoparticles in this research is not directly related to thermophysical properties. Therefore, an extensive study on the effect of

functionalization in the perspective of chemical structure, which can influence the stability, thermal conductivity, and viscosity of nanofluids for different functionalized materials should be performed in order to determine their correlation. This is to give a better understanding on how the functionalized nanomaterials will affect the performances or properties of the prepared functionalized nanomaterials.

Systematic studies about these aspects of functionalized GNPs will give valuable information in order to enhance the properties and provide optimum performance for the applications.

3. As an extension of understanding the fundamentals of convective heat transfer and thermoelectrochemistry properties, different chemical structures are the topic of interest. Thus, experimental works on convective heat transfer and thermoelectric performances can be extended by incorporating the functionalized materials used in this study. Investigations on heat transfer application can be further conducted at different conditions (e.g., flow rate, temperature, voltage power, and others), as well as for thermoelectrochemistry potential where investigations can be performed by studying the effect of electrolyte ratio and range of temperature for each functionalized GNPs. More theoretical studies can also help in achieving a better understanding of the effect of functionalized GNPs in these applications.

REFERENCES

Abraham, T. J., MacFarlane, D. R., & Pringle, J. M. (2011). Seebeck coefficients in ionic liquids–prospects for thermo-electrochemical cells. *Chemical Communications, 47*(22), 6260-6262.

Abraham, T. J., MacFarlane, D. R., & Pringle, J. M. (2013). High Seebeck coefficient redox ionic liquid electrolytes for thermal energy harvesting. *Energy & Environmental Science, 6*(9), 2639-2645.

Abu-Nada, E. (2008). Application of nanofluids for heat transfer enhancement of separated flows encountered in a backward facing step. *International Journal of Heat and Fluid Flow, 29*(1), 242-249. doi:10.1016/j.ijheatfluidflow.2007.07.001

Agromayor, R., Cabaleiro, D., Pardinas, A. A., Vallejo, J. P., Fernandez-Seara, J., & Lugo, L. (2016). Heat Transfer Performance of Functionalized Graphene Nanoplatelet Aqueous Nanofluids. *Materials, 9*(6).

Ahmadi-Moghadam, B., Sharafimasooleh, M., Shadlou, S., & Taheri, F. (2015). Effect of functionalization of graphene nanoplatelets on the mechanical response of graphene/epoxy composites. *Materials & Design, 66*, 142-149.

Al-Saleh, M. H., Al-Anid, H. K., & Hussain, Y. A. (2013). CNT/ABS nanocomposites by solution processing: Proper dispersion and selective localization for low percolation threshold. *Composites Part A: Applied Science and Manufacturing, 46*, 53-59.

Alexandridis, P., & Tsianou, M. (2011). Block copolymer-directed metal nanoparticle morphogenesis and organization. *European Polymer Journal, 47*(4), 569-583.

Amiri, A., Kazi, S., Shanbedi, M., Zubir, M. N. M., Yarmand, H., & Chew, B. (2015). Transformer oil based multi-walled carbon nanotube–hexylamine coolant with optimized electrical, thermal and rheological enhancements. *RSC Advances, 5*(130), 107222-107236.

Amiri, A., Sadri, R., Ahmadi, G., Chew, B., Kazi, S., Shanbedi, M., & Alehashem, M. S. (2015). Synthesis of polyethylene glycol-functionalized multi-walled carbon nanotubes with a microwave-assisted approach for improved heat dissipation. *Rsc Advances, 5*(45), 35425-35434.

Amollo, T. A., Mola, G. T., Kirui, M. S. K., & Nyamori, V. O. (2018). Graphene for Thermoelectric Applications: Prospects and Challenges. *Critical Reviews in Solid State and Materials Sciences, 43*(2), 133-157.

Amrollahi, A., Rashidi, A. M., Meibodi, M. E., & Kashefi, K. (2009). Conduction heat transfer characteristics and dispersion behaviour of carbon nanofluids as a function of different parameters. *Journal of Experimental Nanoscience, 4*(4), 347-363.

An, S., Lee, M. W., Kim, N. Y., Lee, C., Al-Deyab, S. S., James, S. C., & Yoon, S. S. (2014). Effect of viscosity, electrical conductivity, and surface tension on direct-current-pulsed drop-on-demand electrohydrodynamic printing frequency. *Applied Physics Letters, 105*(21), 214102.

Anno, Y., Imakita, Y., Takei, K., Akita, S., & Arie, T. (2017). Enhancement of graphene thermoelectric performance through defect engineering. *2d Materials, 4*(2).

Antunes, M., Gedler, G., Abbasi, H., & Velasco, J. I. (2016). Graphene nanoplatelets as a multifunctional filler for polymer foams. *Materials Today-Proceedings, 3*, S233-S239.

Aravind, S. J., Baskar, P., Baby, T. T., Sabareesh, R. K., Das, S., & Ramaprabhu, S. (2011). Investigation of structural stability, dispersion, viscosity, and conductive heat transfer properties of functionalized carbon nanotube based nanofluids. *The Journal of Physical Chemistry C, 115*(34), 16737-16744.

Arzani, H. K., Amiri, A., Kazi, S. N., Badarudin, A., & Chew, B. T. (2016). Heat transfer performance of water-based tetrahydrofurfuryl polyethylene glycol-treated graphene nanoplatelet nanofluids. *Rsc Advances, 6*(70), 65654-65669.

Askari, S., Koolivand, H., Pourkhalil, M., Lotfi, R., & Rashidi, A. (2017). Investigation of Fe3O4/Graphene nanohybrid heat transfer properties: Experimental approach. *International Communications in Heat and Mass Transfer, 87*, 30-39.

Azizi, M., Hosseini, M., Zafarnak, S., Shanbedi, M., & Amiri, A. (2013). Experimental analysis of thermal performance in a two-phase closed thermosiphon using graphene/water nanofluid. *Industrial & Engineering Chemistry Research, 52*(29), 10015-10021.

Baby, T. T., & Ramaprabhu, S. (2010). Investigation of thermal and electrical conductivity of graphene based nanofluids. *Journal of Applied Physics, 108*(12), 124308.

Baby, T. T., & Ramaprabhu, S. (2011). Enhanced convective heat transfer using graphene dispersed nanofluids. *Nanoscale Research Letters, 6*.

Bae, S., Kim, H., Lee, Y., Xu, X., Park, J.-S., Zheng, Y., . . . Song, Y. I. (2010). Roll-to-roll production of 30-inch graphene films for transparent electrodes. *Nature Nanotechnology, 5*(8), 574.

Bafana, A. (2016). *Polypropylene nanocomposites reinforced with graphene nanoplatelets*: Lamar University-Beaumont.

Bai, H., Li, C., & Shi, G. (2011). Functional composite materials based on chemically converted graphene. *Advanced Materials, 23*(9), 1089-1115.

Bai, H., Xu, Y., Zhao, L., Li, C., & Shi, G. (2009). Non-covalent functionalization of graphene sheets by sulfonated polyaniline. *Chemical Communications*(13), 1667-1669.

Bai, H., Xu, Y. X., Zhao, L., Li, C., & Shi, G. Q. (2009). Non-covalent functionalization of graphene sheets by sulfonated polyaniline. *Chemical Communications*(13), 1667-1669.

Bai, S., & Shen, X. (2012). Graphene–inorganic nanocomposites. *Rsc Advances, 2*(1), 64-98.

Bianco, V., Manca, O., & Nardini, S. (2011). Numerical investigation on nanofluids turbulent convection heat transfer inside a circular tube. *International Journal of Thermal Sciences, 50*(3), 341-349.

Black, J. J., Murphy, T., Atkin, R., Dolan, A., & Aldous, L. (2016). The thermoelectrochemistry of lithium–glyme solvate ionic liquids: towards waste heat harvesting. *Physical Chemistry Chemical Physics, 18*(30), 20768-20777.

Blasius, H. (1913). The Law of Similarity of Frictional Processes in Fluids (originally in German). *ForschArbeitIngenieur-Wesen, Berlin, 131*.

Bointon, T. H., Barnes, M. D., Russo, S., & Craciun, M. F. (2015). High quality monolayer graphene synthesized by resistive heating cold wall chemical vapor deposition. *Advanced Materials, 27*(28), 4200-4206.

Brink, L. (2014). *NOBEL LECTURES IN PHYSICS (2006–2010)*: World Scientific.

Britnell, L., Gorbachev, R., Jalil, R., Belle, B., Schedin, F., Mishchenko, A., . . . Morozov, S. (2012). Field-effect tunneling transistor based on vertical graphene heterostructures. *science, 335*(6071), 947-950.

Buongiorno, J. (2006). Convective transport in nanofluids. *Journal of Heat transfer, 128*(3), 240-250.

Cabaleiro, D., Colla, L., Barison, S., Lugo, L., Fedele, L., & Bobbo, S. (2017). Heat Transfer Capability of (Ethylene Glycol plus Water)-Based Nanofluids Containing Graphene Nanoplatelets: Design and Thermophysical Profile. *Nanoscale Research Letters, 12*.

Cai, D., & Song, M. (2010). Recent advance in functionalized graphene/polymer nanocomposites. *Journal of Materials Chemistry, 20*(37), 7906-7915.

Cai, D. Y., & Song, M. (2010). Recent advance in functionalized graphene/polymer nanocomposites. *Journal of Materials Chemistry, 20*(37), 7906-7915.

Chen, B., Zhao, X., Liu, Y., Xu, B., & Pan, X. (2015). Highly stable and covalently functionalized magnetic nanoparticles by polyethyleneimine for Cr (VI) adsorption in aqueous solution. *Rsc Advances, 5*(2), 1398-1405.

Chen, J., Yao, B., Li, C., & Shi, G. (2013). An improved Hummers method for eco-friendly synthesis of graphene oxide. *Carbon, 64*, 225-229.

Chen, P., Yang, J. J., Li, S. S., Wang, Z., Xiao, T. Y., Qian, Y. H., & Yu, S. H. (2013). Hydrothermal synthesis of macroscopic nitrogen-doped graphene hydrogels for ultrafast supercapacitor. *Nano Energy, 2*(2), 249-256.

Chieng, B. W., Ibrahim, N. A., & Yunus, W. M. Z. W. (2012). Optimization of Tensile Strength of Poly(Lactic Acid)/Graphene Nanocomposites Using Response Surface Methodology. *Polymer-Plastics Technology and Engineering, 51*(8), 791-799.

Cho, T.-Y., Yoon, S.-G., Sekhon, S., & Han, C.-H. (2011). Effect of Ionic Liquids with Different Cations in I-/I 3-Redox Electrolyte on the Performance of Dye-sensitized Solar Cells. *Bulletin of the Korean Chemical Society, 32*(6), 2058-2062.

Choi, E. Y., Han, T. H., Hong, J. H., Kim, J. E., Lee, S. H., Kim, H. W., & Kim, S. O. (2010). Noncovalent functionalization of graphene with end-functional polymers. *Journal of Materials Chemistry, 20*(10), 1907-1912.

Choi, S., Zhang, Z., Yu, W., Lockwood, F., & Grulke, E. (2001). Anomalous thermal conductivity enhancement in nanotube suspensions. *Applied Physics Letters, 79*(14), 2252-2254.

Chon, C. H., Kihm, K. D., Lee, S. P., & Choi, S. U. (2005). Empirical correlation finding the role of temperature and particle size for nanofluid (Al 2 O 3) thermal conductivity enhancement. *Applied Physics Letters, 87*(15), 153107.

Ciesielski, A., & Samori, P. (2014). Graphene via sonication assisted liquid-phase exfoliation. *Chemical Society Reviews, 43*(1), 381-398.

Ciesielski, A., & Samori, P. (2016). Supramolecular Approaches to Graphene: From Self-Assembly to Molecule-Assisted Liquid-Phase Exfoliation. *Advanced Materials, 28*(29), 6030-6051.

Coleman, J. N. (2013). Liquid Exfoliation of Defect-Free Graphene. *Accounts of Chemical Research, 46*(1), 14-22.

Coleman, V., Knut, R., Karis, O., Grennberg, H., Jansson, U., Quinlan, R., . . . Eriksson, O. (2008). Defect formation in graphene nanosheets by acid treatment: an x-ray absorption spectroscopy and density functional theory study. *Journal of Physics D: Applied Physics, 41*(6), 062001.

Compton, O. C., & Nguyen, S. T. (2010). Graphene Oxide, Highly Reduced Graphene Oxide, and Graphene: Versatile Building Blocks for Carbon-Based Materials. *Small, 6*(6), 711-723.

Conti, S., del Rosso, M. G., Ciesielski, A., Weippert, J., Bottcher, A., Shin, Y. Y., . . . Cecchini, M. (2016). Perchlorination of Coronene Enhances its Propensity for Self-Assembly on Graphene. *Chemphyschem, 17*(3), 352-357.

Craciun, M. F., Khrapach, I., Barnes, M. D., & Russo, S. (2013). Properties and applications of chemically functionalized graphene. *J Phys Condens Matter, 25*(42), 423201.

Cui, X., Zhang, C. Z., Hao, R., & Hou, Y. L. (2011). Liquid-phase exfoliation, functionalization and applications of graphene. *Nanoscale, 3*(5), 2118-2126.

Dai, J., Zhu, L., Tang, D., Fu, X., Tang, J., Guo, X., & Hu, C. (2017). Sulfonated polyaniline as a solid organocatalyst for dehydration of fructose into 5-hydroxymethylfurfural. *Green Chemistry, 19*(8), 1932-1939.

Dai, J. F., Wang, G. J., Ma, L., & Wu, C. K. (2015). Surface Properties of Graphene: Relationship to Graphene-Polymer Composites. *Reviews on Advanced Materials Science, 40*(1), 60-71.

Das, S. K., Putra, N., Thiesen, P., & Roetzel, W. (2003). Temperature dependence of thermal conductivity enhancement for nanofluids. *Journal of Heat transfer, 125*(4), 567-574.

Daungthongsuk, W., & Wongwises, S. (2007). A critical review of convective heat transfer of nanofluids. *Renewable & Sustainable Energy Reviews, 11*(5), 797-817.

de Andres, P. L., Ramirez, R., & Verges, J. A. (2008). Strong covalent bonding between two graphene layers. *Physical Review B, 77*(4).

Deissler, R. G. (1954). Analysis of turbulent heat transfer, mass transfer, and friction in smooth tubes at high Prandtl and Schmidt numbers.

Denaro, T., Baglio, V., Girolamo, M., Antonucci, V., Arico', A. S., Matteucci, F., & Ornelas, R. (2009). Investigation of low cost carbonaceous materials for application as counter electrode in dye-sensitized solar cells. *Journal of Applied Electrochemistry, 39*(11), 2173-2179.

Dittus, F., & Boelter, L. (1930). University of California publications on engineering. *University of California publications in Engineering, 2*, 371.

Dong, X., Wang, P., Fang, W., Su, C.-Y., Chen, Y.-H., Li, L.-J., . . . Chen, P. (2011). Growth of large-sized graphene thin-films by liquid precursor-based chemical vapor deposition under atmospheric pressure. *Carbon, 49*(11), 3672-3678.

Duangthongsuk, W., & Wongwises, S. (2010). An experimental study on the heat transfer performance and pressure drop of TiO2-water nanofluids flowing under a turbulent flow regime. *International Journal of Heat and Mass Transfer, 53*(1-3), 334-344.

Eapen, J., Williams, W. C., Buongiorno, J., Hu, L.-w., Yip, S., Rusconi, R., & Piazza, R. (2007). Mean-field versus microconvection effects in nanofluid thermal conduction. *Physical Review Letters, 99*(9), 095901.

Ejigu, A., Lovelock, K. R. J., Licence, P., & Walsh, D. A. (2011). Iodide/triiodide electrochemistry in ionic liquids: Effect of viscosity on mass transport, voltammetry and scanning electrochemical microscopy. *Electrochimica Acta, 56*(28), 10313-10320.

Emami-Meibodi, M., Vafaie-Sefti, M., Rashidi, A. M., Amrollahi, A., Tabasi, M., & Sid-Kalal, H. (2010). A model for thermal conductivity of nanofluids. *Materials Chemistry and Physics, 123*(2-3), 639-643.

Fan, X., Peng, W., Li, Y., Li, X., Wang, S., Zhang, G., & Zhang, F. (2008). Deoxygenation of exfoliated graphite oxide under alkaline conditions: a green route to graphene preparation. *Advanced Materials, 20*(23), 4490-4493.

Fan, Y., Liu, Y., Cai, Q., Liu, Y., & Zhang, J. (2012). Synthesis of CTAB-intercalated graphene/polypyrrole nanocomposites via in situ oxidative polymerization. *Synthetic Metals, 162*(21-22), 1815-1821.

Fernandez-Seara, J., Uhía, F. J., Sieres, J., & Campo, A. (2007). A general review of the Wilson plot method and its modifications to determine convection coefficients in heat exchange devices. *Applied Thermal Engineering, 27*(17), 2745-2757.

Fesenko, O., Dovbeshko, G., Dementjev, A., Karpicz, R., Kaplas, T., & Svirko, Y. (2015). Graphene-enhanced Raman spectroscopy of thymine adsorbed on single-layer graphene. *Nanoscale Research Letters, 10*(1), 163.

Fu, M., Jiao, Q., & Zhao, Y. (2013). In situ fabrication and characterization of cobalt ferrite nanorods/graphene composites. *Materials Characterization, 86*, 303-315.

Fugallo, G., Cepellotti, A., Paulatto, L., Lazzeri, M., Marzari, N., & Mauri, F. (2014). Thermal Conductivity of Graphene and Graphite: Collective Excitations and Mean Free Paths. *Nano Letters, 14*(11), 6109-6114.

Fuhrer, M. S., Lau, C. N., & MacDonald, A. H. (2010). Graphene: Materially Better Carbon. *Mrs Bulletin, 35*(4), 289-295.

Ge, H., Wang, C., Liu, S., & Huang, Z. (2016). Synthesis of citric acid functionalized magnetic graphene oxide coated corn straw for methylene blue adsorption. *Bioresour Technol, 221*, 419-429.

Geim, A. K. (2012). Graphene prehistory. *Physica Scripta, T146*.

Geim, A. K., & Novoselov, K. S. (2007). The rise of graphene. *Nature Materials, 6*(3), 183-191.

Georgakilas, V., Tiwari, J. N., Kemp, K. C., Perman, J. A., Bourlinos, A. B., Kim, K. S., & Zboril, R. (2016). Noncovalent Functionalization of Graphene and Graphene Oxide for Energy Materials, Biosensing, Catalytic, and Biomedical Applications. *Chemical Reviews, 116*(9), 5464-5519.

Georgiou, T., Jalil, R., Belle, B. D., Britnell, L., Gorbachev, R. V., Morozov, S. V., . . . Mishchenko, A. (2013). Vertical field-effect transistor based on graphene-WS2 heterostructures for flexible and transparent electronics. *Nature Nanotechnology, 8*(2), 100-103.

Ghadimi, A., Saidur, R., & Metselaar, H. S. C. (2011). A review of nanofluid stability properties and characterization in stationary conditions. *International Journal of Heat and Mass Transfer, 54*(17-18), 4051-4068.

Ghasemi, H., & Rajabpour, A. (2017). Thermal expansion coefficient of graphene using molecular dynamics simulation: A comparative study on potential functions. *Eurotherm Seminar No 108 - Nanoscale and Microscale Heat Transfer V, 785*.

Ghozatloo, A., Rashidi, A., & Shariaty-Niassar, M. (2014). Convective heat transfer enhancement of graphene nanofluids in shell and tube heat exchanger. *Experimental Thermal and Fluid Science, 53*, 136-141.

Gibbs, Z. M., Kim, H.-S., Wang, H., & Snyder, G. J. (2015). Band gap estimation from temperature dependent Seebeck measurement—deviations from the 2e| S| maxTmax relation. *Applied Physics Letters, 106*(2), 022112.

Gnielinski, V. (1976). New equations for heat and mass transfer in turbulent pipe and channel flow. *Int. Chem. Eng., 16*(2), 359-368.

Gong, X. Z., Liu, G. Z., Li, Y. S., Yu, D. Y. W., & Teoh, W. Y. (2016). Functionalized-Graphene Composites: Fabrication and Applications in Sustainable Energy and Environment. *Chemistry of Materials, 28*(22), 8082-8118.

Guerrero-Contreras, J., & Caballero-Briones, F. (2015). Graphene oxide powders with different oxidation degree, prepared by synthesis variations of the Hummers method. *Materials Chemistry and Physics, 153*, 209-220.

Guo, B., Fang, L., Zhang, B., & Gong, J. R. (2011). Graphene doping: a review. *Insciences J., 1*(2), 80-89.

Gupta, T. (2017). *Carbon: The Black, the Gray and the Transparent*: Springer.

Gyawali, D., Nair, P., Zhang, Y., Tran, R. T., Zhang, C., Samchukov, M., . . . Yang, J. A. (2010). Citric acid-derived in situ crosslinkable biodegradable polymers for cell delivery. *Biomaterials, 31*(34), 9092-9105.

Haar, S., Ciesielski, A., Clough, J., Yang, H., Mazzaro, R., Richard, F., . . . Morandi, V. (2015). A Supramolecular Strategy to Leverage the Liquid-Phase Exfoliation of Graphene in the Presence of Surfactants: Unraveling the Role of the Length of Fatty Acids. *Small, 11*(14), 1691-1702.

Han, J., Zhang, L. L., Lee, S., Oh, J., Lee, K. S., Potts, J. R., . . . Park, S. (2013). Generation of B-Doped Graphene Nanoplatelets Using a Solution Process and Their Supercapacitor Applications. *Acs Nano, 7*(1), 19-26.

Hasnan, M. M., Abdullah, N., Said, S., Salleh, M. M., Hussin, S. M., & Shah, N. M. (2017). Thermo-eletrochemical generation capabilities of octahedral spin crossover complexes of Mn (II), Fe (II) and Co (II) with N-donor ligands and benzoate counter ion. *Electrochimica Acta*.

Hayyan, M., Abo-Hamad, A., AlSaadi, M. A., & Hashim, M. A. (2015). Functionalization of graphene using deep eutectic solvents. *Nanoscale Research Letters, 10*.

Heris, S. Z., Etemad, S. G., & Esfahany, A. N. (2006). Experimental investigation of oxide nanofluids laminar flow convective heat transfer. *International Communications in Heat and Mass Transfer, 33*(4), 529-535.

Hernandez, Y., Nicolosi, V., Lotya, M., Blighe, F. M., Sun, Z., De, S., . . . Gun'Ko, Y. K. (2008). High-yield production of graphene by liquid-phase exfoliation of graphite. *Nature Nanotechnology, 3*(9), 563.

Heyrovska, R. (2008). Atomic structures of graphene, benzene and methane with bond lengths as sums of the single, double and resonance bond radii of carbon. *arXiv preprint arXiv:0804.4086*.

Hong, W., Xu, Y., Lu, G., Li, C., & Shi, G. (2008). Transparent graphene/PEDOT–PSS composite films as counter electrodes of dye-sensitized solar cells. *Electrochemistry Communications, 10*(10), 1555-1558.

Hsiao, S.-T., Ma, C.-C. M., Tien, H.-W., Liao, W.-H., Wang, Y.-S., Li, S.-M., & Huang, Y.-C. (2013). Using a non-covalent modification to prepare a high electromagnetic interference shielding performance graphene nanosheet/water-borne polyurethane composite. *Carbon, 60*, 57-66.

Hu, R., Cola, B. A., Haram, N., Barisci, J. N., Lee, S., Stoughton, S., . . . Gestos, A. (2010). Harvesting waste thermal energy using a carbon-nanotube-based thermo-electrochemical cell. *Nano Letters, 10*(3), 838-846.

Hu, Y., & Sun, X. (2013). Chemically functionalized graphene and their applications in electrochemical energy conversion and storage *Advances in Graphene Science*: InTech.

Huang, X., Qi, X., Boey, F., & Zhang, H. (2012). Graphene-based composites. *Chemical Society Reviews, 41*(2), 666-686.

Hummers Jr, W. S., & Offeman, R. E. (1958). Preparation of graphitic oxide. *Journal of the American Chemical Society, 80*(6), 1339-1339.

Islam, M. F., Rojas, E., Bergey, D. M., Johnson, A. T., & Yodh, A. G. (2003). High weight fraction surfactant solubilization of single-wall carbon nanotubes in water. *Nano Letters, 3*(2), 269-273.

Ji, L. L., Wu, Y. H., Ma, L. J., & Yang, X. M. (2015). Noncovalent functionalization of graphene with pyrene-terminated liquid crystalline polymer. *Composites Part a-Applied Science and Manufacturing, 72*, 32-39. doi:10.1016/j.compositesa.2015.01.009

Jiang, B. J., Tian, C. G., Wang, L., Sun, L., Chen, C., Nong, X. Z., . . . Fu, H. G. (2012). Highly concentrated, stable nitrogen-doped graphene for supercapacitors: Simultaneous doping and reduction. *Applied Surface Science, 258*(8), 3438-3443.

Jiang, H. F., Li, H., Xu, Q. H., & Shi, L. (2014). Effective thermal conductivity of nanofluids considering interfacial nano-shells. *Materials Chemistry and Physics, 148*(1-2), 195-200.

Jo, W.-G., Khan, M., Tan, L.-S., Jeong, H.-S., Lee, S.-H., & Park, S.-Y. (2017). Polypyrrole nanocomposite with water-dispersible graphene. *Macromolecular Research, 25*(4), 335-343.

Johnson, D. W., Dobson, B. P., & Coleman, K. S. (2015). A manufacturing perspective on graphene dispersions. *Current Opinion in Colloid & Interface Science, 20*(5-6), 367-382.

Kakac, S., & Pramuanjaroenkij, A. (2009). Review of convective heat transfer enhancement with nanofluids. *International Journal of Heat and Mass Transfer, 52*(13-14), 3187-3196.

Kalinina, I., Worsley, K., Lugo, C., Mandal, S., Bekyarova, E., & Haddon, R. C. (2011). Synthesis, Dispersion, and Viscosity of Poly (ethylene glycol)-Functionalized Water-Soluble Single-Walled Carbon Nanotubes. *Chemistry of Materials, 23*(5), 1246-1253.

Kanakia, S., Toussaint, J. D., Chowdhury, S. M., Lalwani, G., Tembulkar, T., Button, T., . . . Sitharaman, B. (2013). Physicochemical characterization of a novel graphene-based magnetic resonance imaging contrast agent. *International Journal of Nanomedicine, 8*, 2821-2833.

Kang, J., Shin, D., Bae, S., & Hong, B. H. (2012). Graphene transfer: key for applications. *Nanoscale, 4*(18), 5527-5537.

Kang, S., Choi, H., Bin Lee, S., Park, S. C., Park, J. B., Lee, S., . . . Hong, B. H. (2017). Efficient heat generation in large-area graphene films by electromagnetic wave absorption. *2d Materials, 4*(2).

Kang, T. J., Fang, S., Kozlov, M. E., Haines, C. S., Li, N., Kim, Y. H., . . . Baughman, R. H. (2012). Electrical power from nanotube and graphene electrochemical thermal energy harvesters. *Advanced Functional Materials, 22*(3), 477-489.

Kaur, P., Shin, M. S., Sharma, N., Kaur, N., Joshi, A., Chae, S. R., . . . Sekhon, S. S. (2015). Non-covalent functionalization of graphene with poly(diallyl dimethylammonium) chloride: Effect of a non-ionic surfactant. *International Journal of Hydrogen Energy, 40*(3), 1541-1547.

Kauzlarich, S. M., Brown, S. R., & Snyder, G. J. (2007). Zintl phases for thermoelectric devices. *Dalton Transactions*(21), 2099-2107.

Kazi, S., Duffy, G., & Chen, X. (2014). Validation of heat transfer and friction loss data for fibre suspensions in a circular and a coaxial pipe heat exchanger. *International Journal of Thermal Sciences, 79*, 146-160.

Khodabakhshi, F., Arab, S. M., Svec, P., & Gerlich, A. P. (2017). Fabrication of a new Al-Mg/graphene nanocomposite by multi-pass friction-stir processing: Dispersion, microstructure, stability, and strengthening. *Materials Characterization, 132*, 92-107

Kim, M., Kim, K.-J., Lee, S.-J., Kim, H.-M., Cho, S.-Y., Kim, M.-S., . . . Kim, K.-B. (2016). Highly Stable and Effective Doping of Graphene by Selective Atomic Layer Deposition of Ruthenium. *Acs Applied Materials & Interfaces, 9*(1), 701-709.

Kim, Y. J., Kim, Y., Novoselov, K., & Hong, B. H. (2015). Engineering electrical properties of graphene: chemical approaches. *2d Materials, 2*(4).

King, J. A., Klimek, D. R., Miskioglu, I., & Odegard, G. M. (2013). Mechanical properties of graphene nanoplatelet/epoxy composites. *Journal of Applied Polymer Science, 128*(6), 4217-4223.

Kitagawa, A., & Murai, Y. (2013). Natural convection heat transfer from a vertical heated plate in water with microbubble injection. *Chemical Engineering Science, 99*, 215-224.

Kline, S., & McClintock, F. (1953). Describing Uncertainties in Single-Sample Experiments,'A SME Mechanical Engineering, Vol. 75.

Kline, S. J., & McClintock, F. (1953). Describing uncertainties in single-sample experiments. *Mechanical engineering, 75*(1), 3-8.

Koch, C. C. (2007). Structural nanocrystalline materials: an overview. *Journal of Materials Science, 42*(5), 1403-1414.

Kotakoski, J., & Meyer, J. C. (2012). Mechanical properties of polycrystalline graphene based on a realistic atomistic model. *Physical Review B, 85*(19).

Kun, P., Tapaszto, O., Weber, F., & Balazsi, C. (2012). Determination of structural and mechanical properties of multilayer graphene added silicon nitride-based composites. *Ceramics International, 38*(1), 211-216.

Kwon, Y., Lee, K., Park, M., Koo, K., Lee, J., Doh, Y., . . . Jung, Y. (2013). Temperature Dependence of Convective Heat Transfer with Al2O3 Nanofluids in the Turbulent Flow Region. *Journal of Nanoscience and Nanotechnology, 13*(12), 7902-7905.

Lee, C., Wei, X., Kysar, J. W., & Hone, J. (2008). Measurement of the elastic properties and intrinsic strength of monolayer graphene. *science, 321*(5887), 385-388.

Lee, J. H., Hwang, K. S., Jang, S. P., Lee, B. H., Kim, J. H., Choi, S. O. U. S., & Choi, C. J. (2008). Effective viscosities and thermal conductivities of aqueous nanofluids containing of Al2O3 low volume concentrations nanoparticles. *International Journal of Heat and Mass Transfer, 51*(11-12), 2651-2656.

Lee, K. R., Lee, K. U., Lee, J. W., Ahn, B. T., & Woo, S. I. (2010). Electrochemical oxygen reduction on nitrogen doped graphene sheets in acid media. *Electrochemistry Communications, 12*(8), 1052-1055.

Lee, M. S., Choi, H. J., Baek, J. B., & Chang, D. W. (2017). Simple solution-based synthesis of pyridinic-rich nitrogen-doped graphene nanoplatelets for supercapacitors. *Applied Energy, 195*, 1071-1078.

Li, D., Müller, M. B., Gilje, S., Kaner, R. B., & Wallace, G. G. (2008). Processable aqueous dispersions of graphene nanosheets. *Nature Nanotechnology, 3*(2), 101.

Li, S., & Eastman, J. (1999). Measuring thermal conductivity of fluids containing oxide nanoparticles. *J. Heat Transf, 121*(2), 280-289.

Li, S. H., Li, Z. L., Burnett, T. L., Slater, T. J. A., Hashimoto, T., & Young, R. J. (2017). Nanocomposites of graphene nanoplatelets in natural rubber: microstructure and mechanisms of reinforcement. *Journal of Materials Science, 52*(16), 9558-9572.

Li, X., Cai, W., An, J., Kim, S., Nah, J., Yang, D., . . . Tutuc, E. (2009). Large-area synthesis of high-quality and uniform graphene films on copper foils. *science, 324*(5932), 1312-1314.

Li, X., Chen, Y., Mo, S. P., Jia, L. S., & Shao, X. F. (2014). Effect of surface modification on the stability and thermal conductivity of water-based SiO2-coated graphene nanofluid. *Thermochimica Acta, 595*, 6-10.

Li, Y. C., Tang, J. G., Huang, L. J., Wang, Y., Liu, J. X., Ge, X. C., . . . Belfiore, L. A. (2015). Facile preparation, characterization and performance of noncovalently functionalized graphene/epoxy nanocomposites with poly(sodium 4-styrenesulfonate). *Composites Part a-Applied Science and Manufacturing, 68*, 1-9.

Lian, M., Fan, J., Shi, Z., Li, H., & Yin, J. (2014). Kevlar®-functionalized graphene nanoribbon for polymer reinforcement. *Polymer, 55*(10), 2578-2587.

Liang, X. H., & Jiang, C. J. (2013). Atomic layer deposited highly dispersed platinum nanoparticles supported on non-functionalized multiwalled carbon nanotubes for the hydrogenation of xylose to xylitol. *Journal of Nanoparticle Research, 15*(9).

Liao, Z., Zhang, T., Qiao, S., & Zhang, L. (2017). *Preparation and Electrochemical Properties of Graphene/Epoxy Resin Composite Coating.* Paper presented at the IOP Conference Series: Earth and Environmental Science.

Lin, Z., Ye, X. H., Han, J. P., Chen, Q., Fan, P. X., Zhang, H. J., . . . Zhong, M. L. (2015). Precise Control of the Number of Layers of Graphene by Picosecond Laser Thinning. *Scientific Reports, 5*.

Liu, J., Wang, B. J., Xu, X. M., Chen, J. G., Chen, L. Y., & Yang, Y. Q. (2016). Green Finishing of Cotton Fabrics Using a Xylitol-Extended Citric Acid Cross-linking System on a Pilot Scale. *Acs Sustainable Chemistry & Engineering, 4*(3), 1131-1138.

Liu, J., Wang, F. X., Zhang, L., Fang, X. M., & Zhang, Z. G. (2014). Thermodynamic properties and thermal stability of ionic liquid-based nanofluids containing graphene as advanced heat transfer fluids for medium-to-high-temperature applications. *Renewable Energy, 63*, 519-523.

Liu, Q. H., Zhou, X. F., Fan, X. Y., Zhu, C. Y., Yao, X. Y., & Liu, Z. P. (2012). Mechanical and Thermal Properties of Epoxy Resin Nanocomposites Reinforced with Graphene Oxide. *Polymer-Plastics Technology and Engineering, 51*(3), 251-256.

Loh, K. P., Bao, Q., Ang, P. K., & Yang, J. (2010). The chemistry of graphene. *Journal of Materials Chemistry, 20*(12), 2277-2289.

Long, D., Li, W., Ling, L., Miyawaki, J., Mochida, I., & Yoon, S.-H. (2010). Preparation of nitrogen-doped graphene sheets by a combined chemical and hydrothermal reduction of graphene oxide. *Langmuir, 26*(20), 16096-16102.

Long, D. H., Li, W., Ling, L. C., Miyawaki, J., Mochida, I., & Yoon, S. H. (2010). Preparation of Nitrogen-Doped Graphene Sheets by a Combined Chemical and Hydrothermal Reduction of Graphene Oxide. *Langmuir, 26*(20), 16096-16102.

Lu, X., Yu, M., Huang, H., & Ruoff, R. S. (1999). Tailoring graphite with the goal of achieving single sheets. *Nanotechnology, 10*(3), 269.

Ma, W. S., Yang, F., Shi, J. J., Wang, F. X., Zhang, Z. G., & Wang, S. F. (2013). Silicone based nanofluids containing functionalized graphene nanosheets. *Colloids and Surfaces a-Physicochemical and Engineering Aspects, 431*, 120-126.

Mahalingam, S., Ramasamy, J., & Ahn, Y.-H. (2017). Synthesis and application of graphene-αMoO 3 nanocomposite for improving visible light irradiated photocatalytic decolorization of methylene blue dye. *Journal of the Taiwan Institute of Chemical Engineers*.

Mahmoud, L., Alhwarai, M., Samad, Y. A., Mohammad, B., Laio, K., & Elnaggar, I. (2015). Characterization of a Graphene-Based Thermoelectric Generator using a Cost-Effective Fabrication Process. *Clean, Efficient and Affordable Energy for a Sustainable Future, 75*, 615-620.

Malard, L. M., Pimenta, M. A., Dresselhaus, G., & Dresselhaus, M. S. (2009). Raman spectroscopy in graphene. *Physics Reports-Review Section of Physics Letters, 473*(5-6), 51-87.

Mandriota, S. J., Tenan, M., Ferrari, P., & Sappino, A. P. (2016). Aluminium chloride promotes tumorigenesis and metastasis in normal murine mammary gland epithelial cells. *International Journal of Cancer, 139*(12), 2781-2790.

Mao, X. W., Rutledge, G. C., & Hatton, T. A. (2014). Nanocarbon-based electrochemical systems for sensing, electrocatalysis, and energy storage. *Nano Today, 9*(4), 405-432.

Mao, Y., Duan, H., Xu, B., Zhang, L., Hu, Y. S., Zhao, C. C., . . . Yang, Y. S. (2012). Lithium storage in nitrogen-rich mesoporous carbon materials. *Energy & Environmental Science, 5*(7), 7950-7955.

McAllister, M. J., Li, J. L., Adamson, D. H., Schniepp, H. C., Abdala, A. A., Liu, J., . . . Aksay, I. A. (2007). Single sheet functionalized graphene by oxidation and thermal expansion of graphite. *Chemistry of Materials, 19*(18), 4396-4404.

Mehrali, M., Sadeghinezhad, E., Akhiani, A. R., Latibari, S. T., Talebian, S., Dolatshahi-Pirouz, A., . . . Mehrali, M. (2016). An ecofriendly graphene-based nanofluid for heat transfer applications. *Journal of Cleaner Production, 137*, 555-566.

Migkovic-Stankovic, V., Jevremovic, I., Jung, I., & Rhee, K. (2014). Electrochemical study of corrosion behavior of graphene coatings on copper and aluminum in a chloride solution. *Carbon, 75*, 335-344.

Mostofizadeh, A., Li, Y. W., Song, B., & Huang, Y. D. (2011). Synthesis, Properties, and Applications of Low-Dimensional Carbon-Related Nanomaterials. *Journal of Nanomaterials*.

Murugan, A. V., Muraliganth, T., & Manthiram, A. (2009). Rapid, facile microwave-solvothermal synthesis of graphene nanosheets and their polyaniline nanocomposites for energy strorage. *Chemistry of Materials, 21*(21), 5004-5006.

Nair, R. R., Blake, P., Grigorenko, A. N., Novoselov, K. S., Booth, T. J., Stauber, T., . . . Geim, A. K. (2008). Fine structure constant defines visual transparency of graphene. *science, 320*(5881), 1308-1308.

Nakayama, M., Sato, A., Ishihara, K., & Yamamoto, H. (2004). Water-tolerant and reusable catalysts for direct ester condensation between equimolar amounts of carboxylic acids and alcohols. *Advanced Synthesis & Catalysis, 346*(11), 1275-1279.

Ni, Z., Wang, H., Kasim, J., Fan, H., Yu, T., Wu, Y., . . . Shen, Z. (2007). Graphene thickness determination using reflection and contrast spectroscopy. *Nano Letters, 7*(9), 2758-2763.

Nika, D., Ghosh, S., Pokatilov, E., & Balandin, A. (2009). Lattice thermal conductivity of graphene flakes: Comparison with bulk graphite. *Applied Physics Letters, 94*(20), 203103.

Nika, D. L., Pokatilov, E. P., Askerov, A. S., & Balandin, A. A. (2009). Phonon thermal conduction in graphene: Role of Umklapp and edge roughness scattering. *Physical Review B, 79*(15).

Nikoofar, K., & Khademi, Z. (2015). A review on green Lewis acids: zirconium(IV) oxydichloride octahydrate (ZrOCl2·8H2O) and zirconium(IV) tetrachloride (ZrCl4) in organic chemistry. *Research on Chemical Intermediates, 42*(5), 3929-3977.

Niu, L., Coleman, J. N., Zhang, H., Shin, H., Chhowalla, M., & Zheng, Z. (2016). Production of Two-Dimensional Nanomaterials via Liquid-Based Direct Exfoliation. *Small, 12*(3), 272-293.

Niyogi, S., Bekyarova, E., Itkis, M. E., Zhang, H., Shepperd, K., Hicks, J., . . . Deheer, W. A. (2010). Spectroscopy of covalently functionalized graphene. *Nano Letters, 10*(10), 4061-4066.

Novoselov, K., Mishchenko, A., Carvalho, A., & Neto, A. C. (2016). 2D materials and van der Waals heterostructures. *science, 353*(6298), aac9439.

Novoselov, K. S., Geim, A. K., Morozov, S., Jiang, D., Katsnelson, M., Grigorieva, I., . . . AA. (2005). Two-dimensional gas of massless Dirac fermions in graphene. *Nature, 438*(7065), 197.

Novoselov, K. S., Geim, A. K., Morozov, S. V., Jiang, D., Zhang, Y., Dubonos, S. V., . . . Firsov, A. A. (2004). Electric field effect in atomically thin carbon films. *science, 306*(5696), 666-669.

Novoselov, K. S., Jiang, Z., Zhang, Y., Morozov, S., Stormer, H. L., Zeitler, U., . . . Geim, A. K. (2007). Room-temperature quantum Hall effect in graphene. *science, 315*(5817), 1379-1379.

Oh, J. S., Kim, K. N., & Yeom, G. Y. (2014). Graphene doping methods and device applications. *Journal of Nanoscience and Nanotechnology, 14*(2), 1120-1133.

Ohtani, Y., & Hoshi, H. (2018). Effect of graphene nanoplatelet edges on the iodide/triiodide redox reaction. *Electrochemistry Communications, 87*, 49-52.

Pak, B. C., & Cho, Y. I. (1998). Hydrodynamic and heat transfer study of dispersed fluids with submicron metallic oxide particles. *Experimental Heat Transfer an International Journal, 11*(2), 151-170.

Panchakarla, L., Subrahmanyam, K., Saha, S., Govindaraj, A., Krishnamurthy, H., Waghmare, U., & Rao, C. (2009). Synthesis, Structure, and Properties of Boron- and Nitrogen-Doped Graphene. *Advanced Materials, 21*(46), 4726-4730.

Panchokarla, L. S., Subrahmanyam, K. S., Saha, S. K., Govindaraj, A., Krishnamurthy, H. R., Waghmare, U. V., & Rao, C. N. R. (2009). Synthesis, Structure, and Properties of Boron- and Nitrogen-Doped Graphene. *Advanced Materials, 21*(46), 4726-+.

Papageorgiou, D. G., Kinloch, I. A., & Young, R. J. (2017). Mechanical properties of graphene and graphene-based nanocomposites. *Progress in Materials Science, 90*, 75-127.

Park, M. J., Lee, J. K., Lee, B. S., Lee, Y. W., Choi, I. S., & Lee, S. G. (2006). Covalent modification of multiwalled carbon nanotubes with imidazolium-based ionic liquids: Effect of anions on solubility. *Chemistry of Materials, 18*(6), 1546-1551.

Park, S., & Ruoff, R. S. (2009). Chemical methods for the production of graphenes. *Nature Nanotechnology, 4*(4), 217.

Park, S. S., & Kim, N. J. (2014). Influence of the oxidation treatment and the average particle diameter of graphene for thermal conductivity enhancement. *Journal of Industrial and Engineering Chemistry, 20*(4), 1911-1915.

Petukhov, B. (1970). Heat transfer and friction in turbulent pipe flow with variable physical properties *Advances in heat transfer* (Vol. 6, pp. 503-564): Elsevier.

Polsen, E. S., McNerny, D. Q., Viswanath, B., Pattinson, S. W., & Hart, A. J. (2015). High-speed roll-to-roll manufacturing of graphene using a concentric tube CVD reactor. *Scientific Reports, 5*, 10257.

Pop, E., Varshney, V., & Roy, A. K. (2012). Thermal properties of graphene: Fundamentals and applications. *Mrs Bulletin, 37*(12), 1273-1281.

Prasher, R., Song, D., Wang, J., & Phelan, P. (2006). Measurements of nanofluid viscosity and its implications for thermal applications. *Applied Physics Letters, 89*(13), 133108.

Prencipe, G., Tabakman, S. M., Welsher, K., Liu, Z., Goodwin, A. P., Zhang, L., . . . Dai, H. J. (2009). PEG Branched Polymer for Functionalization of Nanomaterials with Ultralong Blood Circulation. *Journal of the American Chemical Society, 131*(13), 4783-4787.

Puangbuppha, B., Limsuwan, P., & Asanithi, P. (2012). Non-Chemically Functionalized Graphene Exfoliated from Graphite in Water using Ultrasonic Treatment. *Iseec, 32*, 1094-1099.

Qian, Y., Wu, H., Yuan, D., Li, X., Yu, W., & Wang, C. (2015). In situ polymerization of polyimide-based nanocomposites via covalent incorporation of functionalized graphene nanosheets for enhancing mechanical, thermal, and electrical properties. *Journal of Applied Polymer Science, 132*(44).

Qu, L. T., Liu, Y., Baek, J. B., & Dai, L. M. (2010). Nitrogen-Doped Graphene as Efficient Metal-Free Electrocatalyst for Oxygen Reduction in Fuel Cells. *Acs Nano, 4*(3), 1321-1326.

Radadiya, T. M. (2015). A PROPERTIES OF GRAPHENE. *European Journal of Material Sciences, 2*(1), 6-18.

Rahman, M. J., & Mieno, T. (2014). Water-Dispersible Multiwalled Carbon Nanotubes Obtained from Citric-Acid-Assisted Oxygen Plasma Functionalization. *Journal of Nanomaterials*.

Ramires, M. L. V., Decastro, C. A. N., Nagasaka, Y., Nagashima, A., Assael, M. J., & Wakeham, W. A. (1995). Standard Reference Data for the Thermal-Conductivity of Water. *Journal of Physical and Chemical Reference Data, 24*(3), 1377-1381.

Renteria, J. D., Nika, D. L., & Balandin, A. A. (2014). Graphene Thermal Properties: Applications in Thermal Management and Energy Storage. *Applied Sciences-Basel, 4*(4), 525-547.

Research: Projects: Graphene Chemistry. (2018, June 6). *Organic Surface Chemistry (Aarhus University, Denmark)*. Retrieved from http://surfchem.dk/research/projects/graphene-chemistry/

Rohsenow, W. M., Hartnett, J. P., & Cho, Y. I. (1998). *Handbook of heat transfer* (Vol. 3): McGraw-Hill New York.

Romano, M. S., Gambhir, S., Razal, J. M., Gestos, A., Wallace, G. G., & Chen, J. (2012). Novel carbon materials for thermal energy harvesting. *Journal of Thermal Analysis and Calorimetry, 109*(3), 1229-1235.

Romano, M. S., Li, N., Antiohos, D., Razal, J. M., Nattestad, A., Beirne, S., . . . Wallace, G. G. (2013). Carbon nanotube–reduced graphene oxide composites for thermal energy harvesting applications. *Advanced Materials, 25*(45), 6602-6606.

Romano, M. S., Razal, J. M., Antiohos, D., Wallace, G., & Chen, J. (2015). Nano-carbon electrodes for thermal energy harvesting. *Journal of Nanoscience and Nanotechnology, 15*(1), 1-14.

Rowe, D. M. (2005). *Thermoelectrics handbook: macro to nano*: CRC press.

Roy-Mayhew, J. D., Bozym, D. J., Punckt, C., & Aksay, I. A. (2010). Functionalized Graphene as a Catalytic Counter Electrode in Dye-Sensitized Solar Cells. *Acs Nano, 4*(10), 6203-6211.

Rümmeli, M. H., Rocha, C. G., Ortmann, F., Ibrahim, I., Sevincli, H., Börrnert, F., . . . Shiraishi, M. (2011). Graphene: Piecing it together. *Advanced Materials, 23*(39), 4471-4490.

Sadeghinezhad, E., Mehrali, M., Latibari, S. T., Mehrali, M., Kazi, S. N., Oon, C. S., & Metselaar, H. S. C. (2014). Experimental Investigation of Convective Heat Transfer Using Graphene Nanoplatelet Based Nanofluids under Turbulent Flow Conditions. *Industrial & Engineering Chemistry Research, 53*(31), 12455-12465.

Sadeghinezhad, E., Mehrali, M., Tahan Latibari, S., Mehrali, M., Kazi, S., Oon, C. S., & Metselaar, H. S. C. (2014). Experimental investigation of convective heat transfer using graphene nanoplatelet based nanofluids under turbulent flow conditions. *Industrial & Engineering Chemistry Research, 53*(31), 12455-12465.

Sadeghinezhad, E., Togun, H., Mehrali, M., Nejad, P. S., Latibari, S. T., Abdulrazzaq, T., . . . Metselaar, H. S. C. (2015). An experimental and numerical investigation of heat transfer enhancement for graphene nanoplatelets nanofluids in turbulent flow conditions. *International Journal of Heat and Mass Transfer, 81*, 41-51.

Salavagione, H. J., Gomez, M. A., & Martinez, G. (2009). Polymeric modification of graphene through esterification of graphite oxide and poly (vinyl alcohol). *Macromolecules, 42*(17), 6331-6334.

Salavagione, H. J., & Martínez, G. (2011). Importance of covalent linkages in the preparation of effective reduced graphene oxide− poly (vinyl chloride) nanocomposites. *Macromolecules, 44*(8), 2685-2692.

Sarojini, K. G. K., Manoj, S. V., Singh, P. K., Pradeep, T., & Das, S. K. (2013). Electrical conductivity of ceramic and metallic nanofluids. *Colloids and Surfaces a-Physicochemical and Engineering Aspects, 417*, 39-46.

Sarsam, W. S., Amiri, A., Kazi, S. N., & Badarudin, A. (2016). Stability and thermophysical properties of non-covalently functionalized graphene nanoplatelets nanofluids. *Energy Conversion and Management, 116*, 101-111.

Sarsam, W. S., Amiri, A., Zubir, M. N. M., Yarmand, H., Kazi, S. N., & Badarudin, A. (2016). Stability and thermophysical properties of water-based nanofluids containing triethanolamine-treated graphene nanoplatelets with different specific surface areas. *Colloids and Surfaces a-Physicochemical and Engineering Aspects, 500*, 17-31.

Scaffaro, R., Botta, L., Maio, A., Mistretta, M. C., & La Mantia, F. P. (2016). Effect of Graphene Nanoplatelets on the Physical and Antimicrobial Properties of Biopolymer-Based Nanocomposites. *Materials, 9*(5).

Schedin, F., Geim, A. K., Morozov, S. V., Hill, E. W., Blake, P., Katsnelson, M. I., & Novoselov, K. S. (2007). Detection of individual gas molecules adsorbed on graphene. *Nature Materials, 6*(9), 652-655.

Sen Gupta, S., Siva, V. M., Krishnan, S., Sreeprasad, T. S., Singh, P. K., Pradeep, T., & Das, S. K. (2011). Thermal conductivity enhancement of nanofluids containing graphene nanosheets. *Journal of Applied Physics, 110*(8).

Shahil, K. M. F., & Balandin, A. A. (2012). Thermal properties of graphene and multilayer graphene: Applications in thermal interface materials. *Solid State Communications, 152*(15), 1331-1340.

Shan, C. S., Yang, H. F., Han, D. X., Zhang, Q. X., Ivaska, A., & Niu, L. (2009). Water-Soluble Graphene Covalently Functionalized by Biocompatible Poly-L-lysine. *Langmuir, 25*(20), 12030-12033.

Shearer, C. J., Cherevan, A., & Eder, D. (2014). Application and Future Challenges of Functional Nanocarbon Hybrids. *Advanced Materials, 26*(15), 2295-2318.

Shen, J., Hu, Y., Shi, M., Lu, X., Qin, C., Li, C., & Ye, M. (2009). Fast and facile preparation of graphene oxide and reduced graphene oxide nanoplatelets. *Chemistry of Materials, 21*(15), 3514-3520.

Shen, Z. Q., Ye, H. L., Zhou, C., Kroger, M., & Li, Y. (2018). Size of graphene sheets determines the structural and mechanical properties of 3D graphene foams. *Nanotechnology, 29*(10).

Shin, H. J., Kim, K. K., Benayad, A., Yoon, S. M., Park, H. K., Jung, I. S., . . . Choi, J. Y. (2009). Efficient reduction of graphite oxide by sodium borohydride and its effect on electrical conductance. *Advanced Functional Materials, 19*(12), 1987-1992.

Shoghl, S. N., Jamali, J., & Moraveji, M. K. (2016). Electrical conductivity, viscosity, and density of different nanofluids: An experimental study. *Experimental Thermal and Fluid Science, 74*, 339-346.

Singh, V., Joung, D., Zhai, L., Das, S., Khondaker, S. I., & Seal, S. (2011). Graphene based materials: Past, present and future. *Progress in Materials Science, 56*(8), 1178-1271.

Song, J., Kam, F.-Y., Png, R.-Q., Seah, W.-L., Zhuo, J.-M., Lim, G.-K., . . . Chua, L.-L. (2013). A general method for transferring graphene onto soft surfaces. *Nature Nanotechnology, 8*(5), 356.

Song, M. (2013). Graphene functionalization and its application to polymer composite materials.

Srivastava, A., Galande, C., Ci, L., Song, L., Rai, C., Jariwala, D., . . . Ajayan, P. M. (2010). Novel liquid precursor-based facile synthesis of large-area continuous, single, and few-layer graphene films. *Chemistry of Materials, 22*(11), 3457-3461.

Stankovich, S., Dikin, D. A., Dommett, G. H. B., Kohlhaas, K. M., Zimney, E. J., Stach, E. A., . . . Ruoff, R. S. (2006). Graphene-based composite materials. *Nature, 442*(7100), 282-286.

Stankovich, S., Dikin, D. A., Piner, R. D., Kohlhaas, K. A., Kleinhammes, A., Jia, Y., . . . Ruoff, R. S. (2007). Synthesis of graphene-based nanosheets via chemical reduction of exfoliated graphite oxide. *Carbon, 45*(7), 1558-1565.

Stankovich, S., Piner, R. D., Chen, X., Wu, N., Nguyen, S. T., & Ruoff, R. S. (2006). Stable aqueous dispersions of graphitic nanoplatelets via the reduction of exfoliated graphite oxide in the presence of poly (sodium 4-styrenesulfonate). *Journal of Materials Chemistry, 16*(2), 155-158.

Steinhögl, W., Schindler, G., Steinlesberger, G., Traving, M., & Engelhardt, M. (2005). Comprehensive study of the resistivity of copper wires with lateral dimensions of 100 nm and smaller. *Journal of Applied Physics, 97*(2), 023706.

Stoller, M. D., Park, S. J., Zhu, Y. W., An, J. H., & Ruoff, R. S. (2008). Graphene-Based Ultracapacitors. *Nano Letters, 8*(10), 3498-3502.

Strankowski, M., Piszczyk, L., Kosmela, P., & Korzeniewski, P. (2015). Morphology and the physical and thermal properties of thermoplastic polyurethane reinforced with thermally reduced graphene oxide. *Polish Journal of Chemical Technology, 17*(4), 88-94.

Su, Y. L., Wang, J., & Liu, H. Z. (2002). FTIR spectroscopic study on effects of temperature and polymer composition on the structural properties of PEO-PPO-PEO block copolymer micelles. *Langmuir, 18*(14), 5370-5374.

Sukhadolau, A., Ivakin, E., Ralchenko, V., Khomich, A., Vlasov, A., & Popovich, A. (2005). Thermal conductivity of CVD diamond at elevated temperatures. *Diamond and Related Materials, 14*(3-7), 589-593.

Sun, Y. P., Fu, K. F., Lin, Y., & Huang, W. J. (2002). Functionalized carbon nanotubes: Properties and applications. *Accounts of Chemical Research, 35*(12), 1096-1104.

Sundar, L. S., Singh, M. K., & Sousa, A. C. (2014). Enhanced heat transfer and friction factor of MWCNT–Fe3O4/water hybrid nanofluids. *International Communications in Heat and Mass Transfer, 52*, 73-83.

Taha, A. A., Mousa, A., Al-ott, M., Faroun, M., Assali, M., Gomez, P. R., & Thiab, S. (2016). Non-Covalent Functionalization of Graphene Sheets with Surfactants and their Antibacterial Activity.

Talat, M., Awasthi, K., & Srivastava, O. (2014). Studies on the Dispersion of Carbon Nanotubes and Graphene in Aqueous Solutions with Different Types of Surfactants. *Advanced Science Letters, 20*(5-6), 1163-1169.

Tang, Q., Zhou, Z., & Chen, Z. F. (2013). Graphene-related nanomaterials: tuning properties by functionalization. *Nanoscale, 5*(11), 4541-4583.

Taylor, J. (1997). *Introduction to error analysis, the study of uncertainties in physical measurements*.

Taylor, J. R., & Thompson, W. (1998). An introduction to error analysis: the study of uncertainties in physical measurements. *Measurement Science and Technology, 9*(6), 1015.

Thommes, M., Kohn, R., & Froba, M. (2000). Sorption and pore condensation behavior of nitrogen, argon, and krypton in mesoporous: MCM-48 silica materials. *Journal of Physical Chemistry B, 104*(33), 7932-7943.

Timofeeva, E. V., Routbort, J. L., & Singh, D. (2009). Particle shape effects on thermophysical properties of alumina nanofluids. *Journal of Applied Physics, 106*(1), 014304.

Tiwari, S. K., Kumar, V., Huczko, A., Oraon, R., De Adhikari, A., & Nayak, G. C. (2016). Magical Allotropes of Carbon: Prospects and Applications. *Critical Reviews in Solid State and Materials Sciences, 41*(4), 257-317.

Tohei, T., Kuwabara, A., Oba, F., & Tanaka, I. (2006). Debye temperature and stiffness of carbon and boron nitride polymorphs from first principles calculations. *Physical Review B, 73*(6).

Trancik, J. E., Barton, S. C., & Hone, J. (2008). Transparent and catalytic carbon nanotube films. *Nano Letters, 8*(4), 982-987.

Usachov, D., Vilkov, O., Gruneis, A., Haberer, D., Fedorov, A., Adamchuk, V. K., . . . Vyalikh, D. V. (2011). Nitrogen-Doped Graphene: Efficient Growth, Structure, and Electronic Properties. *Nano Letters, 11*(12), 5401-5407.

Wall, M. (2011). The Raman spectroscopy of graphene and the determination of layer thickness. *Thermo Sci, 5*.

Wallace, P. R. (1947). The band theory of graphite. *Physical Review, 71*(9), 622.

Wang, H., Maiyalagan, T., & Wang, X. (2012). Review on recent progress in nitrogen-doped graphene: synthesis, characterization, and its potential applications. *Acs Catalysis, 2*(5), 781-794.

Wang, J. G., Ma, F. C., Liang, W. J., & Sun, M. T. (2017). Electrical properties and applications of graphene, hexagonal boron nitride (h-BN), and graphene/h-BN heterostructures. *Materials Today Physics, 2*, 6-34.

Wang, X. (2010). N-doping of graphene through electrothermal reactions with ammonia (vol 324, pg 768, 2009). *science, 329*(5998), 1467-1467.

Wang, X., Hu, Y., Li, T., & He, Y. (2017). Experimental Investigation of Graphene Nanofluid and Numerical Simulation of Its Natural Convection in a Square Enclosure. *Nanoscience and Nanotechnology Letters, 9*(5), 640-649.

Wang, X., Zhi, L. J., & Mullen, K. (2008). Transparent, conductive graphene electrodes for dye-sensitized solar cells. *Nano Letters, 8*(1), 323-327.

Wang, X. R., Li, X. L., Zhang, L., Yoon, Y., Weber, P. K., Wang, H. L., . . . Dai, H. J. (2009). N-Doping of Graphene Through Electrothermal Reactions with Ammonia. *science, 324*(5928), 768-771.

Wang, Y., Qiu, B., & Ruan, X. (2012). Edge effect on thermal transport in graphene nanoribbons: A phonon localization mechanism beyond edge roughness scattering. *Applied Physics Letters, 101*(1), 013101.

Wang, Y., Shi, Z., & Yin, J. (2011). Facile synthesis of soluble graphene via a green reduction of graphene oxide in tea solution and its biocomposites. *Acs Applied Materials & Interfaces, 3*(4), 1127-1133.

Wang, Y., Yu, J., Dai, W., Song, Y., Wang, D., Zeng, L., & Jiang, N. (2015). Enhanced thermal and electrical properties of epoxy composites reinforced with graphene nanoplatelets. *Polymer Composites, 36*(3), 556-565.

Wei, D., Liu, Y., Wang, Y., Zhang, H., Huang, L., & Yu, G. (2009). Synthesis of N-doped graphene by chemical vapor deposition and its electrical properties. *Nano Letters, 9*(5), 1752-1758.

Wei, D. C., Liu, Y. Q., Wang, Y., Zhang, H. L., Huang, L. P., & Yu, G. (2009). Synthesis of N-Doped Graphene by Chemical Vapor Deposition and Its Electrical Properties. *Nano Letters, 9*(5), 1752-1758.

Wei, J., Atif, R., Vo, T., & Inam, F. (2015). Graphene nanoplatelets in epoxy system: dispersion, reaggregation, and mechanical properties of nanocomposites. *Journal of Nanomaterials, 16*(1), 374.

Wei, J., & Inam, F. (2017). Processing of epoxy/graphene nanocomposites: effects of surfactants. *Journal of Polymer Science & Applications, 2017*.

Wei, J. C., Atif, R., Vo, T., & Inam, F. (2015). Graphene Nanoplatelets in Epoxy System: Dispersion, Reaggregation, and Mechanical Properties of Nanocomposites. *Journal of Nanomaterials*.

Wei, Q. L., Tong, X., Zhang, G. X., Qiao, J. L., Gong, Q. J., & Sun, S. H. (2015). Nitrogen-Doped Carbon Nanotube and Graphene Materials for Oxygen Reduction Reactions. *Catalysts, 5*(3), 1574-1602.

Wei, Y., & Sun, Z. Y. (2015). Liquid-phase exfoliation of graphite for mass production of pristine few-layer graphene. *Current Opinion in Colloid & Interface Science, 20*(5-6), 311-321.

Wen, D. S., & Ding, Y. L. (2004). Experimental investigation into convective heat transfer of nanofluids at the entrance region under laminar flow conditions. *International Journal of Heat and Mass Transfer, 47*(24), 5181-5188.

Wen, D. S., Lin, G. P., Vafaei, S., & Zhang, K. (2009). Review of nanofluids for heat transfer applications. *Particuology, 7*(2), 141-150.

Withers, F., Del Pozo-Zamudio, O., Mishchenko, A., Rooney, A. P., Gholinia, A., Watanabe, K., . . . Novoselov, K. S. (2015). Light-emitting diodes by band-

structure engineering in van der Waals heterostructures. *Nature Materials, 14*(3), 301-306.

Wu, J., Lan, Z., Lin, J., Huang, M., Huang, Y., Fan, L., & Luo, G. (2015). Electrolytes in dye-sensitized solar cells. *Chemical Reviews, 115*(5), 2136-2173.

Xin, Y. C., Liu, J. G., Jie, X., Liu, W. M., Liu, F. Q., Yin, Y., . . . Zou, Z. G. (2012). Preparation and electrochemical characterization of nitrogen doped graphene by microwave as supporting materials for fuel cell catalysts. *Electrochimica Acta, 60*, 354-358.

Xing, T. T., Lou, Y. B., Bao, Q. L., & Chen, J. X. (2014). Surfactant-assisted synthesis of ZIF-8 nanocrystals in aqueous solution via microwave irradiation. *Crystengcomm, 16*(38), 8994-9000.

Xing, Z., Ju, Z. C., Zhao, Y. L., Wan, J. L., Zhu, Y. B., Qiang, Y. H., & Qian, Y. T. (2016). One-pot hydrothermal synthesis of Nitrogen-doped graphene as high-performance anode materials for lithium ion batteries. *Scientific Reports, 6*.

Xiong, B., Zhou, Y., Zhao, Y., Wang, J., Chen, X., O'Hayre, R., & Shao, Z. (2013). The use of nitrogen-doped graphene supporting Pt nanoparticles as a catalyst for methanol electrocatalytic oxidation. *Carbon, 52*, 181-192.

Xu, Z. Y., Wang, S., Li, Y. J., Wang, M. W., Shi, P., & Huang, X. Y. (2014). Covalent Functionalization of Graphene Oxide with Biocompatible Poly(ethylene glycol) for Delivery of Paclitaxel. *Acs Applied Materials & Interfaces, 6*(19), 17268-17276.

Xue, C. H., Zhou, R. J., Shi, M. M., Gao, Y., Wu, G., Zhang, X. B., . . . Wang, M. (2008). A green route to water soluble carbon nanotubes and in situ loading of silver nanoparticles. *Nanotechnology, 19*(32).

Yadav, R., & Dixit, C. K. (2017). Synthesis, characterization and prospective applications of nitrogen-doped graphene: A short review. *Journal of Science: Advanced Materials and Devices, 2*(2), 141-149.

Yadav, S. K., & Cho, J. W. (2013). Functionalized graphene nanoplatelets for enhanced mechanical and thermal properties of polyurethane nanocomposites. *Applied Surface Science, 266*, 360-367.

Yang, F., Liu, Y., Gao, L., & Sun, J. (2010). pH-Sensitive highly dispersed reduced graphene oxide solution using lysozyme via an in situ reduction method. *The Journal of Physical Chemistry C, 114*(50), 22085-22091.

Yang, H. B., Memon, S. A., Bao, X. H., Cui, H. Z., & Li, D. X. (2017). Design and Preparation of Carbon Based Composite Phase Change Material for Energy Piles. *Materials, 10*(4).

Yang, J. M., Yan, Y. L., Wang, Y. X., & Yang, G. (2014). Improved thermoelectric performance of CuGaTe2 with convergence of band valleys: a first-principles study. *Rsc Advances, 4*(54), 28714-28720.

Yang, S., Li, G., Qu, C., Wang, G., & Wang, D. (2017). Simple synthesis of ZnO nanoparticles on N-doped reduced graphene oxide for the electrocatalytic sensing of l-cysteine. *Rsc Advances, 7*(56), 35004-35011.

Yang, W., Akhtar, S., Leifer, K., & Grennberg, H. (2013). Noncovalent Functionalization of Graphene in Suspension. *ISRN organic chemistry, 2013*.

Yang, Y., Zhang, Z. G., Grulke, E. A., Anderson, W. B., & Wu, G. (2005). Heat transfer properties of nanoparticle-in-fluid dispersions (nanofluids) in laminar flow. *International Journal of Heat and Mass Transfer, 48*(6), 1107-1116.

Yarmand, H., Zulkifli, N. W. B. M., Gharehkhani, S., Shirazi, S. F. S., Alrashed, A. A., Ali, M. A. B., . . . Kazi, S. (2017). Convective heat transfer enhancement with graphene nanoplatelet/platinum hybrid nanofluid. *International Communications in Heat and Mass Transfer, 88*, 120-125.

Yeom, D. Y., Jeon, W., Tu, N. D. K., Yeo, S. Y., Lee, S. S., Sung, B. J., . . . Kim, H. (2015). High-concentration boron doping of graphene nanoplatelets by simple thermal annealing and their supercapacitive properties. *Scientific Reports, 5*.

Young, R. J., Kinloch, I. A., Gong, L., & Novoselov, K. S. (2012). The mechanics of graphene nanocomposites: A review. *Composites Science and Technology, 72*(12), 1459-1476.

Yu, W., France, D., Timofeeva, E., Singh, D., & Routbort, J. (2010). Thermophysical property-related comparison criteria for nanofluid heat transfer enhancement in turbulent flow. *Applied Physics Letters, 96*(21), 213109.

Yu, W., & Xie, H. Q. (2012). A Review on Nanofluids: Preparation, Stability Mechanisms, and Applications. *Journal of Nanomaterials*.

Yu, W. H., France, D. M., Routbort, J. L., & Choi, S. U. S. (2008). Review and comparison of nanofluid thermal conductivity and heat transfer enhancements. *Heat Transfer Engineering, 29*(5), 432-460.

Yuan, C. F., Chen, W. F., & Yan, L. F. (2012). Amino-grafted graphene as a stable and metal-free solid basic catalyst. *Journal of Materials Chemistry, 22*(15), 7456-7460.

Yue, S., Tong, H., Gao, Z., Bai, W., Lu, L., Wang, J., & Zhang, X. Fabrication of flexible nanoporous nitrogen-doped graphene film for high-performance supercapacitors. *Journal of Solid State Electrochemistry*, 1-11.

Zhang, G., Wang, F., Dai, J., & Huang, Z. (2016). Effect of functionalization of graphene nanoplatelets on the mechanical and thermal properties of silicone rubber composites. *Materials, 9*(2), 92.

Zhang, J., Xu, Y., Cui, L., Fu, A., Yang, W., Barrow, C., & Liu, J. (2015). Mechanical properties of graphene films enhanced by homo-telechelic functionalized polymer fillers via π–π stacking interactions. *Composites Part A: Applied Science and Manufacturing, 71*, 1-8.

Zhang, J., Yang, H., Shen, G., Cheng, P., Zhang, J., & Guo, S. (2010). Reduction of graphene oxide via L-ascorbic acid. *Chemical Communications, 46*(7), 1112-1114.

Zhang, L. L., Zhao, X., Ji, H., Stoller, M. D., Lai, L., Murali, S., . . . Ruoff, R. S. (2012). Nitrogen doping of graphene and its effect on quantum capacitance, and a new insight on the enhanced capacitance of N-doped carbon. *Energy & Environmental Science, 5*(11), 9618-9625.

Zhang, S. P., Xiong, P., Yang, X. J., & Wang, X. (2011). Novel PEG functionalized graphene nanosheets: enhancement of dispersibility and thermal stability. *Nanoscale, 3*(5), 2169-2174.

Zhang, T., Liu, J. L., Wang, C., Leng, X. Y., Xiao, Y., & Fu, L. (2017). Synthesis of graphene and related two-dimensional materials for bioelectronics devices. *Biosensors & Bioelectronics, 89*, 28-42.

Zhang, T. P., Liu, P., Sheng, C. R., Duan, Y. X., & Zhang, J. M. (2014). A green and facile approach for the synthesis of water-dispersible reduced graphene oxide based on ionic liquids. *Chemical Communications, 50*(22), 2889-2892.

Zhang, Z., & Lockwood, F. E. (2009). Preparation of stable nanotube dispersions in liquids: Google Patents.

Zheng, W., Shen, B., & Zhai, W. (2013). Surface functionalization of graphene with polymers for enhanced properties *New Progress on Graphene Research*: Intech.

Zhou, Y., Bao, Q. L., Tang, L. A. L., Zhong, Y. L., & Loh, K. P. (2009). Hydrothermal Dehydration for the "Green" Reduction of Exfoliated Graphene Oxide to Graphene and Demonstration of Tunable Optical Limiting Properties. *Chemistry of Materials, 21*(13), 2950-2956.

Zhu, G., Xu, T., Lv, T. A., Pan, L. K., Zhao, Q. F., & Sun, Z. (2011). Graphene-incorporated nanocrystalline TiO2 films for CdS quantum dot-sensitized solar cells. *Journal of Electroanalytical Chemistry, 650*(2), 248-251.

Zhu, H. T., Zhang, C. Y., Tang, Y. M., Wang, J. X., Ren, B., & Yin, Y. S. (2007). Preparation and thermal conductivity of suspensions of graphite nanoparticles. *Carbon, 45*(1), 226-228.

Zhu, Y., Stoller, M. D., Cai, W., Velamakanni, A., Piner, R. D., Chen, D., & Ruoff, R. S. (2010). Exfoliation of graphite oxide in propylene carbonate and thermal reduction of the resulting graphene oxide platelets. *Acs Nano, 4*(2), 1227-1233.

Zhu, Y. W., Murali, S., Cai, W. W., Li, X. S., Suk, J. W., Potts, J. R., & Ruoff, R. S. (2010). Graphene and Graphene Oxide: Synthesis, Properties, and Applications (vol 22, pg 3906, 2010). *Advanced Materials, 22*(46), 5226-5226.

Zu, S. Z., & Han, B. H. (2009). Aqueous Dispersion of Graphene Sheets Stabilized by Pluronic Copolymers: Formation of Supramolecular Hydrogel. *Journal of Physical Chemistry C, 113*(31), 13651-13657.

Zyla, G., Fal, J., Traciak, J., Gizowska, M., & Perkowski, K. (2016). Huge thermal conductivity enhancement in boron nitride - ethylene glycol nanofluids. *Materials Chemistry and Physics, 180*, 250-255.

LIST OF PUBLICATIONS AND PAPERS PRESENTED

1) Shazali, S. S., Amiri, A., Zubir, M. N. M., Rozali, S., Zabri, M. Z., & Sabri, M. F. M. (2017). Colloidal stability measurements of graphene nanoplatelets covalently functionalized with tetrahydrofurfuryl polyethylene glycol in different organic solvents. *Current Applied Physics*, *18*. 209-219.
2) Shazali, S. S., Amiri, A., Zubir, M. N. M., Rozali, S., Zabri, M. Z., Sabri, M. F. M., & Soleymaniha, M. (2018). Investigation of the thermophysical properties and stability performance of non-covalently functionalized graphene nanoplatelets with Pluronic P-123 in different solvents. *Materials Chemistry and Physics, 206*, 94-102.
3) Shazali, S. S., Rozali, S., Amiri, A., Zubir, M. N. M., Sabri, M. F. M., & Zabri, M. Z. (2018). Evaluation on stability and thermophysical performances of covalently functionalized graphene nanoplatelets with xylitol and citric acid. *Materials Chemistry and Physics, 212*, 363-371.
4) Shazali, S. S., Amiri, A., Zubir, M. N. M., Rozali, S., Zabri, M. Z., & Sabri, M. F. M. (2018). Facile hydrothermal method for synthesizing nitrogen-doped graphene nanoplatelets using aqueous ammonia: dispersion, stability in solvents and thermophysical performances. *Materials Research Express, 5*(3), 1-17.